LEVEL 2

PROCEEDINGS

CONFERENCE ON
THE EFFECTS OF
HELICOPTER DOWNWASH
ON FREE PROJECTILES

US ARMY AVIATION SYSTEMS COMMAND

ST. LOUIS, MISSOURI

78 08 10 067

Best
Available
Copy

(6)

Proceedings of the

TECHNICAL CONFERENCE ON
THE EFFECTS OF HELICOPTER DOWNWASH
ON FREE PROJECTILES,

held at Bridgeton, Missouri,

on 12-14 August 1975.

11 Nov 75

12, 305 p.

PROCEEDINGS

NOVEMBER 1975

78 08 10 067
404 318

PREFACE

This proceeding of the conference on "The Effects of Helicopter Downwash on Free Projectiles" is published by the US Army Aviation Systems Command and includes all reports and formal papers presented during the conference.

A chronological bibliography on Rotor Downwash from 1922 to 1975 is included, courtesy of Mr. R. Blattner, US Army Materiel Systems Analysis Activity.

PROCEEDING

This summary of the conference on "The Effects of Helicopter Downwash and Free Projectiles", held at the Red Carpet Inn, Bridgeton, Missouri, and Mart Building, St. Louis, Missouri, 12-14 August 1975, is a record of the presentations and transactions of the meeting.

The registered attendance of the meeting is as follows: 75 persons, representing 20 companies, 16 US Government Agencies and 1 Foreign Government.

There were 18 formal papers presented. All papers are published in this proceeding unless otherwise noted.

Two major projects which the Army will pursue, resulted from the conference. The projects will be directed by a committee headed by LTC John Topp. The committee held its first meeting 28 August 1975.

OPENING SESSION
Tuesday, 12 August, 9:00 A.M.

Formal opening of the Helicopter/Rocket Airflow Conference, General Chairman R. Reeves.

This session was formally opened by the General Chairman R. Reeves, who called attention to the program of events that were to follow during the two day conference. The meeting was then turned over to the Session Chairman, R. Bergman.

Partial contents)

DOWNWASH EFFECTS
Chairman R. Bergman

WELCOME - R. Long, Deputy Director of Research, Development and Engineering, US Army Aviation Systems Command.

INTRODUCTION AND ASSESSMENT OF THE PROBLEM - G.R. Marner, presented by the Author.

THE PERTURBED FLOW ENVIRONMENT ABOUT HELICOPTERS AND ITS EFFECT ON FREE ROCKETS. - B.Z. Jenkins, presented by the Author.

SOME PRACTICAL ASPECTS OF ROTOR WAKE EFFECTS ON ROCKET ACCURACY. - H.A. Morse, presented by the Author.

DOWNWASH EFFECTS ON ROCKET TRAJECTORIES, EMERSON REPORT 2418 - presented by R. Bauman and R. Figueras.

AH-1G HELICOPTER FIELD FLOW SURVEY. - B.H. Boirun and E. Bailes presented by F. Dominick.

(p 2)

1

DOWNWASH EFFECTS
Tuesday, 12 August, 1:15 P.M.
Chairman R. Frank

TOTAL QE COMPONENT VARIATION UNDER HOVER DOWNWASH CONDITIONS FOR LONG RANGE TARGETS (3-6KM), - R. Lent and W. Garner, presented by Authors.

MOVIE/INTRODUCTION TO THE EFFECTS OF ROTOR-WAKE ON ROCKETS. - R. Bergman, presented by the Author.

ROTOR-WAKE INDUCED FLOW ALONG HELICOPTER ROCKET TRAJECTORIES - A. Landgrebe and T.A. Egolf, presented by Authors.

PRELIMINARY ANALYSIS OF THE EFFECTS OF CALCULATED DOWNWASH DISTRIBUTION ON FLIGHT PERFORMANCE OF THE 2.75-INCH ROCKET - S. Wasserman, presented by the Author.

AIR DATA SENSORS
Wednesday, 13 August, 9:00 A.M.
Chairman L. Bolmarick

THE MEASUREMENT OF HELICOPTER AIR DATA USING SURVEILLING PITOT STATIC PRESSURE PROBES - J. Carter, presented by the Author.

THE CORRELATION OF ACTUAL INDUCED FLOW WITH THEORY FOR BELL NUH-1M HELICOPTER ROTOR OPERATING IN LEVEL FLIGHT - J. Carter, presented by the Author.

REVIEW OF LORAS CHARACTERISTICS - D.L. Green, presented by the Author.

GENERAL REQUIREMENTS FOR OMNI DIRECTIONAL LOW RANGE AIRSPEED SYSTEM - D.L. Green, presented by the Author.

LORAS DISPLAYS - D.L. Green, presented by the Author

ULTRASONIC WIND VECTOR SENSOR - F.J. Ferrin and M. Yurescko, presented by the Author.

AIR DATA SENSORS
Wednesday, 13 August, 1:15 P.M.
Chairman L. Bolmarick

APPLICATION OF REMOTE WIND SENSORS - D.H. Dickson, presented by the Author.

EFFECTS OF AIRFLOW ON JETTISON OF MULTI-TRACK LAUNCHERS FROM HELICOPTERS.- E.S. Stoops and R.D. Enrich, presented by E.S. Stoops

VA 210-220 SERIES, LOW SPEED INDICATOR, 1 to 150K AND AIR SPEED/DIRECTIONAL SENSOR, 2 AXIS, VT1003. R. Colton and R. Joy, presented by the Authors.

2

An interesting and informative open discussion followed which revealed many good points on airflow and air data sensors. Closing remarks were made by L. Bolmarick, G.R. Marner, and R. Reeves.

GOVERNMENT RECAP
Thursday, 14 August, 9:00 A.M.
Chairman R. Reeves

Government representatives met in Conference Room #2 of the Mart Building to recap the events of the prior two days and discuss means of accomplishing the planned goals. After discussing a number of proposals, it was decided to concentrate AVSCOM's efforts on two major projects. LTC John Top, Systems Integration Project Manager, AVSCOM, was selected and accepted responsibility for assembling a task team. This team will outline the programs and act as a decision making body to solve the low speed hover firing problem.

Although the conference title related to free projectiles, most of the papers were directed at the 2.75 inch rocket and related subsystems. The papers were well received by those in attendance and considerable discussion ensued following the formal presentation. All who heard the presentation will now have a deeper appreciation of the complexity of the downwash problem.

THE EFFECTS OF HELICOPTER DOWNWASH ON FREE PROJECTILES

INTRODUCTION AND ASSESSMENT OF THE PROBLEM

GENE R. MARNER
U.S. ARMY AVIATION SYSTEM
ST. LOUIS, MISSOURI

The helicopter is an agile, flexible, and adaptable vehicle. It has proved to be of great utility as a weapon platform under complex battlefield conditions. This adaptable utility gives the helicopter a major role in America's deterent forces. If these forces are to be effective peacekeepers, they must be adaptable to many different conditions of terrain, weather and threat, since we live in a complicated world in which tensions in many locations threaten world peace.

The capability of the helicopter weapon system is under challenge. Conventional anti-aircraft weapons are being developed with better search capability, greater range and more rapid response. They are being fielded extensively on mobile armored platforms. Missiles are being fielded in large numbers with highly portable launching platforms and sophisticated guidance systems. Thus, we find that the helicopter must operate at low altitudes, must take advantage of terrain features, must work at greater stand-off distances and must develop even greater hover and maneuver capability.

Now, while the helicopter has many merits, it has limitations. It must conform to severe weight restrictions in order to attain hover and maneuver capability. It is a sensitive, vibrating platform. It is clear that helicopter-borne weapons systems must attain better precision at greater ranges while operating at hover or low speed maneuvers.

This brings us, therefore, to the subject of this conference. The free aerial rocket, which is launched at low velocity and has no terminal guidance, is significantly affected by rotor downwash. This downwash is, of course, largest during hover, so it is expected to be of considerable importance in the future. It appears that we need to know more about the translation and rotation effects as a function of downwash characteristics, that we need a method of measuring downwash characteristics during flight, and that we need the capability to use the derived data in a fire control system.

Unfortunately, we seem to be in the early stages of learning insofar as this problem is concerned. The 2.75" Project Manager sponsored a 2.75 Inch Rocket/AH-1G System Baseline Accuracy Test which was a detailed analysis of the helicopter/rocket system performance at airspeeds of 90 and 120 knots. The major conclusion of the test was that helicopter rocket fire control was needed to accomplish a significant improvement in system effectiveness. The lack of appropriate instrumentation was a prime factor in not acquiring the same type of data for hover and low forward air speeds. Currently, instrumentation has still not advanced sufficiently to provide adequate experimental data on airflow under the Cobra rotor disc throughout the weapon launch envelope at low airspeeds. Discussions with the aeronautical laboratories revealed that no definite data existed on the area of interest. Rocket ballistic simulations had to be performed utilizing assumed data generated with standard momentum theory based on the size of the rotor and gross helicopter weight. Airflow perturbations within the rotor downwash were unknown.

After determining that there existed a large gap in data on airflow in the rocket launch envelope at low airspeed, the 2.75 Inch Rocket Project Manager accepted a proposal from United Aircraft Research Laboratories (UARL) to acquire basic information utilizing computer simulation. The computer simulation techniques developed by UARL are unique in the capability to provide instaneous and time-averaged airflow vectors in both distorted and undistorted rotor wakes.

The Aeroballistics Section at Picatinny Arsenal followed through with the data presented in the UARL report to calculate the effects of the airflow on the rocket trajectory. The rocket will usually be influenced by the passage of approximately two rotor blades during its exit from the weapon launch envelope. During preliminary simulations with a six degree of freedom rocket ballistic simulation, it was found that at ranges below 2000 meters, a variation in impact distance could be detected as a function of the blade position and instantaneous velocities at the time of firing. At ranges greater than 2000 meters the impact point was not detectably influenced by variation in firing time relative to rotor position.

In hover firing tests at Yuma Proving Ground in 1974, the 2.75" rocket achieved an impact distance of 4500 meters when fired at 30 feet above the target with a 3° launch angle. On the other hand, firings at 90 knots at 300 feet altitude required a 7° launch angle to reach 4000 meters. It is evident that the upward weathervaning effect in hover has a significant effect on trajectory. We anticipate hearing a great more detail from these research efforts.

In the past few years there has been rapid progress in the techniques of low velocity airspeed measurement. Adaptations of the pitot technique, new methods of vortex trail measurement, and doppler laser techniques all give promise for measuring downwash velocities. We hope these techniques will make it possible to obtain precise empirical data for fire control application. We look forward to several papers concerning these techniques.

I hope that this conference will focus attention on the downwash problem and will accelerate progress which is badly needed.

THE PERTURBED FLOW ENVIRONMENT ABOUT HELICOPTERS
AND ITS EFFECT ON FREE ROCKETS

BILLY Z. JENKINS
US ARMY MISSILE COMMAND
HUNTSVILLE, ALABAMA

ABSTRACT

The use of rotary-wing aircraft as launching platforms for rockets
or missiles is complicated by the transient environment which exists
before and during launch and through the first six or eight meters of
flight. Not the least important of these is rotor downwash. Current
concepts in air launched weapons emphasizes launch from very low
speed or hover, conditions at which downwash effects are maximal.
The round is, moreover, most vulnerable to upsetting disturbances
at the low speed, initial segment of its trajectory.

Results are presented for flight test surveys of the downwash
velocities as well as analytical predictions of these velocities.
A UH-1M helicopter bearing an array of 3-vector hot film anemometers
was flown at the US Army Engineering Flight Activity at Edwards Air
Force Base in California. Velocity data were gathered at a variety
of speeds from hover to 90 knots at an altitude above ground effect.
In addition to results, some of the problems peculiar to such a test
are discussed. A similar test on the AH-1G is underway and will be
discussed pending its success. The helicopter flow field for steady
straight (no side-slip) and level flight has been modelled using a
source-sink distribution to simulate the fuselage effect and a shed
rolled-up vortex filament system to simulate the rotor. The fuselage-
downwash representatives are iterated in leap-frog fashion until a
periodic flow included their interaction is reached. A comparison
of theory and experiment is shown which indicates a good agreement
in some cases, and poor agreement in others.

Trajectory simulation is included to show the effects of downwash on
free rockets. In many cases, it is seen that the round cannot respond
to the fluctuating component of the velocity but can significantly be
influenced by the time averaged component.

Introduction

The Army is deeply committed to the concept of an attack helicopter - one which may be armed with conventional firearms as well as guided missiles or free rockets. A helicopter is not the most ideal launch platform for rockets and missiles due to the numberous launch transients involved. These transients, principally vibration, rotor downwash, and translation and rotation of the launch platform, have not been properly investigated as sources of rocket dispersion. In an effort to assess the importance of rotor downwash on the dynamics of the round during its first few feet of flight, it is first necessary to determine the induced velocity field about the helicopter in flight. Knowing the properties of the environment which the rocket must traverse, aerodynamic forces derived therefrom may be used in simulating the rocket's trajectory. A theoretical capability to define the helicopter's downwash properties exists at MICOM through a computer program developed over the past eight years. To verify and supplement this, a flight test experiment was begun in 1973 and is still being conducted.

Description of Analytical Technique

The computer program being used at MICOM and the analysis upon which it is based are described in Refs. 1, 2, and 3. Basically, the resultant flow in the domain of interest is assumed to be a superposition of three elements: the freestream, the fuselage represented by a distribution of sources and sirks, and the rotor wake represented by line vortices shed from each blade (Fig. 1). Obviously, the representation of the fuselage and the representation of the rotor downwash are interdependent and should be periodic functions of time. In the

7

program, the initial representation of the wake is chosen to be helical
(one for each blade) and slanted aft in accordance with momentum theory.
The fuselage representation is initially taken to be that resulting from
the freestream only. The rotor representation is then advanced by
marching timewise for several revolutions of the rotor. The fuselage
representation is then recalculated using the time averaged values for
the downwash effect in accounting for flow nonuniformity. This pro-
cedure is then repeated until a nearly periodic flow is established -
usually, approximately four complete passes. It is seen that the sol-
ution found is not completely interactive - the fuselage representation
resulting is the one that would result from the time average of the
periodic flow. The influence of the fuselage is relatively small com-
pared to the other sources and this shortcoming is not very important.
There is another shortcoming which is potentially more serious. The
shed vortex sheet from along the blades is ignored or lumped into the
vortex filaments being shed by the blade tips. More recent downwash
simulation programs which account for this effect indicate that it is
important.

Consideration of the model representation of the flow field reveals
several important facets of the resulting flow:

(a) areas of strong velocity gradients and high velocites will
occur near the vortices distributed through the flow;

(b) the position of the boundaries of the rotor wake is strongly
influenced by the aircraft's speed. For rockets launched from the
helicopter in a conventional fashion, there exists a maximum airspeed
for which the rotor downwash intersects the rocket's flight path;

8

(c) the weight of the aircraft influences the vertical downwash component almost linearly; and

(d) the incidence of the rotor disk to the freestream, α_T, is important for characterization of the downwash properties and is largely determined by aircraft drag and weight.

Description of Experiments

The most direct quantities for defining the aerodynamic environment occurring about helicopters are the time dependent velocity components throughout the region of interest. This was undertaken, but for economy of effort the rotor wake boundary as a function of airspeed was first undertaken to fix the forward limit of the survey. Virtually all the experimental data given can also be found in Ref. 4.

a. Aircraft and Range

The flight tests were conducted by the US Army Aviation Engineering Flight Activity located at Edwards Air Force Base, California. Based primarily on aircraft availability, a UH-1M helicopter was selected as the test vehicle. A drawing of the aircraft, showing the coordinate system, is presented in Fig. 2.

b. Instrumentation and Procedure

The wake boundary surveys were made using an Elliott dual-axis low airspeed system. The Elliott system was mounted at Y = -65, Z = 29 for various X positions and at Y = -65, Z · 88 for various X positions. The flow angularily in the helicopter pitch plane was noted for various forward speeds of the aircraft. As the foremost boundary of the rotor wake passed the Elliott probe a pronounced change in the flow angularity occurred, allowing the X coordinate of the wake boundary to be deter-

mined as a function of airspeed for two outboard stations (Fig 3).
It is seen that the weapon mount location, typically forward of fuse-
lage station 120, will be free of downwash effects for true airspeeds
greater that 45 ft/sec.

The flow field velocity survey was conducted using an array of
seven split film 3-component anemometers mounted linearly on a lateral
rack, 8.5 in. apart (Fig. 2). Plans were to make successive flights,
repositioning the rack between flights until the entire volume of
interest had been covered. During each flight a number of data re-
cords were to be taken at a predetermined set of flight conditions.
Complete descriptions and specifications are given in Ref. 1.

Unfortunately, the tolerance of the anemometers to vibration had
not been determined and insufficient vibration isolation had been built
into the support structure. The sensors failed subsequent to the first
flight with the rack in the first position. The probe locations for
the first rack position are given in Table 1. During this test flight,
data were taken for a variety of forward velocities. As Table 1 indi-
cates, only five of the seven sensors were fully operative throughout
the flight.

TABLE 1. PROBE LOCATIONS

Probe No.	X (in.)	Y (in.)	Z (in.)	Comments
1	111.885	-109.56	58.928	
2	111.885	-101.06	58.928	Operative in one axis only
3	111.885	-92.56	58.928	
4	111.885	-84.06	58.928	
5	111.885	-75.56	58.928	Inoperative
6	111.885	-67.06	58.928	
7	111.885	-58.56	58.928	Data noisy (perhaps due to turbulence)

Flight data records were taken at airspeeds of approximately 8, 18, 54, 75, 393, 113, 135 and 153 ft/sec. The helicopter was flying with zero sideslip, straight and level out of ground effect. Gross weight was 7400 to 7500 lbs and rotor speed was nominally 324 rpm.

c. Velocity Survey Results

Velocity-time curves for each component, sensor, and flight record are presented for the entire measurement interval in Ref. 1. This time interval is large compared to the period of the fluctuating velocity, making it hard to distinguish details of the curve shape over only one period (~ 0.095 sec). In Ref. 5, these data are represented over an interval of only six periods allowing the scatter in data, repeatability from cycle to cycle, and variability of data quality from flight record to flight record to be readily seen. One of these

11

plots is shown in Fig. 4. Note in particular:

(a) the passage of the vortex filaments as indicated by the fast velocity change in all components but principally V_X and V_Y;

(b) the low amplitude of the fluctuations of vertical downwash component;

(c) the weakness of the lateral component of velocity at this station. According to analysis, this is true even at station located near the wake boundaries;

(d) the unusually high value for V_X (30 to 40 ft/sec) is unrealistic for a forward velocity of only 7.7 ft/sec. All theoretical methods indicate the mean value of V_X should be on the order of $7.7 + V \sin \alpha_T$ $= 7.7 + 75 \cdot \sin 2^\circ = 10$ ft/sec. The measured values were repeatable between different data records of approximately 5 sec each.

Comparison of Theory and Experiment

Theoretical simulations were conducted for several of the experimental flight records. One of the critical input variables is the incidence of the rotor tip path plane to the freestream (α_T). This quantity varies with airspeed and aircraft weight and center of gravity location and was not directly measured during the experiment but inferred from aircraft attitude measurements. Since rotor flapping angle was not measured, the angle of the tip plane relative to the aircraft coordinate system was unknown. For the values of α_T derived from experiment, the flapping angle was assumed to be zero; therefore, α_T may be in error by the amount of the true flapping angle. If the available data for aircraft weight and drag is used, α_T may be calculated by balancing

12

forces at the rotor hub. The comparison of the values obtained in
these two different methods is shown in Fig. 5. Disagreements between
theory and experiment which correspond to up to 4° of flow incidence in
the pitch plane may be expected to be found.

a. Time Dependent Data Comparison

Since the period of the velocity fluctuations is governed by
the rotation of the rotor, the time coordinate was replaced with rotor
position. For a two-bladed rotor, such as that of the UH-1M, each blade
contributes to the flow velocity experienced by a point in the wake;
therefore, the period is 2 per revolution or 180° of rotation of the
rotor. Instead of plotting rotor position as an ever increasing angle
for successive periods, it was plotted modulo 180°. In this way all
the periods are superimposed on each other in the same 0 to 180° range.
This is called a folded plot. For flight record 1, the absolute value
of rotor position was measured with 0 and 180° corresponding to align-
ment of the rotor with the fuselage centerline. This measurement sub-
sequently became inoperative; therefore, for the remaining flight
records the experimental values for rotor position are known relative
to each other but not with respect to any reference position as was
the case for flight record 1. As a result, in comparing theory with
experiment using Figs. 6 through 8, it must be realized that theory
and experiment can be arbitrarily displaced relative to each other
along the abscissa.

During the course of the experiment, the rotational velocity of the
rotor was nominally 324 rpm which would correspond to a period of 0.0926
sec. However, in plotting the folded data it was found that slightly

13

higher values for the period gave much better results in that there was less scatter in the data. The value used for the period is indicated on each graph of Figs. 6 through 8.

Instead of plotting flow velocity components along the three coordinate axes (Fig. 4), velocity magnitude and direction are shown in Figs. 6 through 8. θ_Y and θ_Z are the angles between the flow velocity vector and the Y and Z axes, respectively. In this manner differences in flow direction between theory and experiment are put in proper perspective whereas in plotting VX, VY, and VZ a small error in flow direction can overwhelm a small component, such as VY, making it scattered to the point of being useless.

The inconsistency mentioned earlier in velocity measurement is shown in Fig. 8 as a 10 to 15° direction error. Since this occurred at the most outboard probe, flow interference is unlikely-deflection of the probe and for rack is more likely. These angular inconsistencies were present for most flight records and probes, increasing with proximity to the fuselage. The velocity magnitude error is considered less alarming.

b. Time Averaged Data

In many cases the frequency of the flow fluctuation (≈ 10Hz) is high enough that objects of interest which are immersed in the flow cannot respond to it. In this case time dependent details of the wake flow can be ignored and the time averaged flow velocity and direction can be used to determine the behavior of the object. Theoretical and experimental flow magnitude and direction were time averaged and plotted

14

(Fig. 9) as a function of Y for fixed X and Z locations corresponding to the sensor rack position (Table 1). Gaps in the experimental data correspond to positions of the malfunctioning sensors Nos. 2, 5, and 7.

Elaboration of a Typical Situation

Having devoted some time to qualitatively describing the flow field and justifying the application of the downwash computer program, typical conditions existing along the path of a rocket fired from the AH-1G wing will be presented, based on calculated results (Fig. 10).

Figure 11 shows the downwash velocity components as a function of displacement along the trajectory of a 2.75 in. rocket. The conditions used in generating the data for this plot along with implications are as follows:

(a) The aircraft is hovering. Forward velocity would diminish the vertical downwash while enhancing the component along the trajectory, thus decreasing cross flow angles and increasing dynamic pressure. Moreover, the rocket would be immersed in the downwash over a shorter distance for higher airspeeds and be entirely free of it at approximately 36 knots.

(b) The round is launched from a position at butt line 42, water line 55, and fuselage station 148 corresponding to an inboard launcher position. Changes in the velocity-position profiles resulting from changes in launcher position within reasonable limits are minimal at hover. Moving outboard or forward results in a quicker exit from the wake, moving downward tends to reduce crossflow. If ground effect were to be considered, the induced vertical velocity component would be somewhat less depending on hover altitude.

15

(c) The quadrant elevation of the round is 9.8°. The influence of changes in this parameter is to increase time of immersal and intensity of downwash if increased and vice-versa.

(d) The solid lines were drawn corresponding to an instantaneous rotor position of alignment with the fuselage; the dashed lines-time average velocities and the shaded areas, the limits for other instantaneous values at various rotor positions and for the other side of the helicopter. The regions of greatest fluctuations were associated with the zone of passage of the vortex filaments.

Figure 12 relates the information of the previous slide to the angles of attack in pitch and yaw experienced by the 2.75 in. rocket. In this case the instantaneous values of downwash are used which are calculated at the time when the rocket nose occupies that point. In Fig. 11, time is constant along the solid line and is averaged out for the dashed line. These curves are specific to the 2.75 in. rocket since its forward velocity and elapsed time at each point figure in the computation.

Finally, to show the effect that this environment can have on the rocket dispersion, suppose that the trajectory to impact is computed, assuming the rocket is fired from 30 ft. above the plain. Neglecting downwash entirely, the round impacts at approximately 12,000 ft. with only 1-1/2 ft. crossrange deflection. If a constant downwash of 50 ft/sec over the entire rotor disk shadow is assumed, the round impacts at approximately 14,000 ft. with less than 3 ft. of crossrange deflection. With the indicated profile (Fig 11 and 12) the round impacts at near 14,000 ft. but has flown to the left approximately 120 ft. In both cases

16

of downwash assumptions, the rocket is high in the air (several hundred feet) when it is 12,000 ft. downrange.

If the trajectory is calculated with different phasing of the launch-rotor positions, little change results; only 10 to 25 ft. in crossrange or downrange. It would suffice in the case of the 2.75 in. rocket to consider time average downwash properties. It was noted, however, that a constant downwash model cannot properly predict cross-range effects. (These results are subject to mitigation by ground effect.)

Conclusions and Recommendations

The downwash can significantly affect the trajectory of rockets launched from rotary wing aircraft at low speed or hover; however, the magnitude of these effects in relation to other launch transients is unknown and are not readily separable in firing tests. In the past, firing techniques have emphasized deployment from a dive at approximately 60 knots but current emphasis is on fire and forget tactics making use of popup and shoot at near hover. The role of downwash, in fact all launch transients, must be effectively assessed.

Further trajectory simulation is required for rockets having different aerodynamic and dynamic properties. The moderating effect of ground proximity and influence of drift and gusts should be considered.

When the aerodynamic environment is accurately known, the aerodynamic force calculations should allow for gross nonuniformity of the flow. The flow properties can change significantly over the length of the rocket.

Flight tests are in progress to survey the flow field about the AH-1G from the launcher attachment point to the nose of the aircraft.

17

These data will be used to verify the analytical technique further and will provide better definition of the aerodynamic environment for further trajectory simulation.

REFERENCES

1. Crimi, Peter: <u>Theoretical Prediction of the Flow in the Wake of</u> <u>a Helicopter Rotor, Part 1</u>, September 1965, CAL Report No. BB-1994-S-1.

2. Crimi, Peter: <u>Theoretical Prediction of the Flow in the Wake of a</u> <u>Helicopter Rotor, Part 2</u>, September 1965, CAL Report No. BB-1994-S-2.

3. Crimi, Peter and Trenka, Andrew: <u>Theoretical Prediction of the Flow</u> <u>in the Wake of a Helicopter Rotor, Addendum</u>, August 1966, CAL Report No. BB-1994-S-3.

4. Boirun, Barclay, Jefferis, Robert, and Holasek, Ronald: <u>Rotor</u> <u>Flow Survey Program UH-1M Helicopter</u>, May 1974, Final Report on USAASTA Project No. 72-05.

5. Jenkins, B. Z. and Marks, A. S.: <u>Rotor Downwash Velocities About</u> <u>the UH-1M Helicopter - Flight Test Measurements and Theoretical</u> <u>Calculations</u>, 1 January 1975, MICOM Technical Report RD-75-27.

Freestream

Vortices shed by rotor

Fuselage element
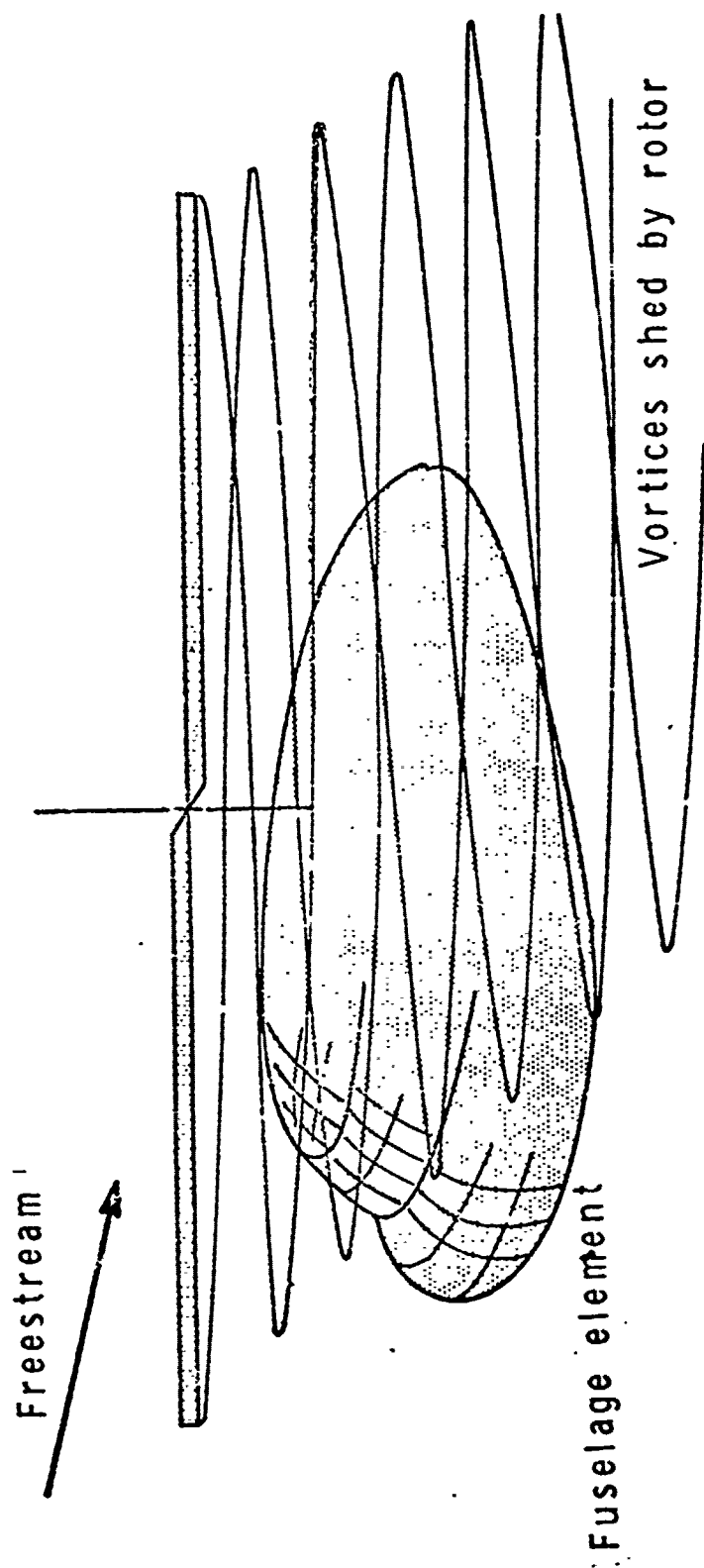
Figure 1. Schematic representation of flow field.

ELLIOTT PROBE

BALLAST BOX

RAKE
POSITION NO. 1

WATERLINE (Z) (in.)

150
100
50
0

FUSELAGE STATION (X) (in.)

0   100   200   300   400   500

ELLIOTT PROBE

BALLAST
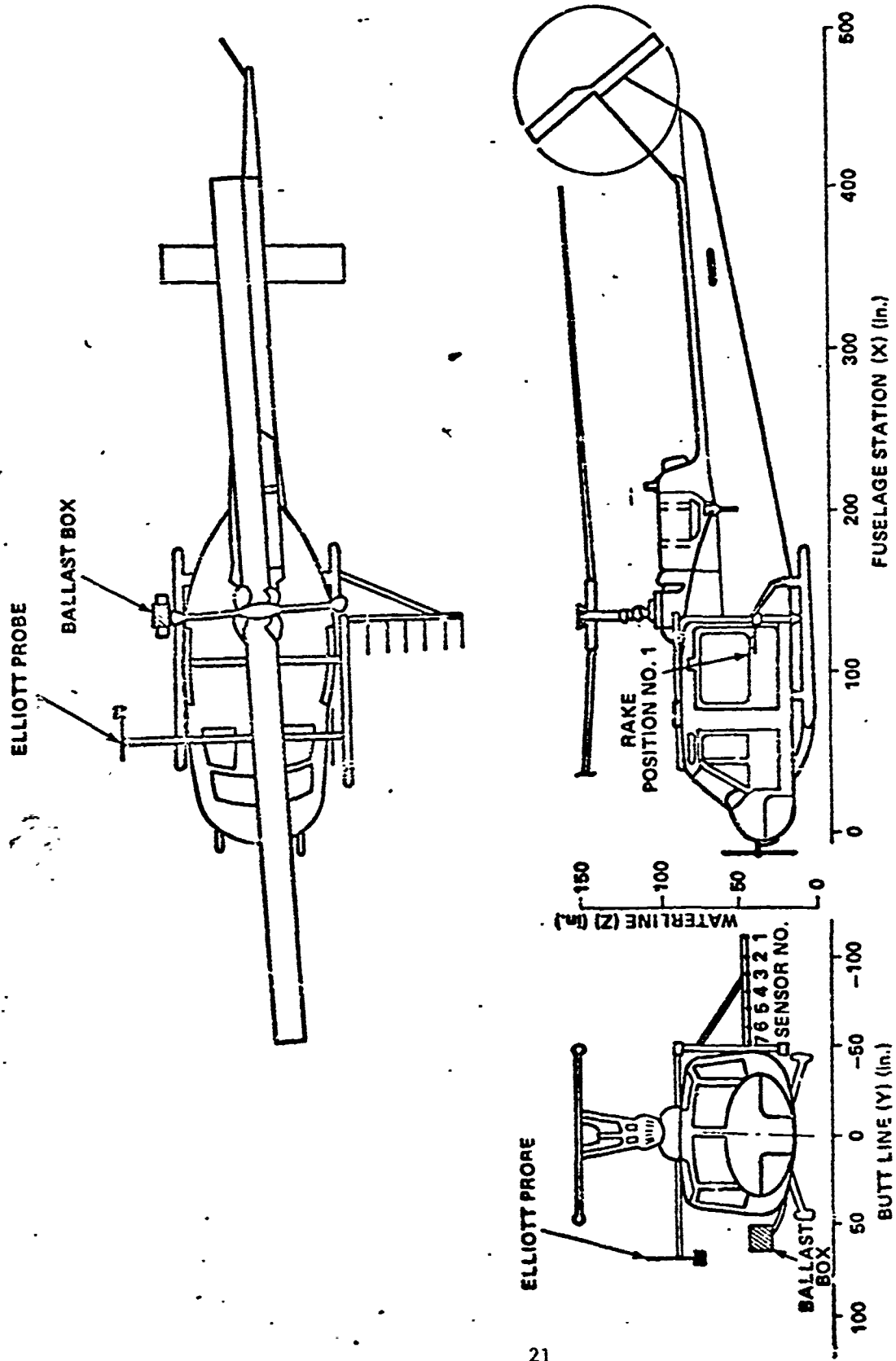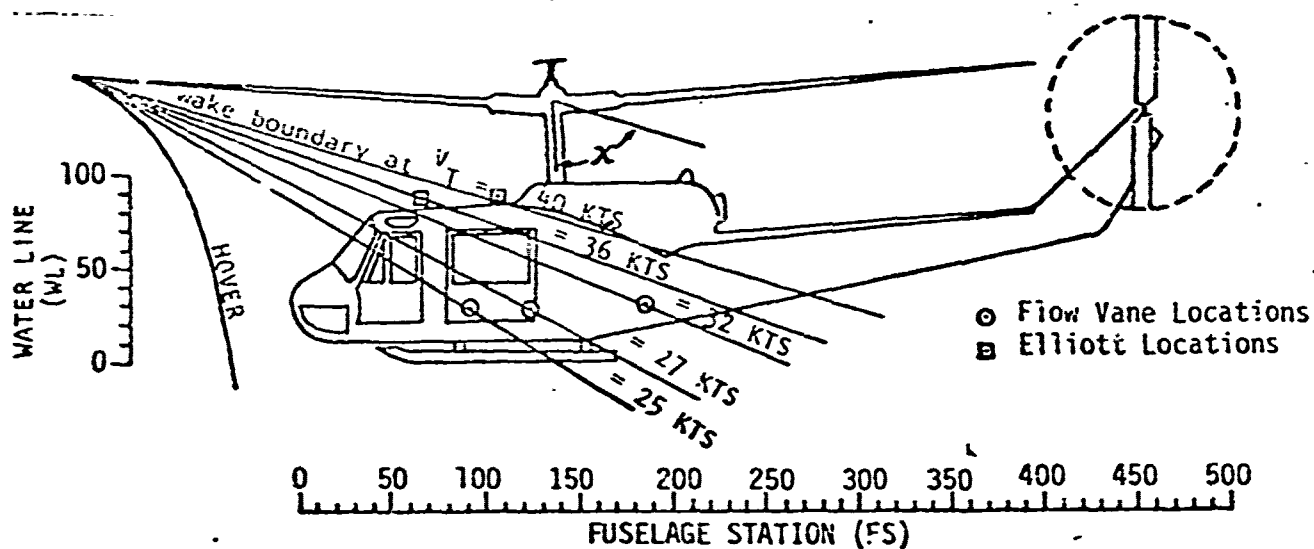BOX

7 6 5 4 3 2 1 SENSOR NO.

BUTT LINE (Y) (in.)

100   50   0   -50   -100

Figure 2. Aircraft coordinate system showing probe locations.

21

NOTES: 1. Data shown for buttline -65.
2. Data not corrected for displacement due to rotor flapping with increased forward speed.
3. Waterline stations are 83 and 29.
4. Average Conditions:
Gross Weight = 7500 pounds.
Density Altitude = 2500 feet.

Figure 3. Rotor wake boundaries in forward flight.
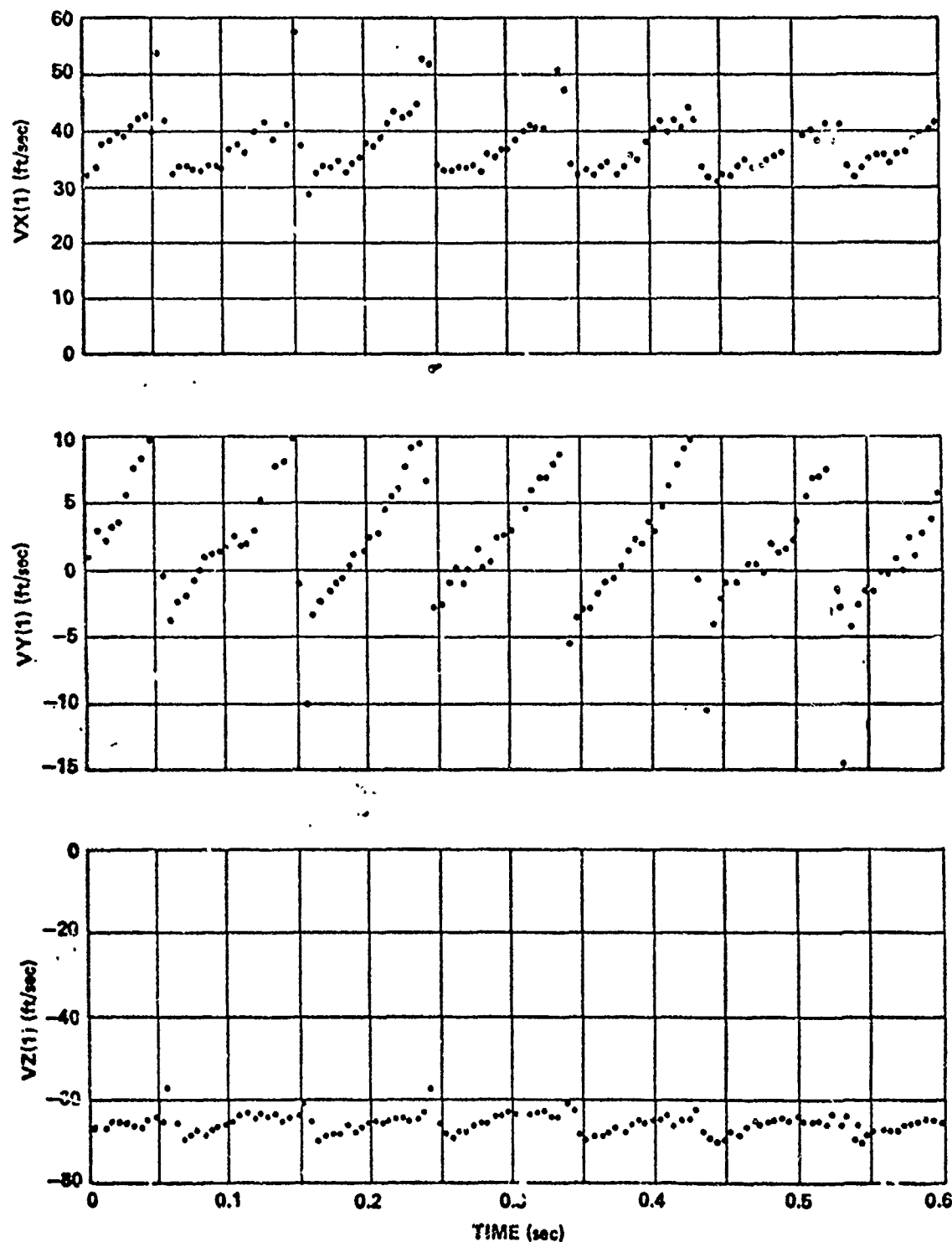
Figure 4. UH-1M helicopter flow field velocity components –
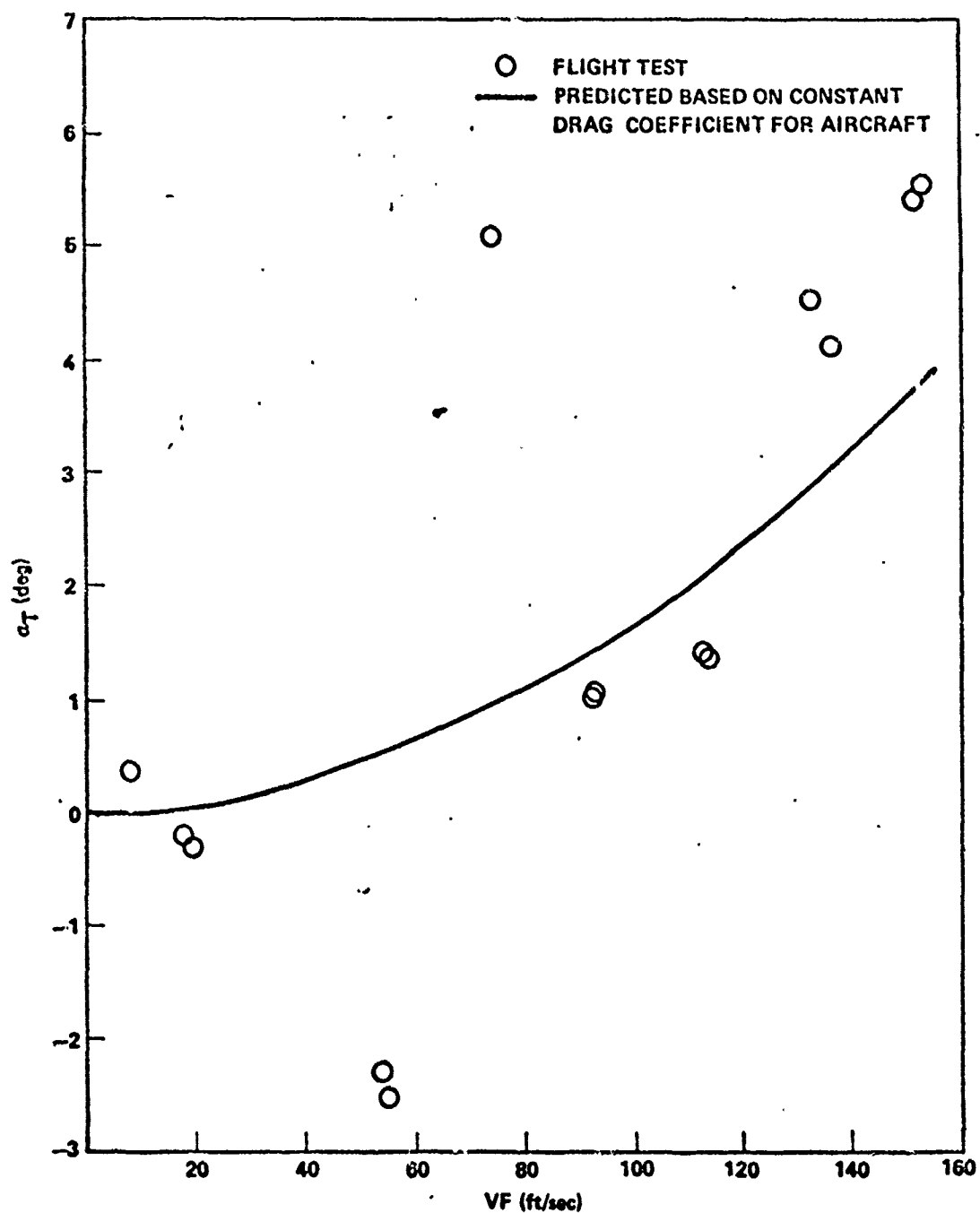7.7 ft/sec airspeed, sensor No. 1.

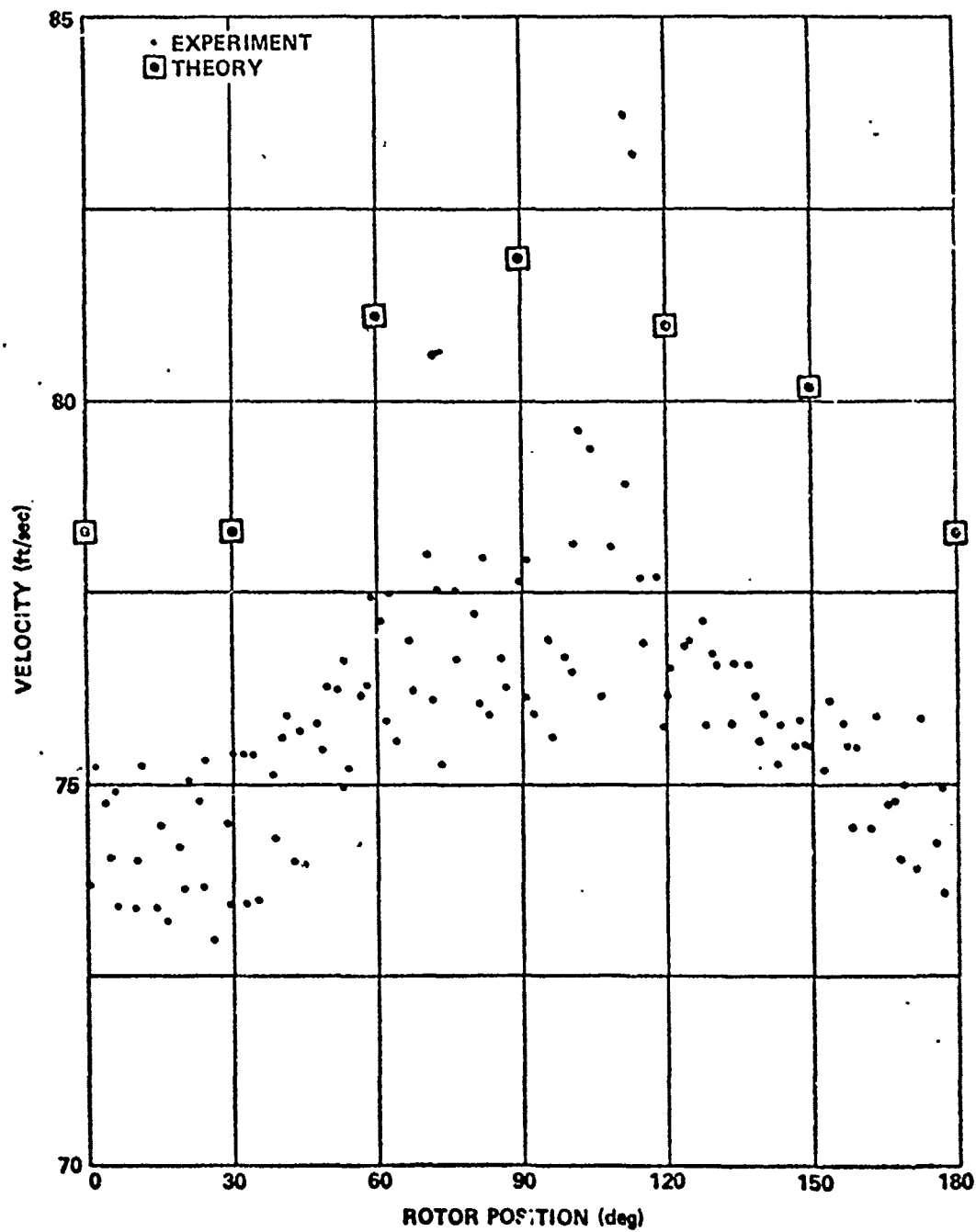Figure 5. Variation of inclination of tip path plane of helicopter to freestream with helicopter airspeed.

Figure 6. Folded comparison – 7.7 ft/sec airspeed, sensor No. 1, and trial period 0.094500.
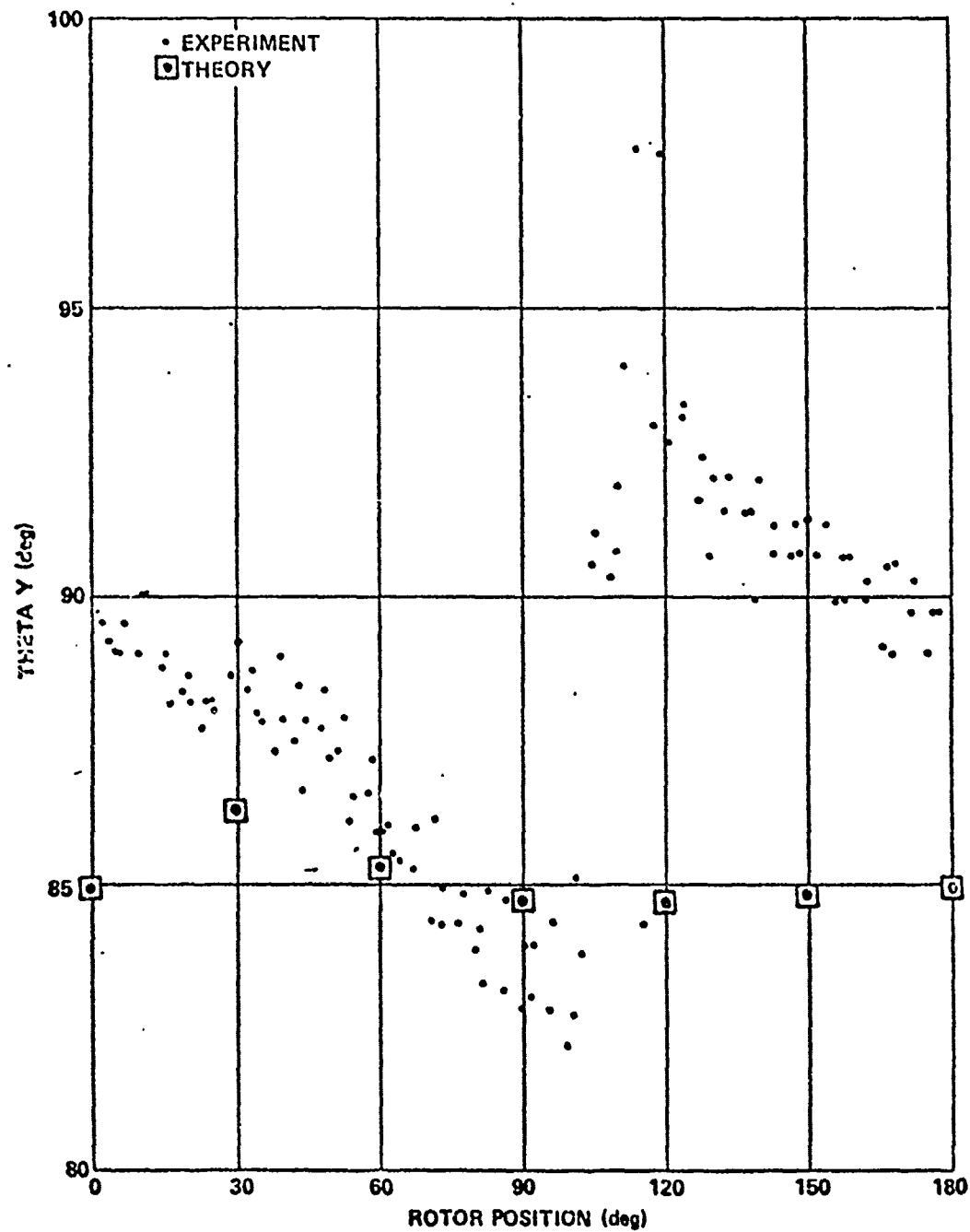
Figure 7. Folded comparison – 7.7 ft/sec airspeed, sensor No. 1, and trial period 0.094500.
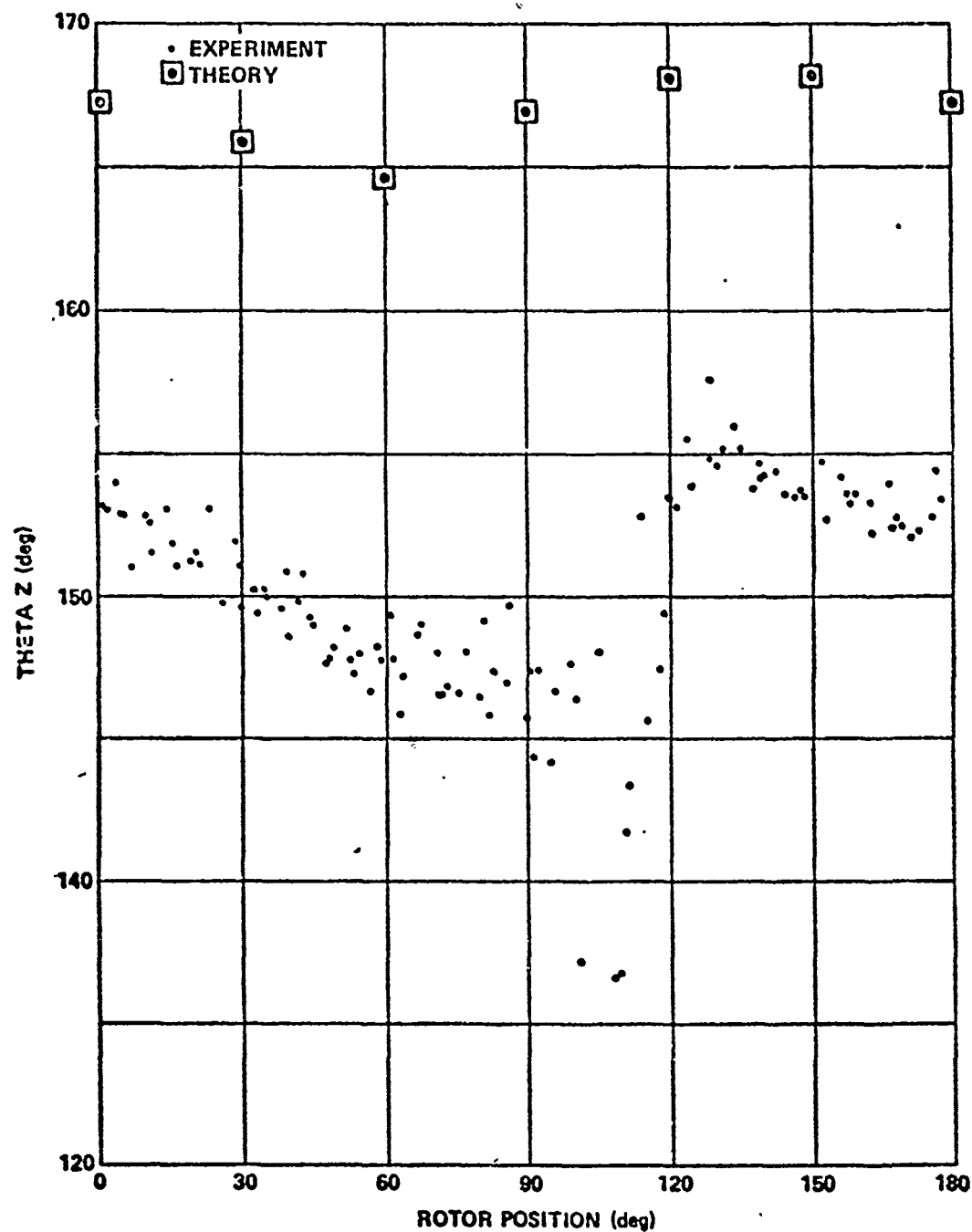
Figure 8. Folded comparison – 7.7 ft/sec airspeed, sensor No. 1, and trial period 0.094500.
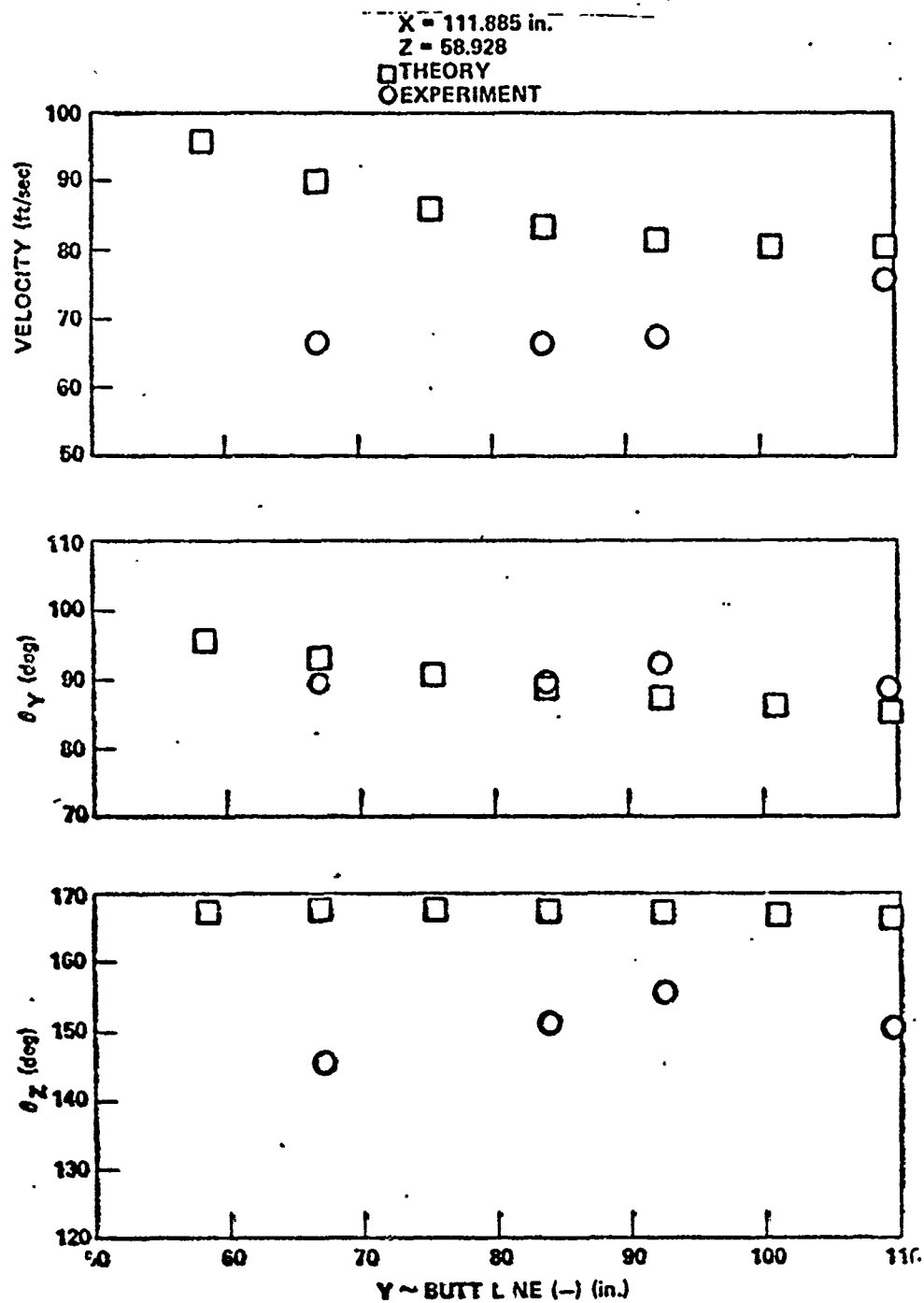
Figure 9. Comparison of time averaged velocity predictions with experiment, 7.7 ft/sec airspeed.
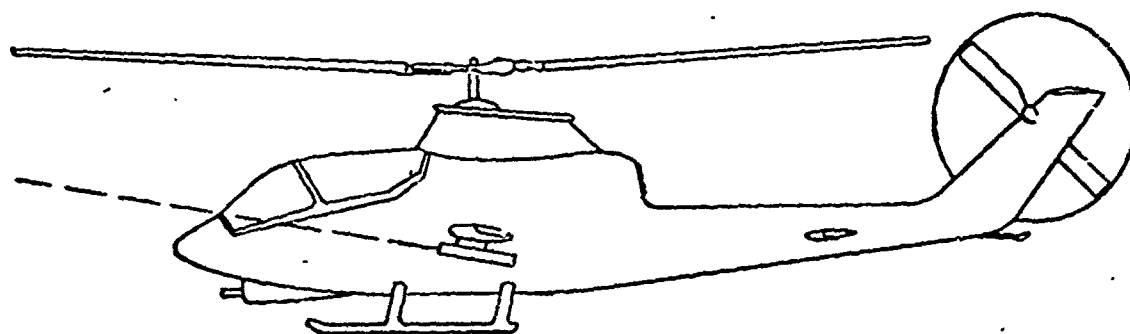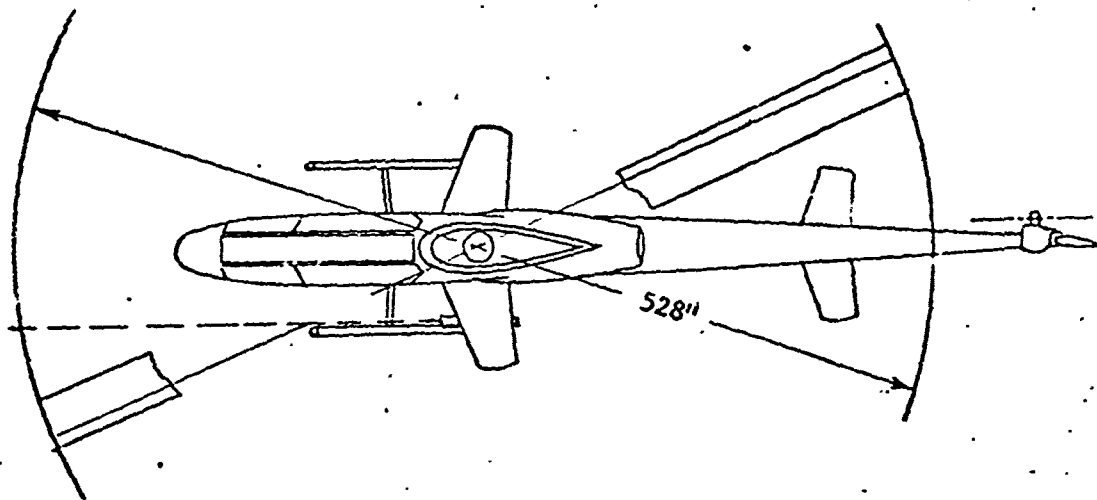
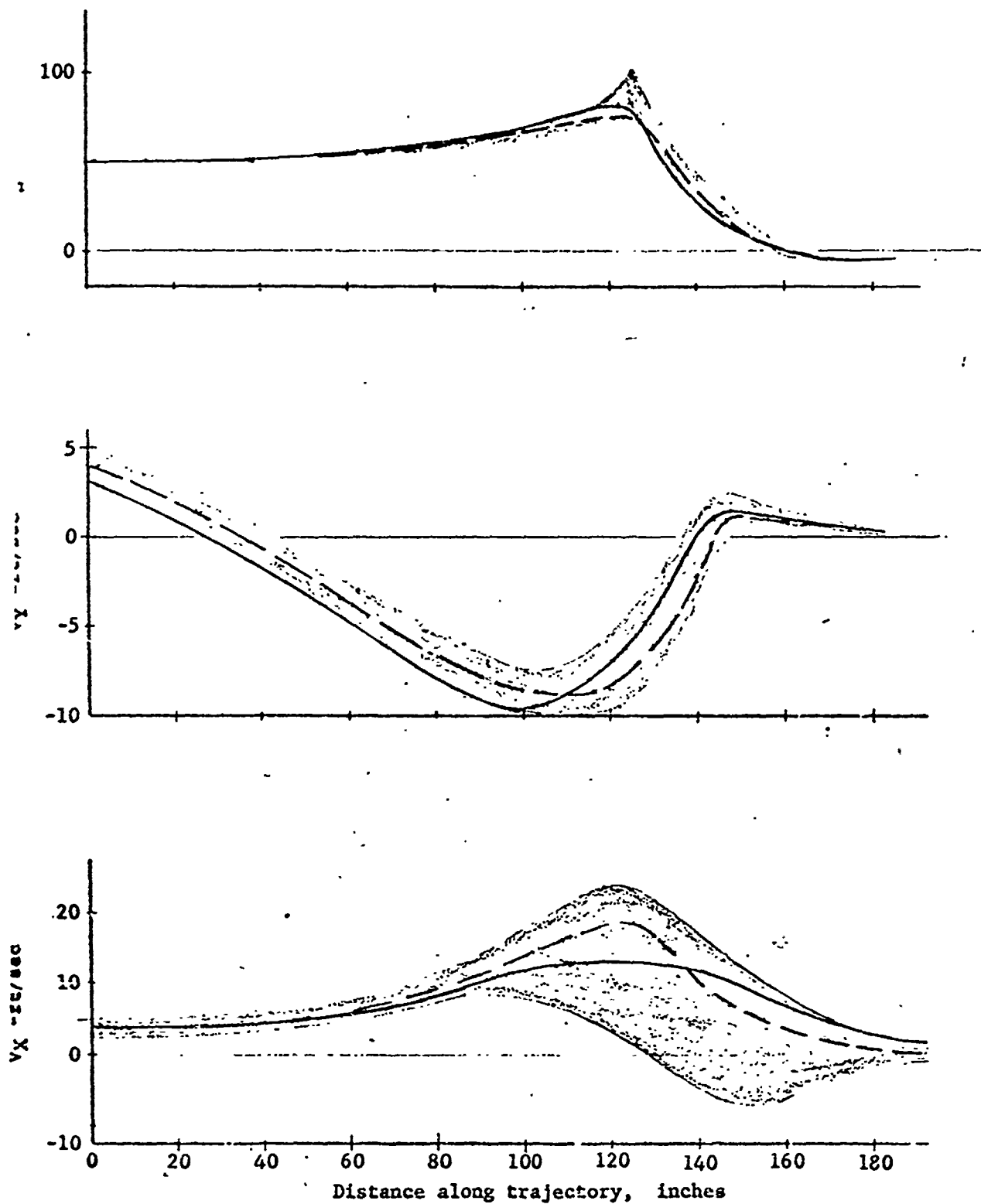Figure 10. AH-1G aircraft showing typical 2.75" rocket flight path.

528"

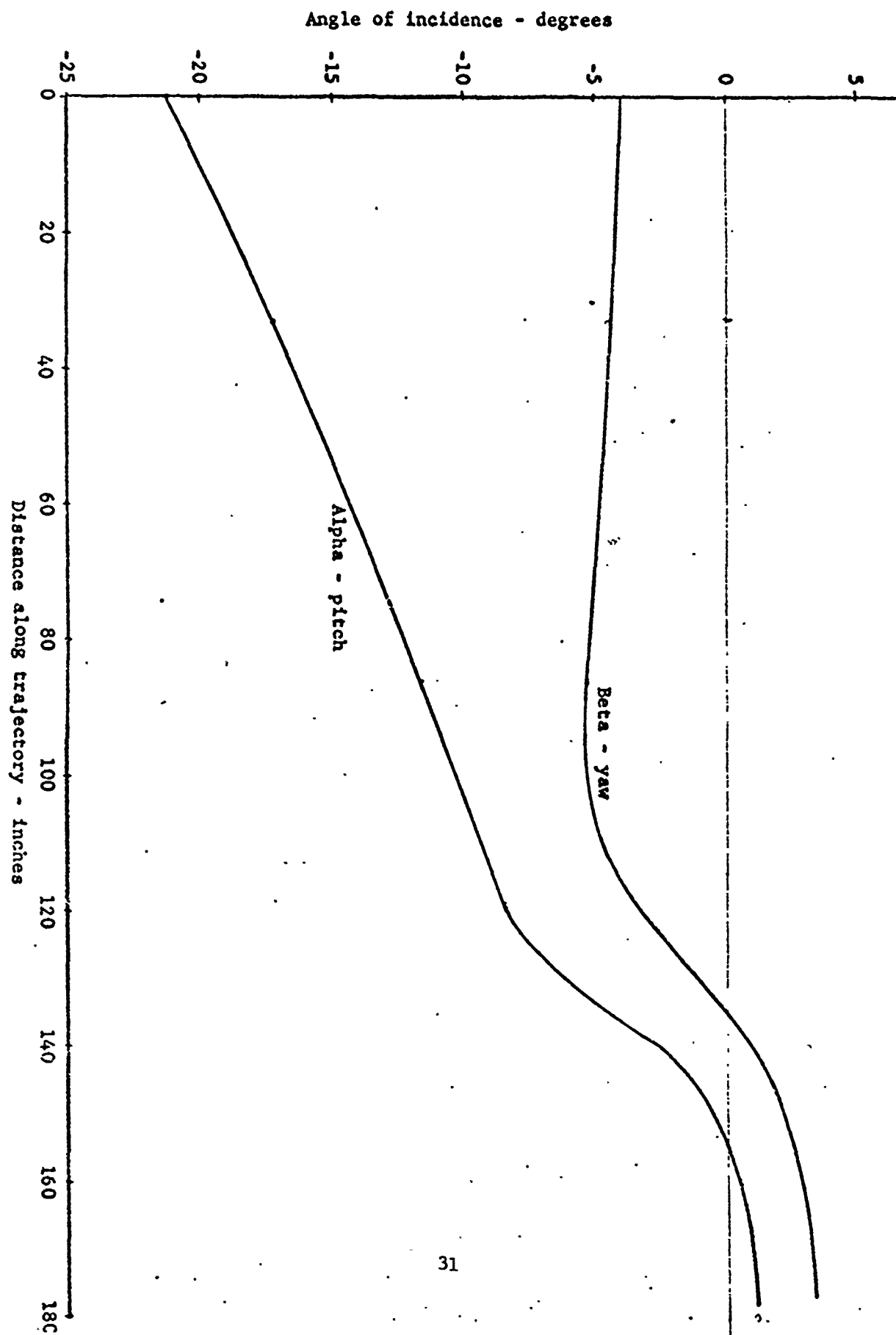Figure 11. Downwash induced velocity components along a typical 2.75"
rocket flight path.

Figure 12. Typical incidence angle history of 2.75" rocket immersed in helicopter downwash.

Angle of incidence - degrees

Distance along trajectory - inches

Alpha - pitch

Beta - yaw

31

SOME PRACTICAL ASPECTS OF ROTOR WAKE
EFFECTS ON ROCKET ACCURACY

H. ANDREW MORSE
US ARMY AIR MOBILITY R&D LABORATORY
MOFFETT FIELD, CALIF

ABSTRACT

Helicopter rocket weapons, such as the 2.75 Inch Rocket, possess a large stand-off capability and have a tremendous advantage in low round cost over guided missiles. To maximize the cost effectiveness of these weapons, emphasis should be placed on improving accuracy with minimum increase in complexity. At low forward speeds the launched rocket must pass through the rotor wake for short distances immediately after launch. This distance decreases as forward speed increases until the rotor wake passes behind the rocket launcher at velocities of approximately 30 kts. Effects of wake unsteady flow, and velocity gradients of the rotor wake free stream boundary are considered in a practical sense as to their influence upon rocket trajectory. Basic considerations of automatic fire control systems and their potential for improved cost effective delivery of helicopter launched rocket systems are considered.

Some Practical Aspects of Rotor Wake Effects of Rocket Accuracy

H. Andrew Morse
U.S. Army Air Mobility R&D Laboratory
Ames Directorate
Moffett Field, CA 94035

INTRODUCTION

Helicopter rocket weapons, such as the 2.75" rocket, possess a large stand-off capability and have a tremendous advantage in low round cost over guided missiles. Our overall objective, therefore, must be to damage or destroy targets by use of helicopter launched weapons—with a minimum loss of men or equipment—and it is very important that we do this at minimum complexity which will minimize cost. Consider the tradeoffs available. The rocket has advantages of low round cost and is jam proof. The primary disadvantage being the accuracy with which the rocket can be placed on targets. On the other end of the spectrum, the missile has advantages of high accuracy and disadvantages of high round cost and susceptibility to countermeasures.

To define the problem at hand more accurately (see Fig. 3) we would like to improve the accuracy while retaining the cost advantages. To review those items which determine the trajectory of a rocket fired from a helicopter, it is convenient to break the problem into two parts (see Fig. 4). The firing platform must be positioned in space and aimed accurately. This position must be maintained until the rocket has passed from the influence of the launcher. In multiple firing the launcher's special position must be maintained until the last rocket has passed from the influence of the launcher. Once the rocket leaves the influence of the launcher, its flight

path is then determined by the gravitational effects--which are constant and predictable--and the aerodynamic effects and another very important parameter which I neglected to include on this figure, the thrust and duration of thrust of the rocket.

In considering the stability of the firing platform, the type of rotor system is very important. With articulated or teetering rotors, the helicopter hangs from what amounts to a universal joint. Yaw control inputs result in a direct force applied at the aft end of the fuselage structure; and with most configurations, they are only second-order effects of yaw control inputs on roll attitude and negligible effects on the pitch attitude. Pitch and roll inputs are accomplished by applying forces above the CG at the rotor hub position. This application of force results in translations and the net effect is a strong coupling in pitch, roll and yaw. On the other hand, hingeless rotors have the capability of applying forces and moments at the rotor hub. With a hingeless rotor, the pilot has higher control forces; and the controls are more directly applied to the launcher attitude position. Helicopter automatic stabilization would therefore be more effective in stabilizing the launcher attitude when utilized on a helicopter with a hingeless rotor (see Fig. 5).

The most direct, but also most costly method, would be to independently stabilize the launcher system. Considering the influences of the trajectory, (see Fig. 6) the trajectory from launch to burnout is highly influenced by aerodynamic effects. This sensitivity is maximum at the time the rocket leaves the launch tube and decreases, because of increased velocity, to the point of burnout. A rocket with high directional static stability tends to weather-vane into the relative wind. With high accelerations along the longitudinal

34

axis, the rocket can experience large changes in effective launch angle. When the rocket's velocity becomes large relative to the cross wind, rockets with high static stability will experience only very small angle changes. The trajectory from burnout to impact has a much lower sensitivity to cross winds, and it is highly desirable that the rocket have a high static stability. During this phase, the rocket continues under its own momentum; and the primary aerodynamic effect of cross winds is to create a drag effect normal to the flight path. In this situation, it is highly desirable that the rocket have high static stability so that it will weathervane into the relative wind thus minimizing drag.

Considering the possibility of minimizing or correcting for the aerodynamic effects, it is convenient to break the trajectory into two parts. One where the rocket is in the influence of the rotor wake; and two, where the rocket is under the influence of surface winds. During this second part of the trajectory, the rocket has relatively high forward speeds in comparison to expected wind velocities. It is difficult, if not impossible, to correct for the unsteady components of surface winds. However, steady wind velocities could be measured prior to launch and corrections made by the fire control system based on the assumptions that the wind velocity and magnitude would remain constant during the time the rocket is in flight (see Fig. 7).

Systems which measure the wind velocity must be free from rotor downwash effects. There are two known concepts with this capability. The LORAS system, developed by Cornell, has been shown to provide a good measure of the wind velocity and direction which is relatively independent of the flight condition of the helicopter. Another concept which should

35

provide even better measurements was developed by the National Research Council in Canada, but is not commercially available. This system measures the tip speed as a function of time and the rotor azmuth position. The difference between the advancing blade tip speed and the retreating blade tip speed is twice the wind velocity while the phase relationship between the maximum velocity and a known rotor position determines the wind direction. When the rocket is launched from helicopter forward speeds of approximately 30 knots or less the rocket must pass through some of the rotor downwash fields during the intial portion of its trajectory. The 2.75" rocket leaves the launch tube with relatively low velocity; it has a high acceleration and a large static directional stability. While the rotor downwash has reasonably large steady-state values, high velocity gradients, and high unsteady velocity components.

If we consider the hover situation, which is a worse case, the 2.75" rocket passes through the rotor downwash for a distance of four or five times its own length. The steady-state downwash goes from very low values increasing to about 70 ft a second for the UH-1 or AH-1 type helicopters. Then, in a few inches changes to an upwash of 10 to 20 ft a second. While the 2.75" rocket passes through this wake in the time of a few tenths of a second, the angle of attack on the stabilizing fins reaches values in excess of 20 degrees. Steady-state aerodynamics cannot predict the forces and moments applied to the rocket during this time interval. The unsteady downwash components result primarily from tip vortices shed from rotor blades. These strong tip vortices induce

36

large local velocities whose magnitude increase according to the square of the distance from the core, build up to a maximum, change signs across the core, and then reduce again according to the square of the distance from the core. This spatial distribution of the unsteady velocity, then, is small compared to the length of the rocket. If we assume that the primary influence of the vortex has a spatial resolution of approximately two rocket fin lengths and that the rocket is traveling at a mean velocity of approximately 200 ft a second, then the fin will experience a decrease in angle-of-attack through stall, then a rapid change to a positive stall angle, and then return again to low values, all in the period of approximately 1/500 of a second. Unsteady aerodynamics are required if calculations of loads are to be attempted. In a practical sense, these loads applied for such short periods of time cannot cause significant changes in rocket attitude. The net result is the creation of vibratory loads due to the unsteady downwash components. Considering the complexity of predicting the rotor downwash (see Fig. 8) a reasonable approximation for steady downwash can be obtained with a relatively few input parameters. The steady downwash can be predicted with reasonable accuracy if the weight, airspeed, and density altitude are known. Knowing the tip path plane angle, in addition, would improve the capability of predicting the downwash freestream boundary. To make a reasonable prediction of the unsteady components or rotor downwash, many additional inputs will be required. Pilot control inputs, wind velocity and direction, rotor azimuth position, and ground effect can all have pronounced effects on the time dependent rotor wake velocity.

To give a better feel for the cause and magnitudes of the unsteady

37

downwash, some laser velocimeter measurements on a model rotor will be
presented. Figure 9 shows the laser velocimeter system. An ARGON laser
is used. The beam is split into the two most powerful colors--blue and
green. Each of these beams is split into two additional beams which are
then focused at the point of measurement in the wake of the model rotor
(see Fig. 10). The laser velocimeter provides high spatial resolution
and time dependent measurements. Data obtained from these experiments,
(see Fig. 11) show the time averaged velocity (the square symbols) and
the instantaneous velocity (round symbols). In the streamwise direction,
the time averaged instantaneous velocities are in reasonably good agree-
ment. In the downwash direction, the instantaneous velocities reach
values several orders of magnitude greater than the time averaged
velocity. These measurements were made relatively close to the plane
of the rotor, but there would be little decay in peak velocities by
the time the wake moved down to intersect the trajectory of the rocket. As
the rotor blade makes one revolution, it experiences large angle-of-attack
changes; and under highly loaded conditions, dynamic stall occurs on the
retreating side.

Figure 12 shows a 4 ft chord oscillating airfoil that was tested in
the Ames Directorate 7x10 ft wind tunnel. The flow conditions experienced
by the two-dimensional oscillating airfoil are very similar to the flow
conditions experienced by the rotor blade. The large chord provides the
capability of testing at high Reynolds numbers, and also provides relatively
thick boundary layers where detailed measurements can be made. A short
movie film shows the time variation of detailed pressure measurements on

38

a rotor blade; some flow visualization of oscillating airfoils showing
the nature of dynamic stall and the shedding of the bound vortex; some
tip vortices flow visualization; and finally, some flow visualization
movies of an AH-1G model tested in ground effect. In the later sequences
of the AH-1G model, the ground horseshoe vortex and details of the wake
free-stream interaction are visualized both with smoke and hydrogen bubbles.

In summary Fig. 13 indicates what must be done to obtain accuracy
improvements for low-speed launch of the 2.75" rocket. The items are
listed in what is felt to be the proper order of importance for improving
accuracy. A stabilized launcher appears to be necessary to provide
accuracy of multiple firing when launched from the AH-1G helicopter at
low forward speeds. When a 2.75" rocket is launched, a large reaction
force is applied to the launcher; and as stated previously on this
helicopter with a teetering rotor, the launcher and fuselage swing
back. In order to correct for the pitch, the pilot must put in aft cyclic
which puts an aft force on the top of the mast. With both forces in the aft
direction, the helicopter tends to accelerate in the rearward direction.
When forward speed is reduced, or rearward velocities initiated, power
required increases. In hover, when the pilot is using a ground point for
reference, the pilot tends to pull in collective pitch to maintain this
same relative position of the reference point. All of these forces and
moments, plus the couplings, produce a very unstable firing platform. To
counteract this problem, the rocket's static directional stability can be
reduced during the first few 1/10 of seconds of flight. This is high on
the list because of its low cost and high probability of success.

39

We can conclude that the forces and moments, both steady and unsteady, are destabilizing while the rocket is   the rotor wake. By reducing the static directional stability, the f' .   ath should be more repeatable and experience much less perturbation. Ground wind velocity and direction can be measured prior to launch a: d the information fed to the fire control system.

Lastly, a simple representation of downwash can be obtained and fed to the fire control system. Since the mean dynamic pressure in the rotor wake is determined only by the rotor disk loading and the advance ratio, a relatively simple correction for the steady downwash could be provided the fire control system for aiming corrections. Techniques for measuring the unsteady components of the rotor downwash, and providing that information to the fire control system, would be complex, costly, and totally unwarranted.

OBJECTIVE:

EV ...
...R
ENGAGED
WEAPONS

DAMAGE
OR
DESTROY
TARGETS

WITH:

- MINIMUM LOSS OF MEN
  AND/OR EQUIPMENT

- FOR MINIMUM COST

Figure 1

TRADE OFF

	ROCKET	MISSILE
ADVANTAGES		
	• LOW ROUND COST	• HIGH ACCURACY
	• JAM PROOF	
DISADVANTAGES		
	• LOW ACCURACY	• HIGH ROUND COST
		• COUNTERMEASURES

Figure 2

42

PROBLEM DEFINITION
FOR 2.75 IN. ROCKET

- IMPROVE ACCURACY

- RETAIN COST ADVANTAGE

Figure 3

CONTROL OF ACCURACY

FIRING PLATFORM

- AIMING ACCURACY
- MULTIPLE FIRE STABILITY

FLIGHT PATH DETERMINATION

- GRAVITATIONAL EFFECT
- AERODYNAMIC EFFECTS

Figure 4

44

FIRING PLATFORM STABILITY

ARTICULATED & TEETERING ROTORS

HINGELESS ROTORS

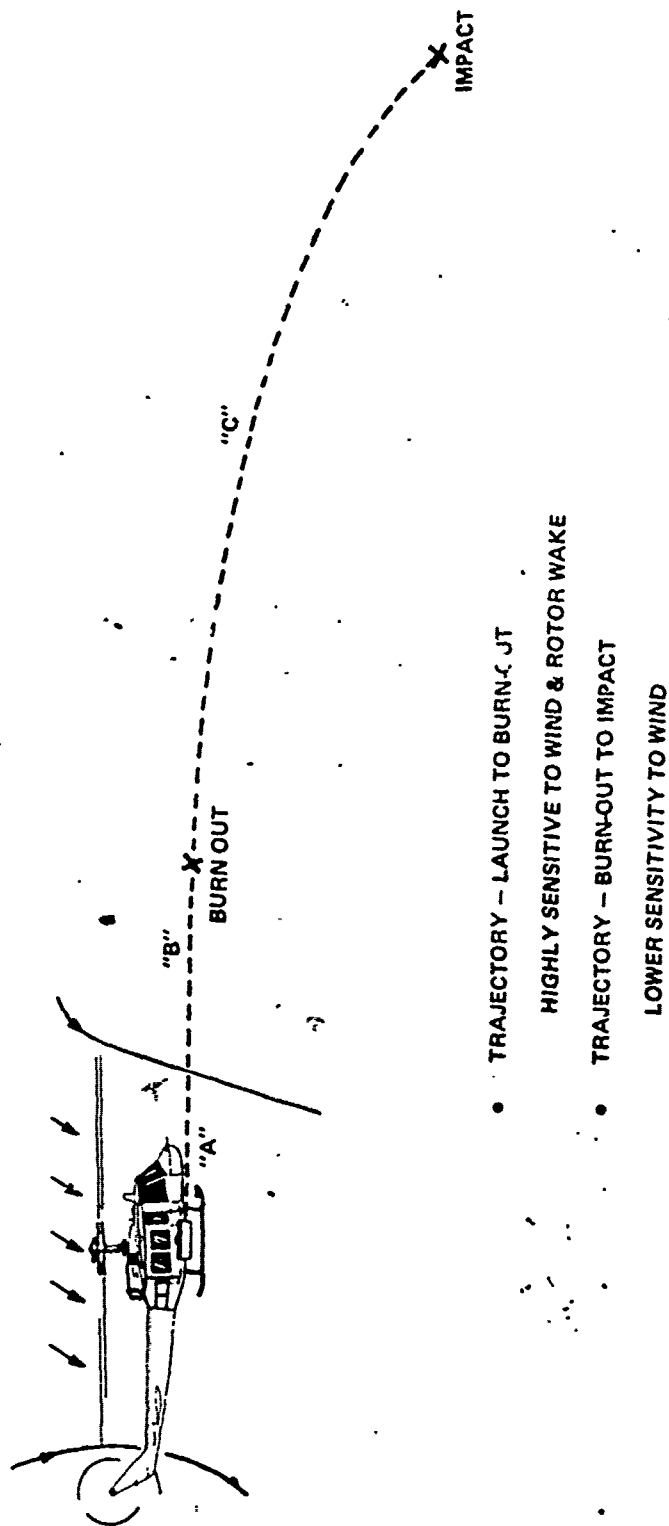## INDEPENDENT LAUNCHER STABILIZATION

Figure 5

45

FLIGHT PATH DETERMINATION

"B"

"A"

BURN OUT

"C"

IMPACT

- TRAJECTORY – LAUNCH TO BURN-OUT
  HIGHLY SENSITIVE TO WIND & ROTOR WAKE

- TRAJECTORY – BURN-OUT TO IMPACT
  LOWER SENSITIVITY TO WIND

Figure 6

46

WIND PREDICTABILITY

MEASURE WIND VELOCITY & DIRECTION

- LORAS — CORNELL

- $V_T f(t)$ — NRC

Figure 7

47

DOWNWASH PREDICTABILITY

STEADY APPROXIMATION

- WEIGHT
- AIR SPEED
- DENSITY ALTITUDE
- TIP PATH PLANE ANGLE

UNSTEADY COMPONENT

- CONTROL INPUTS
- WIND VELOCITY AND DIRECTION
- ROTOR AZIMUTH POSITION
- BLADE STRUCTURAL RESPONSE
- GROUND EFFECT
- FUSELAGE ACCELERATIONS
- NONLINEARITIES AND COUPLINGS
- ETC.

Figure 3

Figure 9

Figure 10
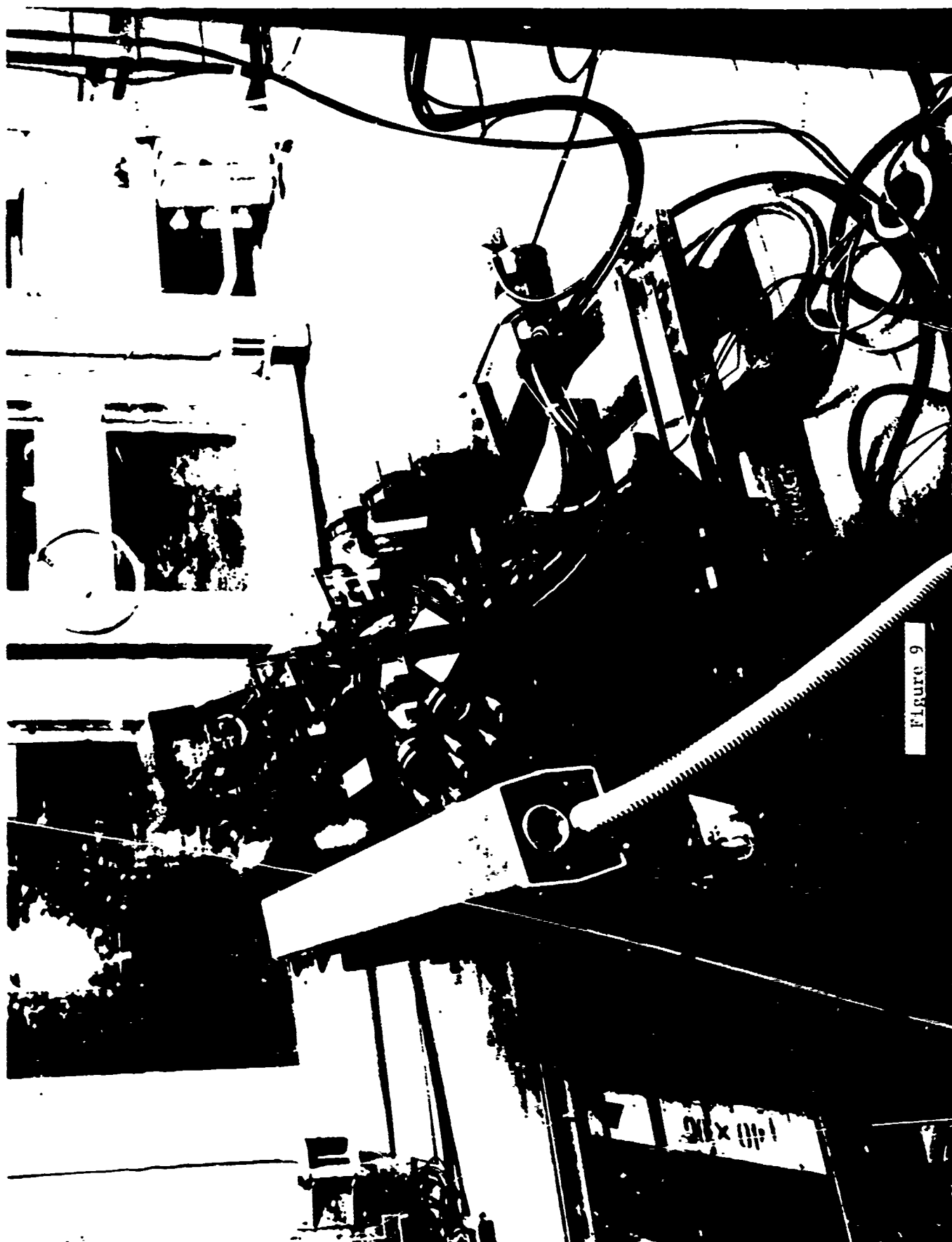
50

LASER MEASUREMENTS OF ROTOR DOWNWASH

$V_\infty / \Omega R = 0.18$

Figure 11
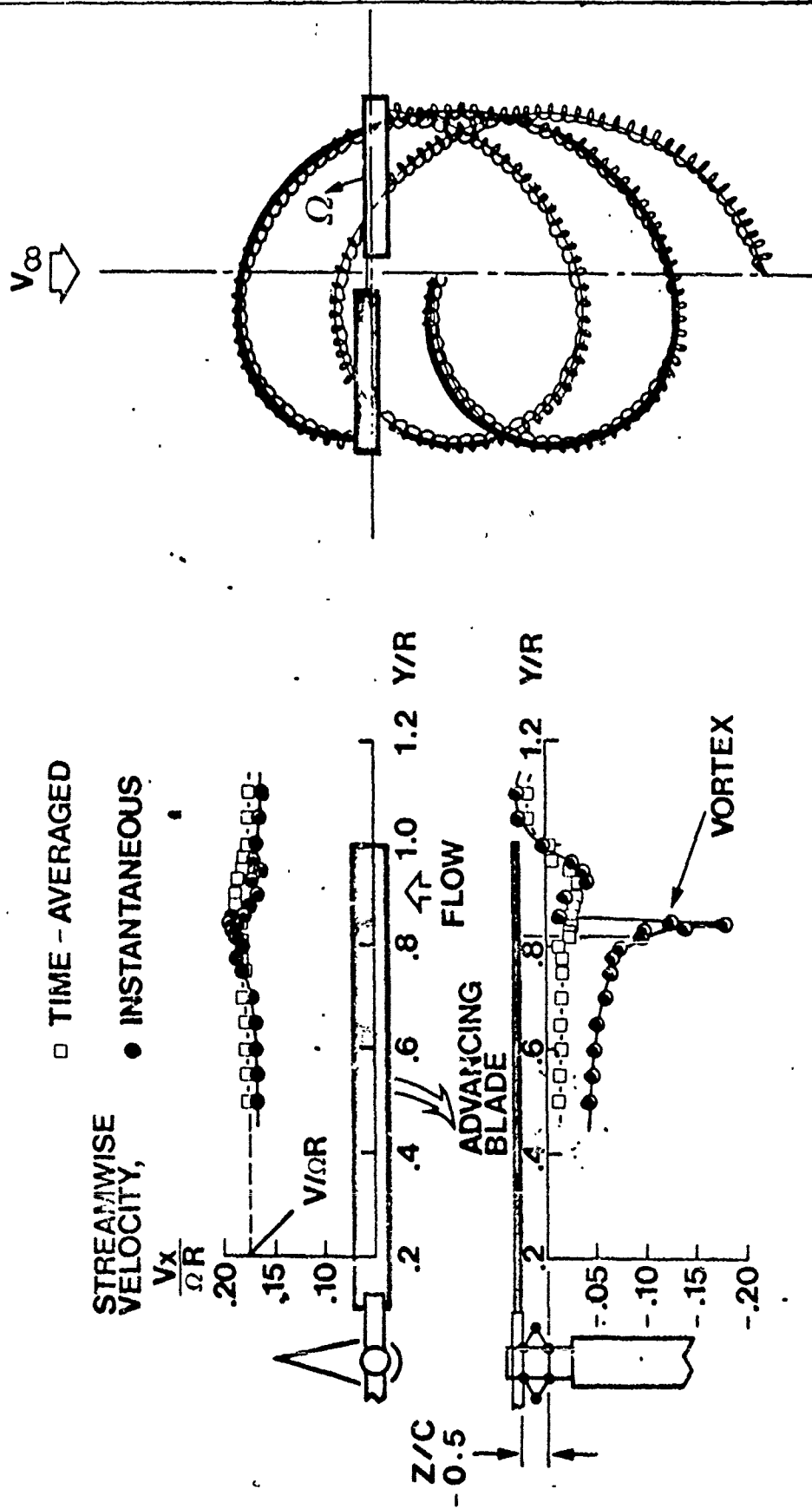
Figure 12

ACCURACY IMPROVEMENTS FOR LOW SPEED LAUNCH OF 2.75 IN. ROCKET

1. STABILIZE LAUNCHER

2. REDUCE ROCKET STABILITY

3. MEASURE WIND VELOCITY & DIRECTION

4. SIMPLE MOMENTUM DOWNWASH

Figure 13

DOWNWASH EFFECTS ON ROCKET TRAJECTORIES

DICK FIGUERAS and ROBERT BAUMAN
ELECTRONICS & SPACE DIVISION
EMERSON ELECTRIC CO.
ST. LOUIS, MISSOURI

ABSTRACT

In support of a joint Emerson/Boeing Vertol proposal effort, Emerson
has conducted downwash modeling studies and rocket trajectory simulations
to determine the effects of the helicopter downwash field on rocket
delivery accuracy.

The following conditions were investigated:

    Aircraft Gross Weight - 14000 lbs
    Flight speed - hover
    Downwash model: Triangular and constant inflow
                     with both steady and pulsating
                     vertical flow components
    Rockets: 105mm ANSSR (Aaerodynamically Neutral Spin
              Stabilized Rocket) and 2.75 In FFAR (MK40,
              M151 whd)

Results show that downwash effect on the ANSSR trajectory results in
a maximum angular error of only about 2 mils and thus, from a practical
standpoint, can be ignored with regard to fire control compensation.
Downwash effects on the 2.75 FFAR however, are significant, including
bias components (i.e., variations in MPI) of 35 to 64 mils for tri-
angular and constant inflow fields respectively.

Furthermore, the effects of launcher in phase of out-of-phase with
rotor blade passage can contribute 2-4 mils random (precision) error
components to the 2.75 FFAR trajectory under the assumed ± 15 percent
variation in downwash velocity amplitude.

INTRODUCTION AND SUMMARY

This Emerson Electric Co. report defines helicopter downwash effects on the trajectory characteristics of airborne tactical rocketry. The report documents results of the initial phase of an investigation being conducted in cooperation with the Boeing Vertol Company. The joint Emerson/Vertol program objective is improvement of helicopter/rocket system delivery accuracy, specifically during hover deployments. Fur_her investigation areas are also identified.

Since 1962 Emerson Electric has participated in the design and development of helicopter-borne armament systems. Related experience includes exploratory development of a unique, free flight rocket concept which is specifically designed for accurate payload delivery within helicopter launch environments, (i.e., rocket is insensitive to angle-of-attack and launch platform angular rate disturbances).

This report identifies the effects of rotor downwash on rocket flight characteristics and recommends topics requiring further investigation with regard to improvement of system accuracy potential for helicopter/hover deployments of free flight rockets.

Based on study results, the most direct approach to minimizing system dispersion during hover deployments is the Aerodynamically Neutral Spin Stabilized Rocket (ANSSR) configuration. During passage through a typical downwash field the ANSSR configuration accrues trajectory errors which are only five percent of those accrued by the 2.75 in. FFAR. For example, deployment from a typical downwash field imparts a 1.7 mil trajectory error to ANSSR as opposed to 35.5 mils for a 2.75 in. FFAR.

Improved finned rocket system accuracy during hover deployments requires more accurately identified downwash environments and effects on rocket trajectories to determine the limiting accuracy potential and fire control requirements. Downwash pulsations themselves may introduce significant errors (i.e., 4 mils for the 2.75 in. FFAR) and may not be correctable, even with fire control compensation.

DOWNWASH FIELD

The rotor downwash field consists of a cylindrical region of downwash directed air flow which emanates from an overhead, multi-bladed rotor. The vertical air flow velocity is assumed invariant with vertical distance below the rotor plane, but, within any horizontal plane, the downwash velocities varies with the radial distance from the rotor center and the position relative to the individual rotor blades.

Downwash velocity magnitude and spatial distribution data were obtained from the Boeing/Vertol Company and are representative of a typical, single rotor, utility helicopter with a gross weight of approximately 14000 pounds and rotor diameter of 50 feet. Typical downwash velocity profiles are shown in Figure 1 for:

A constant inflow rotor (i.e., blade twist angle varies from minimum at tip to a maximum value at the rotor center)

A triangular distribution wherein the blade twist angle is constant along the blade length

Figures 2 and 3 show the physical profiles of rotor wake for forward and sideward flight respectively.

These data represent assumed steady state velocities. That is, the downwash velocity magnitude at any location within the rotor wake is assumed invariant with individual blade position.

Experimental data [1] indicates that the magnitude of the vertical velocity component does in fact depend upon blade position and may be represented as a sinueoidal distribution with the peak value occurring when the blade is directly overhead. The velocity history at any specific location within a horizontal plane beneath the rotor is represented as a periodic function with an average value proportional to helicopter gross weight and the radial distance from the rotor center (i.e., data of Figure 1). The minimum and maximum velocity excursions respectively occur when the point of interest is exactly between adjacent blades or directly beneath any single blade. Downwash velocity dependence upon blade position can be defined as a time dependent through the relationship with rotor rotational speed (assumed constant).

Relating downwash velocity to time (t) is essential in determining the influence on a projectile launched from within the velocity field. With time as the independent variable, it is possible to exactly compare the trajectory characteristics of arbitrary projectile configurations which traverse the downwash field. The downwash velocity equation at any arbitrary position within the field is given in Figure 4.

The coordinate system associated with downwash velocity simulation is defined in Figure 5 (i.e., equations (1) and (2)). Downwash velocity direction is defined as normal to the range-deflection plane (shown in Figure 5) as is positive in the downward direction.

---

1 Heyson, H., Measurements of the Time-Averaged and Instantaneous Induced Velocities in the Wake of a Helicopter Rotor Hovering at High Tip Speeds, NASA TN D-393, July 1960.

56

Simulation of downwash velocity as defined by equations (1) and (2) is accomplished within the existing Emerson six degree of freedom computerized trajectory simulator. Trajectories of both the ANSSR III and 2.75 in. FFAR were simulated within various velocity fields. Simulated downwash velocities encountered by the rockets during passage through the rotor wake are shown in Figures 6 through 9. The data in each figure corresponds to a two bladed rotor, operating at a 300 rpm rotation rate. Three distinct conditions of downwash dynamic behavior are presented. These include:

Steady state (No periodicity)

$\pm$ 15 percent amplitude variation with rocket launch position coincident with overhead passage of rotor blade, and

$\pm$ 15 percent amplitude variation with rocket launch position ninety degrees ahead of the advancing blade (i.e., midway between blades)

The rocket is launched along the "x" axis (Figure 5) from an initial position which is one foot from the rotor center. Figures 6 and 7 refer to the 105mm ANSSR III configuration within constant and triangular velocity fields respectively. Figures 8 and 9 refer to the 2.75 in. FFAR within the same downwash fields. As indicated on these plots, minor differences in rocket acceleration (and resulting differences in velocity and displacement histories) cause each rocket to encounter a slightly different downwash velocity environment as it passes through the field. The response of the rocket trajectory to the downwash induced angle of attack disturbances are discussed later in this report.

ROCKET TRAJECTORY SIMULATIONS

Rocket trajectories were computated by using a six degree of freedom, computerized math model. The model computes rigid body motion of arbitrary projectile configurations with respect to a flat earth and uses the 1959 ARDC standard atmosphere simulation. The computer model is currently programmed for use on either the IBM 360/195 or CDC 6600 high speed digital computers. Program formulation was specifically selected for economical flight simulation of high spin rate projectiles.

Input data consists of projectile mass properties, propulsion characteristics, aerodynamic coefficients and launch conditions. Specified launch conditions include aircraft velocity, altitude and attitude angles in addition to rocket velocity and attitude with respect to the launch aircraft. The computer simulation also includes provisions for inputting relative velocity of the air mass (in any of three coordinate directions) with respect to the inertial reference system. This option permits inputting of a vertical air flow field of an arbitrary nature (i.e., downwash field previously discussed).

57

Simulations were conducted for two rocket configurations, namely the ANSSR III and 2.75 in. FFAR rockets. Rocket characteristics are summarized in Table 1. Detailed rocket characteristics for ANSSR were obtained from Reference 2 and from Analysis of ANSSR III experimental (flight test) date. Data for the 2.75 in. FFAR was obtained from Reference 3.

DOWNWASH EFFECTS ON ROCKET TRAJECTORIES

Time histories of rocket flight path and attitude angles during the boost phase of flight are shown in Figures 10 and 12. End-of-boost flight path angle variations (i.e., with respect to nominal or non-disturbed values) are generally accepted as reasonable approximations for normal plane impact errors. Normal plane accuracy is measured in a plane perpendicular to the rocket trajectory at impact. By this correlation, it is possible to evaluate rocket accuracy by examining the response of the end-of-boost flight path angle to any given disturbance which occurs prior to motor burnout.

Vertical flight path angle history for the 2.75 in. FFAR in the presence of a triangular downwash field and in the absence of downwash is shown in Figure 10. As indicated, the flight path angle difference between the nominal (no downwash) and disturbed trajectories is approximately two degrees (35 milliradians). If, during a hover deployment, the 2.75 in. FFAR were aimed at a specified target, and no aiming compensation were provided to account for downwash, the rocket impact (in a normal plant coordinates) would occur approximately 35 mils above the intended target. For fin stabilized rockets, trajectory errors generally occur in the same plane as the disturbing force. Therefore, no appreciable impact azimuth impact error will results from passage through a vertically directed downwash field.

Vertical and horizontal end-of-boost flight path angle histories for ANSSR III are shown in Figures 11 and 12 respectively. As indicated, passage through the triangular downwash field results in a vertical and horizontal path angle variation of 0.08 and 0.06 degrees respectively from the nominal (no downwash) condition. The total flight path angle error (magnitude) is represented by the vector (RSS) sum of the horizontal and vertical flight path angle differences respectively (i.e., approximately 0.1 degrees). This 1.8 mil error is only five percent of the 35 mil error accrued by the 2.75 in. FFAR during passage through the identical downwash field. In general, this characteristic of relative insensitivity to angle of attack disturbances represents the primary advantage of the ANSSR concept.

The end-of-boost flight path angle variations for both ANSSR and the 2.75 in. FFAR for various downwash conditions (as shown in Figures 6 through 9) are summarized in Tables 2 and 3. The trajectory error due to downwash is indicated

Reference 2. Letter from Emerson to MICOM (AMSMI-RDF), subject: ANSSR III Aerodynamic Coefficients, 16 May 1973.

Reference 3. Office of the Project Office Manager, 2.75 Inch Rocket System, 2.75 Inch Rocket/AH-1G Baseline Accuracy Test, AD524878, March 1973.

as the difference between the nominal (no downwash) and disturbed trajectories respectively. The effects of both steady state and pulsating downwash fields are shown. In regard to the ANSSR configuration, the error due to a triangular, steady state downwash is 1.77 mils. As the downwash velocity is permitted to vary by $\pm$ 15 percent about its mean value, the trajectory error is either 1.81 or 1.70 mils respectively, depending upon whether the rocket is launched in-phase or 90 degrees out-of-phase with blade passage.

The 2.75 in. FFAR, on the other hand, experiences a 35.5 mil trajectory in the presence of the steady state triangular downwash field and 37.7 or 33.8 mils error when in-phase or out-of-phase with a pulsating field ($\pm$ 15 percent amplitude).

Trajectory errors are also down for constant velocity downwash fields, both steady and pulsating. The sensitivity of both rocket configurations to the constant velocity downwash field is much greater than for the triangular distribution. This is primarily due to the increased angle of attack at launch resulting from the high downwash velocity in the launcher vicinity. The error producing mechanism depends primarily upon the tendency of the rocket to rotate (pitch or yaw) about its mass center. This rotation tendency is proportional to both the rocket static margin and the impressed angle of attack. Thus an increase in downwash velocity at launch re-enforces the rotation (weathercocking) tendency because the impressed angle of attack is amplified. During passage through the constant velocity downwash field (Figures 1, 6, and 8) the 2.75 in. FFAR experiences a 62.9 mil flight path error whereas the 105mm ANSSR configuration accrues only a 2.2 mil error. In this case, ANSSR sensitivity to downwash is only three percent of that associated with the 2.75 in. FFAR.

The rocket trajectory error due to in-phase and out-of-phase pulsations varies by only a few percent from the steady state error for triangular and constant velocity fields. This variation, which comprises approximately 0.33 mils for ANSSR and 3.98 mils for the 2.75 in. FFAR, represents a component of system dispersion which will exist even if the effect of steady sta.e triangular downwash velocity can be perfectly compensated by aiming corrections.

Although related studies were not completed within the scop. of this report analysis, it is felt that the dispersion due to differences in phasing between the rocket (at launcher) and blade passage will be proportional to the amplitude of the downwash velocity pulsations as well as the frequency. Since the limiting accuracy potential for any proposed compensation technique will be primarily determined by this effect, it is critical that an accurate definition of the downwash dynamic characteristic be obtained as part of follow-on efforts.

CONCLUSIONS/RECOMMENDATIONS

Trajectory simulation results have demonstrated that helicopter downwash can be a major source of error, especially for conventional fin stabilized rockets which are inherently sensitive to angle of attack disturbances. Design and mechanization of an accurate fire control system for use with finners will be

difficult because of the dynamic (pulsating) nature of the downwash field, the influences of aircraft geometry and deployment conditions on the downwash field, and the dependence of trajectory errors on the rocket launch position (i.e., phasing with respect to rotor blades). For this reason, it is concluded that the best approach for minimizing trajectory errors associated with downwash is that of minimizing rocket sensitivity (i.e., ANSSR) to a level such that fire control compensation is either not required or is greatly simplified.

If conventional (fin stabilized) rockets are to be accruately deployed from within the wake of a helicopter rotor, it will be necessary to define:

Rotor wake characteristics to a high degree of accuracy

A technique for sensing appropriate parameters and for computing aiming corrections.

Methods and/or mechanisms for aiming the launcher to compensate for downwash effects

Study results to date (reported herein) include estimates of only one of the several potential error sources associated with hover firings. These results indicate that even when perfect aiming compensation is provided for the average (steady state) triangular downwash velocity, the periodicity effect (i.e., rocket launching "in" or "out-of-phase" with a rotor blade) will produce trajectory errors of approximately four mils for the 2.75 in. FFAR. For aircraft gross weights of 14,000 lbr., it will be necessary to provide aiming angle (launcher elevation) corrections of two to 3.5 degrees respectively, depending upon whether the downwash velocity distr   ion is triangular or constant along the blade length.

It is recommended that the following areas be investigated as part of any future program directed at improvement of rocket delivery accuracy from helicopter/hover deployments:

More accurately define rocket aerodynamic characteristics to ensure accuracy of simulation results. Current simulations use aero data derived for low angle of attack regimes and for uniform (constant) velocity fields.

Determine limiting accuracy potential through consideration of launcher location, tactics (pair vs. ripple firings), downwash pulsations (rotor speed and number of blades), and other error sources for which aiming compensation cannot be provided.

Define downwash field velocity perturbations and resulting rocket trajectory deviations due to tip vortices, presence of fuselage and adjacent structures, variations in helicopter weight, altitude (i.e., ground effects and air density variations), atmospheric winds, helicopter attitude, and translational velocity (fore/aft and lateral).

Define a suitable sensor and accessories array to provide fire control compensation during flight conditions where rotor downwash significantly influences system delivery accuracy (i.e., from hover to forward flight speeds when rotor wake is aft of launcher face).

60

HELICOPTER AIR FLOW CONFERENCE

ROCKET CHARACTERISTICS

PARAMETER	ANSSR	2.75 IN. FFAR
GROSS WEIGHT (LBS)	52.74	20.20
WARHEAD (LBS)	25	M151 - 10
LENGTH (IN)	49.5	54.72
BURN TIME (SEC)	1.500	1.576
AVG. ACCELERATION (G'S)	32.7	34.8
LAUNCH VELOCITY (FPS)	66	109
BURNOUT VELOCITY (FPS)	1703	1891
AT 22-FOOT RANGE:		
TIME (SEC)	0.195	0.216
VELOCITY (FPS)	247	247

TABLE 1

ELECTRONICS AND SPACE DIVISION

EMERSON

HELICOPTER AIR FLOW CONFERENCE

TRAJECTORY ERROR SUMMARY - CONSTANT INFLOW

ROCKET	FLIGHT PATH ANGLE	NO DOWNWASH (NOMINAL)	DOWNWASH FIELD		
			CONSTANT-INFLOW HALF AMPLITUDE (%V)		
			0	15	15
			STEADY STATE	IN PHASE	90° OUT OF PHASE
105-MM ANSSR	VERT. - ∂(DEG)	5.162	5.230	5.230	5.227
	HORIZ. - σ(DEG)	-0.533	-0.433	-0.427	-0.437
	DIFFERENCE (MILS)*		2.15	2.24	2.07
2.75 IN. FFAR	VERT. - ∂(DEG)	3.415	6.951	7.035	6.905
	HORIZ. - σ(DEG)	-0.014	0.054	0.054	0.052
	DIFFERENCE (MILS)*		62.87	64.37	62.06

* DIFFERENCE $= \left\{ (\partial_{DWN} - \partial_{NOM})^2 + (\sigma_{DWN} - \sigma_{NOM})^2 \right\}^{\frac{1}{2}}$

TABLE 2

HELICOPTER AIR FLOW CONFERENCE

TRAJECTORY ERROR SUMMARY · TRIANGULAR

ROCKET	FLIGHT PATH ANGLE	NO DOWNWASH (NOMINAL)	DOWNWASH FIELD TRIANGULAR HALF AMPLITUDE (%V)		
			0 STEADY STATE	15 IN PHASE	15 90° OUT OF PHASE
105-MM ANSSR	VERT.· ∂(DEG)	6.162	5.236	5.230	5.237
	HORIZ.· σ(DEG)	-0.533	-0.466	-0.457	-0.474
	DIFFERENCE (MILS)*		1.77	1.88	1.70
2.75 IN. FFAR	VERT.· ∂(DEG)	3.415	5.412	5.538	5.314
	HORIZ.· σ(DEG)	-0.014	0.022	0.025	0.020
	DIFFERENCE (MILS)*		35.51	37.75	33.77

* DIFFERENCE $= \left\{ (\partial_{DWN} - \partial_{NOM})^2 + (\sigma_{DWN} - \sigma_{NOM})^2 \right\}^{\frac{1}{2}}$

AUG 75

TABLE 3

ELECTRONICS AND SPACE DIVISION

EMERSON

63

HELICOPTER AIR FLOW CONFERENCE

STEADY STATE DOWNWASH VELOCITY - HOVER

HELICOPTED GROSS WEIGHT — 14,000 LBS
HOVERING OUT OF GROUND EFFECT
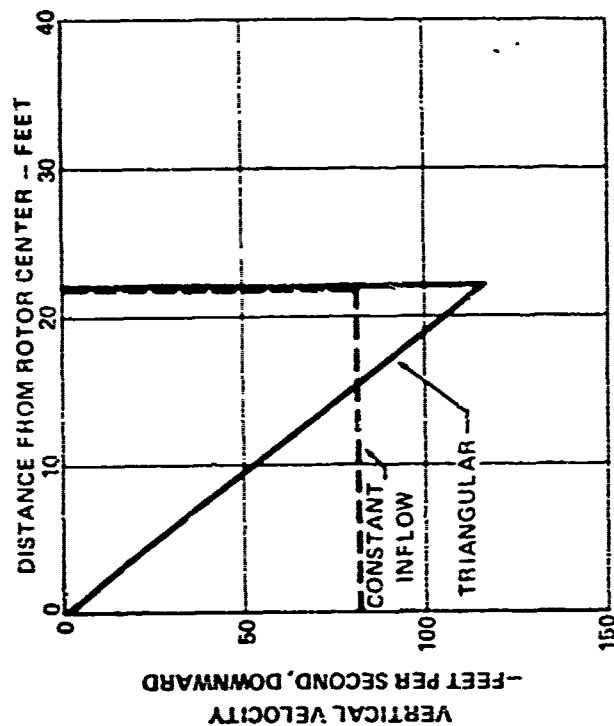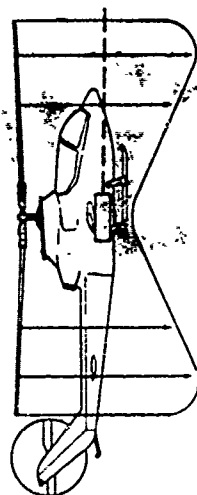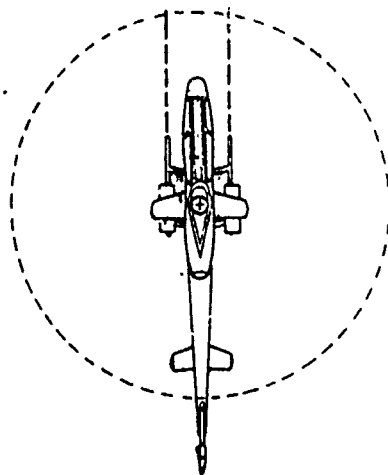ROTOR DIAMETER — 50 FT
ROTOR SPEED — 300 RPM

FIGURE 1

HELICOPTER AIR FLOW CONFERENCE

ROTOR WAKE - FOREWARD FLIGHT
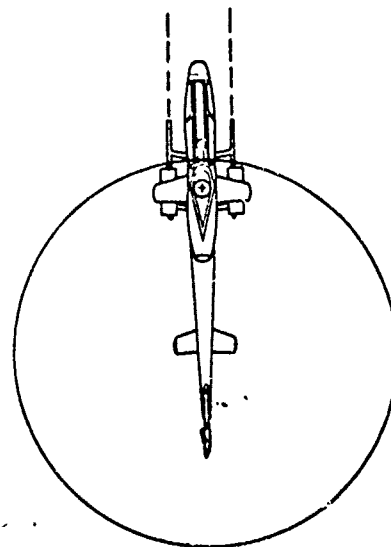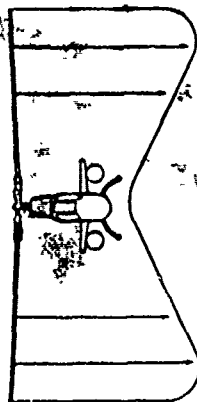
HOVER
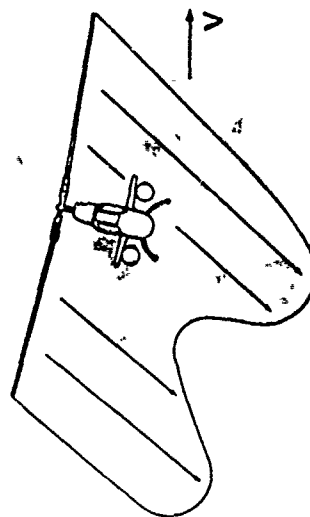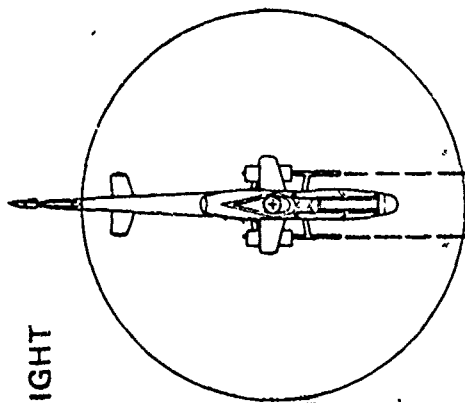
FWD FLIGHT

FIGURE 2

ELECTRONICS AND SPACE DIVISION

65

HELICOPTER AIR FLOW CONFERENCE

ROTOR WAKE - SIDEWARD FLIGHT

HOVER

SIDEWARD FLIGHT

FIGURE 3

66

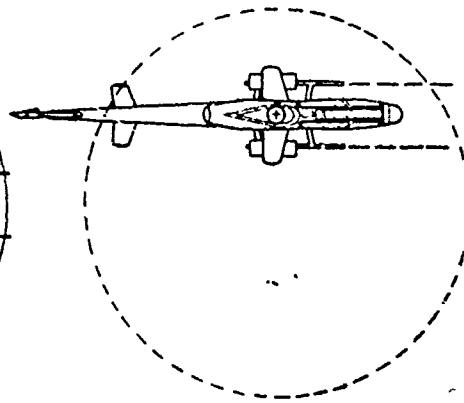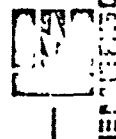# HELICOPTER AIR FLOW CONFERENCE

AUG 75

DOWNWASH VELOCITY EQUATION

$$V_z(r, \psi) = V_z(r)[1 + K\cos(n\psi)]$$

where: $V_z(r, \psi)$ = magnitude of instantaneous vertical velocity

$V_z(r)$ = magnitude of average vertical velocity as determined by radial distance from rotor center.

K = maximum downwash velocity excursion about average value (half amplitude)

ψ = azimuth coordinate of projectile relative to advancing blade

n = number of blades

$$\psi(t) = [\alpha_{BO} - \Omega_B t] - \tan^{-1}(Y_M / X_M)$$

where: $\psi(t)$

α_{BO} = azimuth coordinate projectile relative to blade

= initial angular position of arbitrary advancing blade

Ω_B = rotor rotation rate

t = time from rocket ignition

X_M, Y_M = rocket range and deflection coordinates

FIGURE 4

HELICOPTER AIR FLOW CONFERENCE

ROTOR BLADE/ROCKET COORDINATES
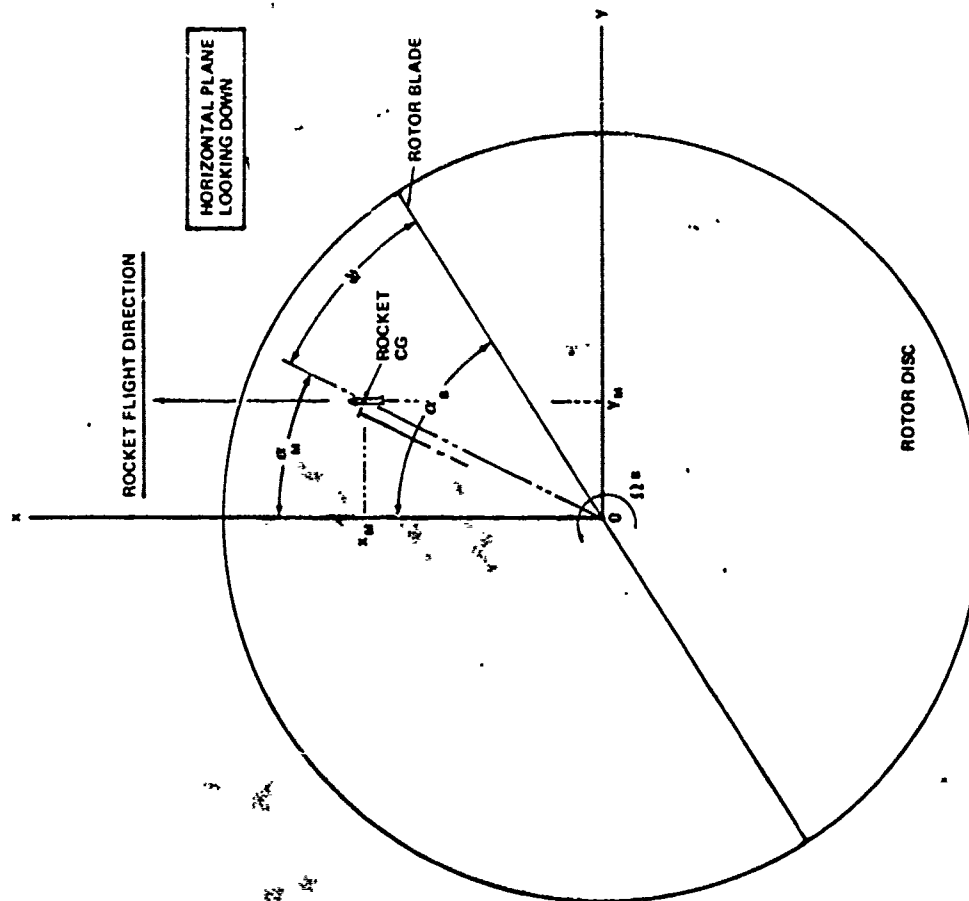
FIGURE 5

ELECTRONICS AND SPACE DIVISION
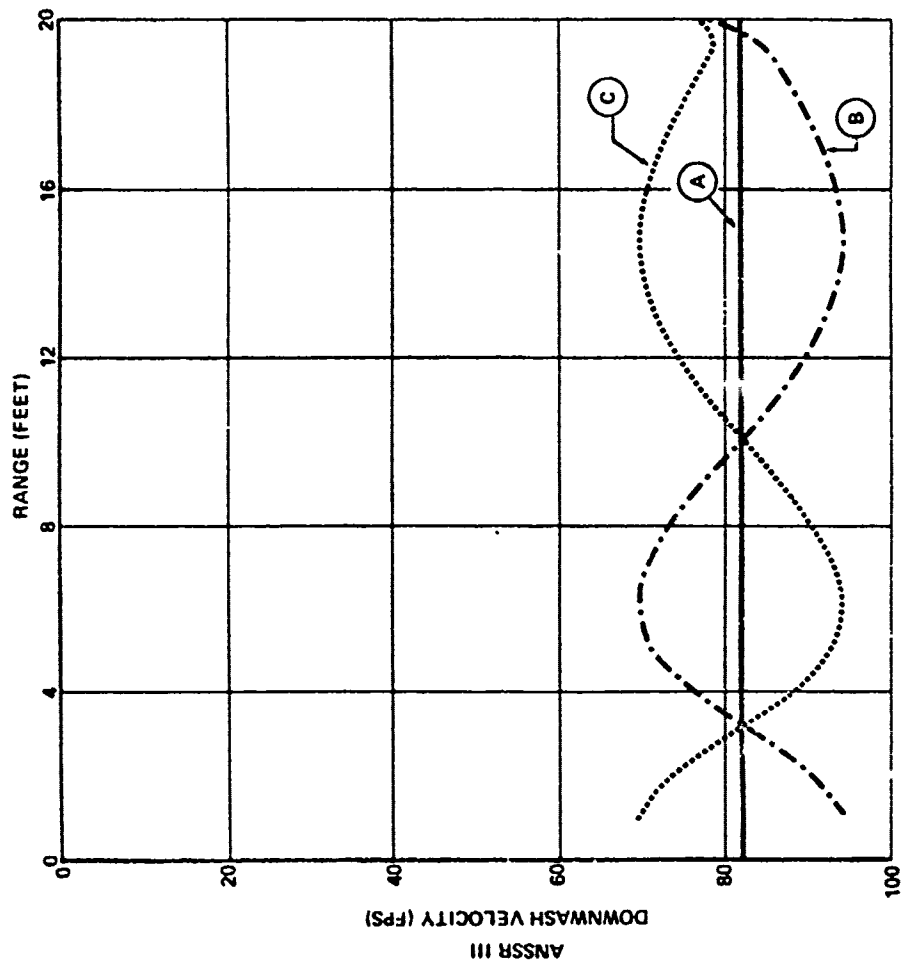
EMERSON

68

FIGURE 6   DOWNWASH VELOCITY-CONSTANT INFLOW-ANSSR ROCKET

SYMBOL	HALF AMPL-TUDE (% VEL)	PHASE AT LAUNCH (ROCKET W/R BLADE)
A	0	NOT APPLICABLE
B	15	0 DEG
C	15 ·	90 DEG

ROTOR SPEED = 300RPM
NO OF BLADES 2
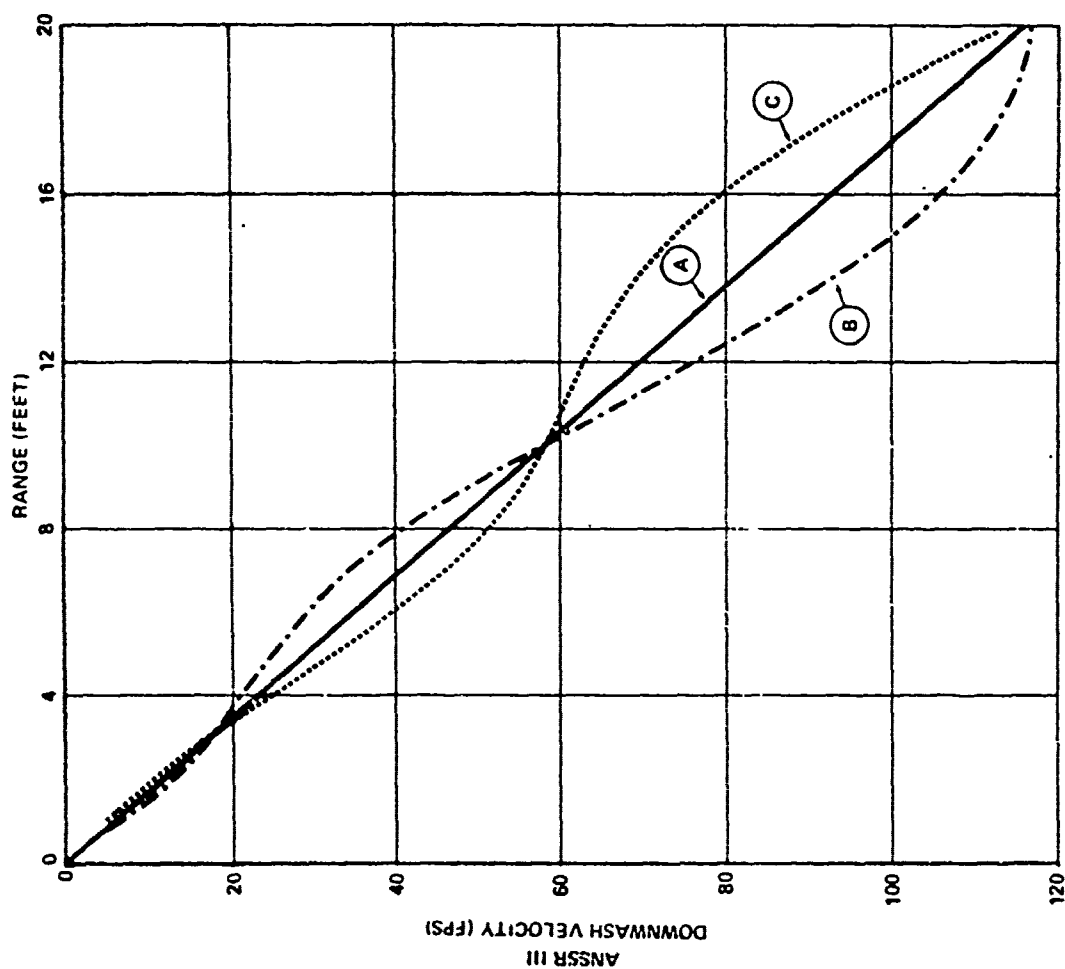
FIGURE 7   DOWNWASH VELOCITY-TRIANGULAR DISTRIBUTION-ANSSR ROCKET

FIGURE 8   DOWNWASH VELOCITY-CONSTANT INFLOW-2.75 IN. FFAR

71

SYMBOL	HALF AMPL-TUDE (% VEL)	PHASE AT LAUNCH (ROCKET W/R BLADE)
A	·)	NOT APPLICABLE
B	15	0 DEG
C	15	90 DEG

ROTOR SPEED = 300RPM
NO. OF BLADES - 2
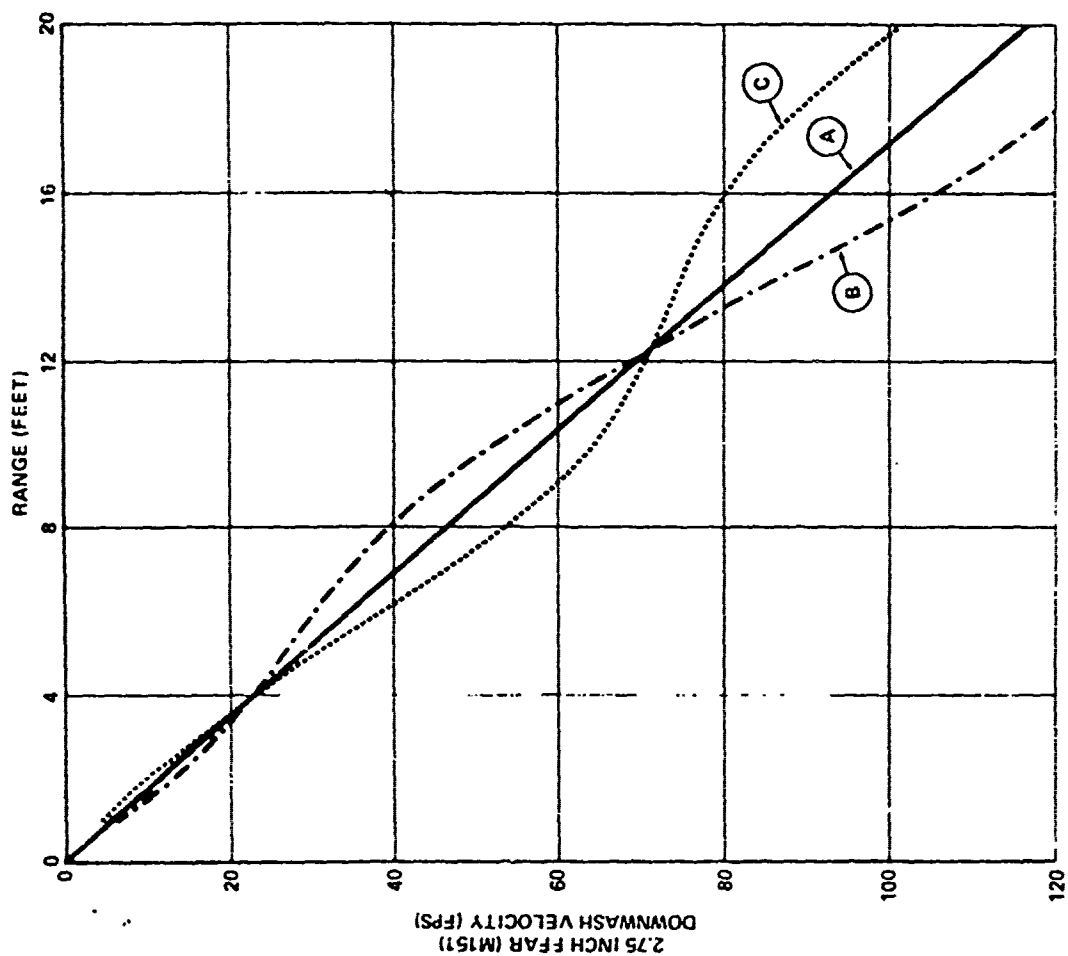
FIGURE 9   DOWNWASH VELOCITY-TRIANGULAR DISTRIBUTION-2.75 IN. FFAR

72.

HELICOPTER AIR FLOW CONFERENCE

VERTICAL TRAJECTORY RESPONSE - 2.75 FFAR/TRIANGULAR

FIGURE 10

ELECTRONICS AND SPACE DIVISION

EMERSON

HELICOPTER AIR FLOW CONFERENCE

VERTICAL TRAJECTORY RESPONSE: ANSSR / TRIANGULAR
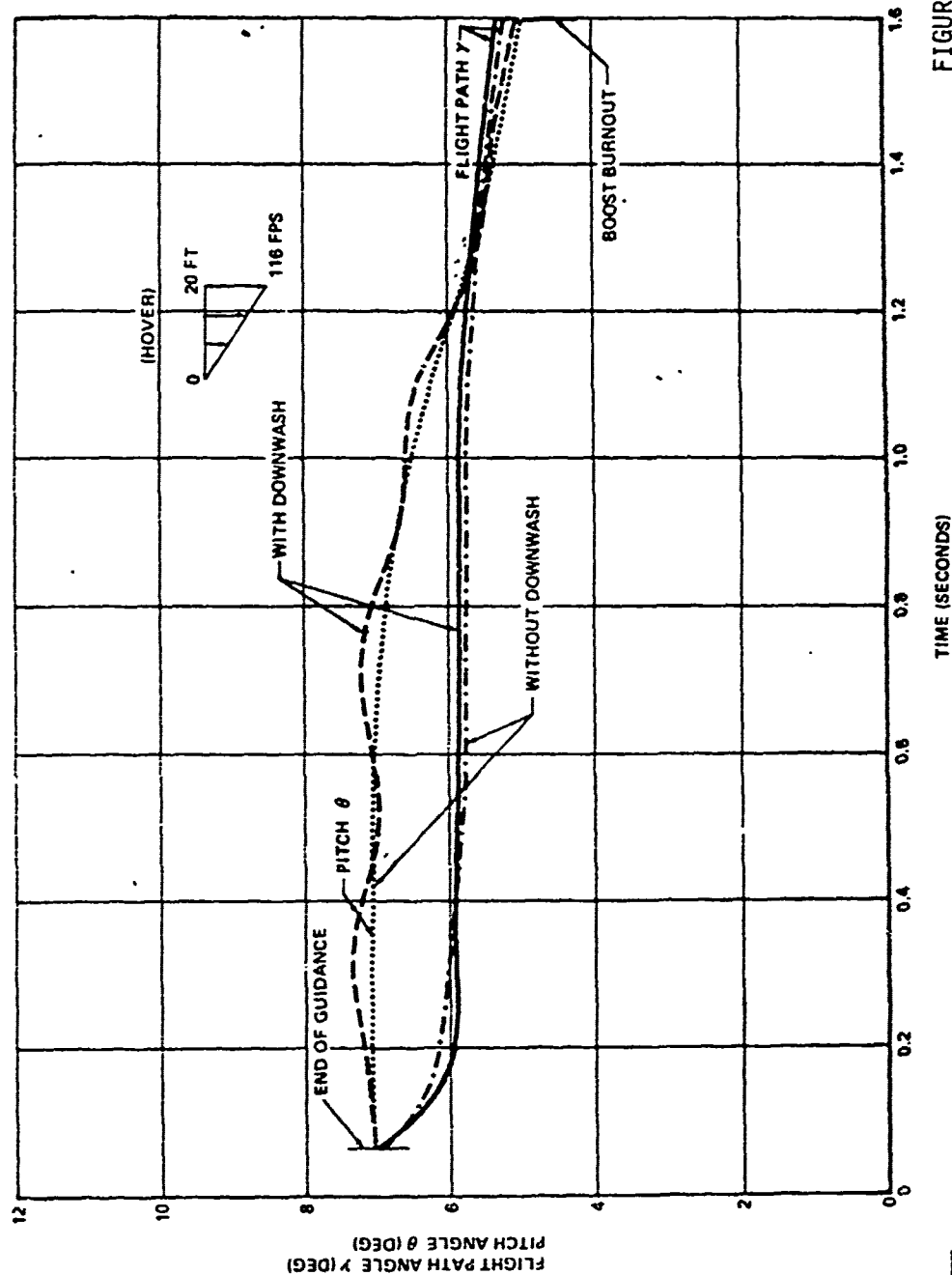
FIGURE 11

ELECTRONICS AND SPACE DIVISION

EMERSON

74

HELICOPTER AIR FLOW CONFERENCE

HORIZONTAL TRAJECTORY RESPONSE: ANSSR/TRIANGULAR
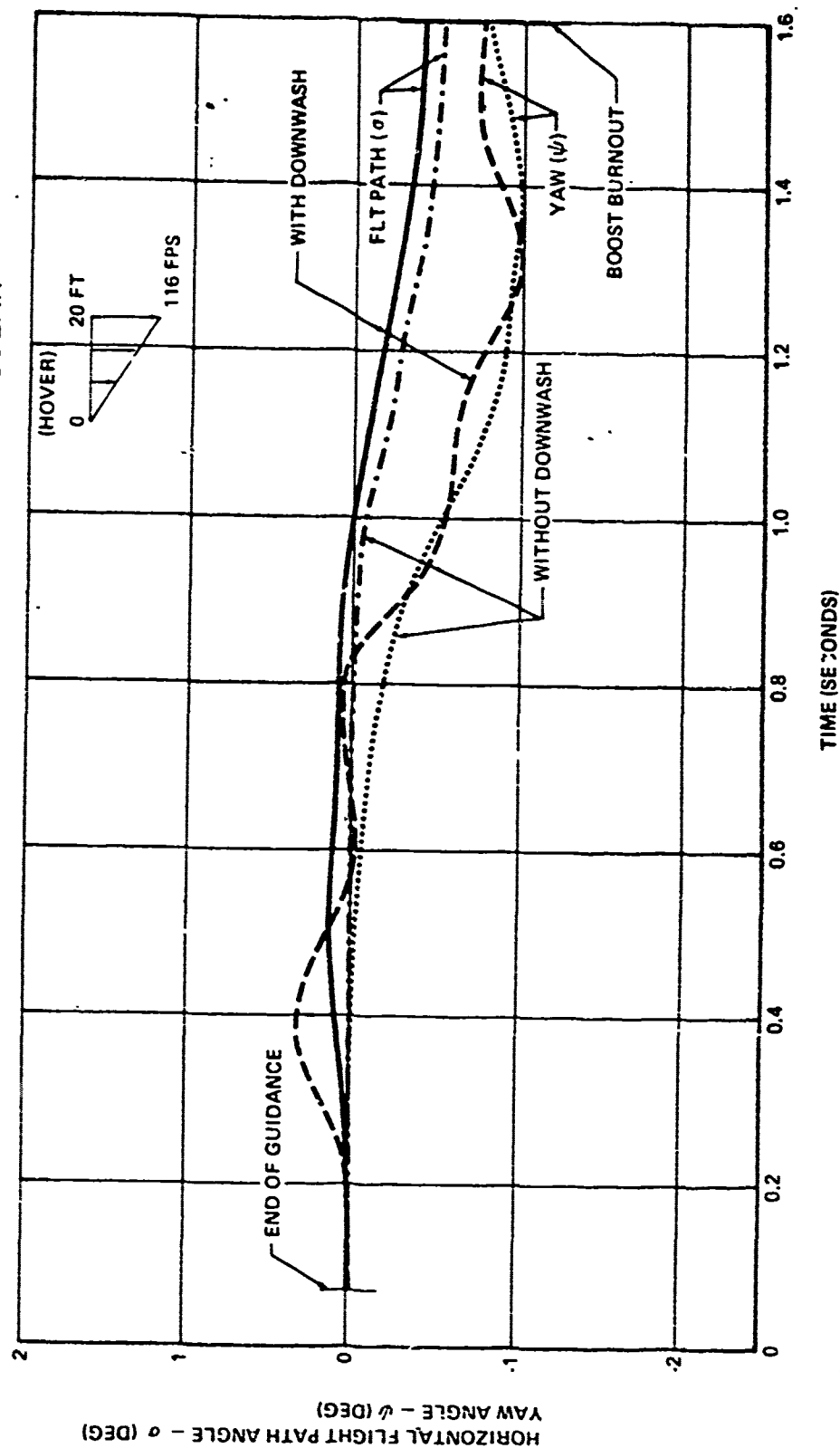
FIGURE 12

AH-1G HELICOPTER FLOW FIELD SURVEY

BARCLAY H. BOIRUN and EDWARD E. BAILES
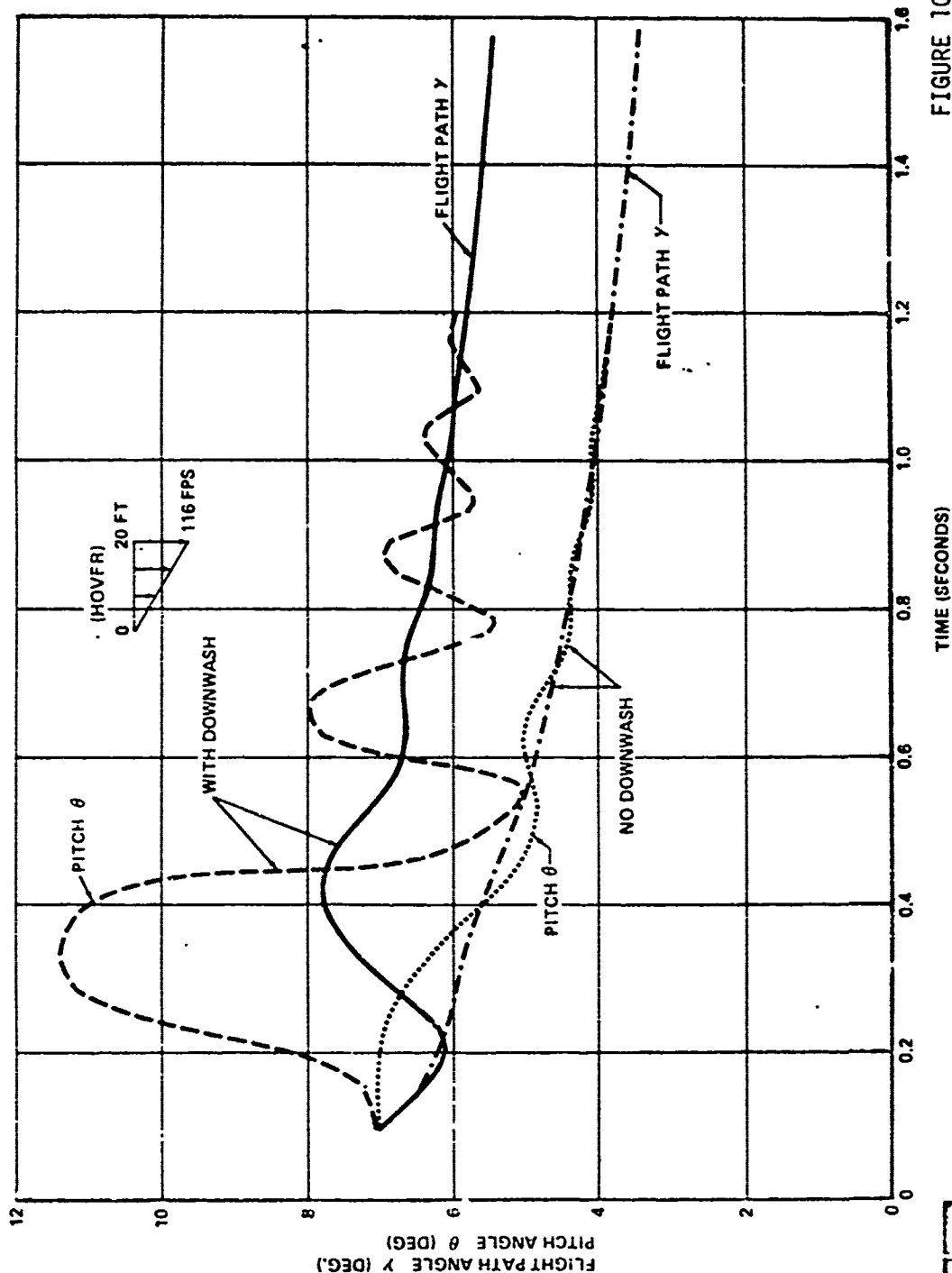US ARMY AVIATION ENGINEERING FLIGHT ACTIVITY
EDWAR'·S AIR FORCE BASE, CALIF.

ABSTRACT

The US Army Engineering Flight Activity (USAAEFA) is currently
conducting an extensive airflow survey on an AH-1G helicopter. This
program is a follow-on to the airflow testing previously reported on
the UH-1M helicopter (USAAEFA Project No. 72-05). The test volume
includes the flight path of any rockets fired from the wing-mounted
store locations. Airflow velocity and direction data are being
measured by six tri-axial split film anemometers, which are arranged
in a 2 x 3 rectangular matrix with 18-inch spacing on a supporting
rake structure. The rake may be moved forward in 18-inch increments
from the leading edge of the wing to just past the aircraft nose.
The test helicopter, operations, and test results obtained to date
will be presented. The presentation may include a 16mm film of a
flight test, slides of the helicopter configuration, and view
graphs of selected flow data.

76

INTRODUCTION

BACKGROUND

1. The current Army requirement for firing small, unguided missiles from helicopters in hover and low-speed conditions has created a need to accurately predict the airflow environment through which the missile must travel. To meet this need, the Aeroballistics Directorate of the United States Army Missile Command (MICOM) requested the United States Army Aviation Systems Command (AVSCOM) (ref 1, app A) to provide representative flight test airflow data. These data were required to determine the early flight behavior of the missiles, and to assess the accuracy of theoretical flow-field prediction models. AVSCOM directed the United States Army Aviation Engineering Flight Activity (USAAEFA) to conduct a flow-field survey to meet the MICOM requirements (ref 2). The UH-1M helicopter was used to develop instrumentation and test methodology for this first survey reported in reference 3 (Project No. 72-05). It was then necessary to repeat the test to obtain data for the AH-1G, which is the primary Army aircraft utilized for missile firing. Instrumentation techniques and experience obtained during the UH-1M Project No. 72-05 have been applied to the AH-1G airflow survey.

2. The airflow mapping is being conducted with total vector split-film anemometers, mounted on a support structure specifically designed to eliminate the anemometer failures caused by vibration during the UH-1M testing. The AH-1G rake structure was designed and tested by the MICOM Structural Dynamics Laboratory through a contract with the Sperry-Rand Corporation.

77

TEST OBJECTIVE

3. The general test objective was to determine the instantaneous flow-field characteristics in a test volume adjacent to the AH-1G helicopter as specified in reference 1, appendix A. The specific objectives were as follows:

    a. Determine the rotor-wake boundary position in the vicinity of the weapons-mount location as a function of forward airspeed.

    b. Determine instantaneous three-dimensional velocity components of airflow in the test volume as a function of forward airspeed.

    c. Determine the effect of aircraft sideslip and angle of attack on the velocity components at a given forward airspeed.

    d. Determine the effects of rotor blade position on the instantaneous velocity components.

4. The measured air velocity is to be analyzed by MICOM for improving the design of the missile launchers and for comparison with analytical airflow prediction methods.

DESCRIPTION

5. The testing is being conducted on an AH-1G helicopter, USA S/N 67-15844, manufactured by the Bell Helicopter Company. A detailed description of the AH-1G is contained in the operator's manual (ref 4, app A). An external structure designed to alleviate vibration levels proven destructive to the airflow sensors, is attached to the AH-1G wing stores to support an airflow instrumentation rake. Versatility of the rake structure and mounting points allows longitudinal adjustments forward and aft, as well as vertical adjustment by means of inverting the rake structure. The structure can be mounted on either side of the helicopter. The test volume encompassed by use of the rake structure is shown as figure A. Six airflow sensors are supported by the rake structure as shown in figure B. They are split-film total vector anemometers, which are manufactured by Thermo-Systems, Incorporated of Bloomington, Minnesota (ref 5, app A), and are described in detail in appendix B. These airflow sensors are capable of measuring instantaneous velocity vectors with a wide dynamic range for large-scale fluctuations, and their frequency response is flat to 1 KHz. The spatial resolution of the hot-film probe is approximately 0.027 inches, which is much smaller than any multi-axis probe. This type of sensor also has the ability to accommodate flow direction over the full solid angle (4 ~ steradians). The specified accuracy over a 300-foot per second velocity range is ±3 percent of reading in magnitude, and ±1.5 percent in direction.

78

FIGURE A. AH-1G AIRFLOW SURVEY TEST VOLUME

FS 490
FS 178.5
BL 30 C
BL 68 0
WL 74 0
WL 20.0

⌐ ¬
└ ┘ = AIRFLOW SURVEY TEST VOLUME
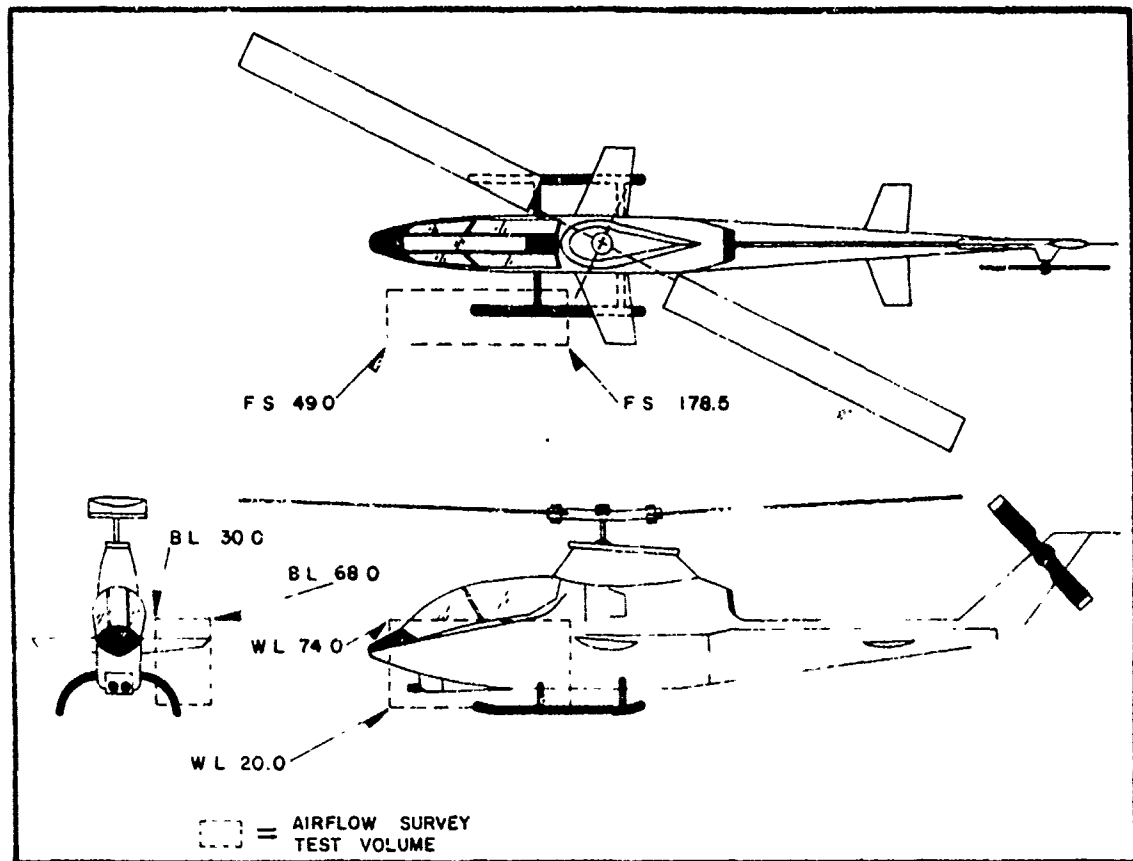
FIGURE B. AIRFLOW RAKE GEOMETRY

18"   18"   PROBE NO. 6

5   3   1

NOTE: VIEW LOOKING AFT

18"

6   4   2

79
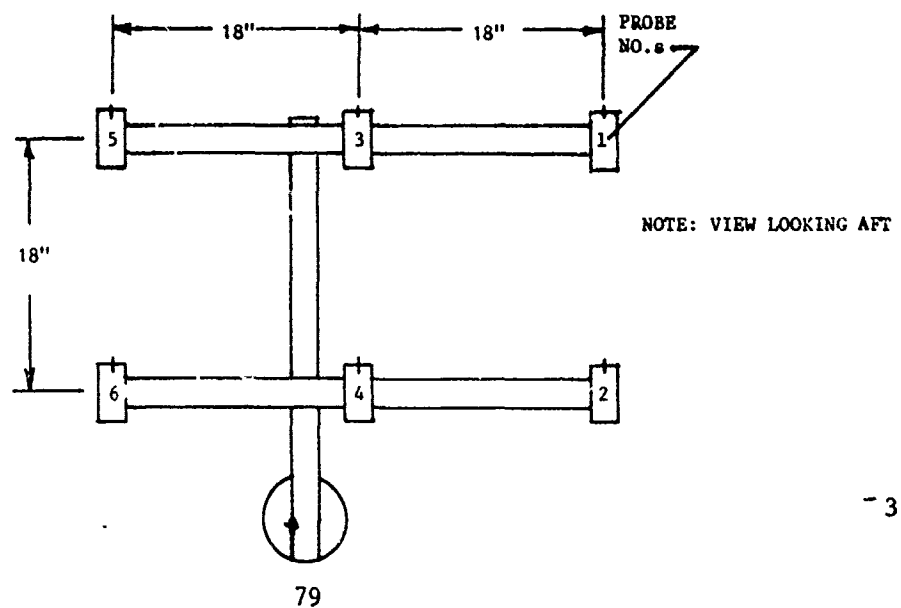
6. Low forward airspeeds are measured by the LORAS II airspeed system, which is mounted above the main rotor head, and includes a sensor unit, airspeed computer, control panel and longitudinal and lateral airspeed indicators. The sensor unit consists of two rotating venturi tubes oriented on opposite ends of a tubular rotor. The venturies are connected to a differential pressure transducer. The rotating assembly is 13.0 inches in diameter and is driven at a constant speed of 720 rpm. The total velocity at each tube consists of a steady component from the constant rotational speed, and a sinusoidal component at a rotational frequency from the translational velocity. The differential pressure transducer converts the sinusoidal velocity component into an electrical signal. This signal is resolved into longitudinal and lateral velocity components and then filtered to remove the modulation frequency which results in average steady-state values. Optional outputs, which are selected from the control panel include, total velocity and either true or indicated airspeed. The system was designed to operate from -50 to 200 knots longitudinal and ±50 knots laterally and be insensitive to vertical airspeed.

DETAILS OF TEST

<u>GENERAL</u>

7. The flow field under the main rotor of the AH-1G is being defined
in stabilized level flight and hover. The conditions shown in table 1
are being flown at a constant thrust coefficient (C_T) of .00475 and
repeated for each of the 20 rake positions required to define the test
volume shown in figure A. Following a successful survey of the base
line test volume, additional tests will be made with variations of C_T
and sideslip angle. Also, the effects of climbing and descending flight
and turbulence on the flow field characteristics will be investigated.
The test aircraft is configured to simulate missile armament and ballast
is added as required to maintain constant gross weight and center of
gravity. The LORAS II and the aircraft standard pitot-static airspeed
systems were calibrated using the trailing oomb and pace vehicle test
methods prior to commencing airflow survey flights.

Table 1. AH-1G Airflow Survey Test Conditions[1]

Point No.	True Airspeed (KTAS)	Advance Ratio (μ)	Forward Velocity (ft/sec)
	Zero (hover)	Zero	Zero
1	5.9	.0134	10
2	11.8	.0268	20
3	17.8	.0402	30
4	23.7	.0536	40
5	30.0	.068	51
6	35.5	.0804	60
7	59.2	.1340	100
8	71.0	.1608	120
9	88.8	.201	150
10	118.5	.268	200

[1]Average test conditions:

Gross weight: 8250 pounds.
Density altitude: 5000 feet.
Rotor speed: 324 rpm.
Thrust coefficient: 00475.
Longitudinal cg: 196.
Lateral cg: zero.

81

SENSOR OUTPUT IN STEADY LEVEL FLIGHT

8. Each anemometer outputs 6 voltages which are an indication of the instantaneous velocity on each film. Therefore, the nature of the airflow can be readily observed from direct strip chart output. Figures C through I present the hover to wake transition speed data in level flight for the lower outboard anemometer (fuselage station (FS) = 162., buttline (BL) = 74., waterline (WL) = 49.). The fundamental frequency shown on all figures was 2/rev of the main rotor (10.8Hz). The maximum amplitude of ~1 volt occurs on film C1, which indicates a maximum oscillation of ~50 ft/sec on one of the velocity components. The character of the flow slightly changes at each velocity as the vortex boundary approaches the sensor location, then rapidly reduces to a small 2/rev fluctuation after the vortex has passed at the 36-knot velocity (figure I). At higher speeds, the average voltages increased, but the oscillation remained basically the same as figure I.

SENSOR OUTPUT IN ACCELERATING FLIGHT

9. Figures J through L present anemometer data obtained while accelerating from hover to ~40 KTAS in forward, left lateral, and right lateral flight, respectively. In figure J, the portion of the data showing vortex passage is presented. The fundamental frequency throughout the run was 2/rev of the main rotor. The approach and passage of the wake vortex boundary is clearly shown. The TIP vortex begins to influence the airflow at the probe location (FS = 164., BL = 56., WL = 67.), at a forward speed of 30 KTAS. The core of the vortex appears to pass the probe at ~36 KTAS and be dissipated by ~40 KTAS. These velocities appear to be slightly higher than for steady level flight conditions by the probe in figure H, which was 18 inches further outboard than the probe in figure I, and is at a higher thrust and angle of attack condition.

10. Figure K shows a similar vortex passage for pure left lateral flight condition. However, figure L shows that at ~6 KTAS in right lateral flight, the airflow at the sensor location was significantly disrupted by a combination of rotor downwash and fuselage interference. All of the other sensors also showed a similar flow disruption in right lateral flight.

VELOCITY COMPONENTS

11. The airflow data from each sensor (as presented in figures C
through L) are being recorded on the FM data system described in
appendix B. These data will be digitized and converted to velocity
components at the rate of ⌃830 samples per second. Each data run
has been set at a 1-second length, which is sufficient for 5.4
rotor revolutions. The data run is initiated by a rotor blip flag
to correlate blade position with flow velocity. As each data run
is processed, the averaged values are output on a printer, and time
varient data will be stored on magnetic tape. The tapes will be
transmitted to USAMICOM for final analysis.

SUMMARY OF TEST TO DATE

12. Mass tuning of the AH-1G airflow rack structure has reduced
maximum acceleration values to ⌃1g at 10.8Hz (2/rev) and significantly
reduced many higher frequencies altogether. The current vibration level
appears to be acceptable because there have not been any inflight
anemometer failures.

13. The primary vibration problem occurs at approximately 135Hz where
it influences the directional velocity data. A dynamic filter will be
used to remove data in this frequency range prior to final data processing.

14. Preliminary data analysis has indicated that the AH-1G airflow
instrumentation system will provide accurate and instantaneous velocity
and direction data in both low and high-speed flight. The system also
seems to be sufficiently accurate for wave form reproduction during
TIP vortex passage.

15. The structural delicacy and electronic complexity of the anemometer
has lead to numerous ground accidents and program delays. If no further
problems are encountered, the currently planned testing should be
completed by October 1975.

TYPICAL VOLTAGE DATA FROM SENSOR NO 2

STEADY FORWARD FLIGHT $V_T = O.$ (HOVER)

FILM VOLTAGE

A1

A2

⊢ 1 SEC ⊣

B1

B2

C1 ≈ 40 FT/SEC

C2

TIME
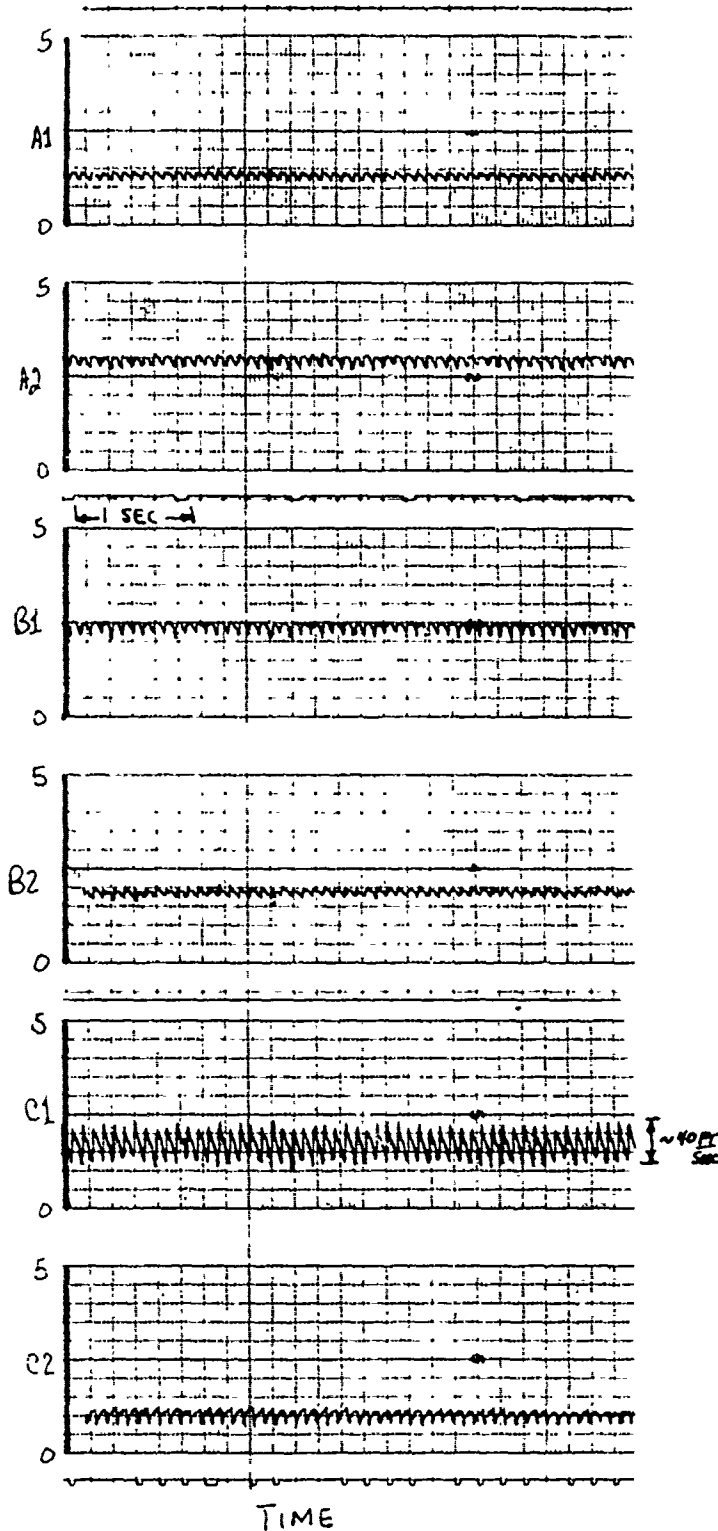
FIGURE D
TYPICAL VOLTAGE DATA FROM SENSOR NO. 2
STEADY FORWARD FLIGHT $V_f = 6.0$ Ktas

85
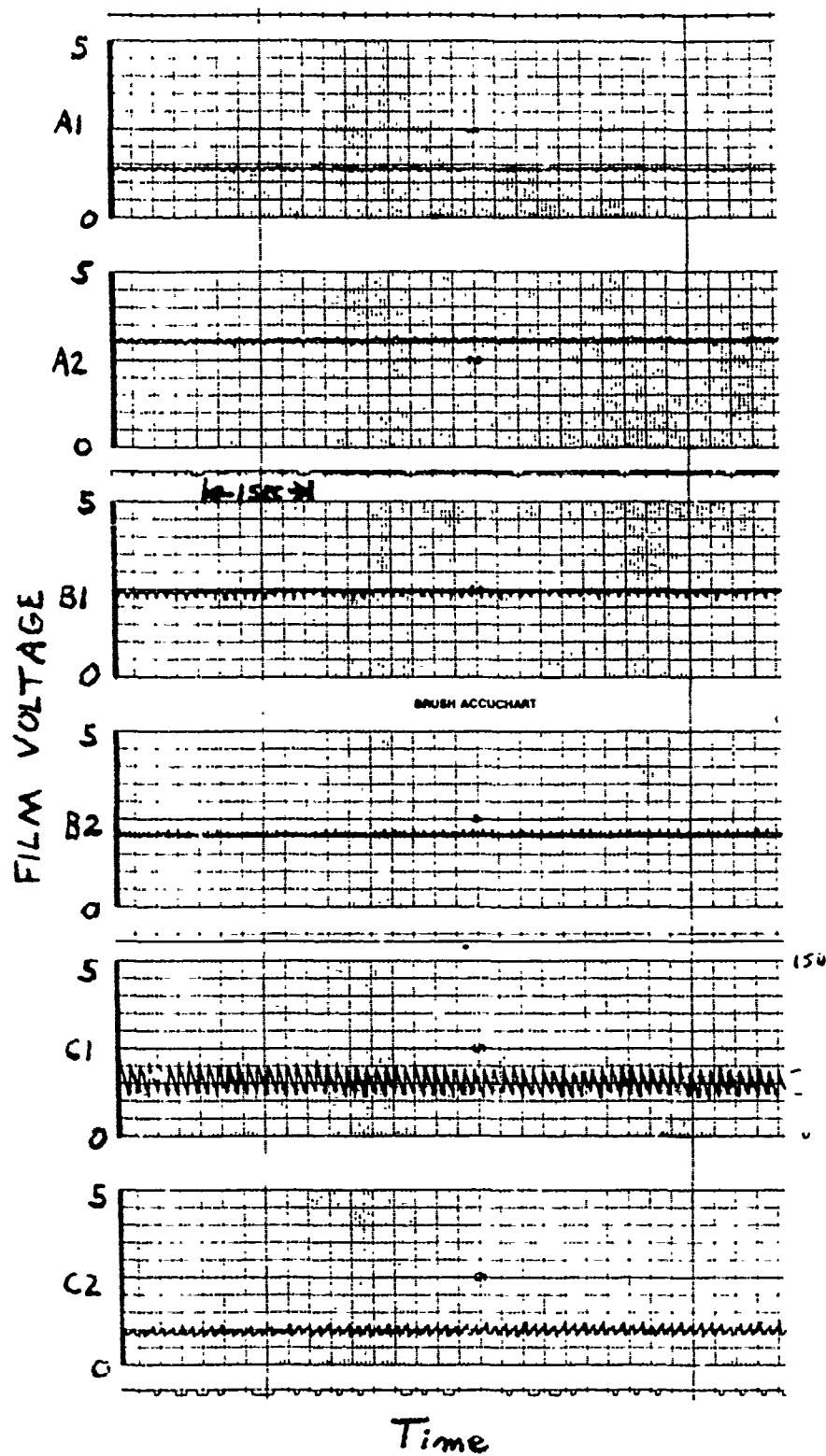
FIGURE E
TYPICAL VOLTAGE DATA FROM SENSOR NO. 2
STEADY FORWARD FLIGHT $V_T = 12$ KTAS

FILM VOLTAGE

TIME
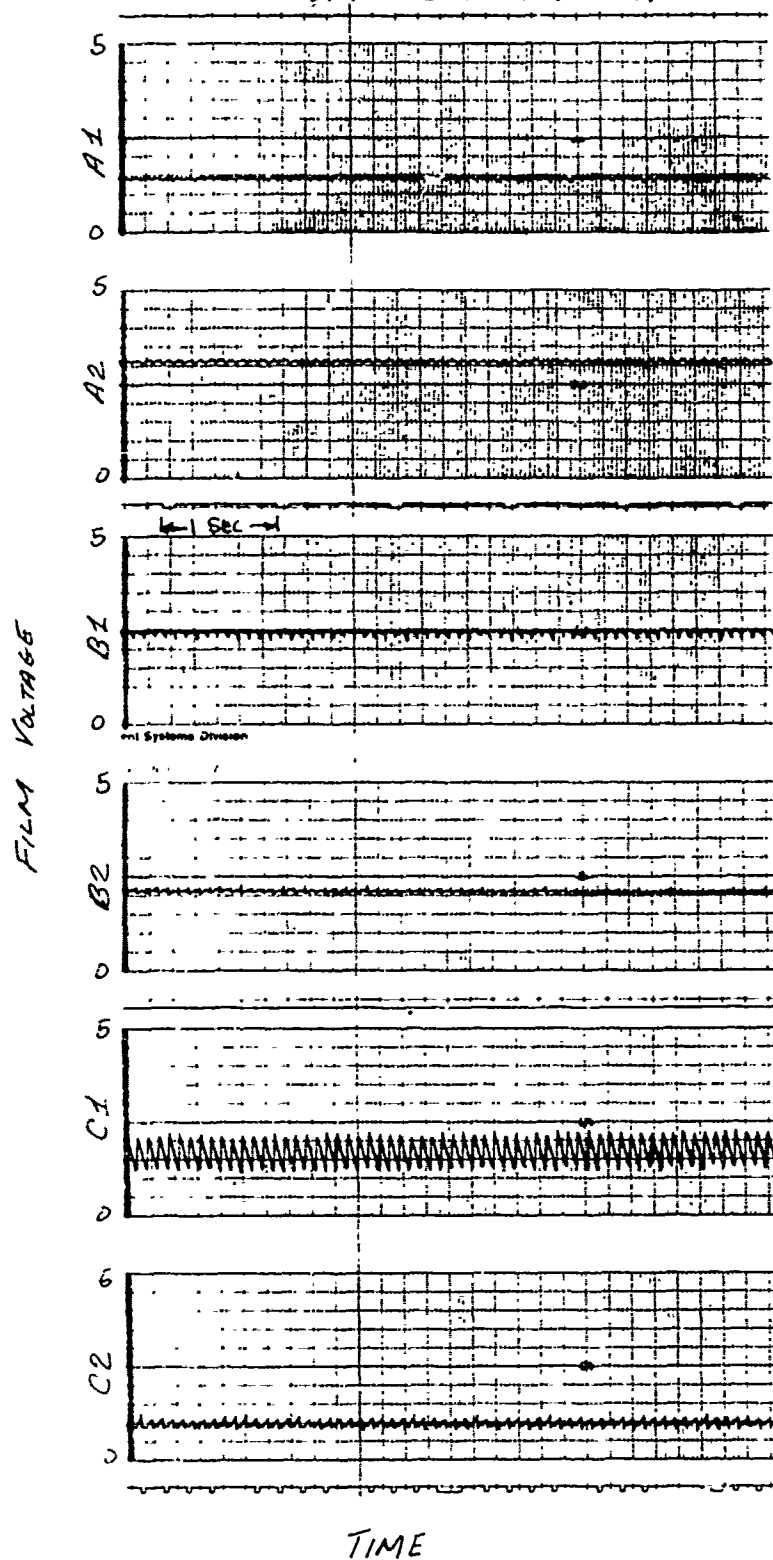
TYPICAL VOLTAGE DATA FROM SENSOR NO 2

STEADY FORWARD FLIGHT $V_T = 18$ KTAS

FILM VOLTAGE

TIME
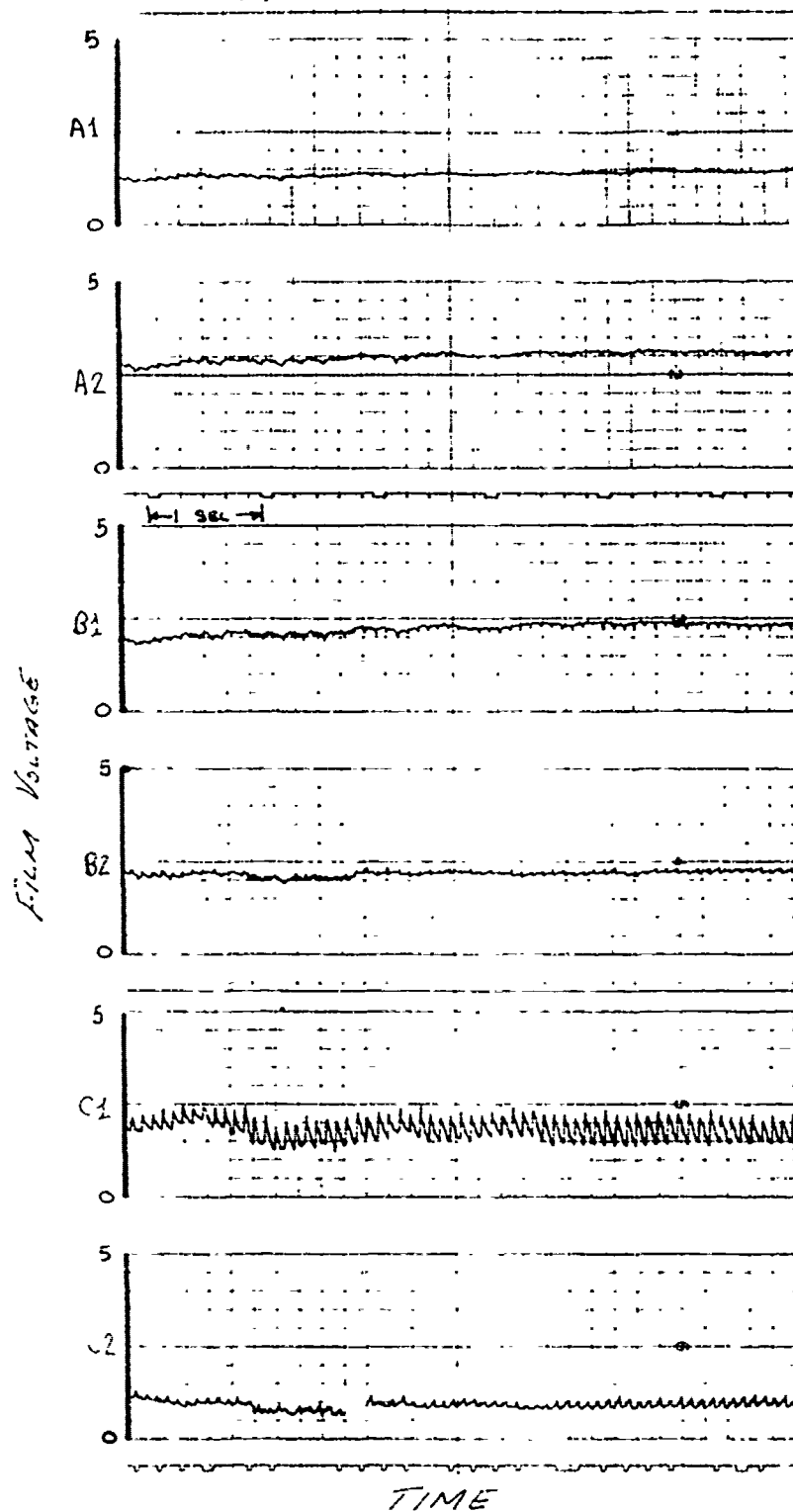
FIGURE G.
TYPICAL VOLTAGE DATA FROM SENSOR NO. 2.
STEADY FORWARD FLIGHT $V_T = 24$. KTAS
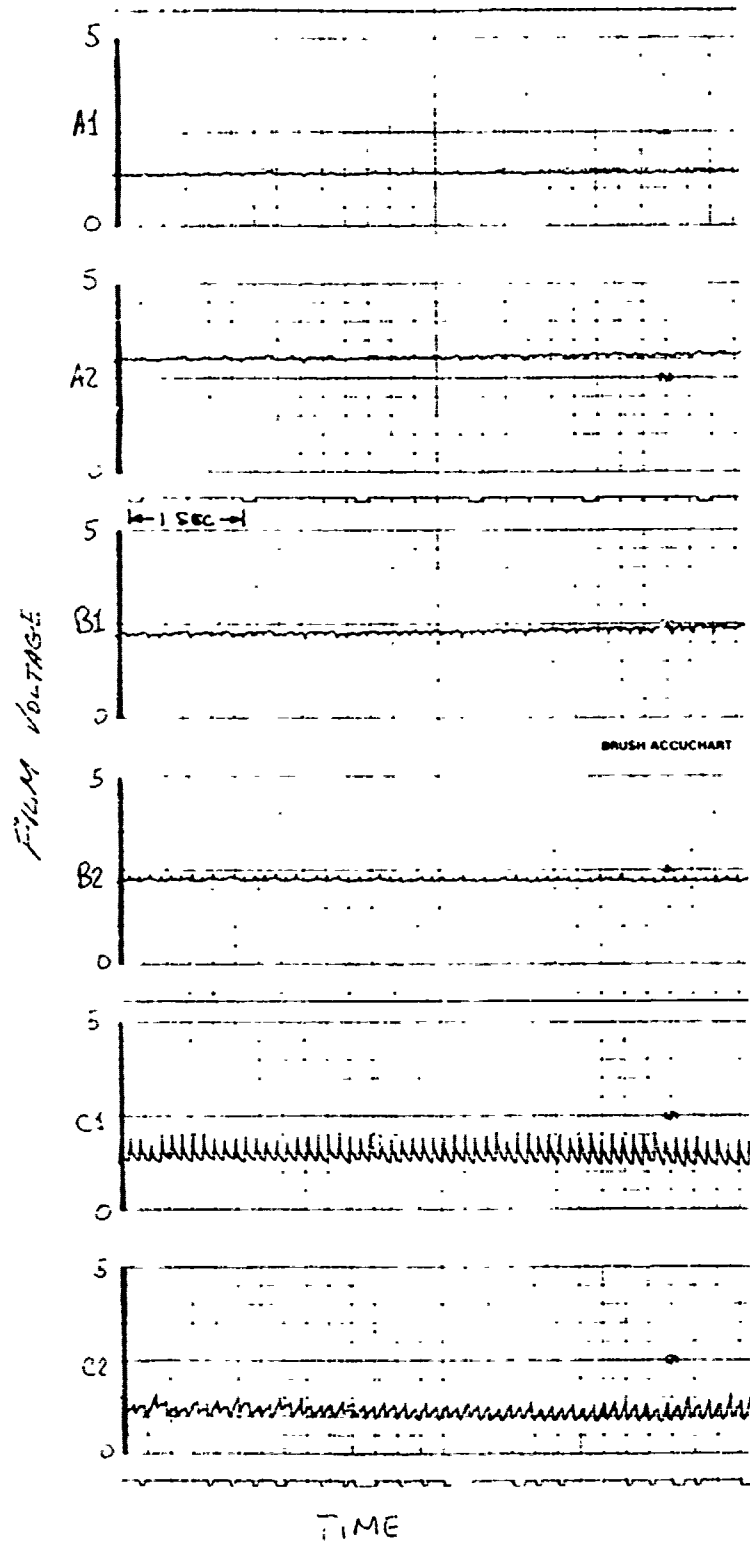
FIGURE 4.
TYPICAL VOLTAGE DATA FROM SENSOR NO 2
STEADY FORWARD FLIGHT $V_T = 30.$ KTAS

TIME

89
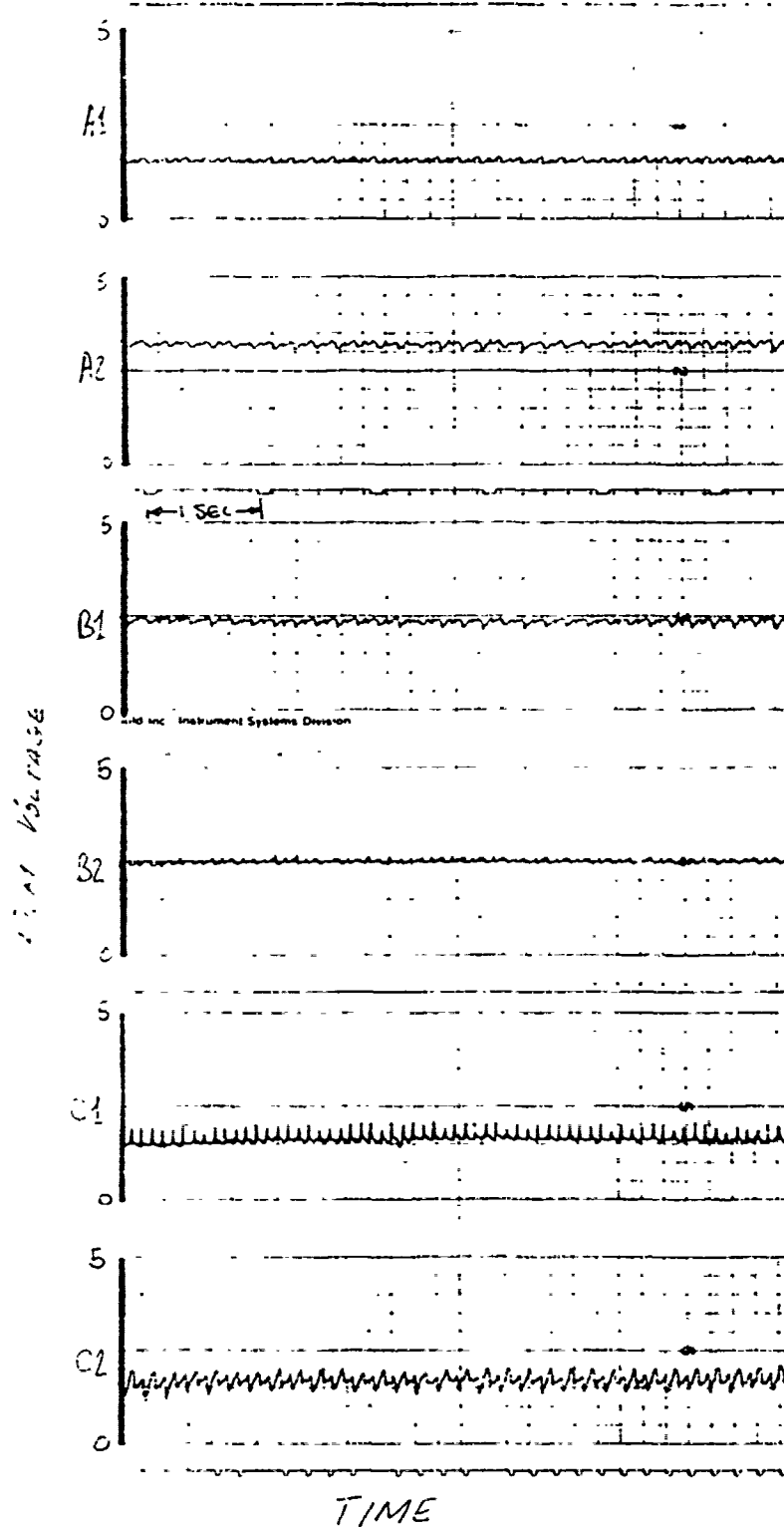
FIGURE 1
TYPICAL VOLTAGE DATA FROM SENSOR NO. 2
STEADY FORWARD FLIGHT $V_T = 35.5$ KTAS

FILM VOLTAGE

A1

A2

B1

B2

C1

C2

TIME

FIG. 5

TYPICAL VOLTAGE DATA FROM SENSOR Nº 4
DECELERATING FORWARD FLIGHT

$V_T \cong 40\,kTAS$

$V_T \cong 36\,kTAS$

$V_T \cong 30\,kTAS$

1 SEC

FILM Voltage

FIG. F

TYPICAL VOLTAGE SWING FROM SENSOR No. 3
ACCELERATING LEFT LATERAL FLIGHT

$V_T \approx 35$ Kras
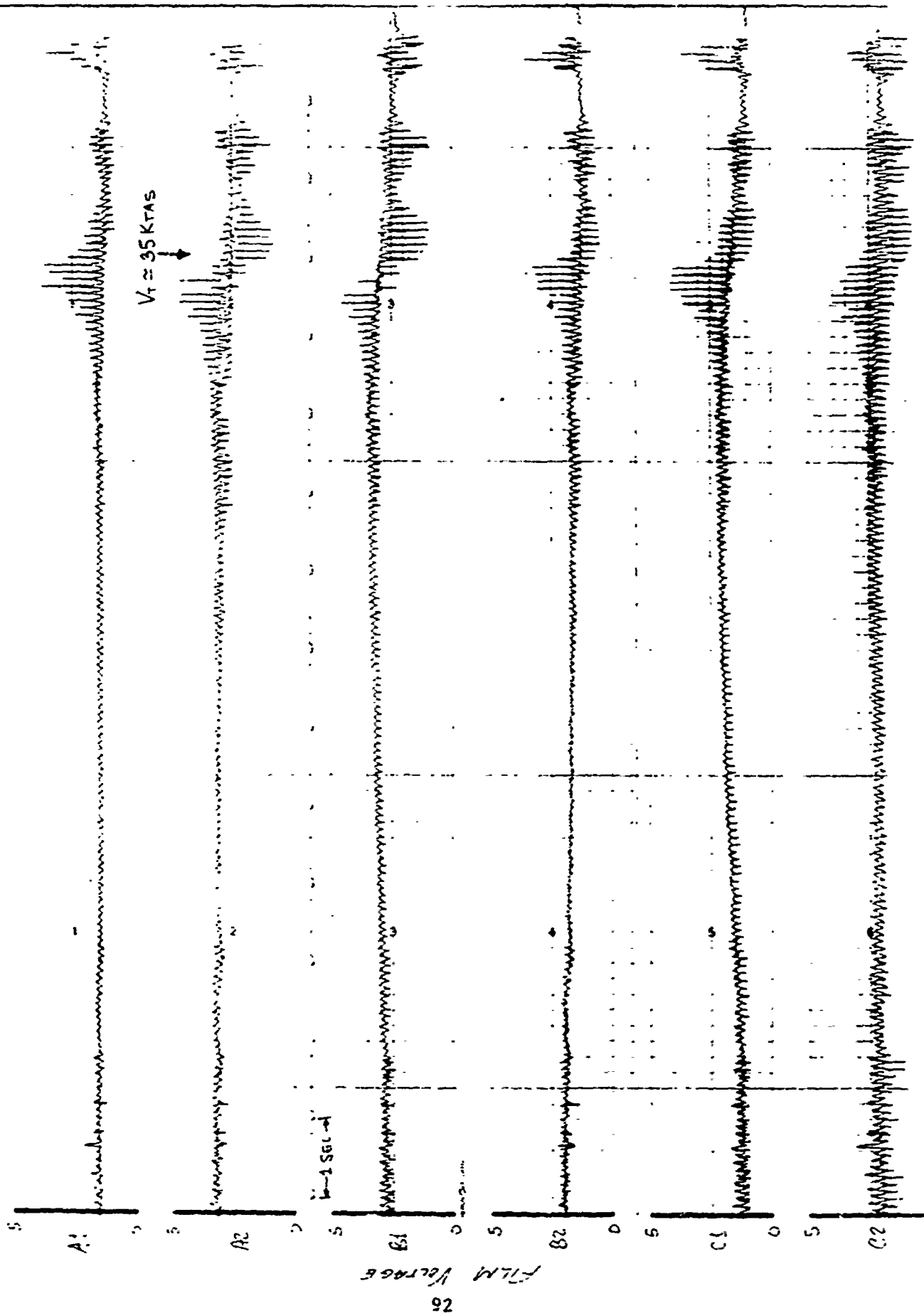
FIG. 1.

TYPICAL VOLTAGE DATA FROM SENSOR NO 6
ACCELERATING RIGHT LATERAL FLIGHT

$V_r \cong 20$

$V_r = 6$ KTAS

GOULD Inc. Instrument Systems Division
BRUSH ACCUCHART

FILM VOLTAGE
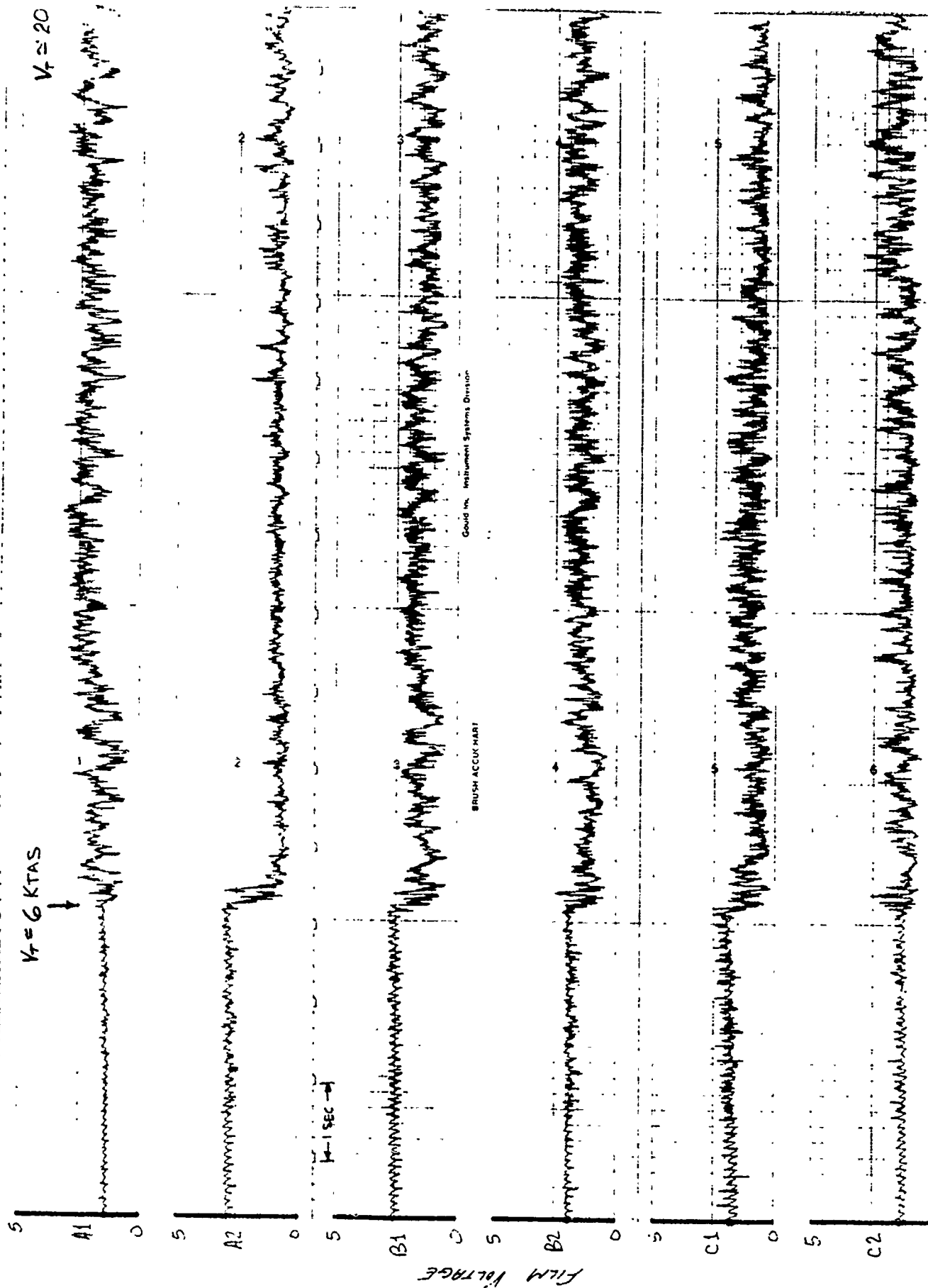
APPENDIX A. REFERENCES

1. Letter, MICOM, AMSMI-RDK, 18 October 1961, subject: Helicopter Flow Measurement Flight Test.

2. Letter, AVSCOM, AMSAV-EFT, 3 February 1972, subject: Test Directive No. 72-05, Helicopter Flow Field Survey.

3. Final Report, USAAEFA, Project No. 72-05, *Rotor Flow Survey Program, UH-1M Helicopter,* May 1974.

4. Technical Manual, TM 55-1520-221-10, *AH-1G Operations Manual,* April 1967.

5. Technical Manual, Thermo-Systems, Incorporated, *Operating and Service Manual for Model 2080 and Model 1080D Total Vector Anemometer,* 1973.

APPENDIX B. INSTRUMENTATION

1. Figure 1 shows the flow survey anemometer signal flow. Airflow was sensed by six Thermo-Systems, Incorporated, Model 1080 total vector anemometers. Each anemometer included a Model 1296F probe and a companion 1083 signal conditioning module. A Model 1088-C rack with a 1082 control circuit completed the anemometer system.

2. Each probe (shown in figures 2 and 3) consists of 3 sensor rods, a support shaft, a copper-constantan temperature sensor mounted between the rods, and a pneumatic probe tip shield. the 3 rods are supported in such a way that an orthogonal three-dimensional coordinate system is formed by the 6 independent films (2 per rod, separated azimuthally). :ach of the film sensors forms one leg of a bridge circuit which is completed by components in the associated 1083 control circuit module. The 1083 module regulates bridge excitation power so that a constant temperature ratio is maintained between each film and a nominal room temperature value (actually controlled by bridge completion resistors). The bridge excitation voltage is scaled for a zero to 5 volts direct current (VDC) output for an airflow scale of zero to 150 feet per second. In addition to the 6-bridge and scaling circuits, each 1083 provides a compensated reference junction for the tip thermocouple. Compensated thermocouple electro-motive force (EMF) is amplified and a linear zero to 5-VDC analog temperature output is provided for correcting flow vectors measured at nonstandard conditions. In practice, the tip thermocouples and pneumatic shield actuators were not used. A single Rosemount type 102AU2CK platinum resistance total temperature probe and a Rosemount 510BF signal conditioning amplifier were used for ambient temperature measurements. This subsystem yielded higher accuracy than the tip thermocouples could have, and only one data channel was required. The probe shields were activated manually to eliminate the need for pneumatic valves, plumbing, and gas storage bottles on the aircraft.

3. Six single-ended, high-level velocity signals (from each probe) were routed directly to a Vector, Incorporated constant bandwidth subcarrier oscillator rack. Each rack contained six constant bandwidth voltage controlled oscillators (VCOS), a 120KHz reference oscillator, and a mixer amplifier. VCO deviation was ±4KHz from a center frequency of 25, 40, 55, 70, 85, or 100KHz for a zero to 5 VDC input. The discriminators used for data reduction were EMR Model 4150's. They incorporated low pass output filters with a constant amplitude response (7-pole butterworth) and a cutoff frequency of 2KHz. The output of a mixer amplifier was routed directly to a tape track and to a telemetry switch for real time monitor selection. The reference oscillator signals were used to provide tape speed compensation during data reduction.
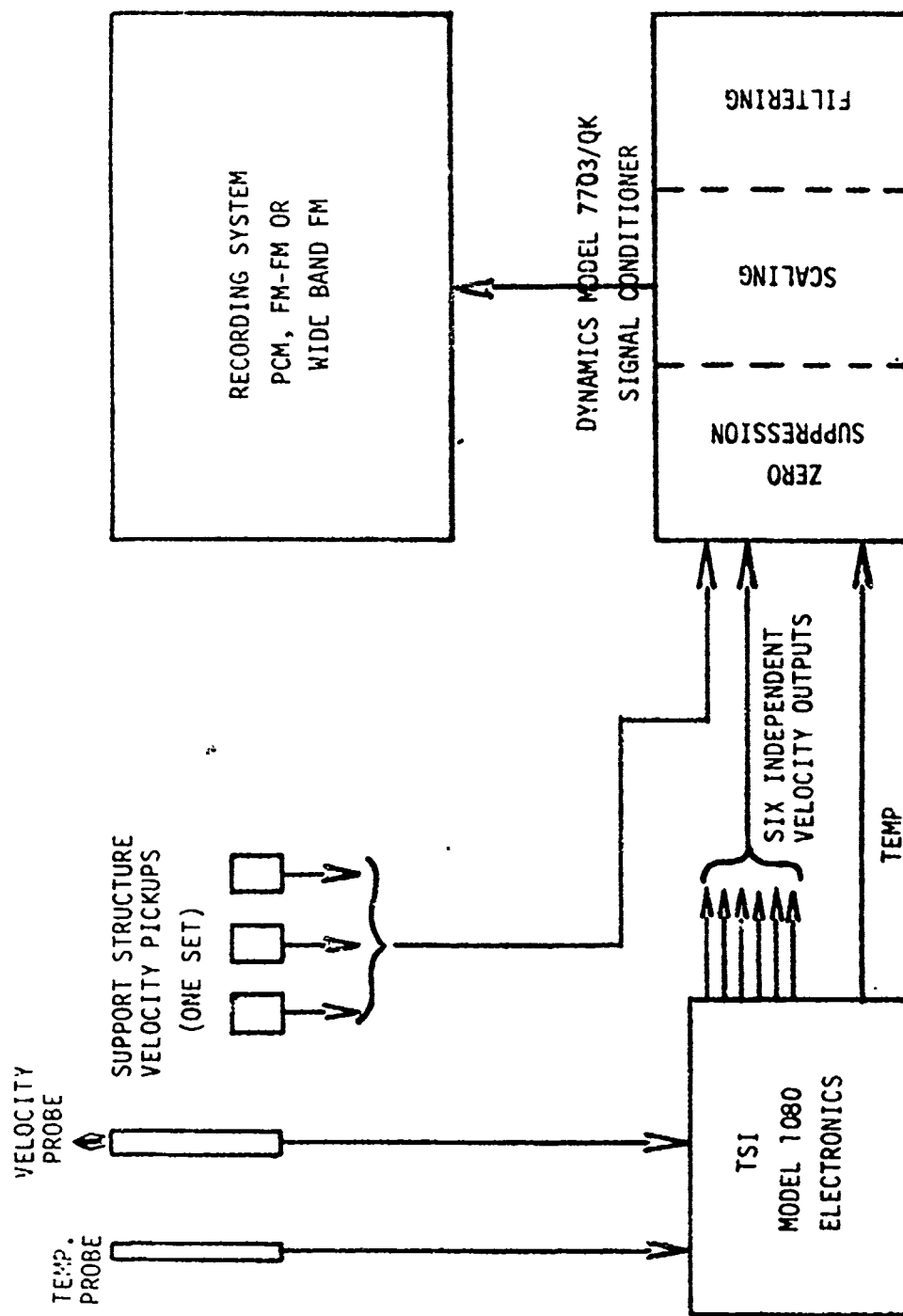
Figure 1. Instrumentation Scheme

Figure 2. Model 1296F Probe

97
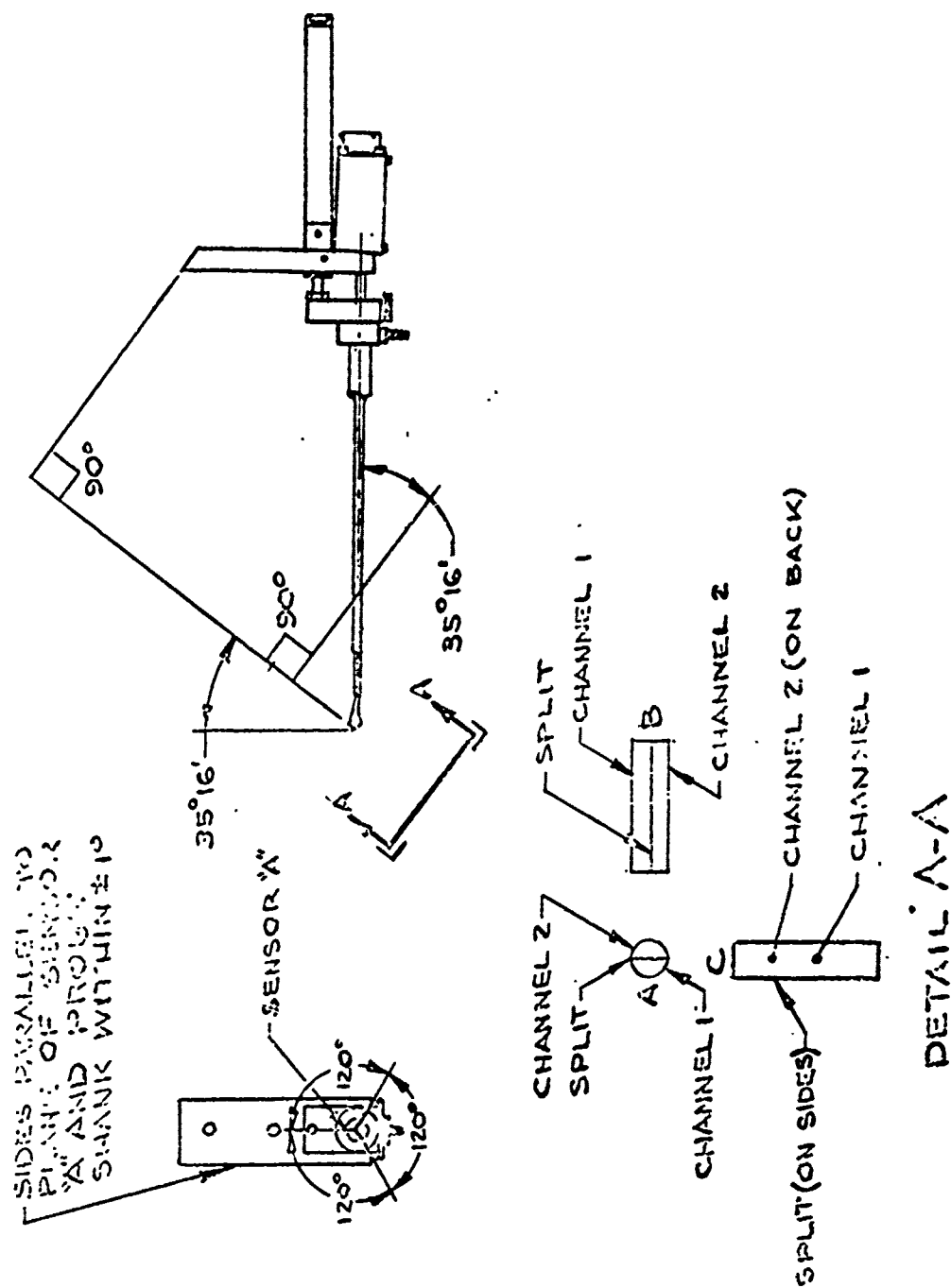
Figure 3. Probe Mount and Sensor Orientation

4. The aircraft parameters were recorded in a PCM format. Spacecraft, Incorporated, built the PCM units that are standard equipment in USAAEFA at this time. Each unit contains a 64-channel, high-level analog multiplexer (tiered groups of 8), a 112-bit discrete bi-level multiplexer (14 transistor logic compatible 8-bit words), an analog buffer/sample and hold amplifier, an 8-bit, 0-5VDC successive approximation analog to digital converter, and all control and formatting circuits required to construct a serial IRIG compatible NRZC PCM bit stream suitable for magnetic tape recording or radio frequency (RF) telemetry. The complete analog portion has been proven to be a monotonic ±0.5-percent full-scale system with a maximum nonlinearity of ±1/2 least significant bit (LSB). Bit rates are hardware programmable in powers of 2 from 32 K-bits per second to 512 K-bits per second, yielding fixed main frame rates from 50 frames per second to 800 frames per second. This test used a frame rate of 100 frames/second (100 samples/second/parameter).

5. All of the airflow data were set up for automatic queing and synchronization with rotor azimuth by an event pulse in the PCM frame. The flight engineer would turn the tape recorder on while a desired flight condition was being established. When he decided that valid data were available, he activated an event switch on his console to arm the event pulse circuit. An optical proximity sensor mounted on the rotor swashplate defined rotor azimuth once per rotor revolution and the armed event circuit activated the event pulse as soon as a rotor azimuth pulse was received. The event pulse had a fixed duration of one second and was supercommutated in the PCM unit to a sample rate of 800 samples/second, allowing automatic data queing to rotor azimuth with an uncertainty of ±2.4 degrees at a rotor speed of 324 rpm.

6. An IRIG-B time code generator provided parallel binary coded decimal (BCD) time-of-day information for inline timing in the PCM main frame and a modulated 1-KHz serial code on an independent tape track for automatic tape searching.

7. As indicated, all of the data were recorded on magnetic tape. An Ampex AR-700 Intermediate Band recorder was used with a tape speed of 30 inches/second with the following track layout:

Track	Signal	Format
1	Voice (intercom)	Direct
2	Time	1KHz Mod Code
3	PCM	Serial BØC
4	Probe # 1	FM/FM CBW
5	# 2	FM/FM CBW
6	# 3	FM/FM CBW
7	# 4	FM/FM CBW
8	# 5	FM/FM CBW
9	# 6	FM/FM CBW
10	Rack vibrations	FM/FM CBW
11	Rack vibrations	FM/FM CBW
14	Tach reference	Direct

8. Preflight anemometer performance checks were made at a zero velocity point, and at a standard flow setting using the manufacturer-supplied calibration data. Integral to each probe tip shield is a sonic orifice which serves to establish a self-test flow point when a regulated 50-PSIG gas supply is applied to the rear of the shield. Bridge output ratios were checked against manufacturer-suggested tolerances with a voltage divider and null detector at the test flow point. Absolute accuracy was checked against the anemometer specifications. Manufacturer-supplied airflow data, exact pressure measurements of the test gas source, barometric pressure readings, and ambient temperature readings were put into the probe data reduction equations for these checks.

TOTAL QUADRANT ELEVATION VARIATION FOR HOVER
DOWNWASH CONDITION AND LONG RANGE TARGETS (3-6 KM)

ROBERT E. LENT
Northrop Corporation
Anaheim, California

WILLIAN G. GARNER
US Army Missile Command
Redstone Arsenal, Alabama

ABSTRACT

This paper presents preliminary test results of a potentially severe variation
in rocket trajectories which a helicopter fire control system will have to
address. The variation in the total QE components, that is, aircraft attitude
and rocket pod elevation, resulted in marked trajectory differences for ranges
of 3 to 6 KM. The rocket systems used were the 2.75 inch and the Arrow. The
tests were conducted at Hover and Altitude above the ground of 100-150 feet and
above the target of 30 feet.

INTRODUCTION

A free rocket, when fired from a helicopter, at low speed
will initially be traveling at a speed which is of the same
order of magnitude as the rotor downwash velocity. Since large
angles of attack result, the trajectory can be significantly
affected by the downwash flow field. These effects necessitate
some form of aiming assistance and compensation (Fire Control
System). Simplistic assumptions of pitch rates proportional to
an average constant downwash have been thought to be adequate
for prediction of the rocket response; with a small amount of
concern that blade passage pulseing might be significant. Recent
test results from the Selective Effects Armament Subsystem (SEAS)
program indicate that interface geometry and pilot/aircraft
closed loop dynamics add significant complexity to trajectory
prediction.

At the conclusion of the SEAS development phase in June 1974,
four rocket systems were evaluated in a competitive flight test
program at Yuma Proving Ground (YPG). The rocket systems were:

o   ANSSR

                    SEAS Candidates

o   ARROW

o   2.75" (MK 40) Army

o   2.75" (MK 66) Navy

Approximately seventy rockets of each system were evaluated.
Evaluation consisted of hover fire and 90 knot running fire to
a target range of 4 kilometers. A 2 kilometer range demonstra-
tion was also fired. The data collected during this test program
provided the base that was utilized in a technology evaluation
program that followed.

During the period of January to March 1975, rocket technology
was evaluated with tests conducted on:

o   Fire Control

o   Maximum range (Hover)

o   Lead Prediction sight

o   Total QE variation effect

The technology program and SEAS Competitive Flight Test Program utilized the same aircraft, pilot, test engineer, and rocket systems. The hover tests were conducted at 10 meters above the target and 30 - 50 meters above the ground so as to be out of ground effects. The aircraft was tracked by several contraves camera stations with their independent outputs resolved to a composite real time readout at mission control. The pilot was given a voice countdown of range and altitude position to permit holding them constant from run to run without diverting his visual attention from target track. The wind was monitored and limited to 5 knots crossing. The aircraft sight (XM-73) and rocket pods boresight were monitored and controlled after each sortie. The impacts were recorded by use of overhead movie and TV cameras.

GEOMETRY

As shown in Figure 1, the total quadrant elevation (QE_T) is defined as the sum of the pod elevation (θ_E) with respect to the aircraft datum line (ADL) and the sight setting. The sight setting angle is comprised of two components, i.e., the aircraft hang or trimmed attitude angle (θ_{TRIM}) which is a function of aircraft weight, center of gravity, flight conditions, and the line of sight (LOS) angle to the target. The LOS angle is also defined as the angle in which the aircraft will have to move (control angle from trim) in order that the QE_T will be correct with respect to horizontal at the moment of rocket firing. Therefore, the relations are:

$$QE_T = \theta_E + \theta_{SIGHT}$$

$$= \theta_E + \{\theta_{TRIM} + \theta_{LOS}\}$$

$$= \theta_E + \{\theta_{TRIM} + \theta_{CONTROL}\}$$

BRIEF DESCRIPTION OF TOTAL ANOMALY

During a test series in which the four competing rocket systems were to demonstrate a six kilometer range capability from hover, a total quadrant elevation anomaly was discovered with the ARROW system. In order to approach the required range with the other three systems it was necessary to use the maximum pod elevation of +160 mils and a sight setting of +50 mils.

The ARROW system, due to its performance characteristics, extrapolated from the SEAS baseline data (Figure 2) and utilized a pod elevation of 88 mils. As indicated in Figure 2, the mean range of the two pair firings was 4.8 kilometers. With a pod elevation of 78 mils, a range of 5.6 kilometers had been attained in a QE test shot during the baseline tests.

The helicopter sight and pod boresight were checked and the sight film reviewed for pilot effects. Data indicated that the boresight and pilot procedure were within limits set by the SEAS baseline results. The test was repeated a week later with two single firings which produced the same results.

These tests confirmed a range versus total QE anomaly of significant magnitude. Additional tests were needed to determine if it was a function of the rocket system or an interface condition between the aircraft and rocket.

Rocket System Evaluation

In order to isolate the anomaly, a test program was set up in which the rocket system could be evaluated as the source. This test series consisted of selecting a pod elevation (71.5 mils) which would remain constant and vary the aircraft attitude from +75 mils to -10 mils. The results presented in Figure 3, showed that the ARROW rocket system range versus total QE was a reasonably smooth profile despite a hint of multiple curves. The anomaly appeared to be the result of an aircraft-rocket interface.

AIRCRAFT-ROCKET INTERFACE

Analysis of the SEAS baseline data in regard to trajectory, impacts, pilot's flight procedure, environmental and aircraft conditions indicated two interface possibilities:

o Critical Pod Elevation

o Aircraft Dynamics

The following sections will discuss in detail the above items.

104

VARIATION OF ROCKET LAUNCH ATTITUDE

In order to test the range sensitivity of the rocket to variation in the rocket pod attitude (θ_E), a pod angle test point well above that of the baseline data, but far below the 160 mil maximum was fired.

The test results are presented in Figure 4 and show the effect discussed. It should be noted that the rate of change of range with QE_T is greater for the lower pod elevation relative to ADL. The pod elevation approaching normal to the downwash flow field as it approaches zero angle relative to ADL.

Test points were selected for the 2.75" FFAR (Mark 40). Firing results shown in Figure 5 confirm an anomaly. However, the direction of discontinuity is reversed.

As shown in Figure 6, the rocket pod elevation relative to the downwash velocity vector varies the amount of aerodynamic downwash influence experienced by the rocket. The rocket will exhibit maximum weathercocking when the pod is normal to the flow field and the effect will decrease as pod elevation is changed from the normal toward alignment with the downwash vector.

This may be the dominant influence for ARROW, but it does not xplain the reversed direction of discontinuity for the 2.75" rocket. It appears that a more dominant force than the downwash induced moment and counter thereto exists for this rocket. The data is too meager to draw a firm conclusion, but it may be that the 2.75" tipoff launcher permits a negative moment downwash induced reinforcement of the tipoff which is not overcome by the stable moment influence before the downwash flow field is transited. Since ARROW has a non tipoff launcher, no counter moment to the negative nose moment exists to produce a couple and its rate buildup prior to positive stability onset could be much less.

An interesting side note to the ARROW rocket system tests was that the standard deviation in range about the MPI was less than that in the yaw plane. This indicates that one can take advantage of the downwash when adequately defined, instead of trying to minimize its effect. Expensive and complex concepts of rocket fin deployment, delay systems and synchronization of the rocket firing times with rotor position are probably not necessary; but launch line to downwash vector angle cannot be ignored.

AIRCRAFT DYNAMICS

Throughout the flight test program, aircraft physical properties, boresight and pilot flight procedures were monitored and controlled. A test series in which the effect, if any, of aircraft weight, center of gravity (c.g.) and flight characteristics could be studied was conducted.

Test instrumentation was removed from the ammunition bay which reduced the aircraft weight (100 - 150 pounds) and moved the c.g. aft so that the aircraft trim angle was 4 mils higher. The SEAS baseline test configuration of pod elevation and sight setting were repeated with the modified aircraft.

Shown in Figure 7, are the results utilizing the ARROW rocket system. A marked change in the range for a given total quadrant elevation was noted. The results with the lighter aircraft and aft c.g. show a reduction in range.

Analysis of the results of this test series indicate that the following was changed during the tests:

o Aircraft weight

o Aircraft center-of-gravity

o Pilot/aircraft dynamics

A discussion of each of their possible effects to produce the observed results follows.

AIRCRAFT WEIGHT

The aircraft weight was reduced by approximately 100 - 150 pounds. The rotor, for identical conditions, would be required to produce less lift to maintain the same firing conditions. Assuming the same flying conditions, the 2 percent change in weight is so small that the rotor downwash flow field effect would not be measurable. The weight change was concluded to be insignificant.

PILOT/AIRCRAFT DYNAMICS

The air temperature and aircraft weight variation was minimal and concluded not to produce the observed effect. The logical explanation had to be with the pilot/aircraft closed-loop dynamics or how the helicopter is flown.

There are two possible sources that could produce the observed anomaly. The first being rates induced by the pilot during the firing procedure and the second being how the downwash changes with application of control.

PILOT INDUCED RATES

The pilot induced rates at the firing has been documented during the SEAS baseline data. The pilot typically maintained a trimmed attitude during the countdown, at approximately T-10 seconds, he would attempt to put the pipper on the target and fire rockets when it was accomplished, independent of countdown. During the SEAS baseline tests, the sight setting required that he nose up the aircraft from trimmed attitude by 2.5 mils. This would produce a pitch up rate.

During the test series with the modified loading in which the aircraft c.g had moved aft, for the same sight setting as before, the pilot had to nose down the aircraft from trimmed attitude by 3 mils. This would produce a pitch down rate. The test results indicated that the SEAS baseline data achieved a longer range than that with the modified aircraft which is consistent with the analysis that the SEAS baseline data had a pitch up rate at firing.

This analysis is based on the assumption that the pilot, once he started his motion toward the target fired the rockets on his first pass. A preliminary analysis on the sight camera data indicated that this was true sometimes. To date, a qualitative analysis of aircraft rate and individual rocket impacts has not been completed to determine any correlation.

DOWNWASH VELOCITY VECTOR MAGNITUDE VARIATION

Assuming a constant collective power setting at hover and zero cyclic input, a flow field vector diagram can be visualized as represented by the top sketch of Figure 8. There is a steady state balance of flow fore and aft through the rotor. Only the forward semicircle of the downwash is seen by a rocket being launched. Now if a stick forward cyclic is input, the flow field changes to that shown in the middle sketch. An increase in flow through the rear sector and a corresponding decrease in flow through the forward sector occurs. Since the area of the flow pattern is fixed, the change in flow is due to a change in velocity. A reduced forward disk sector downwash velocity occurs· with the nosedown cyclic input and conversely an increase occurs with the nose up cyclic as represented in the lower sketch. A rocket launched under nose down cyclic induced flow change will experience less weathercocking than one launched at zero cycl'c input. From the small data base represented pitch rate effect and downwash magnitude effect are inseparable. However, they are directionally additive; and since the differential force change

drives the rate, and sight film often shows slewing an opposite direction rate at trigger, downwash magnitude appears to be the prime source of the rocket pitch rate variation. The other evidence of high weathercock response also supports this conclusion.

Although no data has been taken, a similar downwash interface characteristic should be expected in the transverse plane that will differentially affect left and right rounds simultaneously fired. Roll rate would be directionally additive as was pitch. This effect may be expected to dominate the geometric reduction of θ_{TRIM} due to roll angle in producing range spread of a left-right pair. A small roll angle at launch coupled with a strong cyclic input to remove it could be the dominant source of trajectory crossover.

CONCLUSIONS

The tests were conducted on two fin-stabilized rocket systems and both demonstrated a range anomaly with total quadrant elevation variation. The rocket systems themselves did not cause the observed effect. It was shown that a helicopter-rocket interface anomaly exists in at least two situations.

One parameter is the rocket pod attitude relative to downwash flow field. Two distinct range versus total QE profiles were obtained. The profile for the pod elevation of 40 - 78 mils had a larger slope than that for the pod elevation of 80 - 160 mils.

Additional data from these tests indicated that the downwash flow field should be taken advantage of, instead of trying to minimize its effect. No evidence was seen that expensive and complex concepts of rocket fin deployment, delay mechanisms or attempts at synchronization of the rocket firing with rotor position is necessary.

The other parameter is the pilot/aircraft dynamics which consist of pilot induced rates and downwash velocity vector magnitude variation. The test results did indicate that the pilot can induce both at the time the rockets are fired. Preliminary analysis indicate the rate and downwash magnitude effects are directionally additive but inseparable without special isolation tests.

Due to the lack of rockets to test, the cross-coupling of critical pod elevation, and pilot/aircraft dynamics was not analyzed but the possibility that there is a cross-coupling is high.

RECOMMENDATIONS

The need for future evaluation (both analytical and empiri-
cal) is required in order to establish any correlation in the
pod elevation angle, pilot/aircraft dynamics and cross coupling.
The data would be utilized in establishing new fire control
equations that would account for the observed anomalies.

It is necessary that the equations be established because
current ones cannot handle the whole problem and additional
sensors are required to supplement the equations. Possible
additional sensors would be engine torque monitor, pitch and yaw
rate gyros, and downwash flow field magnitude.

CRITICAL GEOMETRY

POD
ELEVATION

AIRCRAFT
DATUM LINE

HORIZONTAL

θ_E

TRIM

$\theta_{CONTROL}$

CONTROL
LINE OF SIGHT

QE_{TOTAL}

TARGET

RANGE

ALTITUDE
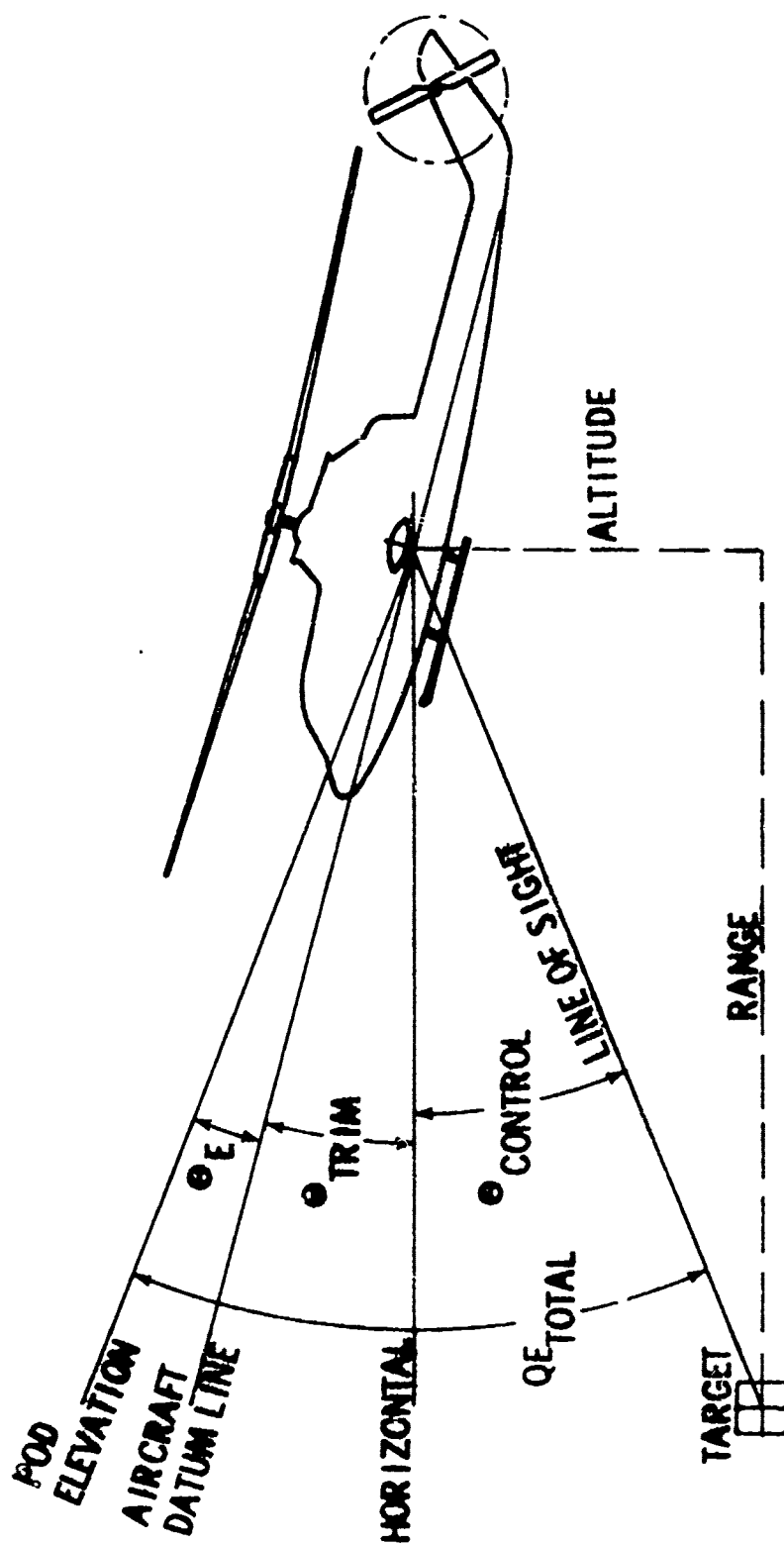
$QE_{TOTAL} = \theta_E + A/C$

$A/C = TRIM + CONTROL = SIGHT$

$QE_{TOTAL} = \theta_E + SIGHT$

FIGURE 1

110

IDENTIFY ANOMALY

ROCKET SYSTEM EVALUATION
(ARROW)

CONSTANT POD ELEVATION
71.5 MILS

TOTAL QUADRANT ELEVATION - MILS

RANGE - KILOMETERS
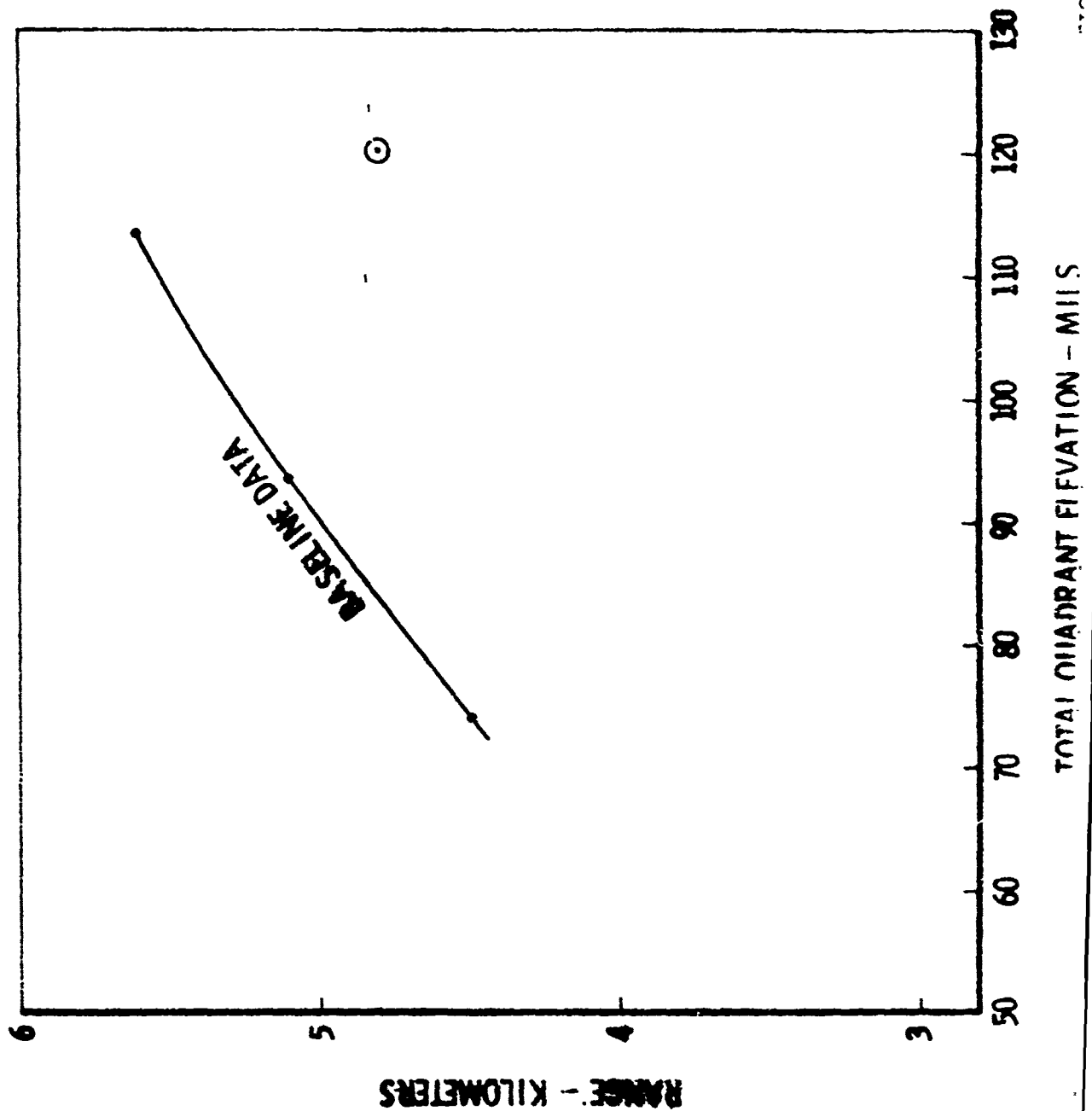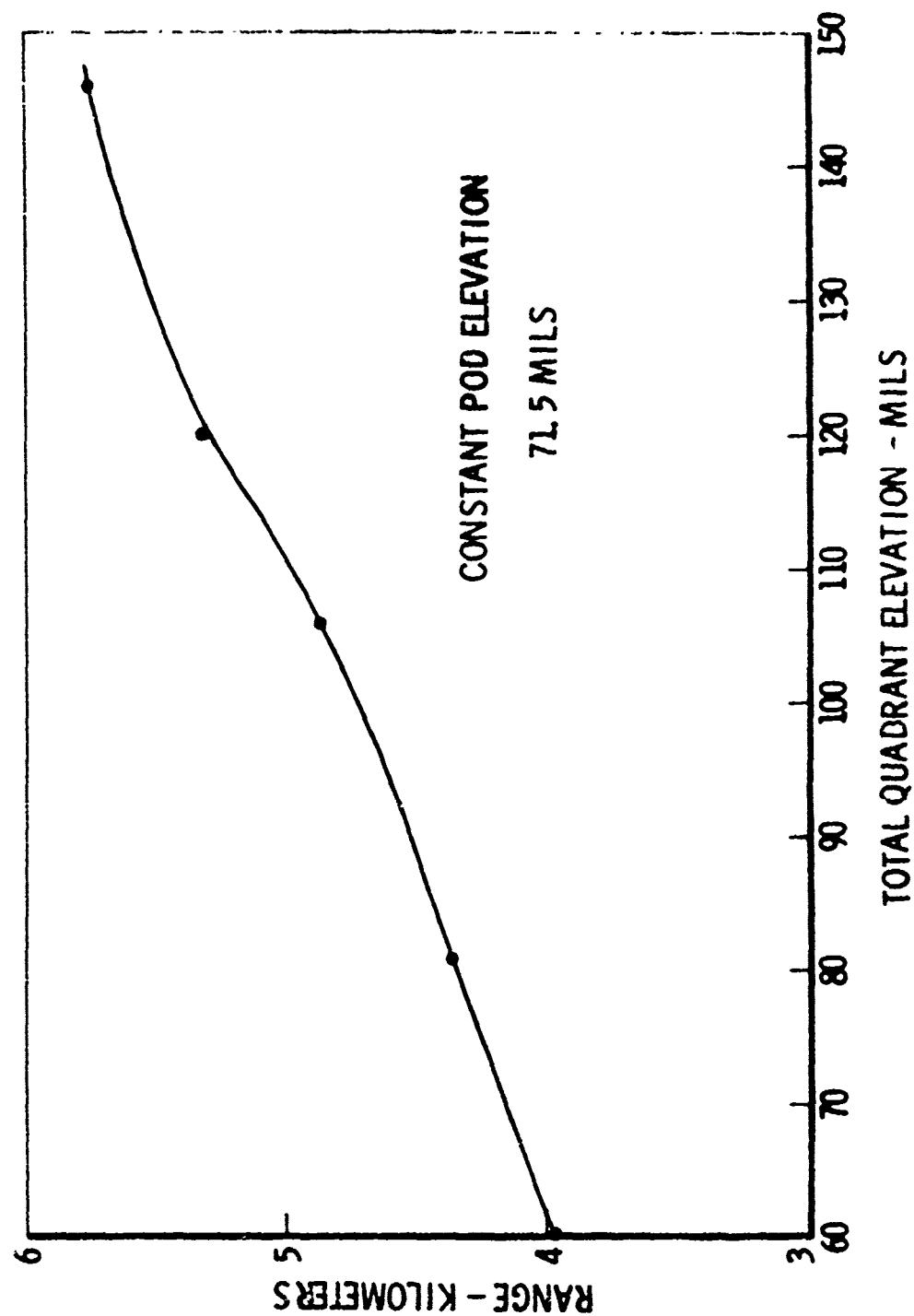
FIGURE

POD ELEVATION EFFECT
(ARROW)

POD ELEVATION

A 40 – 78 MILS

B 88 – 160 MILS

TOTAL QUADRANT ELEVATION – MILS

RANGE – KILOMETERS

FIGURE 4

113
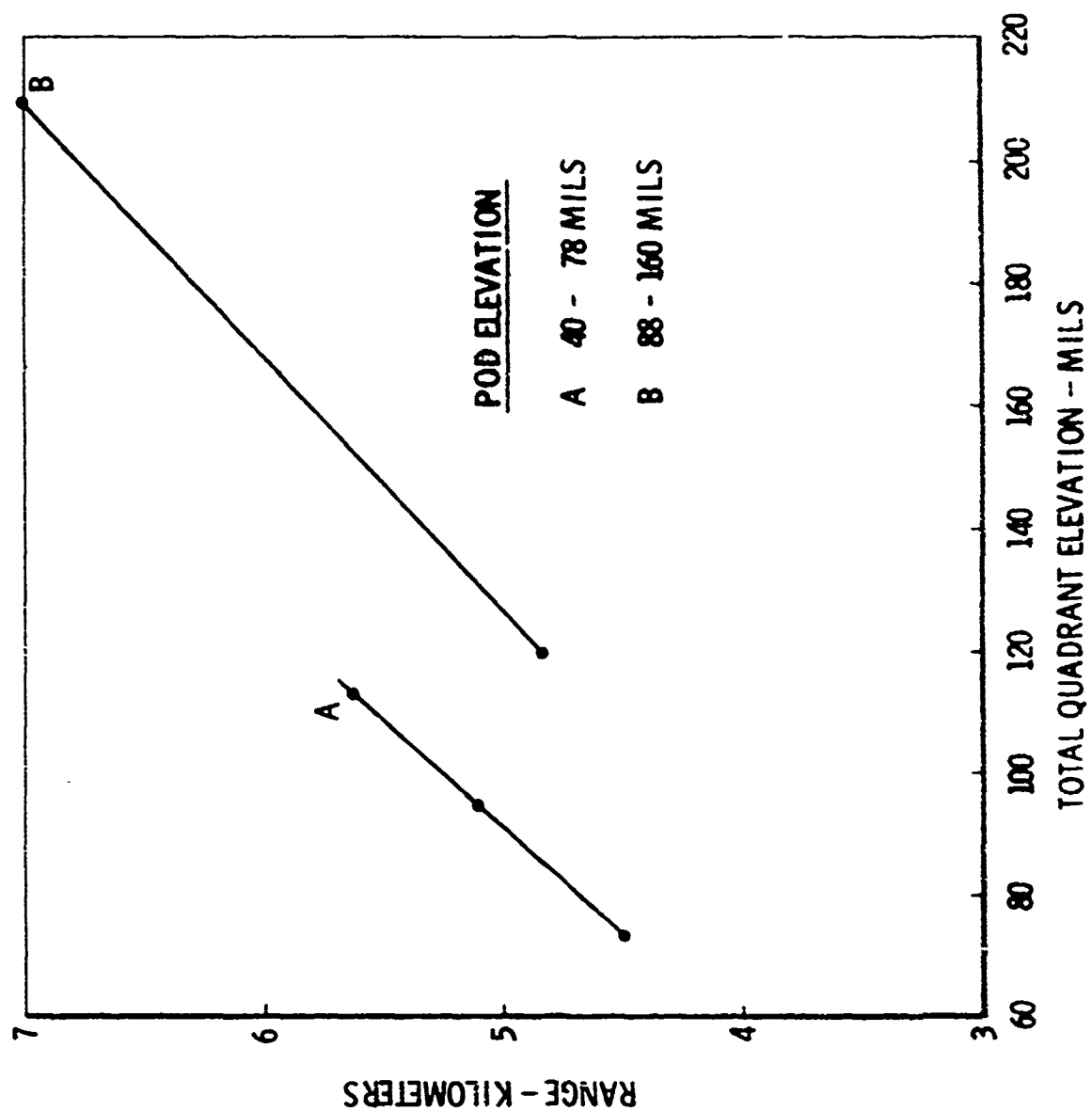
DOWNWASH AND/OR DYNAMICS
EFFECTS — 2.75″ FFAR

POD ELEVATION
o 100 to 160 MILS
□ 72 MILS

TOTAL QUADRANT ELEVATION — MILS

RANGE — KILOMETERS

FIGURE 5

114

AIRCRAFT – ROCKET INTERFACE

POD ELEVATION

ROCKET TRAJECTORIES

DOWNWASH – HOVER

FIGURE 6

115
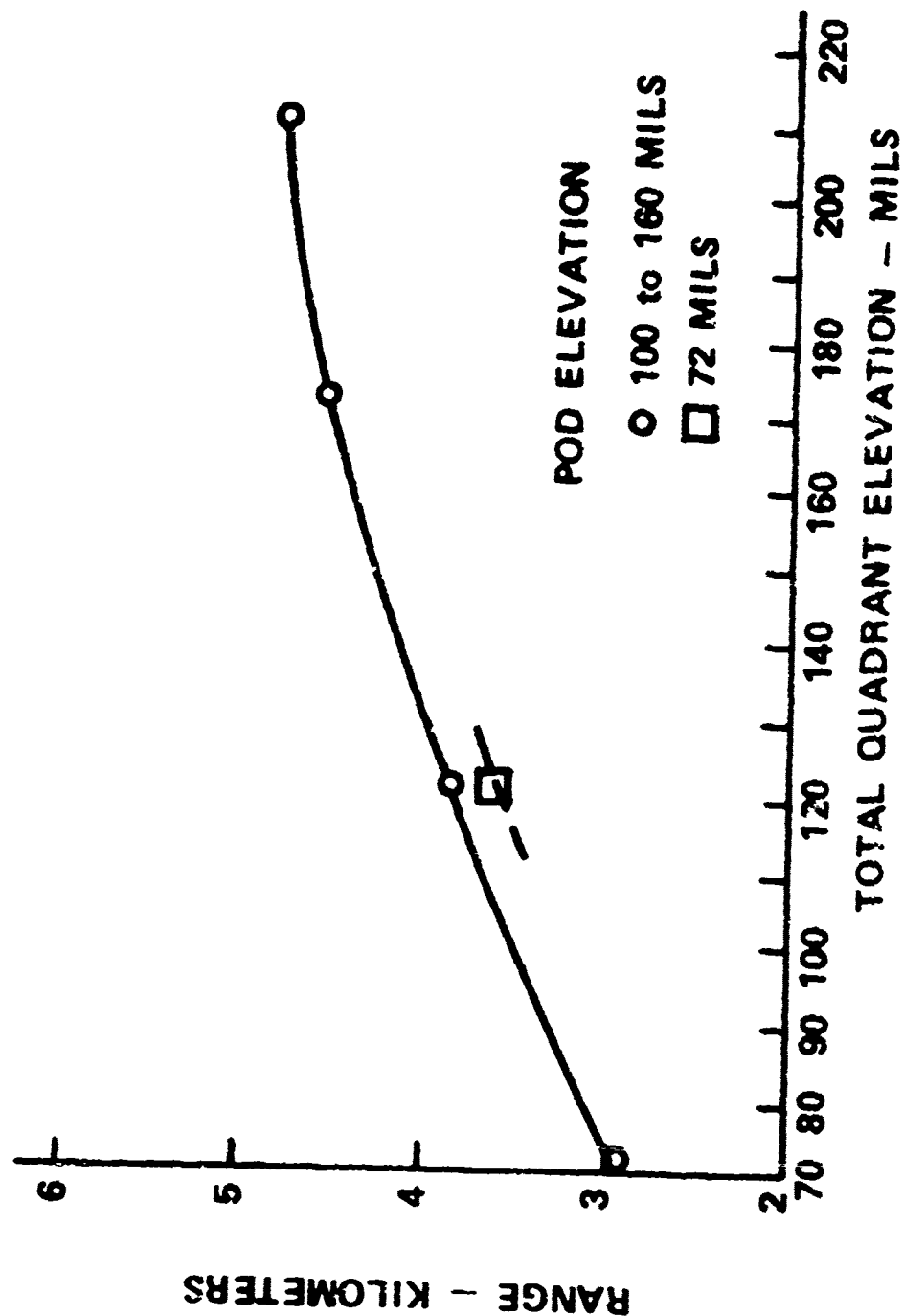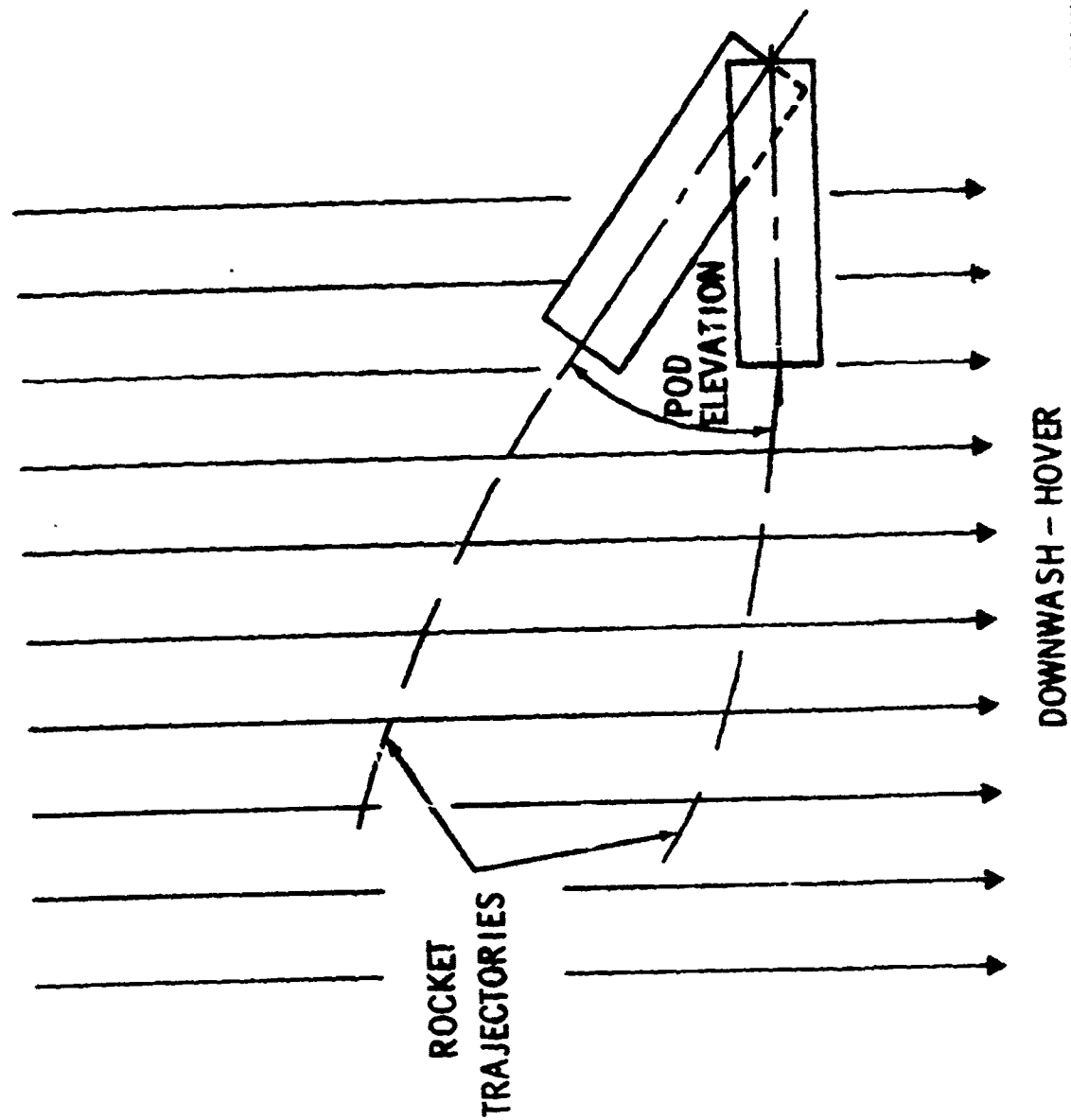
AIRCRAFT Θ_{TRIM} EFFECT

(ARROW)

VELOCITY MAGNITUDE SHIFT
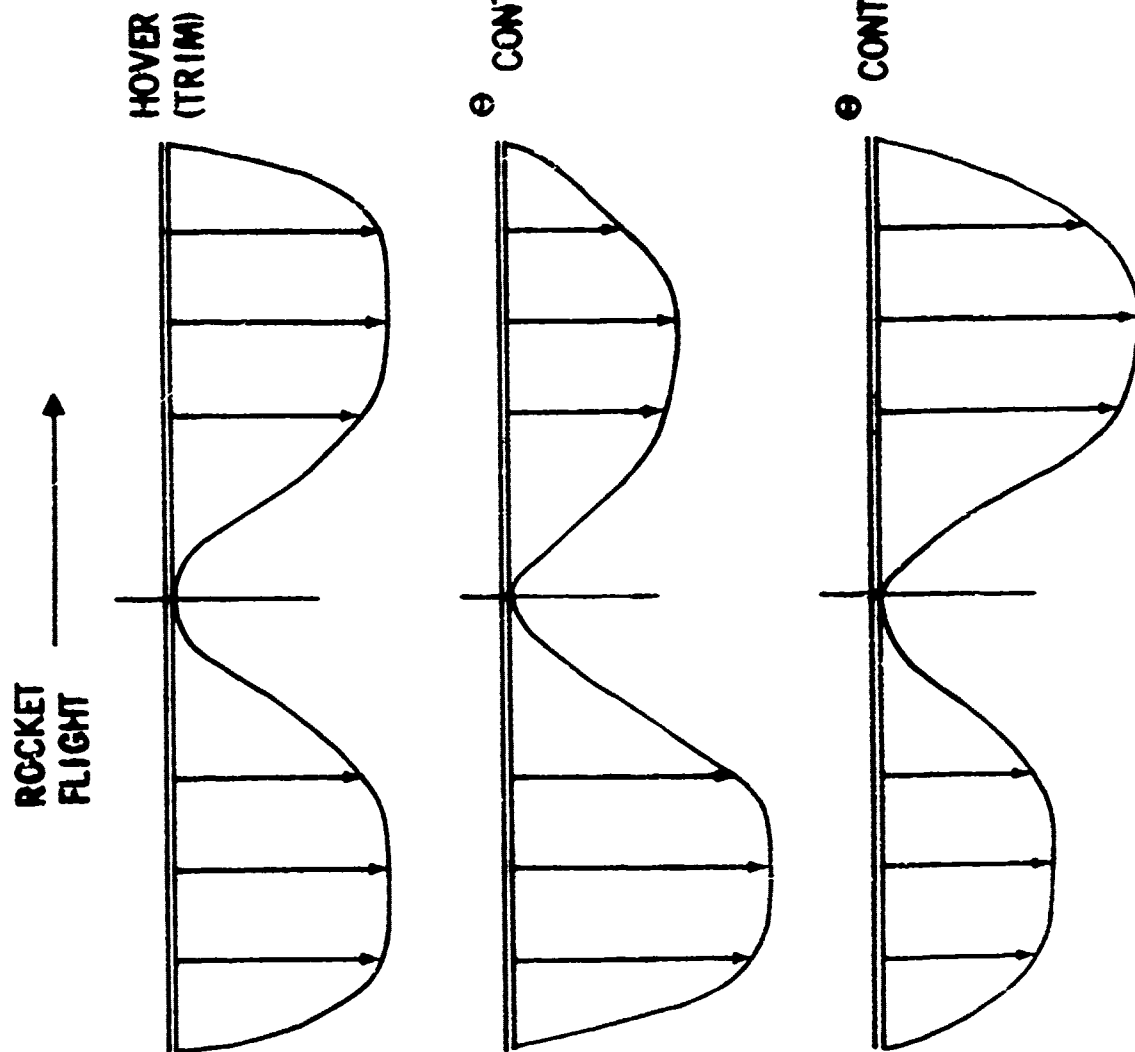
ROCKET
FLIGHT

HOVER
(TRIM)

Θ CONTROL (-)

Θ CONTROL (+)

FIGURE 8

117

INTERACTION OF AIR FLOW AND HELICOPTER
CHARACTERISTICS ON THE 2.75 INCH ROCKET SYSTEM

ROBERT BERGMAN
2.75 INCH ROCKET PROJECT MANAGER'S OFFICE
HUNTSVILLE, AL

ABSTRACT

The 2.75 Inch Rocket Project Manager sponsored the initial Rocket/Air Flow
Research Project. This presentation is short, general in information and
serves to introduce the next two presentations which will be more detailed.

A short silent film will be presented. The films were taken during a MASSTER
Test at the Naval Weapons Center. This presentation includes narrative
for the movie.

INTERACTION OF AIR FLOW AND HELICOPTER
CHARACTERISTICS ON THE 2.75 INCH ROCKET SYSTEM

INTRODUCTION

My briefing will be short and general in information. I want to describe
why this old rocket system is so interested in air flow and resolving its
effects. The two presentations following will be more detailed.

Most of you are familiar with the 2.75 Inch Rocket, however, just in case,
I wanted everyone to review its configuration. The MK 40 motor for low speed
aircraft was adopted from a Navy design, the MK 4 motor which is still launched
from fixed wing aircraft. The MK 40 rocket nozzles are scarfed to impart a
low spin rate after it exits the launcher. The fins are deployed by a piston
after exit. This rocket happens to have a 10 pound white phosphorus warhead
with a mechanical point detonating fuze.

One of the standard AH-1G loading configurations is the "Light Hog" with 2-7
tube launchers on the out-board stations and 2-19 tube launchers on the in-
board stations. The rocket, warheads, fuzes and launchers have been the limit
of the mission of our office.

SYSTEM DEVELOPMENT

To review the progress of the rocket system development, the baseline system
in Column 1 of Figure 1 is what is currently being used by the Army.

The AH-1G has a fixed sight and a simple intervalometer. Our Office manages
the launcher and rocket production.

In the last 1960's, the Army identified a need for remotely setting fuzes
while in flight. This has become known as the Product Improvement Program
(PIP), column 2 of Figure 1. Picatinny Arsenal and MICOM worked on the
development of a fuzing system and launcher to fire two types of remotely set
fuzes: The M433 for high explosive warheads, and the M439 for flechette warheads.
During the same timeframe, we did some work on methods for rapidly rearming the
Cobra for quick turn-around.

This fiscal year, our work with TRADOC has developed into a program to
provide the 2.75 Inch Rocket System with necessary improvements as shown
in Column 3 of Figure 1.

The Cobra Product Manager has been assigned the responsibility to develop
an integrated helicopter fire control. This will also include a Stores
Management and Remote Fuze Setting combination which will be lighter than the
existing XM 40 Fuze Setter.

119

TRADOC has identified the need for lighter weight launchers to allow a larger ordnance load. The self-loading adapter will satisfy the need for rapid rearm by being able to crank a fully loaded launcher into place.

Our Office is reviewing the possibility of transferring some of the technology developed under the SEAS Program to the MK 40 motor. The new fuzing system will still control the same electronic fuzes. The M255 warhead with M439 fuze then will become the basis for a family of common canister warheads which can contain smoke canisters, submunitions, an illumination candle, Chaff or target marking materiel.

2.75/AH-1G SYSTEM

However, being only responsible for the last two items on Figure 2 does not mean we're not interested in the rest of the system and how it works. We can not address one piece of the system in isolation from the rest, even back to the pilot's input.

We view the need for air flow information to be related to the fire control area in order to achieve a predicted impact point for the pilot sight. But even air flow research must not be totally extracted from the context of the system.

MOVIE

In Vietman, the standard attack helicopter technique was high angle, diving fire from relatively short range. Under these conditions, the pilot could adjust his fire and become expert in putting the weapon effects where he wanted.

Diving fire was used with most weapons and the effect of range estimation error and variation in aircraft flight attitudes were minimized.

Since the attack helicopter environment has changed to one of highly lethal air defense, the attack technique has been changed to low level flight or terrain flying. The object is to stay as close to the deck as possible.

These films were taken during a MASSTER Test at the Naval Weapons Center last fall.

The MASSTER Tests included running fire with forward airspeed, direct hover fire and indirect fire.

In many cases, the terrain at the launch points was below that of the target so that the pilots were in effect, firing up-hill or at their same altitude.

The quick climb, fire and back down, reduces aircraft exposure time to air defense units.

This is a view through the standard fixed reticle sight on a Cobra during the rocket run. Notice the movement in the pitch dimension as the rockets are fired.

Although the aircraft pitches, the stable rockets weathervane back into line with the aircraft vector and the impact pattern basically stays together. Fire Control will help put the pattern on the target.

The investigation into the effects of airflow must include the accurate resolution of the forward airspeed vector if we are to have a good fire control system.

MASSTER achieved good target coverage with these standard rockets with inert warheads by knowing the range and developing a standard firing technique. Fire control with full resolution of all the aircraft factors will allow placement of the weapon pattern on target under combat conditions.

Changing now to the hover fire tactics: Some of the best film that I have access to is this series taken when the UH-1 was first armed by MICOM with the 2.75 Inch Rocket. Most of these films were taken with the aircraft at low level, so there was definite ground effect. The fact that the helicopter is hovering in ground effect, significantly reduces the vertical velocity and thereby, the rocket response.

Notice how the aircraft position changes significantly, and no doubt his aim point during this ripple of 24 pairs of rockets.

The MK 40 rocket motor was originally designed for high altitude launches, so the large fins give it a high stability margin when launched at helicopter altitudes.

The stability of the rocket causes it to weathervane up into the downwash air flow. The degree of pitch up depends upon air flow velocity and the length of the trajectory through the downwash. This trajectory length changes dynamically in the hover regime.

MASSTER tried hover firing from both low level and higher altitudes.

The gun camera film illustrates the basic oscillation of the Cobra at hover. The best the pilot can do is pickle off the rockets when the pipper is close to the target. Then the sight pictu: : changes as soon as the first rockets are launched.

On this run, the sight picture was a little off the gun target line when the trigger was pressed.

The resolution of the hover fire problem will have to include the variability in aircraft attitude as well as the air flow parameters.

Note that on some of these ripples that the Cobra ends up flying backward and has to then dump the nose the fly forward to get back to the original fire point. This aspect amplifies the variability of hover fire.

121

This sequence shows the MASSTER Test phase when two aircraft were fired from hover for indirect fire. The rockets were launched over a hill to a target whose range and azimuth were known. In a pop-up maneuver, the aircraft will be starting at low level, attaining a vertical acceleration in order to achieve sufficient altitude to acquire a line of sight to the target. The weapon will have to be fired sometime during the pop-up and the aircraft has to have sufficient performance to recover before he crashes.

In any case, the object is to provide the pilot with a continuously predicted impact point so he can put the rounds on target at any airspeed.

HELICOPTER RESPONSE

To detail the characteristics of a Cobra helicopter at hover, Figure 3 shows the results of a 19-pair ripple of rockets during a test at Yuma Proving Ground last fall. You will notice that the pitch changed 2 degrees and the yaw changed 4 degrees during the time the rockets were exiting the launchers. This data validates the need for better helicopter stability, particularly if accurate hover fire is the goal.

HOVER FLIGHT REGIME-TACTICS

After MASSTER had conducted their experiment 1053, two years ago, we came up with the conclusions shown in Figure 4 about the hover flight regime. The recent movies and tests verify the aim instability. The research into air flow will tell us what is happening in the turbulent downwash and how much rotor wake to expect. The pilot is probably more concerned with the fact that at hover, his ordnance load is severely reduced from what he can carry if he is in forward flight.

HOVER FLIGHT REGIME-DETAILS

When one looks at the effect of hover flight, and the effects of downwash on the rocket, we decided the items shown on Figure 5 were important factors to be considered. At that time I could only find limited information on these components. Consequently, our Office took advantage of an opportunity to sponsor the air flow study which Dr. Landgrebe will address in the next presentation.

HELICOPTER AIR FLOW

To summarize the view of our Office with regard to air flow research, we see the need to accomplish objectives shown in Figure 6 for both current and future helicopters. Next, the effect on the rocket or other weapons needs to be evaluated. We also need improved air data sensors for fire control and air flow research.

Finally, the overall information needs to be applied to the fire control solution.

I will leave the details of the air flow study and rocket analysis to Dr. Landgrebe and Mr. Wasserman. I might say that our office appreciates the extra-ordinary initiative and effort that these two gentlemen have put into this task.

2.75 INCH ROCKET SYSTEM DEVELOPMENT

BASELINE SYSTEM	PIP PROGRAM	IMPROVED SYSTEM
AH–IG AIRCRAFT		
M73 FIXED SIGHT	—	INTEGRATED FIRE CONTROL
MOD C INTERVALOMETER	—	STORES MANAGEMENT
—	XM40 RC FUZE SETTER	REMOTE FUZE SETTER COMBINATION
LAUNCHER		
M158 – 7 TUBE	—	7 TUBE – LIGHTWEIGHT
M200 – 19 TUBE	XM227 RC LAUNCHER	19 TUBE – LIGHTWEIGHT
STANDARD PACKING	RAPID REARM	SELF-LOAD ADAPTER
ROCKET		
MK40 MOTOR	—	SFAS TECHNOLOGY
HE WHDS	HE/M433 RC FUZE	HE/M433 RC FUZE
FLECHETTE WHD	M255/M439 RC FLECHETTE	M255/M439 RC FLECHETTE
		(BASIS FOR COMMON CANISTER FAMILY)
WP WHD	—	SMOKE SCREEN WARHEAD
		MULTIPURPOSE SUBMUNITION WARHEAD
		ILLUMINATION WARHEAD
		CHAFF WARHEAD
		DAY/NIGHT MARKER WARHEAD

FIGURE 1

123

SYSTEMS INTEGRATION

2.75 INCH ROCKET/AH—1G SYSTEM

COMPONENT:	FUNCTION:
PILOT	TACTICAL EMPLOYMENT
AH—1G	OPERATIONAL VEHICLE
FIRE CONTROL	SYSTEM INTEGRATION
	PREDICTED IMPACT POINT
	RANGE
REMOTE SET FUZE SYSTEM	CONTROL WARHEAD EFFECTS
LAUNCHER	STORAGE AND LAUNCH
ROCKET—WARHEAD—FUZE	DESTRUCTIVE VEHICLE

FIGURE 2

124

6

AIRCRAFT RESPONSE DURING RIPPLE FIRE FROM HOVER
19 PAIRS AT 160 msec INTERVAL

FIGURE 3

125
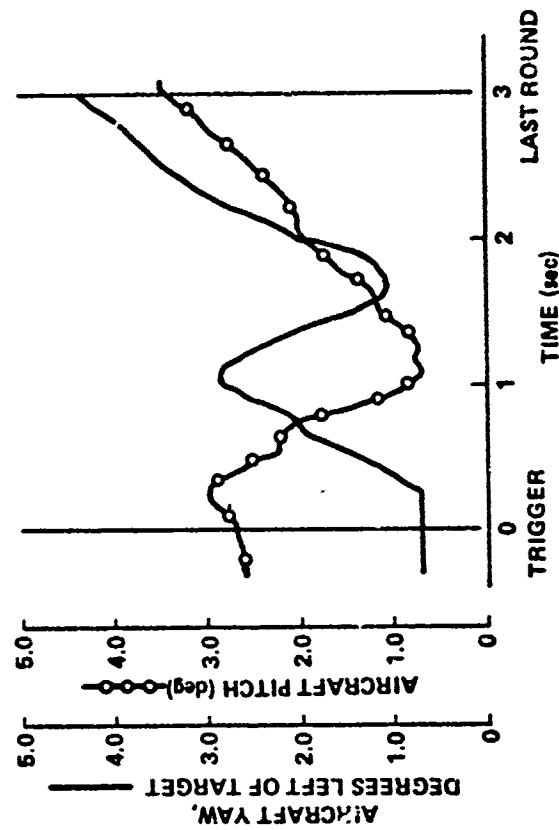
HELICOPTER HOVER FLIGHT REGIME

AIM INSTABILITY

PULSATING TURBULENCE

VARIABLE EFFECT OF ROTOR WAKE

23 NOV 73

FIGURE 4

HELICOPTER HOVER FLIGHT REGIME

- TIP VORTEX
- VORTEX SHEET
- TURBULANCE IN LAUNCH ENVELOPE
- LOCATION OF ROTOR WAKE
- EFFECT OF FUSELAGE

FIGURE 5

127

HELICOPTER AIRFLOW

OBJECTIVES:

- DETERMINE DOWNWASH CHARACTERISTICS (CURRENT AND FUTURE HELICOPTERS)

- ANALYZE EFFECTS ON ROCKET TRAJECTORY

- DEVELOP IMPROVED FIRE CONTROL AIR DATA SENSORS

- APPLY INFORMATION TO FIRE CONTROL SOLUTION

FIGURE 6

Anton J. Landgrebe
Supervisor, Rotary Wing Technology
and
T. Alan Egolf
Associate Research Engineer

United Technologies Research Center
East Hartford, Connecticut

SUMMARY

An analytical investigation was conducted to predict the rotor wake induced flow velocities along the trajectories of rockets fired from an Army AH-1G helicopter. The three components of both the time-averaged and instantaneous induced velocities were predicted at selected points along the trajectories of rockets fired from four wing locations. Three flight conditions with helicopter flight speeds of 0, 15, and 30 knots were investigated. The sensitivity of the predicted induced velocities to rotor wake model, rocket launch attitude, and rocket launch position was also investigated. Velocities induced by tip vortices near the intersections of the rocket trajectories with the wake boundary were found to be similar in magnitude to the launch velocity of the 2.75 in. rocket currently in use on AH-1G aircraft. Values of the downward induced velocity component as high as 70 fps (time-averaged) and 130 fps (instantaneous) were predicted for the hover condition, and the velocities decrease with increasing flight speed. For flight speeds greater than approximately 30 kts, the rotor wake passes behind the rocket launch position which significantly reduces the wake induced effects. The location of the rotor wake boundary relative to the rocket trajectories is a major determinant of the induced velocity distribution along the trajectories. Thus, the use of an accurate wake geometry was found to be important for accurate calculations of the induced velocities at the rocket.

The results of this analytical investigation were published in March 1975 in U.S. Army Picatinny Arsenal Technical Report 4797, "Prediction of Rotor Wake Induced Flow Velocities Along the Rocket Trajectories of an Army AH-1G Helicopter." This paper, presented on August 12, 1975 at the Conference on the Effects of Helicopter Downwash on Free Projectiles sponsored by the U.S. Army Aviation Systems Command, is a condensation of that report.

R	rotor radius, ft
V	forward flight velocity, fps
v_{x_T}, v_{y_T}, v_{z_T}	instantaneous induced velocity components in rocket trajectory coordinate system (x_T, y_T, z_T); sign convention is consistent with coordinate definition, fps
$v_{x_{T_{AVG}}}$, $v_{y_{T_{AVG}}}$, $v_{z_{T_{AVG}}}$	time averaged induced velocity components in rocket trajectory coordinate system (x_T, y_T, z_T); same sign convention as v_{x_T}, v_{y_T}, v_{z_T}, fps
x, y, z	hub centered axis system coordinates nondimensionalized by R, x-y plane parallel to rotor tip path plane, right handed coordinate system with positive x downstream (see Fig. 5)
x_T, y_T, z_T	rocket trajectory axis system coordinates nondimensionalized by R, centered at intersection of axis of rocket launch positions and fuselage centerline, left handed coordinate system with positive x_T in direction of rocket travel (see Fig. 1)
μ	rotor advance ratio, component of V parallel to rotor tip path plane nondimensionalized by rotor tip speed
ψ	blade azimuth angle measured from x axis (see Fig. 1), positive in the direction of rotation, deg

INTRODUCTION

The accurate determination of the flow field around a helicopter is required when the helicopter is used as a weapons platform. Since a free-flight projectile such as a rocket, when fired from a helicopter, may initially be travelling at a speed which is of the same order of magnitude as the flow velocities, the flow field induced by the rotor wake system can have a significant effect on the rocket trajectory. This may necessitate some form of aiming compensation or special firing techniques -- particularly at the low helicopter flight speeds at which rockets are to be fired in accordance with current Army tactical concepts.

To assess the influence of the rotor/wake flow field on the flight path of a rocket fired from the Army AH-1G helicopter when hovering or flying at low forward speeds, computer analyses developed at the United Technologies Research Center, UTRC (formerly the United Aircraft Research Laboratories) were used to predict the induced flow velocities along the rocket trajectories. The four rocket trajectories of the AH-1G helicopter (commonly referred to as the Cobra) are shown in Fig. 1. The results of the Army sponsored investigation have been presented in Ref. 1, and this paper is a condensation of that reference report. The induced velocity results from this investigation have recently been used in Army trajectory analyses to assess the influence of the aerodynamic interference of the rotor wake on rocket trajectories (Ref. 2).

Included herein are (1) a brief description of the computer analyses used, (2) a description of the flight conditions and wake models used in the analyses, (3) presentation of selected induced velocity results for the three flight conditions analyzed, and (4) conclusions and recommendations.

BRIEF DESCRIPTION OF THEORETICAL METHODS

The basic components of the UTRC Rotor Analysis are shown in Fig. 2. Brief descriptions of the Prescribed Wake Rotor Inflow Analysis and the Wake Geometry Analysis are presented below.* More detailed information on the contents, assumptions and applications of the methods is contained in Refs. 3 through 8.

Prescribed Wake Rotor Inflow Analysis

The function of the UTRC Prescribed Wake Rotor Inflow Analysis is to compute the time varying circulation and induced velocity distributions along the rotor blades

---

* Blade motions and control settings were provided by the Bell Helicopter Company. Thus, the blade response analysis in Fig. 2 was not used for this study.

131

and in the wake that are compatible with a prescribed set of blade section operating conditions and a prescribed wake geometry. Each blade is represented by a segmented lifting line, and the wake is represented by a finite number of segmented vortex filaments trailing from the blade segment boundaries. The fundamental relations of blade circulation to lift coefficient, angle of attack, blade motions, control settings, induced velocity, and wake geometry are used in this analysis. Once the circulations are computed, the velocities induced at and away (e.g., at rocket trajectories) from the rotor disc by the bound and trailing vorticity of the rotor are determined through application of the Biot-Savart law which relates the induced velocity at a point in space to the circulations and wake geometry. The induced velocity is proportional to the summation of the products of the circulation strength and the geometric influence coefficient of each element of vorticity in the rotor-wake system. The geometric coefficient is related only to the relative geometry between a wake element and the point at which the induced velocity is being computed. Since the wake geometry is prescribed, the wake may vary from an undistorted wake model to a complex experimental or distorted analytical wake model with tip vortex roll-up and vortex core effects mathematically modeled.

Wake Geometry Analysis

The Rotor Inflow Analysis requires that the rotor wake geometry be specified in order for circulations and induced velocities to be determined. There are several alternatives for rotor wake geometry. Appropriate experimental wake data is certainly most desirable, but, except for hover, is not currently available for most rotor configurations and forward flight conditions.

In its simplest form, the wake from each blade can be assumed to be a classical undistorted skewed helical sheet of vorticity defined from momentum considerations (hereafter referred to as the undistorted wake). Sample undistorted wake representations are shown in Figs. 3(b) and 4 for hovering and forward flight conditions, respectively.

To eliminate the necessity for prescribing an undistorted wake geometry, an analytical method for computing more realistic wake geometries was developed at UTRC. The basic approach of this method, entitled the UTRC Rotor Wake Geometry Analysis, involves the following. First, an undistorted wake model is defined along with the distribution of circulation strengths of the various vortex elements comprising the wake. The classical Biot-Savart law is then applied to determine the velocities induced by each vortex wake element at numerous points in the wake. These distorting velocities are then numerically integrated over a small time increment to obtain new wake element positions. The process of alternately computing new velocities and positions is continued until a converged, periodic distorted wake geometry is attained.

For hovering conditions, systematic model rotor wake geometry data have been acquired experimentally at UTRC. The data have been generalized in Ref. 3 to facilitate the rapid estimation of wake geometry for a wide range of rotor designs and operating conditions and have been used to accurately predict the hover performance for a wide range of full-scale helicopters. A special computer subroutine has been prepared to model the hovering rotor wake in accordance with the generalized data. A comparison of the experimental hovering wake representation with the undistorted wake representation is presented in Fig. 3.

DESCRIPTION OF WAKE GEOMETRIES USED IN THE ANALYSES

For this investigation, the wake geometry analysis was used to generate wakes for the forward flight conditions, and the generalized experimental wake geometry was used for the hover condition.

The wake representation used in the analyses consisted of 10 finite vortex filaments trailing from each blade. These vortex filaments were divided into straight vortex elements at azimuth intervals corresponding to 15 degrees of blade rotation. The extent of the filament geometry was prescribed by 6 wake revolutions from the rotor except for the hover condition for which it was 8 revolutions. The five outer vortex filaments were combined beyond a 15 degree azimuth distance from the blade to simulate the roll-up of the tip vortex. Both undistorted and distorted wake models, described previously, were used to show the sensitivity of the results to wake geometry. For the undistorted vortex filaments, the vortex elements were positioned in a direction normal to the rotor disc in accordance with the mean induced velocity as determined from momentum theory at the rotor disc. The values of this momentum induced velocity for the 0, 15, and 30 kt flight conditions are -36.3, -31.6, and -22.9 fps, respectively. For the distorted wake representations, only distortions of the tip vortices were calculated for the two forward flight conditions and an undistorted inboard wake model was assumed. The latter assumption may be justified considering the relatively higher circulation strength of the rolled up tip vortices compared to that of the inboard vortex filaments.

The undistorted and experimental distorted tip vortex geometries for the hover condition are presented in Figs. 5 and 6. The analytical distorted tip vortex geometries for the 15 and 30 kt conditions are presented in Figs. 7 and 8. The primary difference between the undistorted and distorted wakes (Figs. 5 and 6) for the hover condition is the wake contraction. In addition, as shown Fig. 3, the inboard wake is transported downward with a nonuniform radially varying axial velocity which causes the outer portion to travel faster than the inner portion. At 15 and 30 kts, the tip vortex distortions result in a contraction of the forward boundary of the wake. This contraction of the wake has a predominant effect on the induced velocity distribution along the rocket trajectories in that it moves the intersection point of each trajectory with the wake boundary rearward, and thus decreases the duration of time that the rocket is inside the rotor wake.

133

DESCRIPTION OF FLIGHT CONDITIONS AND AIRCRAFT
CONFIGURATION USED IN THE ANALYSES

Induced velocities were calculated for the Army AH-1G helicopter, commonly referred to as the Cobra. A schematic of the AH-1G helicopter is shown in Fig. 1. The teetering type rotor of this helicopter has a radius of 22 ft. Each of its two blades has a nominal chord of 2.25 ft, a linear twist of -10 deg, a modified 0009 airfoil section, and a preconing of 2.75 deg.

The calculations were performed for a helicopter gross weight of 9500 lbs and a center-of-gravity position at 198.5 in. from the nose of the aircraft. Three flight conditions were investigated corresponding to flight speeds of 0 (hover), 15, and 30 kts. Considering the rotor tip speed of 746 fps, these flight speeds result in rotor advance ratios, μ, of 0, 0.034, and 0.068, respectively. The respective rotor control, flapping, and disc angles used in the analyses are presented in Ref. 1.

Induced velocity calculations were performed for the four rockets mounted at 0.39 R below and 0.034 R foward of the rotor hub, and lateral positions of 0.16 R and 0.22 R on both sides of the fuselage centerline. The rocket launch attitudes were all specified at an elevation of 126 mils (7 degrees) relative to the fuselage water-line except in a sensitivity study where 160 and 195 mils were used. It is noted that each rocket was assumed to be concentrated at a point (center-of-gravity) when determining the launch point. Induced velocities were calculated at increments of 0.1 R along the rocket trajectories from the launch point. The trajectories from the launch point to a distance of one rotor diameter (extent of calculation) were assumed to be straight lines. The coordinate system (x_T, y_T, z_T) used for the predicted induced velocities is referenced to the rocket launch point and the axes are parallel and normal to the rocket trajectories as shown in Fig. 1. Positive directions are also shown in Fig. 1.

DISCUSSION OF INDUCED VELOCITY RESULTS

The three components of induced velocity, v_{x_T}, v_{y_T}, and v_{z_T}, were calculated along each rocket trajectory numbered 1 through 4, as shown in Fig. 1. Since the orientation of the rotor blades and wake relative to a point on a rocket trajectory varies with time, the instantaneous velocity components induced at that point also vary with time. Since steady flight conditions were selected for this investigation, the positions of the blade and wake and the resulting velocities are periodic. The period is the time corresponding to the blade passage interval, which for the 2-bladed AH-1G rotor is the time required for a blade to travel 180 degrees. Thus, time was expressed in terms of increments of rotor rotation designated by rotor position and the corresponding azimuth angles of the two blades. The calculations were performed using an azimuth increment of 15 degrees, which resulted in 12 rotor positions per blade passage interval.* In addition to the instantaneous velocities at each rotor position, the time-averaged velocities were calculated.

The major variables for this investigation and the notation to be used for the plotted results are summarized below:

Major Variables

Flight Conditions	$V = 0, 15, 30$ kt
Wake Models	Distorted, Undistorted
Instantaneous Velocity Components	$v_{x_T}, v_{y_T}, v_{z_T}$
Time-Averaged Velocity Components	$v_{x_{T_{AVG}}}, v_{y_{T_{AVG}}}, v_{z_{T_{AVG}}}$
{Rotor Positions (Time Step)	$1, 2, 3, \ldots, 12$
{Blade Azimuths, ψ, deg	$0, 180; 15, 195; 30, 210; \ldots 165, 345$
{Rocket Number	$1, 2, 3, 4$
{Rocket Lateral Position	$y_T = -0.22, -0.16, 0.16, 0.22$
Position Along Rocket Trajectory	$x_T = 0, 0.1, 0.2, \ldots, 2.0$

In addition to all combinations of these variables, a few computer cases were run to investigate the sensitivity of the results to rocket launch attitude and launch position.

In total, six basic cases (3 flight conditions x 2 wake models) plus three sensitivity variations were run. Considering the 3 velocity components, 4 rockets, 21 rocket trajectory points and the 12 rotor positions plus the time-average velocities, a total of 3276 velocity values were computed for each of the 9 cases. Tabulations of these values have been provided separately to the Army. In Ref. 1 a judicious selection was made of combinations of variables for which velocity data comprising 40 figures

---

* For the AH-1G, and a rocket speed of 100 fps, a rocket travels a distance of 0.42 R during a blade passage interval (one-half rotor revolution).

were presented. A sampling of these figures, selected to convey the primary results for the hover and forward flight conditions, are presented and discussed below.

Condition (V = 0)

The variation of the time- v_{Z_T} velocity along the rocket trajectories of all four rockets, based on the distorted wake model, is presented in Fig. 9. This velocity component normal to each trajectory, increases from approximately 30 to 70 fps (downward) going from the rocket launch position ($x_T = 0$) to the intersection of each trajectory with the wake boundary shown in the top view in Fig. 6, (e.g., at $x_T = 0.77$ for rocket 4). Moving from inside to outside of the wake boundary an abrupt change in velocity occurs in both magnitude and direction (downflow to upflow). The upflow is not as severe as the downflow because the contributions of the tip vortices and the inboard wake are opposing outside of the wake, whereas they are additive just inside the wake. As the rocket moves away from the wake, the velocity decreases as expected. It is also shown in Fig. 9 that the influence of the different lateral positions of the four rocket trajectories on this average velocity component is small.

In Fig. 10, the instantaneous v_{Z_T} velocity component is presented for rocket 4 and four selected rotor positions. Near the wake boundary the instantaneous velocities vary significantly with rotor position. This time variation is clearly shown in Fig. 11 where the v_{Z_T} velocity is plotted versus rotor position for selected trajectory points both near and far from the wake boundary. For the rocket launch point ($x_T = 0$), the variation with rotor position is relatively small. At the farthest point calculated ($x_T = 2.0$), the 2 fps velocity is negligible, considering its effect on the rocket. The variation is generally small for points in the wake up to the region of $x_T = 0.7$ as shown by the abrupt change in the peak-to-peak values between $x_T = 0.6$ and 0.7. At $x_T = 0.7$, the velocity component ranges from 36 to 130 fps in the downward direction. It is noted that the 130 fps flow velocity exceeds the initial rocket launch velocity which is approximately 100 fps. The cyclic nature of the induced flow at a frequency of once-per-blade passage is a direct result of the passage of the tip vortex, and to a lesser extent the inboard vortex sheet, past the trajectory point. The peak downward velocity of 130 fps occurs when the tip vortex is closest to the point. The magnitude of the velocity is low (36 fps) at rotor position 1, because as shown in Fig. 6, the trajectory passes approximately mid-way between the tip vortices at this rotor position. Similar results were generally predicted for the other three rocket trajectories.

Results for the v_{x_T} and v_{y_T} velocities are included in Ref. 1. The time-averaged v_{x_T} velocity was predicted to be in a direction opposite to that of the rocket travel, and the peak value of 23 fps predicted near the wake boundary is significantly less than the 70 fps of the v_{Z_T} velocity component. Instantaneous values as high as 60 fps were predicted. The v_{y_T} velocity component, which is in a direction to influence the lateral motion of the rockets, was predicted to have the lowest magnitude of the three components. The predicted time-average velocity did not exceed 10 fps, and the instantaneous velocity did not exceed 25 fps.

Two primary effects of wake model, distorted versus undistorted, on the induced velocity components were noted. The predominant difference observed from the time-average velocity results in Ref. 1 is the outward shift of the point at which the velocity components change abruptly, caused by the outward shift of the uncontracted wake boundary of the undistorted wake evident in a comparison of Fig. 5 with Fig. 6.

The predominant effect of wake model on the instantaneous velocity components also occurs in the region of the wake boundary, and consists of a shift in the time (rotor position) at which the peak velocities occur at rocket trajectory points in this region. This is evident in a comparison of Fig. 12 with Fig. 11. These differences indicate the importance of accurately representing the wake when predicting induced velocities at rocket trajectories.

In order to show the sensitivity of the induced velocity component to small variations in rocket launch attitude, the launch attitude relative to the fuselage waterline was changed in 2 degree increments for the hovering flight condition. That is, the launch attitude was changed from 7 degrees (126 mils elevation) to 9 and 11 degrees (160 and 195 mils). Since the flight condition and distorted wake geometry were unchanged, the time-averaged velocity components did not change significantly with the small reorientation of the rocket to the time-averaged wake geometry. However, the instantaneous velocity components in the vicinity of the wake boundary experienced a phase shift with rotor position due to the reorientation of the rocket trajectory to the tip vortices at a specific rotor position. This phase shift is shown in Fig. 13.

15 Kt Flight Condition

At the 15 kt flight condition, the wake boundary is skewed back toward the rocket launch point as shown in Fig. 7. The rocket trajectory intersects the distorted wake boundary between an x_T of 0.3 and 0.4. This results in the occurrence of the maximum downward velocity component (v_{z_T}) in that region as shown in Figs. 14 and 15. Thus, the rapid change in the skew angle of the wake with the small change in flight speed from 0 to 15 kts leads to a significant decrease in the distance from the launch point that the rocket is inside the rotor wake ($x_T \approx 0.35$ at 15 kts vs. 0.7/ at 0 kt). The maximum time-average downward velocity ($v_{z_{T_{AVG}}}$) at the four rocket trajectories ranges between approximately 40 and 60 fps (Fig. 14) compared to the 70 fps at 0 kts (Fig. 9). A representative variation of the instantaneous v_{z_T} velocity component for selected rotor positions is shown in Fig. 15.

20 Kt Flight Condition

It is shown in Fig. 8 that the predicted distorted wake is skewed just enough at 20 kt for the tip vortices to pass behind the rocket launch point. This placement of the rocket trajectories outside of the wake results in relatively low magnitudes (less than $\pm$ 10 fps) of all velocity components. This was true for both time-averaged

137

and instantaneous velocities. (Time-averaged velocities are presented in Fig. 16; instantaneous velocities are similar.) Also, only minor variations of the velocity components were predicted between the four rocket trajectories and the various rotor positions. It thus appears that beyond a flight speed of approximatly 30 kt the AH-1G rotor wake is swept behind the rocket trajectories, and the wake induced effects at the rockets are probably insignificant.

Use of an undistorted wake model, for comparison, placed the rocket launch point right at the wake boundary. The resulting close proximity of the tip vortices to the launch point resulted in large instantaneous velocities at certain rotor positions. To show the sensitivity of the induced velocity components to a change in rocket launch position, the launch position was moved forward and down by 0.05 R for the 30 kt flight condition. The selection of this example was based on the intent to show the potential for significantly reducing the induced effects at the rocket by moving the launch point outside the wake. As shown in Fig. 17, moving the launch point outside the undistorted wake by the 0.05 R movements mentioned above, results in a significant decrease in interference similar to that attained through use of the distorted wake model. This emphasizes the importance of accurately locating the wake boundary relative to the rocket launch point. The placement of the launch point inside, at, or outside the wake boundary results in an extreme difference in the predicted induced velocities. Changes in the relative position of the rocket launch point to the wake boundary can be produced by changes in any of the factors determining the wake skew angle (flight speed, aircraft gross weight, and rotor attitude as determined by the aircraft center of gravity location or maneuver condition).

CONCLUSIONS

The following conclusions apply to the AH-1G helicopter operating at hover and low speed flight conditions:

1. The magnitudes of the predicted induced velocity components at the trajectories can exceed the rocket launch velocity. Values of the downward induced velocity component as high as 70 fps (time-averaged) and 130 fps (instantaneous) were predicted.

2. Of the three velocity components, the greatest induced velocities were predicted for the downward component normal to the rocket trajectory. The component along the rocket trajectory was generally next in order of magnitude, and the smallest velocity magnitudes were predicted for the lateral component.

3. As the rocket moves from its launch position, the downward velocity component increases as the wake boundary is approached. As the rocket moves to the outside of the rotor wake the magnitude of the downward velocity decreases abruptly, and becomes insignificant within a distance of one rotor diameter from the launch position.

4. The position of the intersection of a rocket trajectory with the wake boundary is most influential for it determines the length of time that the rocket remains in the higher induced velocity region inside the wake. It also determines the location where the close proximity to a tip vortex can result in a high induced velocity. The importance of the wake boundary location establishes the importance of accurately determining the items which establish the wake skew angle -- flight speed, rotor and aircraft attitude, and aircraft gross weight (rotor thrust).

5. Considering the variation of the predicted induced velocities with flight speed, the influence of the wake aerodynamic interference on the rocket trajectories is expected to decrease with increasing flight speed. In hover, the predicted velocities are the highest, and the rocket remains in the wake for the longest period of time. For flight speeds greater than approximately 30 kts, the rotor wake generally passes behind the rocket launch position which significantly reduces the wake induced effects.

6. Large impulsive type, induced velocity variations with time occur at points on the rocket trajectory near the wake boundary. These variations are caused by the passage of the tip vortices. If the high impulsive type velocities induced by the close passage of a tip vortex are found to significantly alter the flight path of the rocket, a mechanism for synchronizing the rocket firing time with the rotor position for minimum tip vortex interference could be considered.

139

7. The variation of the predicted time-averaged induced velocity components between the four rockets of the AH-1G helicopter is within ±10 fps at similar points along the trajectories.

8. It is necessary to use an accurate rotor wake model in calculations directed toward predicting induced velocities at rocket trajectories. The use of an undistorted wake model rather than a realistic distorted wake model results in significant differences in predicted induced velocities.

9. Small variations (4 degrees) in rocket launch attitude produce small induced velocity changes at the rocket trajectories except near the wake boundary where the variations produce a difference in the phasing of the velocities associated with the relation between rotor position and the passage of a tip vortex. This is generally also true for small variations in rocket launch point. However, vertical and/or longitudinal variations in launch point produce significant variations in induced velocities near the launch point at approximately 30 kts due to the movement of the point from inside to outside of the rotor wake or vice versa. The relative position of the rocket launch point to the wake boundary could also be varied by changes in any of the factors which determine the wake boundary (flight speed, aircraft gross weight, and rotor/fuselage attitude).

RECOMMENDATIONS

1. Several factors which were approximated or neglected in the analytical calculations, should be considered. These are wake instability and dissipation, vortex core size, the selection of the finite spatial and temporal increments used in the analyses, and wing and fuselage interference effects. Also, the possible requirement for iterating between the induced velocities and the rocket trajectory should be considered.

2. Calculations of the effect of the rotor wake induced velocities determined in this investigation on the rocket trajectories should be continued.

3. The rotor wake effects for flight conditions other than the three discussed herein should be determined. In particular, calculations for specific flight conditions for which flight test rocket trajectory data become available should be performed for correlation purposes. Also, the sensitivity of the results to variations of the significant parameters in actual aircraft operation which influence the wake strength and wake/rocket positioning should be investigated, and procedures for generalizing the results should be determined.

4. Model helicopter tests should be conducted to acquire systematic experimental data on this rocket aerodynamic interference problem. Model hovering and wind tunnel facilities and experimental flow measurement and visualization techniques should be used to measure the wake boundaries and flow velocities in the regions of the rocket trajectories. Combined model rotor-fuselage-wing testing, application of flow visualization techniques, and application of laser velocimeter techniques (as reported in Reference 9) to measure flow velocities, should be conducted. The results of such an experimental program would provide data for correlation with theory and for a systematic determination of the total and separate influence of each of the aircraft components (rotor, fuselage and wing) and significant parameters (flight speed, gross weight, aircraft attitude, etc.). In addition, the determination of the velocity field at potential locations for wind sensors mounted on the aircraft would assist in solving the problem of accurately measuring flow velocities at the low aircraft flight speeds required in accordance with current rocket firing tactics.

REFERENCES

1. Landgrebe, A. J. and T. A. Egolf: Prediction of Rotor Wake Induced Flow Velocities Along the Rocket Trajectories of an Army AH-1G Helicopter, Picatinny Arsenal Technical Report 4797, Prepared by the United Aircraft Research Laboratories (presently United Technologies Research Center) for U. S. Army Picatinny Arsenal, Dover, New Jersey, March 1975.

2. Wasserman, S.: Preliminary Analysis of the Effects of Calculated Downwash Distribution on Flight Performance of the 2.75" Rocket, Picatinny Arsenal, Proceedings of the USAAVSCOM Conference on the Effects of Helicopter Down-wash on Free Projectiles, 1975.

3. Landgrebe, A. J.: An Analytical and Experimental Investigation of Helicopter Rotor Hover Performance and Wake Geometry Characteristics, USAAMRDL Technical Report 71-24, Prepared by the United Aircraft Research Laboratories for the Eustis Directorate, U. S. Army Air Mobility Research and Development Laboratory, Fort Eustis, Va., June 1971.

4. Landgrebe, A. J.: The Wake Geometry of a Hovering Helicopter Rotor and Its Influence on Rotor Performance, Jl. American Helicopter Society, Vol. 17, No. 4, October 1972.

5. Landgrebe, A. J. and E. D. Bellinger: An Investigation of the Quantitative Applicability of Model Helicopter Wake Patterns Obtained from a Water Tunnel, USAAMRDL Technical Report 71-69, Prepared by the United Aircraft Research Laboratories for the Eustis Directorate, U. S. Army Air Mobility Research and Development Laboratory, Fort Eustis, Va., December 1971.

6. Landgrebe, A. J.: An Analytical Method for Predicting Rotor Wake Geometry, Jl. American Helicopter Society, Vol. 14, No. 4, October 1969.

7. Landgrebe, A. J. and M. C. Cheney: Rotor Wakes - Key to Performance Prediction, AGARD-CP-111, AGARD Conference Proceedings No. 111 on Aerodynamics of Rotary Wings, Fluid Dynamics Panel Specialists Meeting, September 1972. (Also, paper presented at the Symposium on Status of Testing and Modeling Techniques for V-STOL Aircraft, Mideast Region of the American Helicopter Society, October 1972.)

8. Landgrebe, A. J. and T. A. Egolf: Rotorcraft Wake Analysis for the Prediction of Induced Velocities, USAAMRDL Technical Report 75-45, Prepared by the United Technologies Research Center for the Eustis Directorate, U. S. Army Air Mobility Research and Development Laboratory, Fort Eustis, Va., to be published.

9. Landgrebe, A. J. and B. V. Johnson: Measurement of Model Helicopter Rotor Flow Velocities with a Laser Doppler Velocimeter, Jl. American Helicopter Society, Vol. 19, No. 3, July 1974.
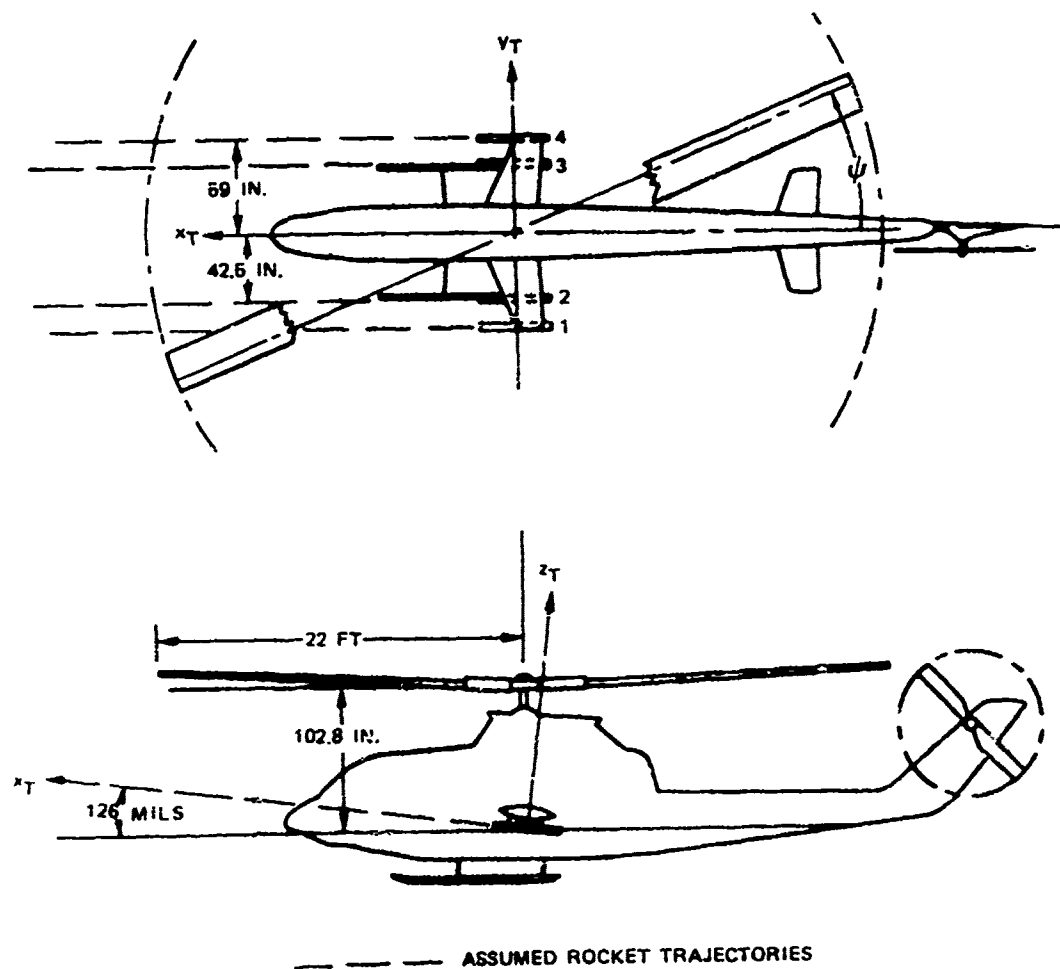
Figure 1.   Schematic of AH-1G Helicopter Showing Assumed Rocket
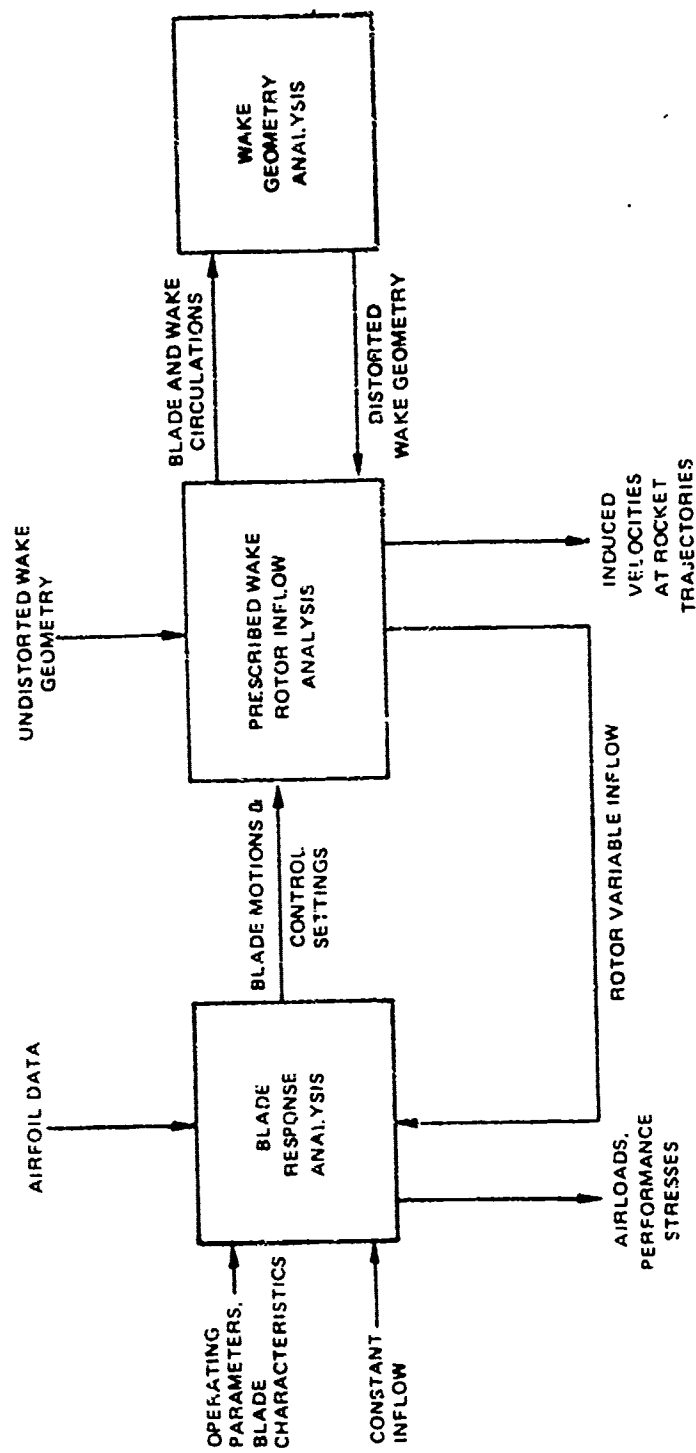Trajectories and Coordinate System.

143

Figure 2. Components of the UTRC Rotor Analysis.
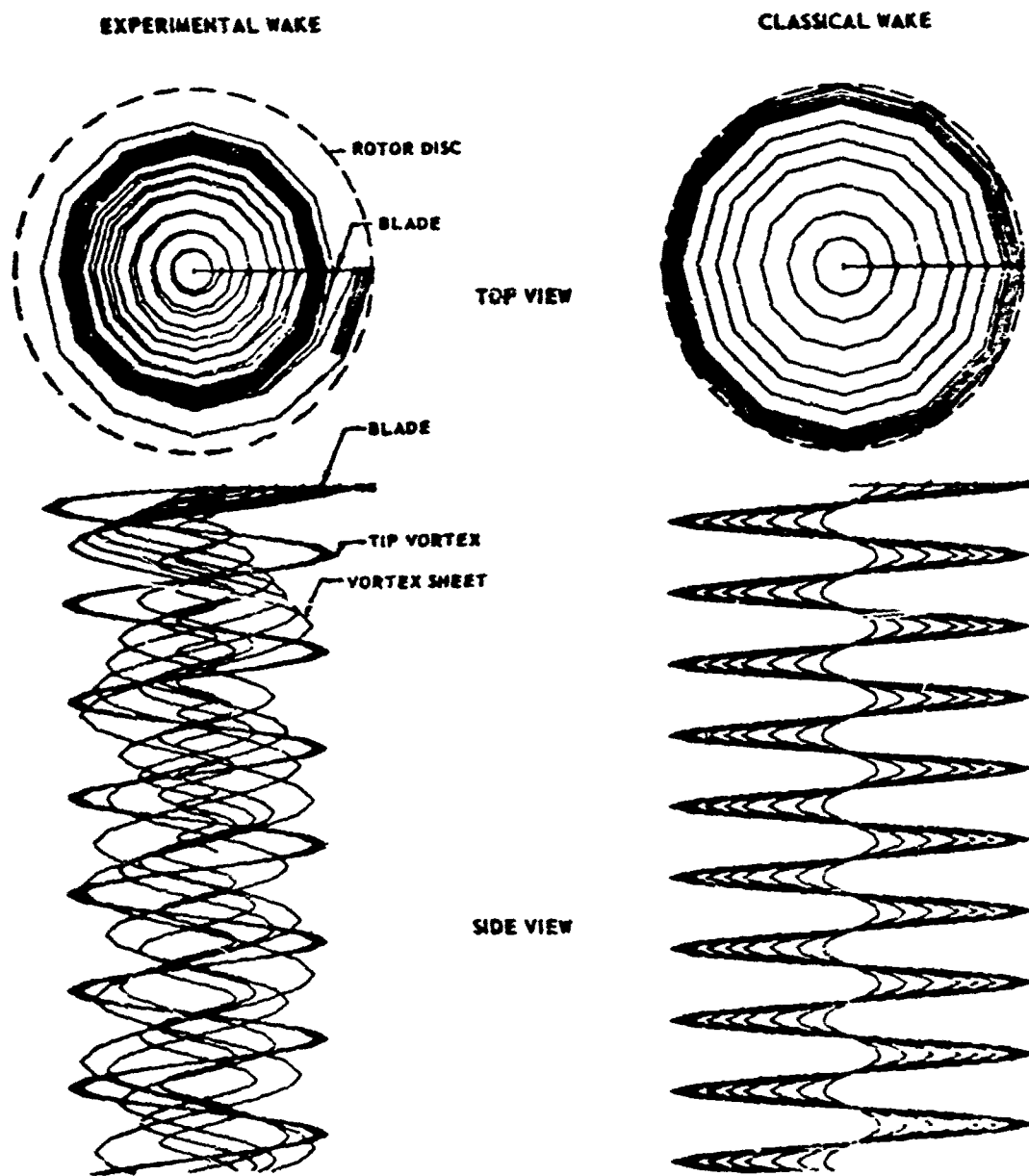
144

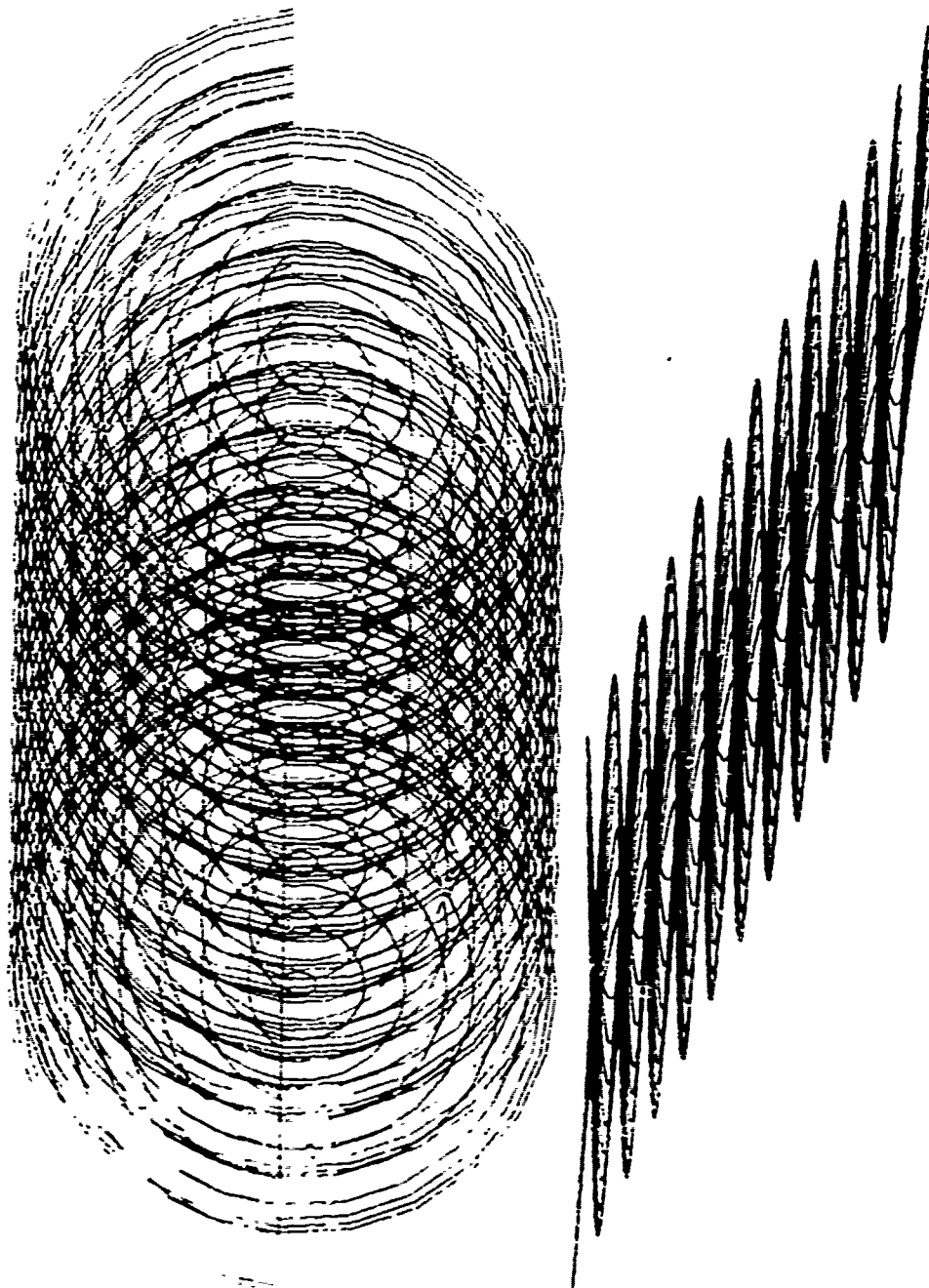Figure 3. Computer Wake Trajectories For One Blade of a Hovering Rotor.

Figure 4.   Computer Wake Representation for a Forward Flight Condition -- Undistorted Wake Model, All Filaments Shown.
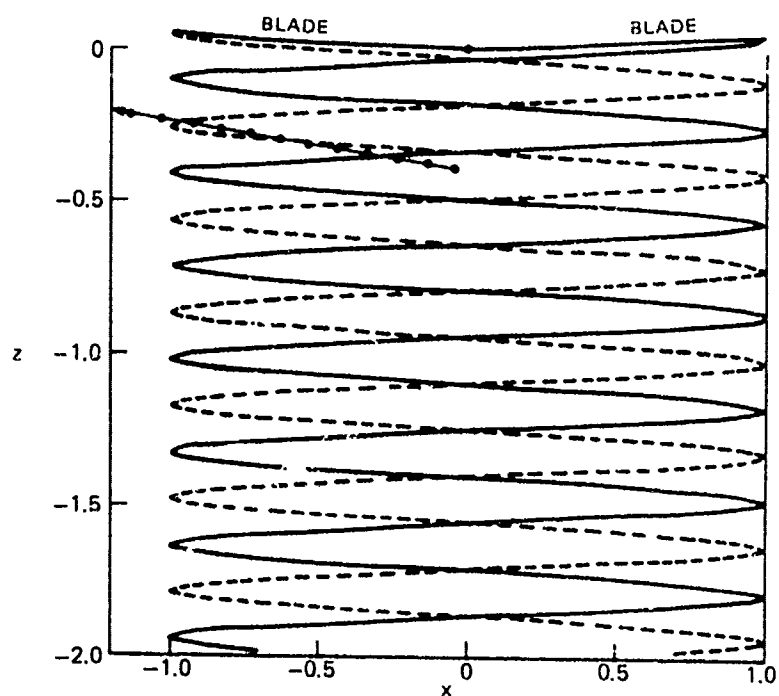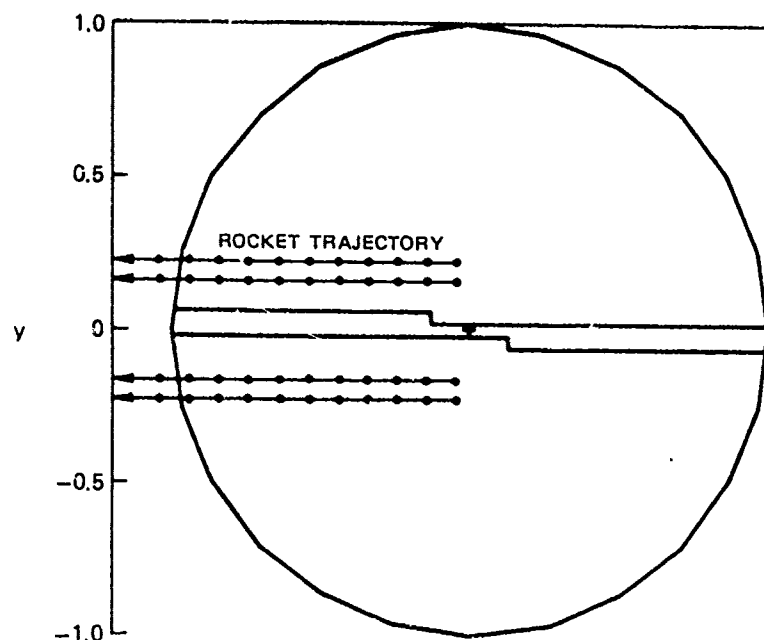
Figure 5.   Undistorted Tip Vortex Geometry for 0 Kt Flight
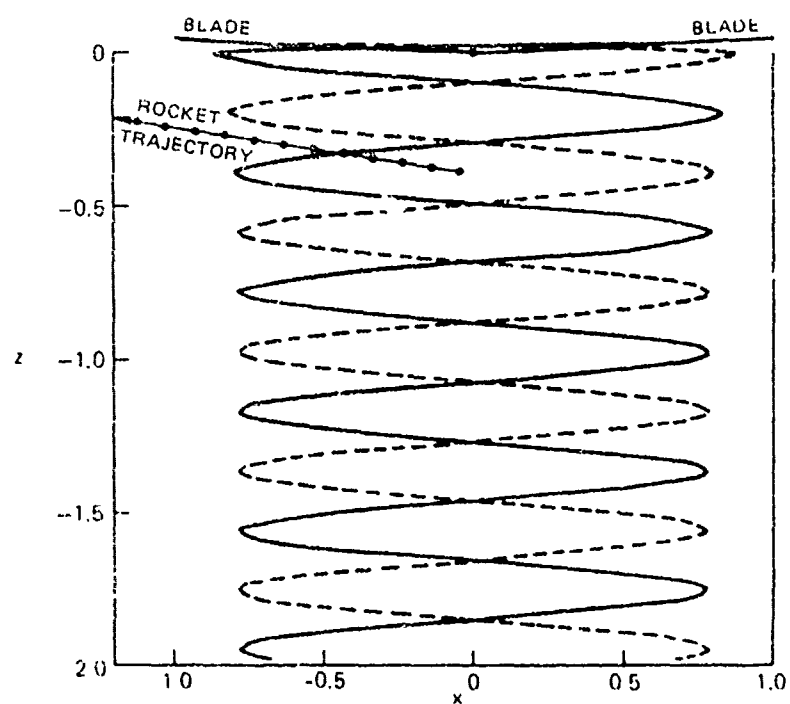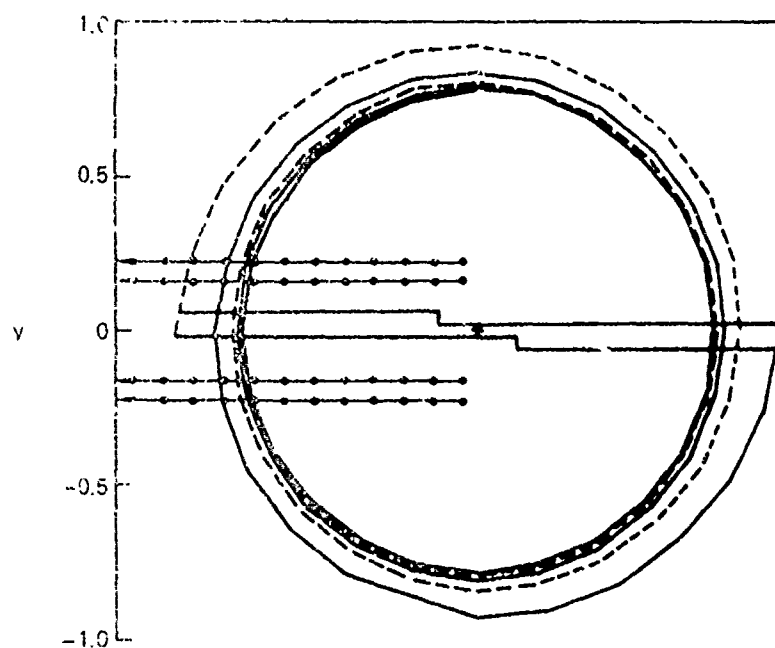Condition and Rotor Position 1.

Figure 6.   Distorted Tip Vortex Geometry (Experimental) for 0 Kt
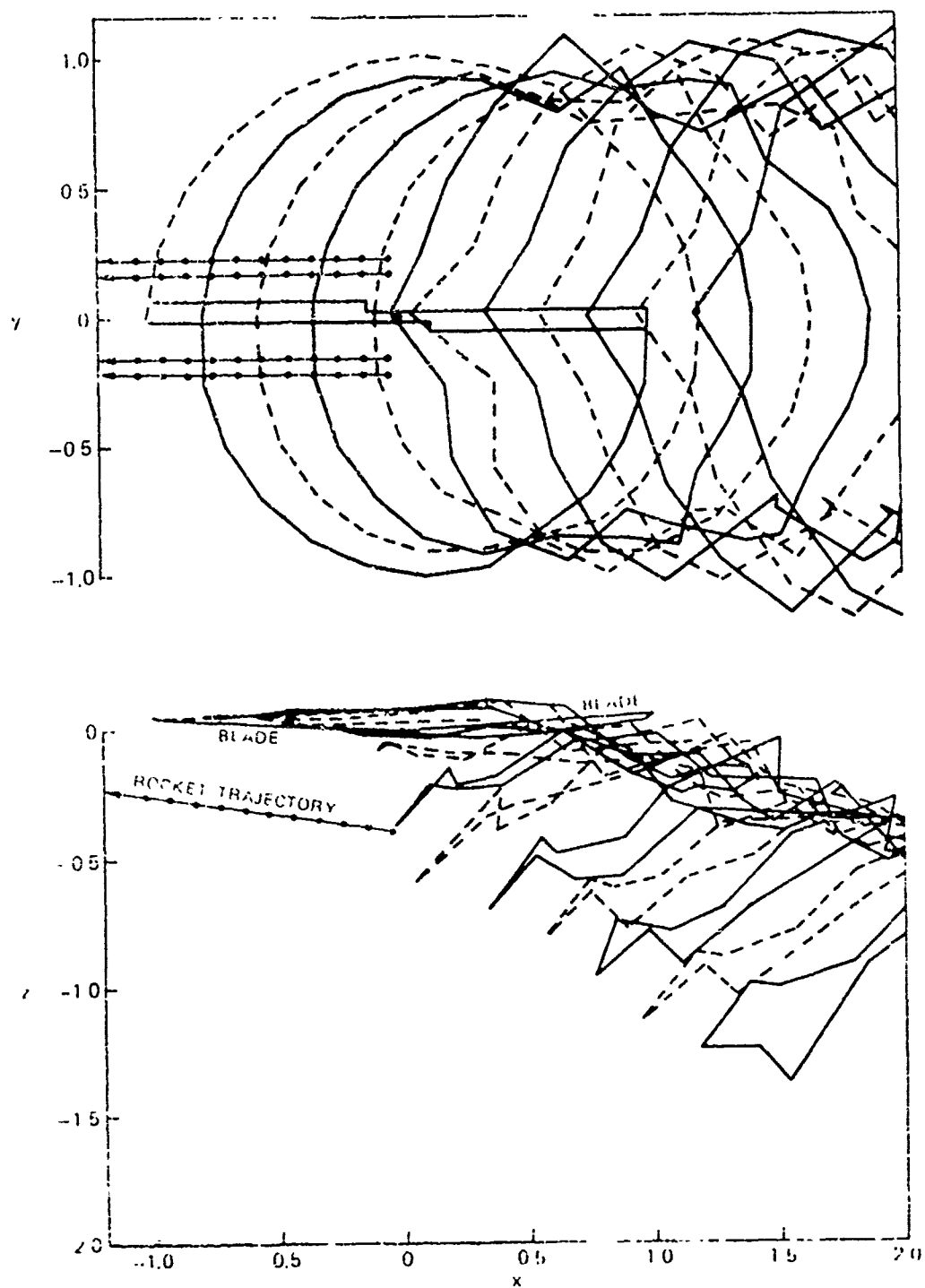Flight Condition and Rotor Position 1.
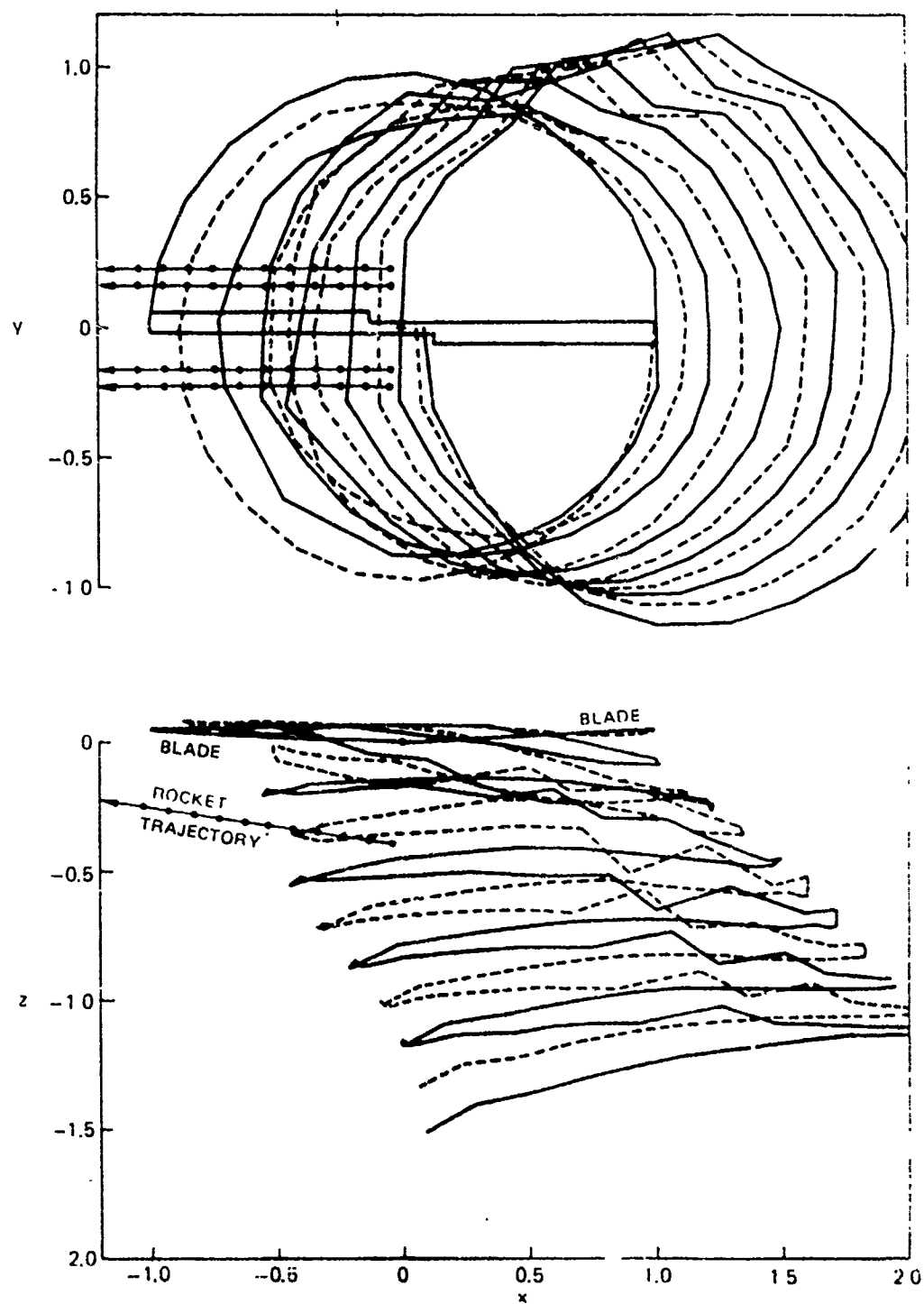
Figure 7. Distorted Tip Vortex Geometry (Analytical) for 15 Kt.
Flight Condition and Rotor Position 1.

149

Figure 6. Distorted Tip Vortex Geometry (Analytical) for 30 Kt
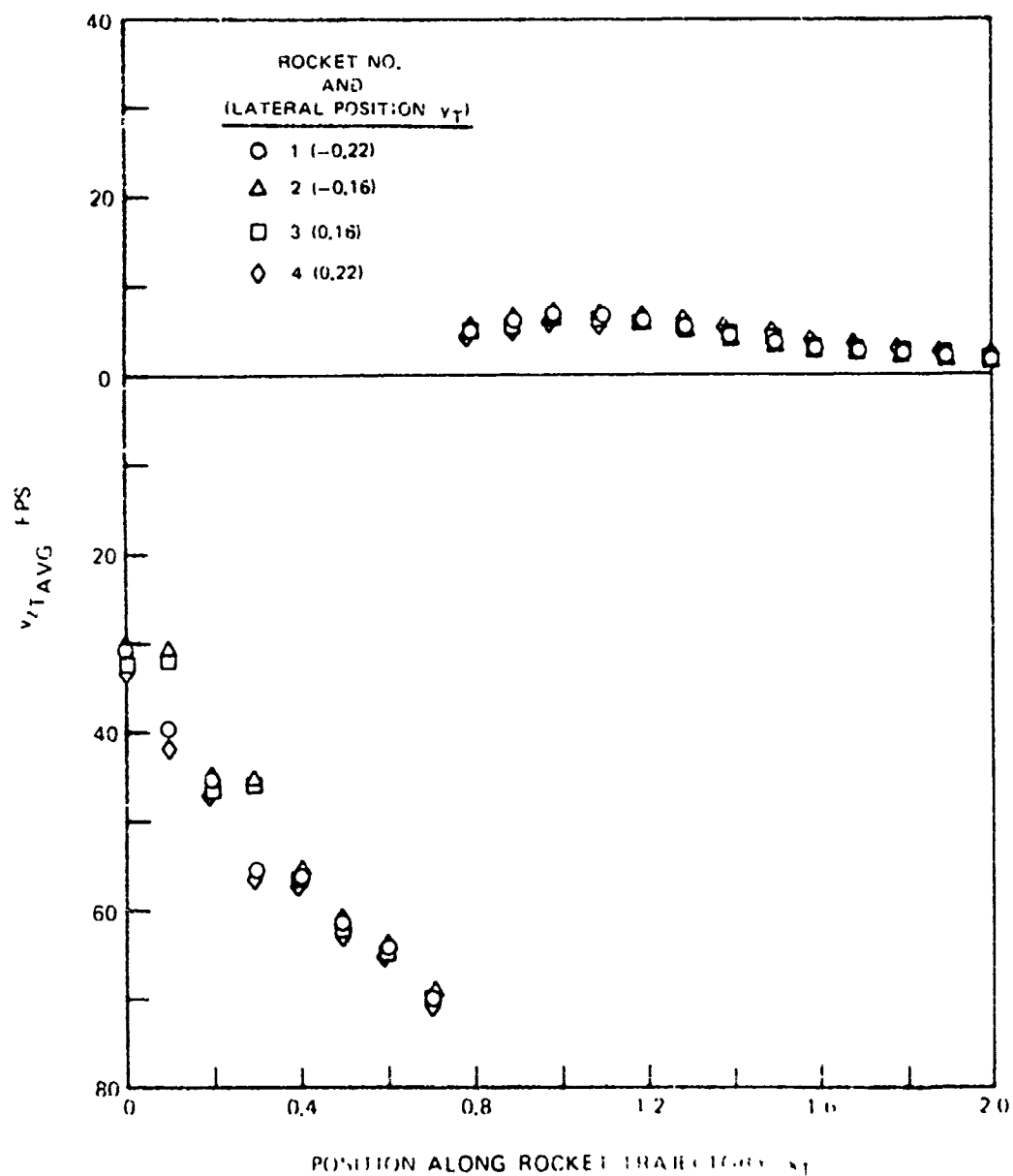Flight Condition and Rotor Position 1.

Figure 9. Variation of Time-Averaged v_T Velocity Component Along the Four Rocket Trajectories -- 0 Kt, in Vortex Wake.
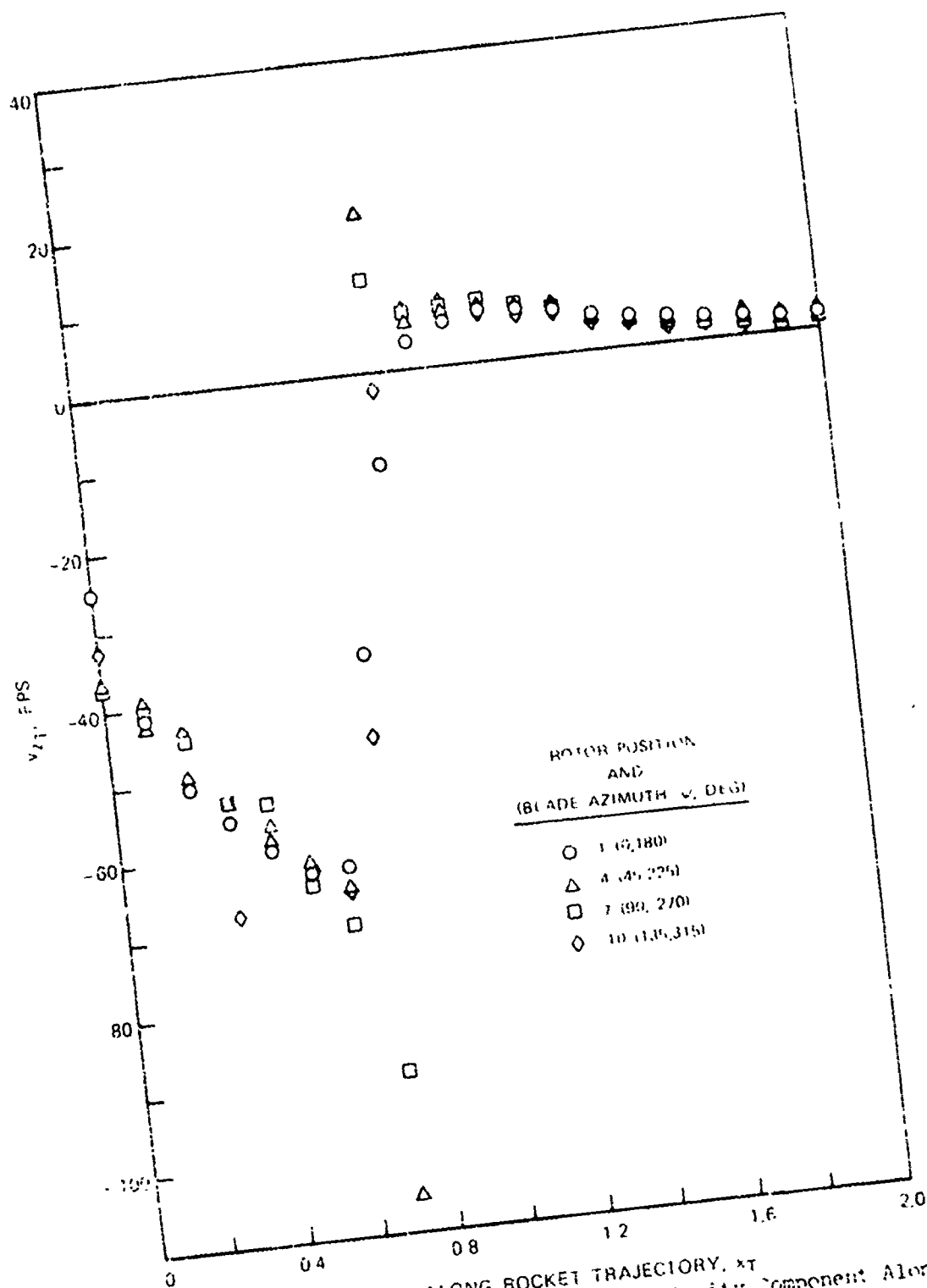
151

Figure 1. Variation of Instantaneous Axial Velocity Component Along One Rocket Trajectory for Selected Rotor Positions -- 0 Kt, Distorted Wake, Rocket No. 4 (V_T = 0.22)
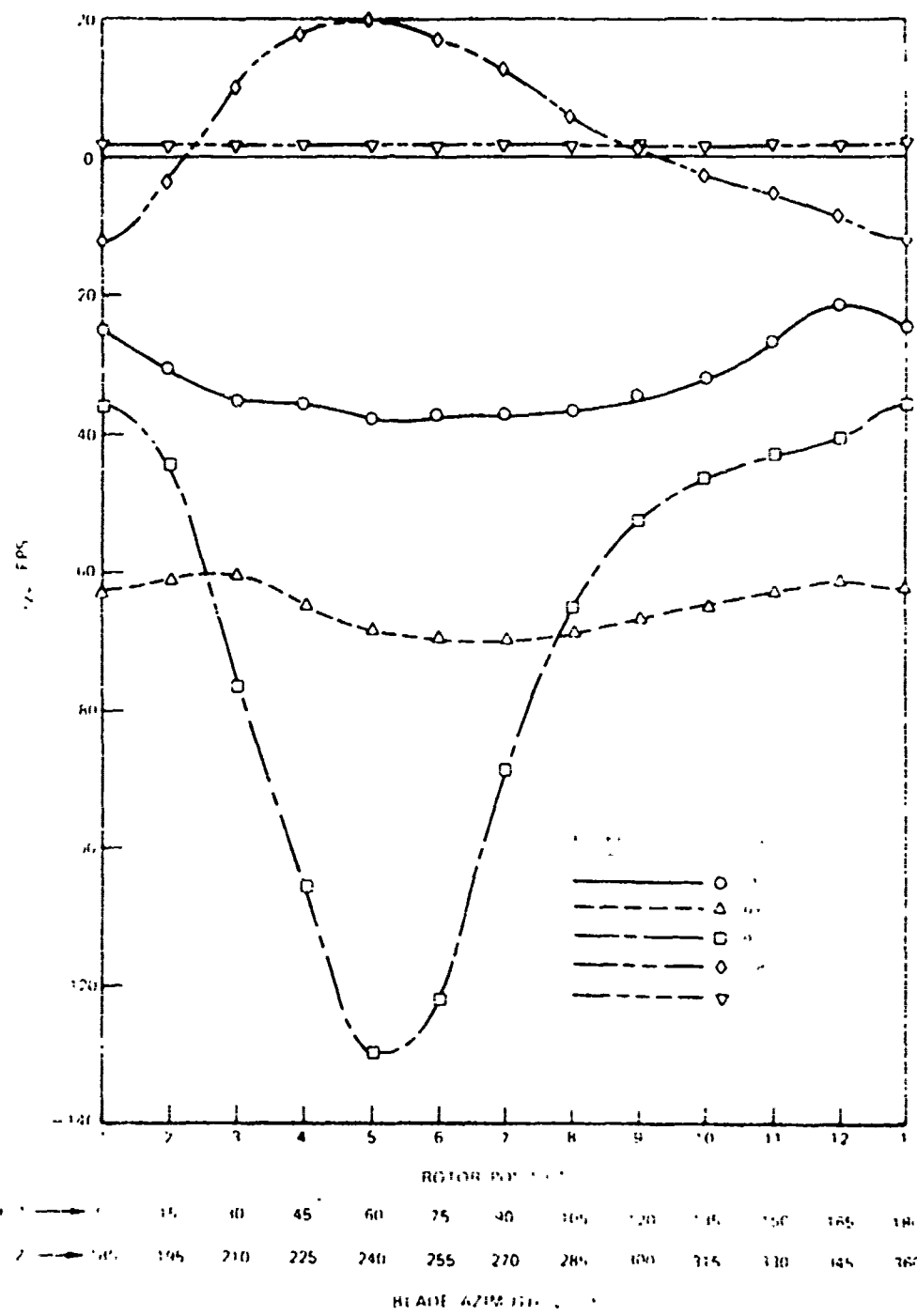
Figure .. Variation of Instantaneous $V_{...}$ Velocity Component With Rotor Position for Selected Points on One Rocket Trajectory -- 0 Kt, Distorted Wake, Rocket No. 4 ($y_T = 0.22$).
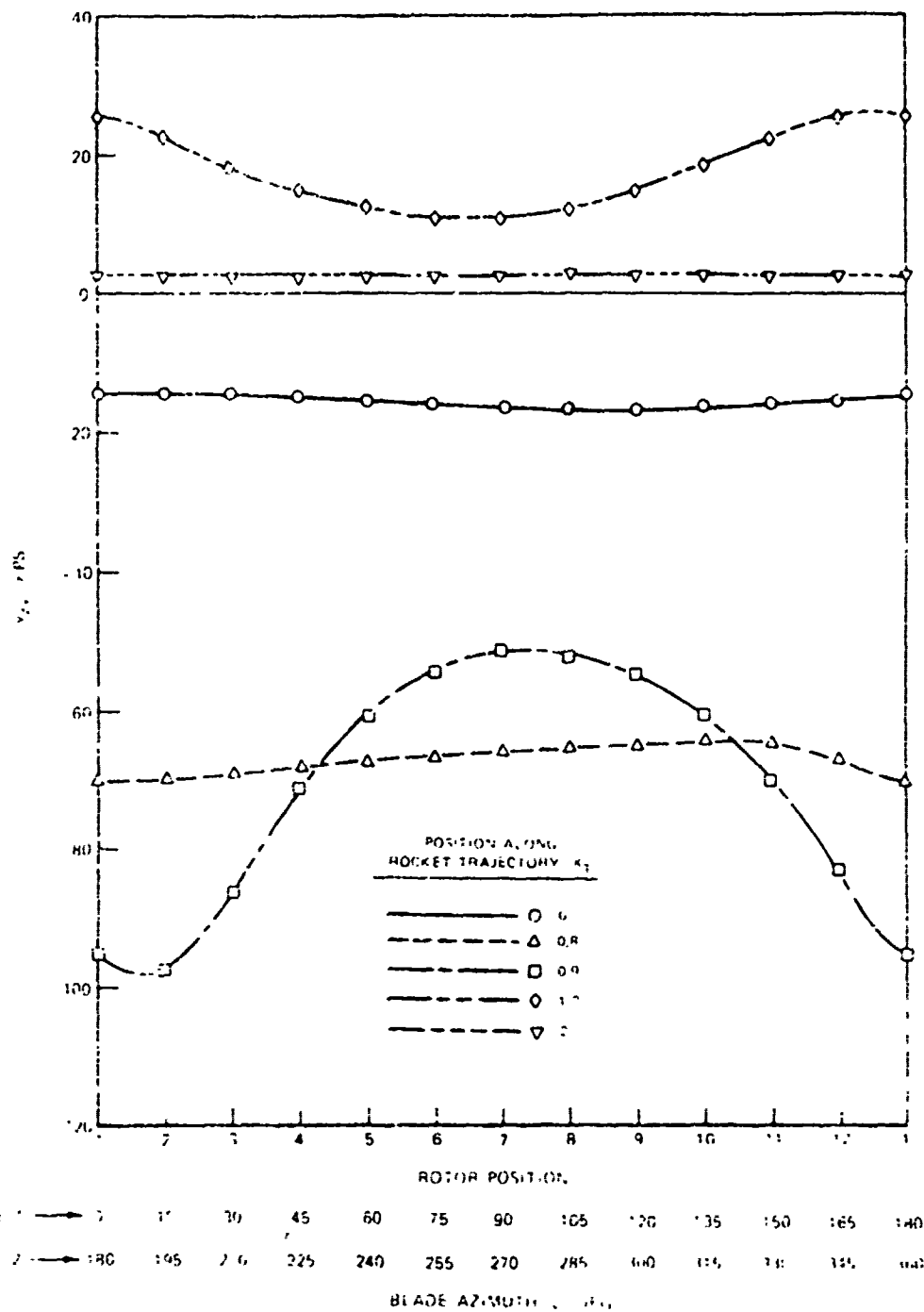
Figure ...   Variation of Instantaneous V_{z_T} Velocity Component With
Rotor Position for Selected Points on One Rocket
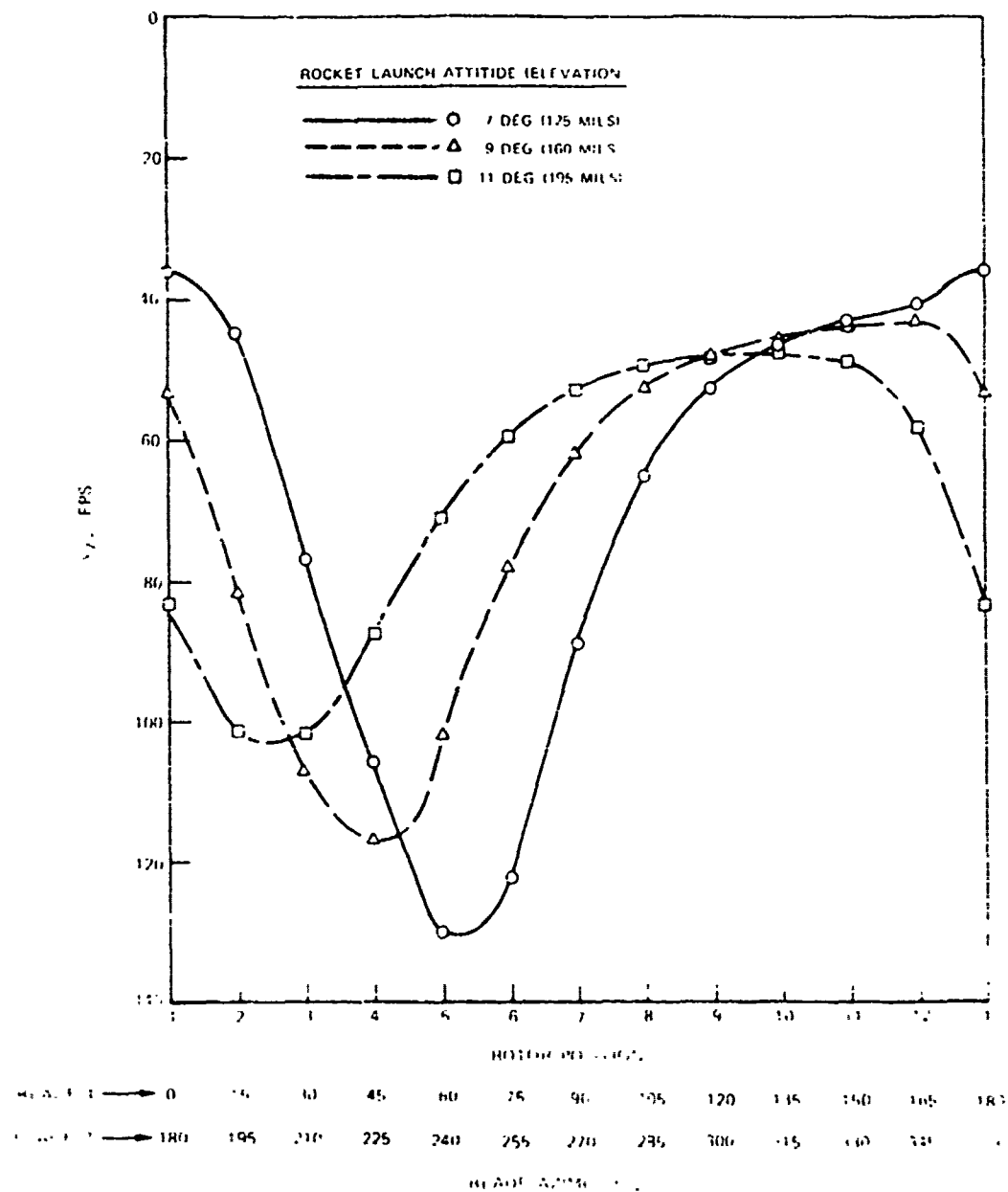Trajectory -- 0 Kt, Undistorted Wake, Rocket No. 1.
$(y_m = 0.22)$.

Figure 3. Effect of Variation of Rocket Launch Attitude on
Instantaneous v_{z_T} Velocity Component Near the Wake
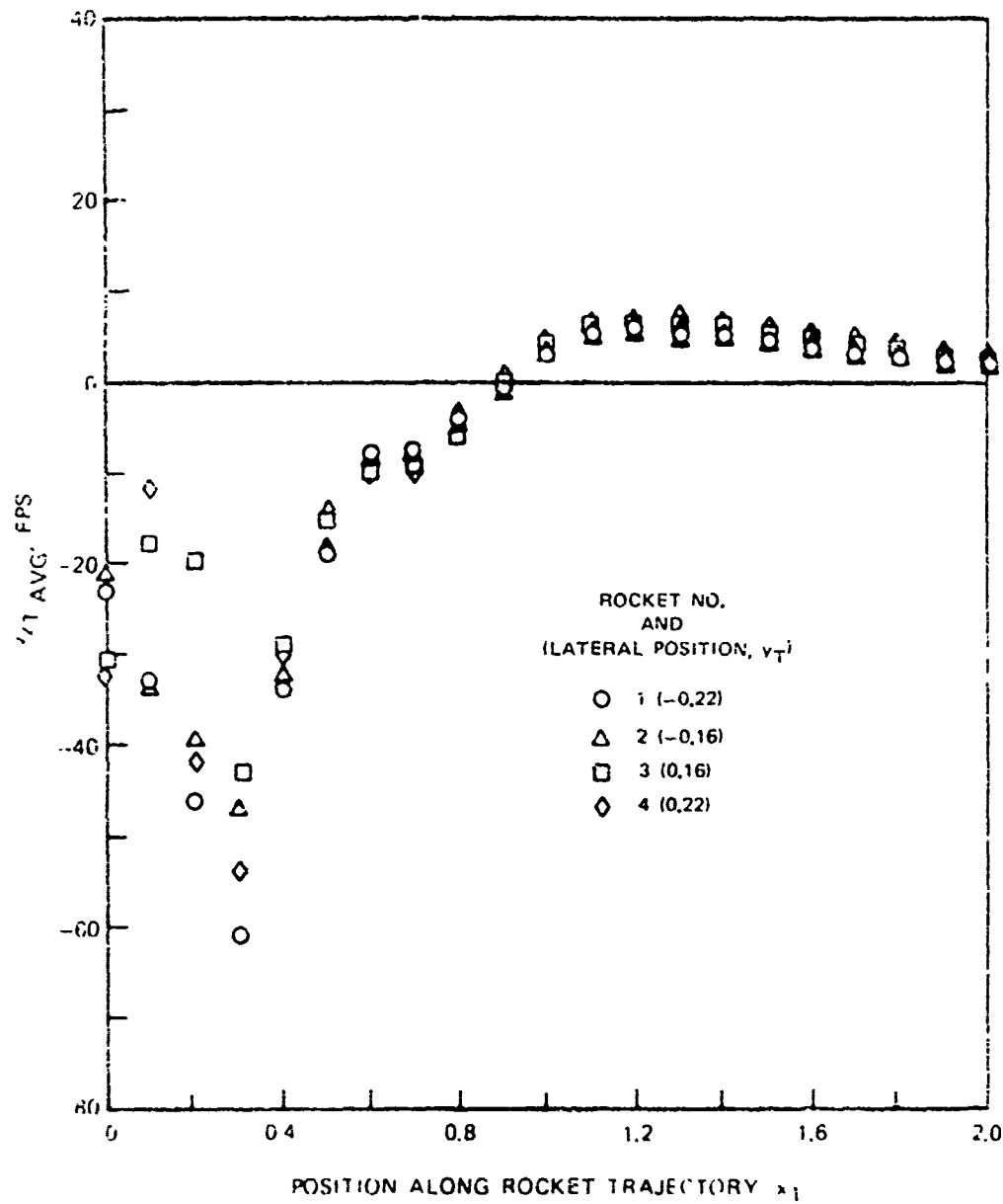Boundary -- 0 Kt. Distorted Wake, Rocket No. 4
($x_i = 0.7$).

155

Figure 14. Variation of Time-Averaged v_{Avg} Velocity Component Along the Four Rocket Trajectories -- 15 Kt, Distorted Wake.
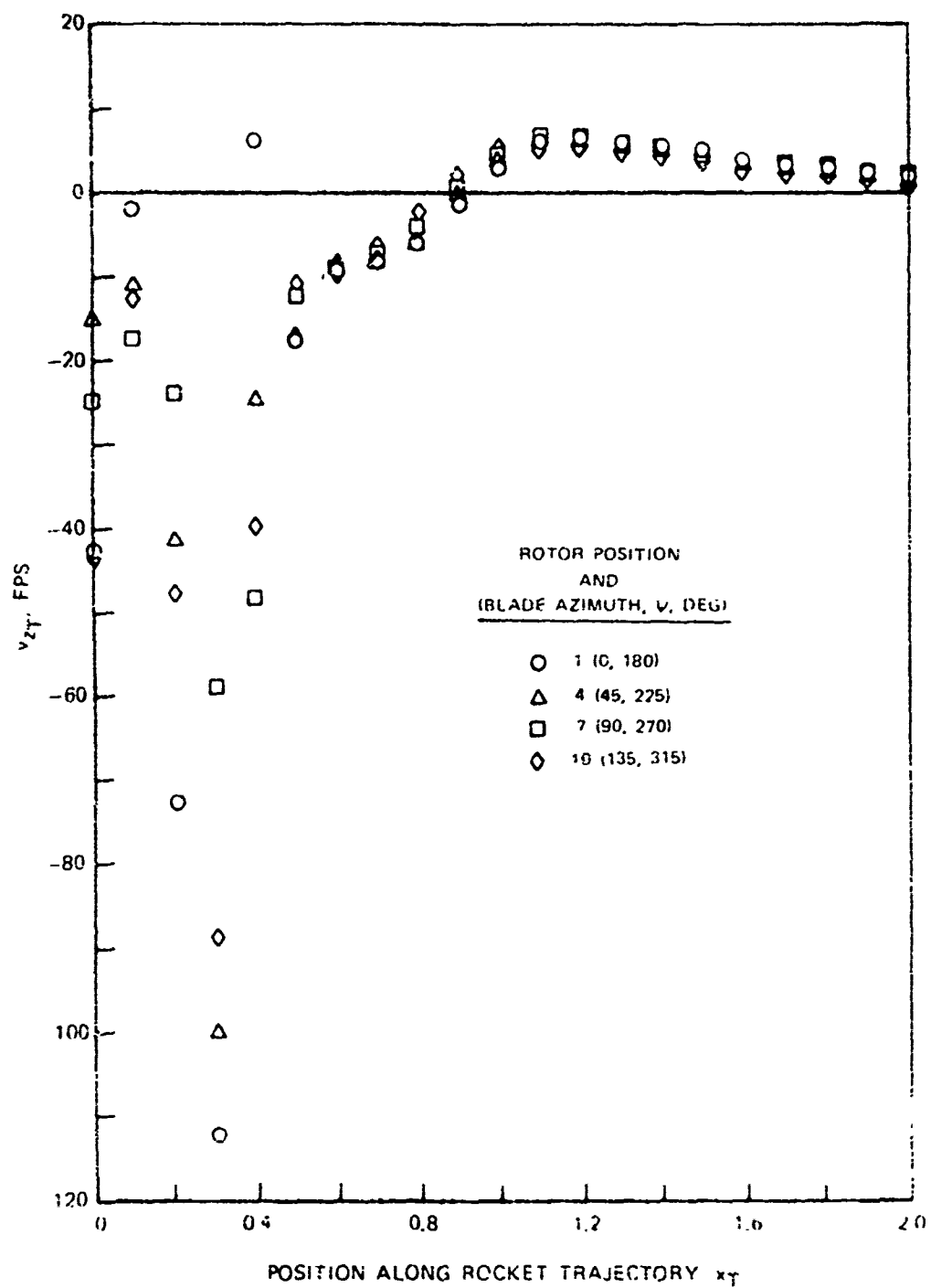
Figure 15. Variation of Instantaneous z-Velocity Component Along One Rocket Trajectory for Selected Rotor Positions — 15 Kt, Distorted Wake, Rocket No. 4 (x_T = 0.27).
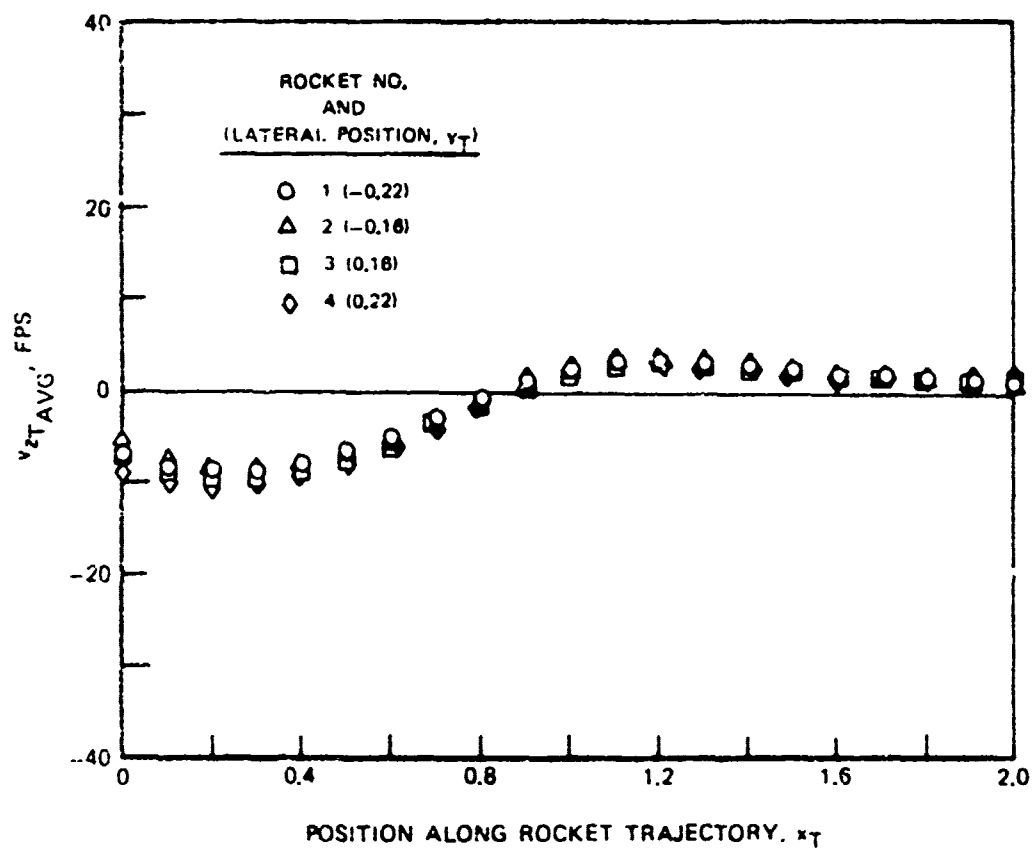
Figure ii. Variation of Time-Averaged v_{z_T} Velocity Component Along the Four Rocket Trajectories -- 30 Kt, Distorted Wake.
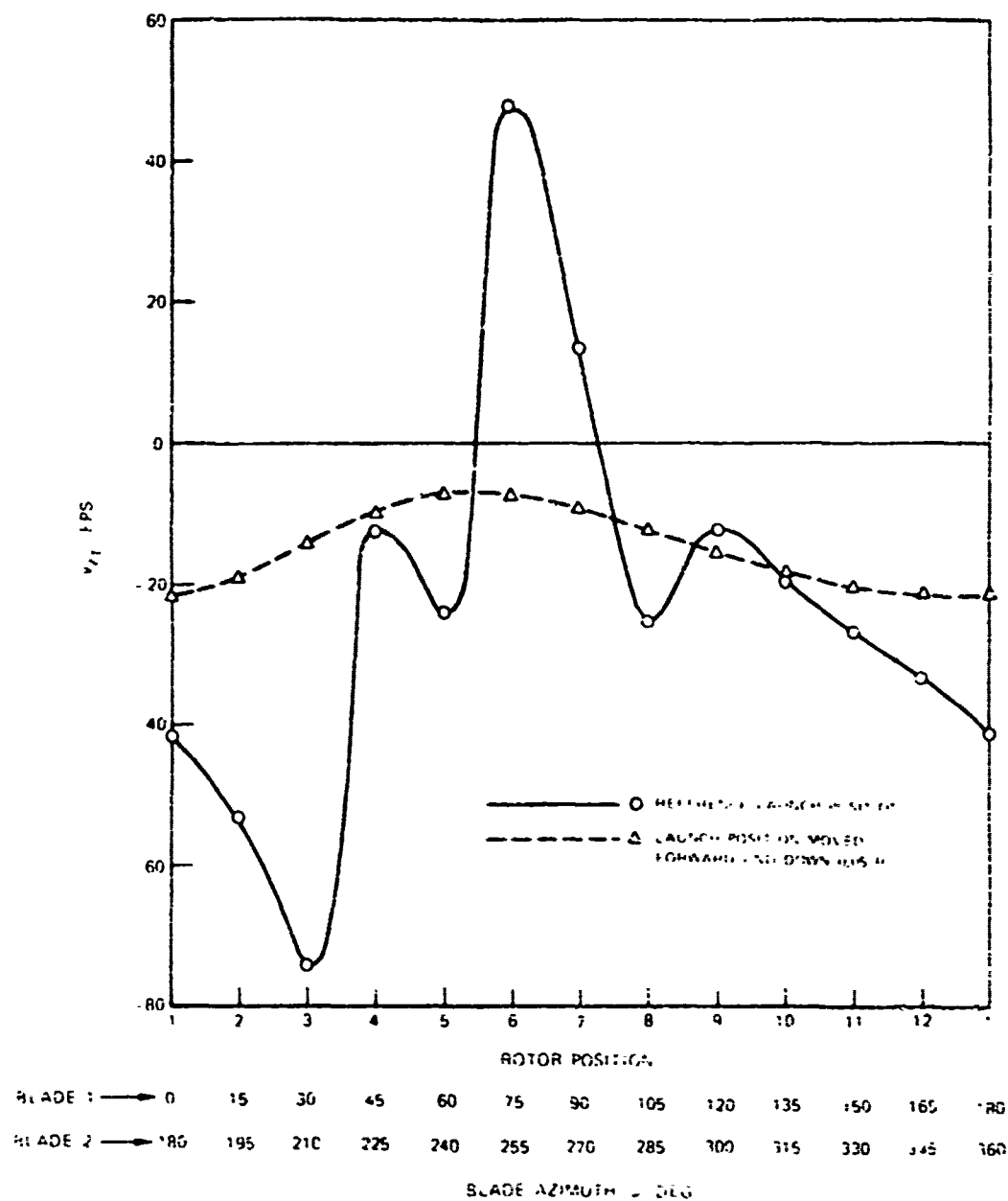
Figure .%   Effect of Variation of Rocket Launch Position on Instantaneous v_{zT} Velocity Component Near the Wake Boundary -- 30 Kt, Undistorted Wake, Rocket No. 4. $(x, \quad 0)$.

PRELIMINARY ANALYSIS OF THE EFFECT OF CALCULATED
DOWNWASH DISTRIBUTIONS ON THE FLIGHT PERFORMANCE
OF THE 2.75 INCH ROCKET

S. WASSERMAN and R. YELLER
Picatinny Arsenal
Dover, New Jersey

ABSTRACT

United Aircraft Research Labs under contract to Picatinny Arsenal has
recently completed a program in which downwash distributions were calculated
for the AH-1G helicopter rotor. These distributions were calculated along
expected rocket trajectory lines from the four rocket launchers to a distance
beyond the rotor tip.

Various 2.75 Inch Rocket six degree of freedom trajectories were calculated
using the UAPL downwash distributions as a function of blade azimuth angle.

Calculated trajectory data are also shown for zero downwash, and two values
of constant downwash.

The effect of rotor downwash distribution over the rocket body length is also
presented and discussed.

Various conclusions and recommendations for future programs are presented.

NOMENCLATURE

$C_{N_{\alpha}2.75}$ Normal Force Coefficient Derivative for the Standard 2.75 inch Rocket

$C_{N_{\alpha}(Downwash)}$ Normal Force Coefficient Derivative for the 2.75 inch Rocket Modified for any given Downwash Distribution

$X'_{cp\ 2.75}$ Normal Force Center of Pressure for the Standard 2.75 inch Rocket (Calibers Aft of the Nose)

$X_{cpW_{z_1}}$ Normal Force Center of Pressure for the Standard 2.75 inch Rocket Based on a Constant Angle of Attack Created by the Downwash at the Tail W_{z_1}

W_{z_1} Downwash Velocity (feet per second) at Tail Section

W_{z_2} Downwash Velocity (feet per second) at Nose Section

V_R Rocket Forward Velocity

$C_{N_{\alpha}Nose} = C_{N_N}$ Normal Force Coefficient Derivative for Nose Alone (assumed to be 2.0)

161

$\mathcal{X}$ cp Nose

Normal Force Center of Pressure for Nose Alone (assumed to be 2.3 calibers aft of nose)

$C_{N_{\bar{d}F}}$

Normal Force Coefficient Derivative for Fins Alone

$\underset{R_R}{\mathsf{T}}$

Rocket Axial Position T with Relation to the Blade Radius (22 feet)

θ

Effective Pitch Angle of Rocket After Being Influenced by the Rotor Downwash

R

Rocket Impact Range

The US Army in recent years has devoted a considerable amount of effort into improving the accuracy and extending the range of rocket munitions launched from helicopters. One of the most critical launch conditions for any rocket fired from a helicopter, as far as accuracy is concerned, is in the hover regime. The lack of detailed test and analytical data for the downwash distributions led to the placement of a very limited contract with the United Aircraft Research Laboratories to provide calculated downwash distributions for hover, 15 knots and 30 knots. The results of this study are presented in a United Aircraft Report published by both United Aircraft and Picatinny Arsenal.

The Rocket Assisted Projectile and Pyrotechnics Branch of Picatinny Arsenal formulated a calculation program using the hover downwash data presented in the UARL report to determine the flight range to be expected for standard 2.75 inch MK40 Rockets with the M151 head. Calculations were also made with the assumption of a 50 fps and a 40 fps constant downwash velocity. A constant downwash velocity of 50 fps has been used to date by the RAP&PB as a typical average for a 9500 pound AH1G helicopter out of ground effect. Results are also tabulated for the ranges calculated with a zero downwash. All range calculations were made with a 6 degree of freedom trajectory program.

The first set of trajectory range calculations were made with the assumption of zero downwash. The results are presented in FIGURE 1.

The second set of calculations used a constant downwash from rocket launch to the rotor tip. Two downwash velocities of 50 feet per second and 40 feet per second were used. The calculated ranges are presented in FIGURE 2 for the standard method of calculation which assumes that the constant downwash acts over the entire body from launch to when the tail clears the point directly under the rotor tip.

The third set of calculations was made with two downwash distributions obtained from Figure 15 of the UARL Report (FIGURE 3). This figure dhows the downwash at particular positions along the rocket trajectory, from the right outboard launcher, as a function of blade orientation angle. The first downwash distribution or minimum downwash distribution was obtained by assuming that the rocket clears the launcher when the blade is at a zero degree azimuth angle. The maximum downwash distribution was calculated for the case where the blade angle is at 60 degrees when the rocket clears the launcher. The calculated maximum and minimum downwash distributions are shown in FIGURE 4. The change in downwash due to a varying blade azimuth angle has been included.

The variable downwash distributions shown in the previous slide were used in one set of calculations with the assumption that the downwash at the tail would apply over the entire rocket. The calculated rocket impact ranges are shown in FIGURE 5. These calculations were made with the standard downwash program.

The fourth set of calculations was made with the minimum and maximum downwash distributions in which the variable downwash distribution over the rocket was accounted for in the following manner. The normal force coefficient for rockets fired in a downwash distribution such as shown by UARL, can be calculated with an assumption that at the time the rocket clears the launch tube the downwash distribution can be broken into two distributions over the length of the body. One is a constant downwash equivalent to the downwash magnitude at the exit of the tube. The other is a triangular downwash distribution with a zero velocity at the launcher exit and a magnitude at the nose of the rocket equivalent to the difference between the actual downwash at the nose and the constant value chosen over the body length. FIGURE 6 depicts the breakdown of a typical downwash distribution.

The simplified formulation assumed that the constant downwash portion of distribution is used to calculate a constant angle of attack over the length of the rocket. This constant angle of attack then leaps to a normal force based on the steady state 2.75 inch Rocket aerodyanmics. The triangular flow distribution, which in the case of the figure shown in FIGURE 6 has a downwash at the nose and none at the tail, is used to modify the normal force by adding an increment of force on the nose. It is assumed that the additional normal force on the nose is created by the incremental downwash $W_{Z_2} - W_{Z_1}$ leading to an angle of attack $\dfrac{W_{Z_2} - W_{Z_1}}{V_R}$ on the nose. The normal force derivative $\left(\dfrac{dC_N}{d\alpha}\right)$ of the nose is assumed to be 2.0. The equation as

165

shown in FIGURE 6 shows the addition of the constant downwash normal

force component which is derived from tabulations of normal force

coefficient vs. angle of attack to the nose incremental coefficient.

The term $\left(\frac{dC_N}{d'\alpha}\right)$ 2.75 $\frac{W_{Z_1}}{V_R}$ is shown only as an indication that the

table lookup for the constant downwash normal force component is

performed. For the point along the rocket trajectory where the down-

wash on the nose is the same as on the tail, the normal force

calculated will be the standard 2.75 inch normal force coefficient

for the angle of attack resulting from the constant downwash. For

the case where, as the rocket passes through the downwash below the

rotor tip, a smaller downwash is observed at the nose than the tail,

the downwash at the tail is assumed to act over the entire body

resulting in a normal force. This normal force is then modified by

allowing a negative downwash operate on the nose section. The

equation of FIGURE 6 would account for the negative downwash in this

case since $W_{Z_2} - W_{Z_1}$ would be negative. All three cases of downwash

distributions which would be handled by the basic formulation are

shown in FIGURE 7.

The center of pressure of the rocket (calibers aft of the nose)

with the various downwash distributions discussed previously can be

calculated in a manner similar to the normal force calculation.

The equation for center of pressure is derived with the following

reasoning (FIGURE 8):

The normal force coefficient due to the flow distribution W_{Z_1} is

located at the 2.75 inch Rocket center of pressure $C_{cp_{W_{Z_1}}}$. The center

of pressure $X_{cp_{W_{Z_1}}}$ which would normally be the resultant center of

pressure, is modified because of the additional flow over the nose.
Again, the difference in downwash velocity between that on the nose
and tail as in FIGURE 8 is assumed to act on the nose at the nose
center of pressure which is taken as 2.3 calibers aft of the tip
of the nose. The force coefficient generated by the downwash is taken

as $C_{N_{\alpha Nose}} \dfrac{(W_{Z_2} - W_{Z_1})}{VR}$ where $CN_{\alpha Nose} = 2.0$. The resultant center

of pressure is then calculated from the sum of the moments about the
nose tip. For the rocket position where the downwash on the nose tip
is equal to the downwash on the tail section the center of pressure
becomes the standard normal force center of pressure for the constant
angle of attack over the body. For the rocket position where the
downwash at the tail is larger than at the nose, the equations for
the normal force derivative and center of pressure will provide the
normal force and center of pressure corresponding to that distribution.
One might question the validity of applying W_{Z_1} over the entire body
and subtracting the contribution of $W_{Z_1} - W_{Z_2}$ over the nose as compared

to using W_{Z_2} over the entire body and adding the contribution of
$(W_{Z_1} - W_{Z_2})$ on the fin normal force. A simple algebraic manipulation
shows that both techniques are valid. The method will not be shown
here but will be presented in the Picatinny Arsenal report of this
work.

Again, the equations can be used to calculate the normal force
center of pressure and normal force coefficient for all downwash
conditions. It is to be noted that the techniques used to calculate

C_N & cp are simplified and will be improved. The results of the range calculations for the condition with the downwash varying over the nose and tail are presented in FIGURE 9. A set of rocket impact ranges was calculated using the variable downwash program and constant downwash of 40 fps and 50 fps. The results are shown in FIGURE 10. The impact ranges differ slightly from those presented in FIGURE 2 for the constant downwash acting over the entire body. The difference in range is due to the variable downwash program giving the rocket nose a zero downwash as the nose clears the rotor tip whereas the conventional program allows the constant downwash over the entire body until the tail clears the rotor tip area. The aerodynamic coefficients for the 2.75 inch Rocket as used in the study are presented in FIGURE 11 and 12. The 6 degree of freedom trajectory program was modified to calculate downwash as a function of rocket range and blade azimuth angle given data as shown in FIGURE 3. The ranges calculated with a zero downwash are, as expected, significantly lower than those calculated with given downwash distributions. The downwash velocity, in combination with the forward velocity of the rocket leads to an angle of attack relative to the longitudinal axis of the rocket. This angle of attack leads to a nose up pitching motion which increases the range over the zero downwash condition.

The dispersion of the rocket when launched at a hover is in part due to the variation in downwash. As was shown, the change in calculated ranges between those for the constant 50 feet per second downwash and the 40 feet per second case are significant. The change in range for the corresponding 10 feet per second change in downwash is greater at the smaller ranges than the larger ranges. The

168

launch elevation at the smaller ranges is lower and therefore the change in range for a change in the effective launch angle $\left(\frac{dR}{d\phi}\right)$ is larger than at the longer ranges.

The downwash would vary in a pure hover mode primarily due to aircraft weight, rotor angular position, and aircraft velocity. Neglecting any change in aircraft pitch angle, the change in aircraft weight would probably lead to the same type of downwash distributions shown in the referenced UARL report but with smaller or larger magnitudes proportional to aircraft weight.

The change in downwash as a function of blade azimuth angle and the resulting change in calculated range can be significant especially for the close-in ranges. At a two degree launch elevation the calculated range difference between the rounds fired with a zero degree rotor azimuth and those fired with a 60 degree rotor azimuth is 290 meters. While this difference is quite significant, it is probably a relatively small percentage of the total ground spread of the rockets fired in hover. Other errors such as round to round error, aim error, helicopter motion during rocket firing, etc., would account for significantly larger ground impact errors at the shorter ranges than the dispersion due to rotor location. With adequate fire control it is possible that most other component errors could be minimized which would then make the dispersion due to rotor position a major part of the gross dispersion. At this point, a method for articulating the rocket firing with rotor angular position might be desirable.

169

At the longer ranges (4700 meters) the difference in calculated range between rounds launched at rotor azimuth angles of 0° and 60° becomes approximately 80 meters. It is felt that there is no need to consider any articulation between rocket launch and rotor position at these longer ranges.

Another method for reducing the dispersion due to downwash for the 2.75 inch Rocket or any rocket fired from a hover is to use a sub-munition warhead with high drag submunitions. The 2.75 inch Rocket PMO is currently sponsoring such a high drag submunition program. The techniques used to minimize range error due to any perturbations in resultant effective pitch launch angle are presented in Reference 2.

The calculated ranges shown for the zero degree and 60 degree initial rotor azimuth angle were averaged at each launch elevation. The resulting ranges would represent expected average ranges if the rockets were fired at random blade orientations from Launcher 4. It is apparent that there is no significant difference between the range calculations using the downwash at the tail or the downwash at the nose and tail. This is primarily due to the very large stabilizing effect of the 2.75 inch Rocket fins. The nose-tail calculation technique should be used for rockets which would have smaller stability margins. The average range data using the tail downwash technique were used to determine the constant downwash that would give the same ranges as the average ranges between zero degree and 60 degree rotor blade angles. The results are shown in FIGURE 13 along with the comparison of ranges between tail technique and nose-tail technique. The average constant downwash results of 41 fps and 39.7 fps agree closely enough so that a value of 40 fps could be used as an overall average.

No attempt has been made in this study to calculate the influence of the V_x and V_y components. Also, no study was made of the 15 knot and 30 knot downwash influence.

Since the downwash at each launcher is dependent on the rotor blade position it is apparent that rockets fired from the left launchers will impact at different ranges from the rounds fired from the right launchers. While no calculations were made in this study specifically to determine the differences in impact range to be expected it is assumed that the magnitude will be similar to the difference in range between the rocket fired at 0 degree rotor position and 60 degree rotor position as presented in this report.

As has been shown, the downwash velocities and the perturbations of the downwash velocities have a very significant influence on the trajectories and dispersion of the 2.75 inch Rockets launched from a hovering helicopter.

A follow on to the United Aircraft study should be initiated to include the detailed effects of the helicopter fuselage. An experimental program should be initiated to verify the results of the calculated downwashes and the calculations presented in this report. The initial experimental program should include downwash measurements on a hover test stand and in a wind tunnel with a model of the AH1G. Rocket firings, should be run in conjunction with full scale downwash tests to verify the downwash calculations and rocket trajectory calculations. Downwash measurement locations for a tactical fire control unit can also be determined from the wind tunnel, hover stand and flight tests. Since the calculated constant downwash which gives the same range as the average downwash distribution is 40 fps it

171

seems that a probe located somewhere along the trajectory where the calculated downwash is 40 fps might be a potential location for a fire control probe. From FIGURE 4, this location would be in the region of r/R_r = .04 to .130.

The final probe location or locations should be determined experimentally taking all interferences into account.

References

1. Landgrebe, A. J. and Egolf, T.A., Prediction of Rotor Wake Induced Flow Along the Rocket Trajectories of an Army AH-1G Helicopter, Picatinny Arsenal Technical Report 4797. Prepared by the United Aircraft Research Laboratories for Picatinny Arsenal, Dover, NJ, March 1975.

2. Goldstein, R., Wasserman, S., Brooks, J., and Smolin, S., Feasibility Study of a High Drag Submunitioned Warhead to Improve the Effectiveness of the 2.75 inch Rocket System, Picatinny Arsenal Technical Report 4750, March 1974.

3. Barnett, B., Trajectory Equations for a Six-Degree-Of-Freedom Missile Using a Fixed-Plane Coordinate System. Picatinny Arsenal Technical Report 3391, June 1966.

172

FIGURE 1

CALCULATED ROCKET IMPACT RANGE (HOVER LAUNCH)

ZERO DOWNWASH   INITIAL ALTITUDE = 25'

OE (Degrees)	RANGE (Meters)
1.0	279
2.0	471
3.0	932
4.0	1610
5.0	2192
6.0	2658
7.0	3053
8.0	3333
9.0	3703
10.0	3978
11.0	4227

FIGURE 2

CALCULATED ROCKET IMPACT RANGE (HOVER LAUNCH)

(50 FPS CONSTANT DOWNWASH)

USING STANDARD 6D PROGRAM   INITIAL ALTITUDE - 25 FEET

LAUNCH θ_L (Deg)	RANGE (Meters)
1.0	1231
2.0	1836
3.0	2407
4.0	2836
5.0	3206
6.0	3523
7.0	3829
8.0	4094
9.0	4337
10.0	4559
11.0	4763

40 fps Constant Downwash

1.0	912
2.0	1601
3.0	2190
4.0	2661
5.0	3069
6.0	3431
7.0	3734
8.0	3986
9.0	4226
10.0	4455
11.0	4660

FIGURE 3

HELICOPTER ROTOR DOWNWASH
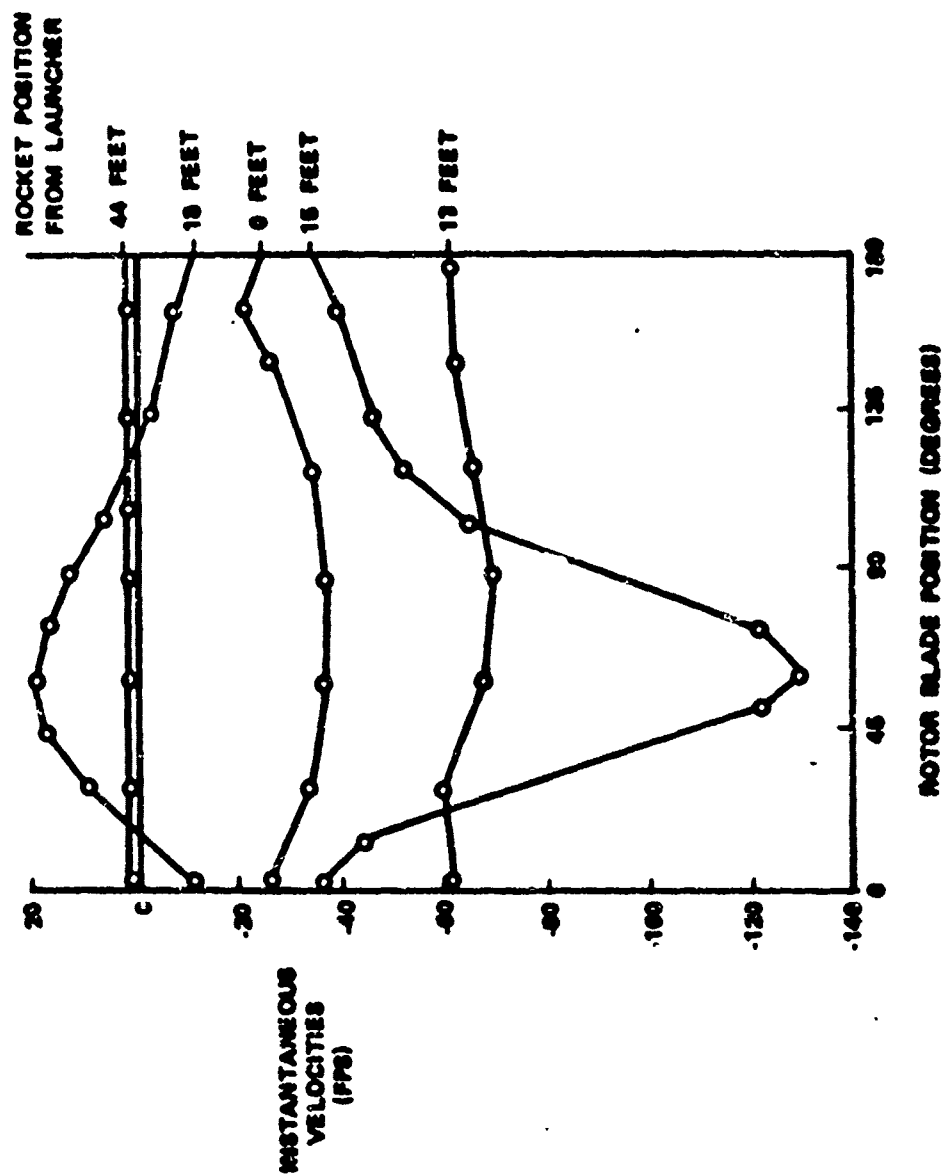
FIGURE 4

MINIMUM AND MAXIMUM DOWNWASH DISTRIBUTIONS

MINIMUM = 0° INITIAL BLADE ANGLE
MAXIMUM = 60° INITIAL BLADE ANGLE

TIME FROM ROCKET LAUNCH (sec)	ROCKET RANGE r/R_R	MINIMUM (fps)	MAXIMUM (fps)
0	0	-25.0	-38.0
.0077	.040	-32.1	-40.1
.0154	.077	-38.2	-42.1
.0231	.130	-41.8	-43.9
.0308	.182	-47.1	-44.1
.0385	.236	-49.6	-43.0
.0462	.291	52.0	44.0
.0539	.355	-55.3	-44.0
.0616	.414	-55.7	-51.2
.0693	.477	-57.8	-54.6
.077	.545	-58.5	-57.9
.0847	.616	-57.6	-70.2
.0924	.691	-40.2	-124.0
.1000	.773	-15.0	-17.8
.1077	.859	+ 4.9	+11.5
.1154	.941	+15.1	+ 6.4
.1230	1.036	+16.5	+ 2.0
.1308	1.123	+13.7	- 0.9
.1385	1.227	+ 3.1	- 4.4

FIGURE 5

CALCULATED RANGE (HOVER LAUNCH)   ALT = 25 FEET

VARIABLE DOWNWASH (MINIMUM)

0 DEGREE INITIAL POSITION AT ROCKET LAUNCH

STANDARD DOWNWASH PROGRAM USING TAIL DOWNWASH

θE (Degrees)	RANGE (Meters)
1.0	816
2.0	1506
3.0	2117
4.0	2600
5.0	3005
6.0	3359
7.0	3671
8.0	1937
9.0	4191
10.0	4435
11.0	4642

60 DEGREE INITIAL ROTOR POSITION AT ROCKET
LAUNCH VARIABLE DOWNWASH (MAXIMUM)
STANDARD DOWNWASH PROGRAM USING TAIL DOWNWASH

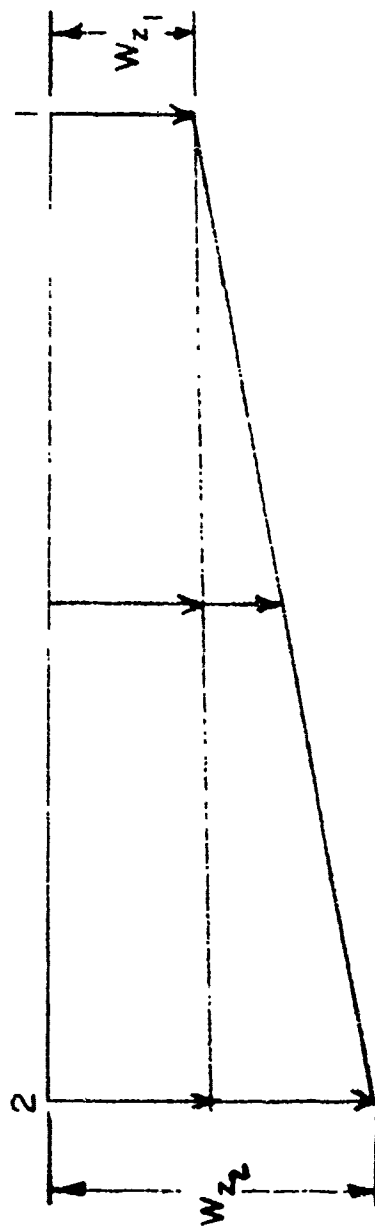|	
1.0	1072
2.0	1796
3.0	2337
4.0	2757
5.0	3144
6.0	3480
7.0	3734
8.0	4052
9.0	4293
10.0	4517
11.0	4722

177

FIGURE 6

$$C_{N(DOWNWASH)} = \left(\frac{dC_N}{d\alpha}\right)_{2.75} \frac{W_{z_1}}{V_R} + \left(\frac{W_{z_2} - W_{z_1}}{V_R}\right) 2.0$$
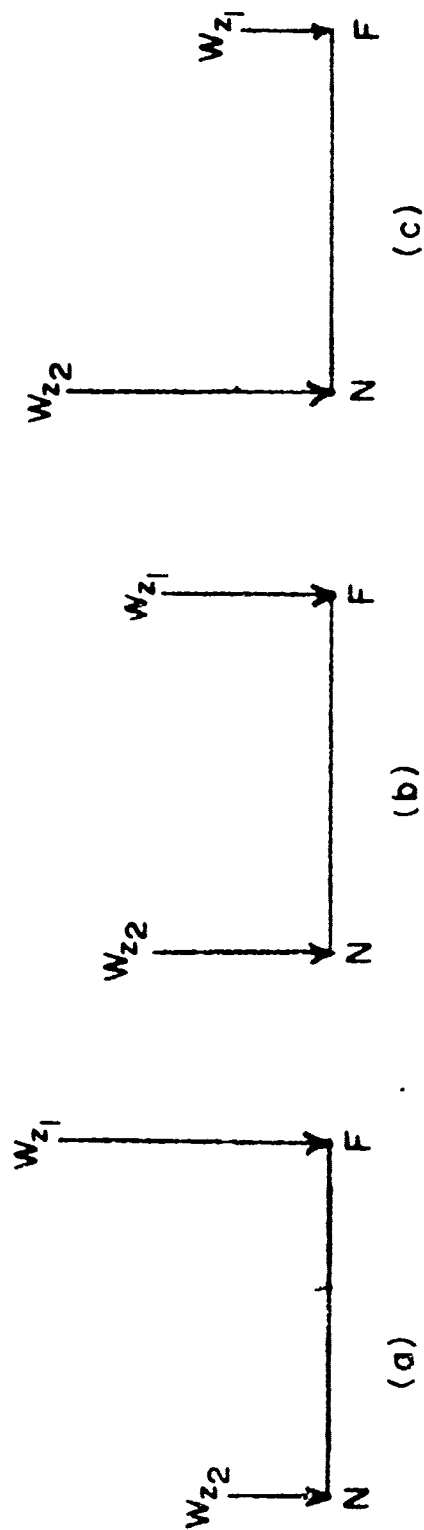
FIGURE 1

FIGURE 7

W_{z_2} → N

W_{z_1} → F

(a)

W_{z_2} → N

W_{z_1} → F

(b)

W_{z_2} → N

W_{z_1} → F

(c)

FIGURE 2

179

FIGURE 8

$$X_{CP(DOWNWASH)} = \frac{2.0(2.3)\left(\dfrac{W_{z_2}-W_{z_1}}{V_R}\right) + C_{N\,2.75}(\text{BASED ON } W_{z_1})\; X_{CP\,2.75}(\text{BASED ON } W_{z_1})}{C_{N(DOWNWASH)}}$$

W_{z_1}

W_{z_2}

2.3 CAL

$2.0\left(\dfrac{W_{z_2}-W_{z_1}}{V_R}\right)$

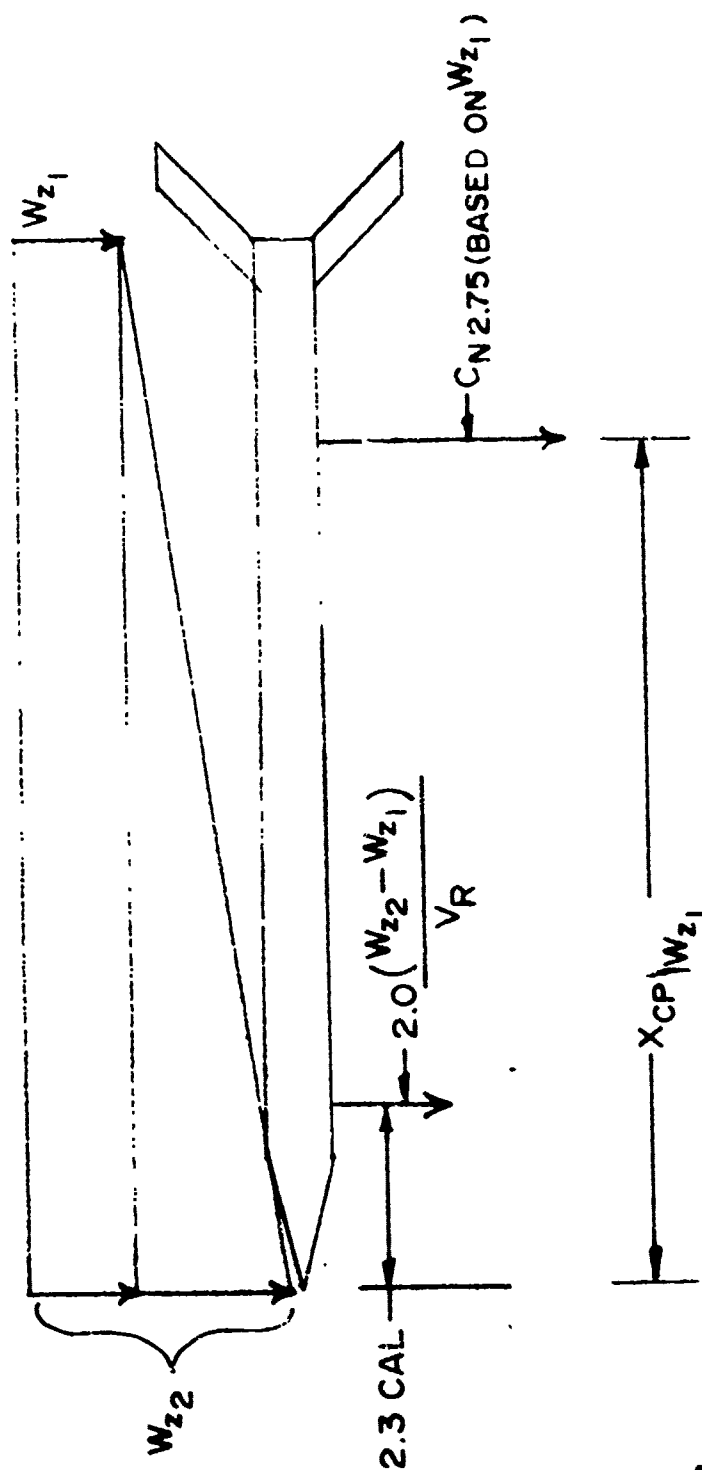$C_{N\,2.75}(\text{BASED ON } W_{z_1})$

$X_{CP}|W_{z_1}$

FIGURE 3

FIGURE 9

CALCULATED RANGE (HOVER LAUNCH)   ALT = 25 FEET
VARIABLE DOWNWASH DISTRIBUTION (MINIMUM)
0 DEGREE INITIAL ROTOR POSITION AT ROCKET
LAUNCH USING DOWNWASH DISTRIBUTION OVER
NOSE AND TAIL

QE	RANGE
1.0	765
2.0	1482
3.0	2206
4.0	2555
5.0	3091
6.0	3428
7.0	3657
8.0	3981
9.0	4265
10.0	4483
11.0	465?

60 DEGREE INITIAL ROTOR POSITION AT RANGE
LAUNCH VARIABLE DOWNWASH DISTRIBUTION (MAXIMUM)
USING DOWNWASH DISTRIBUTION OVER NOSE AND TAIL

1.0	968
2.0	1661
3.0	2126
4.0	2567
5.0	3020
6.0	3351
7.0	3705
8.0	4020
9.0	4225
10.0	4455
11.0	4700

FIGURE 10

CALCULATED ROCKET IMPACT RANGE (HOVER LAUNCH)

(50 FPS CONSTANT DOWNWASH RUN
WITH VARIABLE DOWNWASH PROGRAM)

LAUNCH αE (Deg)	RANGE (Meters)
1.0	1211
2.0	1871
3.0	2397
4.0	2828
5.0	3200
6.0	3534
7.0	3823
8.0	4089
9.0	4331
10.0	4560
11.0	4762

40 fps Constant Downwash Run with Variable
Downwash Program

1.0	880
2.0	1567
3.0	2162
4.0	2637
5.0	3030
6.0	3412
7.0	3718
8.0	3951
9.0	4214
10.0	4443
11.0	4649

FIGURE 11

2.75 inch ROCKET AERODYNAMIC COEFFICIENTS

YAW DAMPING COEFFICIENT ($C_{M_q} + C_{M_{\dot{\alpha}}}$)

MACH NUMBER	$C_{M_q} + C_{M_{\dot{\alpha}}}$
0	920
.6	920
.7	864
.8	879
.9	892
.95	912
1.0	1039
1.05	1068
1.1	978
1.2	897
1.3	627
1.4	497
1.5	474
2.0	239
3.0	131

DRAG COEFFICIENT

M	C_D
0	0.637
.86	0.637
.90	0.650
.93	0.668
.95	0.696
1.03	1.197
2.0	0.981
2.2	0.917

183

FIGURE 12

NORMAL FORCE CENTER OF PRESSURE (CALIBERS AFT OF NOSE) Xcp

Angle of Attack	Mach	0	.6	.7	.8	.9	.95	1.0	1.05
		1.1	1.2	1.3	1.4	1.5	2.0	3.0	4.0
		5.0							
$0°$		15.75	15.74	15.74	15.46	15.19	15.6	16.01	16.01
		15.87	15.87	15.05	14.78	14.65	13.28	12.15	11.48
		10.965							
$4°$		14.92	14.92	15.1	15.05	15.1	15.05	15.33	15.46
		15.19	14.92	14.64	14.37	14.37	13.28	12.15	11.48
		10.965							
$8°$		14.24	14.24	14.1	14.23	14.37	14.37	14.38	14.65
		14.37	14.24	14.1	13.69	13.69	13.28	12.15	11.48
$12°$ & $57.3°$		13.59	13.59	13.69	13.55	13.55	13.56	13.69	13.69
		13.42	13.14	13.14	13.0	12.73	12.44	12.15	11.48
		10.965							

NORMAL FORCE COEFFICIENT (C_N)

Angle of Attack	Mach	0.0	.6	.7	.8	.9	.95	1.0	1.05
		1.1	1.2	1.3	1.4	1.5	2.0	3.0	
$0°$		0	0	0	0	0	0	0	0
		0	0	0	0	0	0	0	
$4°$		1.06	1.06	.996	1.09	1.09	1.09	1.12	1.15
		1.09	1.0	.871	.744	.741	.591	.520	
$8°$		1.94	1.94	1.77	1.87	1.87	1.83	1.99	1.99
		1.93	1.80	1.71	1.55	1.55	1.27	1.24	
$12°$		2.61	2.61	2.55	2.57	2.57	2.55	2.74	2.74
		2.74	2.74	2.65	2.55	2.39	2.14	2.28	
$57.3°$		15.16	15.16	14.27	15.64	15.64	15.64	16.05	16.48
		15.64	14.32	12.48	10.65	10.60	8.46	7.44	

FIGURE 13

AVERAGE RANGE IMPACT RANGE BETWEEN ROCKETS
LAUNCHED AT 0°
ROTOR POSITION AND 60° ROTOR POSITION
FOR LAUNCHER 4

Tail Downwash QE (Degrees)	RANGE (Meters)	Nose-Tail Downwash QE (Degrees)	RANGE (Meters)
1.0	944	1.0	867
2.0	1651	2.0	1572
3.0	2227	3.0	2166
4.0	2679	4.0	2561
5.0	3075	5.0	3056
6.0	3420	6.0	3390
7.0	3728	7.0	3581
8.0	3995	8.0	4000
9.0	4242	9.0	4245
10.0	4476	10.0	4469
11.0	4682	11.0	4676

CONSTANT DOWNWASH REQUIRED TO MATCH ABOVE
RANGES CALCULATED WITH TAIL DOWNWASH

USING VARIABLE DOWNWASH PROGRAM		USING CONSTANT DOWNWASH	
QE	fps	QE	Downwash
1	41.5	1	40.53
2	40.7	2	39.6
3	40.9	3	39.5
4	42.2	4	39.9
5	41.5	5	39.1
6	40.7	6	36.9
7	41.0	7	37.1
8	43.2	8	39.8
9	42.4	9	40.6
10	42.8	10	41.6
11	42.9	11	42.2
Average	41.8	Average	39.7

THE MEASUREMENT OF HELICOPTER AIR DATA USING
A SWIVELLING PITOT-STATIC PRESSURE PROBE

JOHN CARTER
E-A INDUSTRIAL CORPORATION
4500 North Shallowford Road
Chamblee, Georgia   30341

ABSTRACT

This paper describes a system which has been developed to provide accurate air data in helicopters over the complete flight envelope. The system uses a pitot-static pressure probe which aligns with the local airflow under the helicopter rotor. The magnitude and direction of the local airflow is measured and used to determine the forward and sideways aircraft indicated airspeeds. The static pressure source is free from the usual errors associated with helicopter altimetry and is ued to provide accurate altitude and altitude rate data.

This Air Data System has been evaluated in prototype form by US Army Aviation Engineering Flight Activity and preliminary flight test data are presented.

A similar system has been used by US Army Frankford Arsenal as a Relative Wind Sensor for a Fire Control System during 2.75 Inch rocket firing.

It has been found as a result of these test programs that the sensor principle permits the additional derivation of specific airflow data in the rotor induced flow field which can be of assistance in the computation of rocket trajectories. The system is capable of generating outputs of rotor induced flow magnitude and direction. The capability exists of sensing the boundary of the rotor induc_.· flows field to assist in predicting the time of flight during which the ballistic missile is influenced by the rotor.

Additional experiments are planned to use an air data system of this type to map the rotor induced flow field more precisely under varying flight conditions.

1. BACKGROUND

During the first 30 years of operations helicopters have been beset by
a number of technical limitations which have prevented their use as all-
weather, world-wide dedicated vehicles. Most of these limitations were
most severe in the low speed flight region and were due to power and
control margin deficiencies. As a result operational use in the low
speed region was considered to be temporary expedient used only in take-
off and touch down and otherwise to be generally avoided. In this
environment it was not found particularly onerous to make do with velocity
and position data which became inaccurate at low speeds because contact
with the ground was a pre-requisite of low speed operation.

The only agencies with a desire to establish more accurate velocity sensing
devices for helicopters were the test centers involved in defining
performance, stability, aerodynamics etc.

In the last 10 years the helicopter has developed to overcome many of
the low speed limitations of its formative years and now continuous
low speed operation in poor visibility has become an operational necessity.
The roles of search and rescue, submarine detection, mine countermeasures,
front line supply, air-to-ground attack and reconnaisance all demand a
low speed, dirty weather, day or night capability. In its new operating
environment the helicopter has developed an operational need for accurate
low-speed velocity sensing and because it is an aircraft its characteristics
depend on its air velocities and positions.

The conventional methods of measuring air data in airplanes have been in
existence for more than half a century and have not been bettered despite
the rate of technological advancement in most other measurement fields.
The pitot-static pressure tube fixed to the airframe is inherently a
very reliable, simple and low cost source of data.

In conventional aircraft applications airspeed is derived by measuring the
difference between the total pressure (P_t) occuring at a forward-facing
pitot probe mounted on the airframe and the static pressure (P_s) measured
at a static vent also mounted on the airframe. These two sources may be
on the same probe, but more usually are at different sites. Over the
speed range corresponding to helicopter use the indicated airspeed may
be obtained as a very close approximation by determining the square root
of the pressure difference and multiplying by a scale factor thus :

$$V = K . \sqrt{(P_T - P_S)}$$

This relationship is depicted in figure 1 from which
it can be seen that the slope of $(P_t - P_s)$ becomes very small at low airspeeds.
This creates a practical difficulty in that presently available pressure-
measuring techniques which are suitable for aircraft application are poor
at measuring pressure differentials of less than 1/1200 atmospheres which
corresponds to an airspeed of 20 knots.

Various systems have been designed to measure airspeed in a helicopter with varying degrees of success. It is obvious that a fixed pitot probe can never measure airspeed at low velocities particularly in the presence of rotor-induced flow. This same limitation must also apply to any snesor which relies on direct measurement of dynamic pressure or airflow speeds along the flight path for, when hovering, there is no air flow and no dynamic pressure. Such devices, if sufficiently sensitive, may be accurate when the air flow is greater than 5 knots, but sensitivity usually implies lack of ruggedness.

One solution which seemed, a priori , to satisfy both ruggedness and ease-of-installation criteria while offering the promise of providing accurate data through the hover involved the use of a swivelling pitot-static pressure head deliberately mounted within the rotor induced-flow field.

2. PRINCIPLE OF OPERATION

The head has freedom to swivel and is caused to align itself with the resultant airflow vector under the rotor by the 'Weathercock' action of a vane attached to the swivelling probe. Resolvers mounted between the swivelling and airfram-fixed protions of the device, provide a means for measuring the direction of the airflow vector relative to airframe axes.

From these angles and from the value of the magnitude of the resultant airflow vector (as computed from the pitot-static sensor) the horizontal fore-aft component of the airflow vector can be computed.

Figure 2 depicts the induced flow field in the plane of the probe.

Reference to this figure shows that the horizontal component of resultant airflow is given by:

$$\overline{V} \cos\alpha = V + v\sin i.$$

However, in steady state helicopter flight conditions, when the induced velocity v is large, i is a small angle. Conversely, when i is a large angle, the rotor-induced velocity v is low. Hence

$$V >> v \sin i$$

$$\text{and} \quad \overline{V} \cos \alpha \approx V$$

(the horizontal component of result airflow is approximately equal to the forward airspeed). It will be observed that the pressure sensor activated from the probe dynamic pressure input will never have to sense zero airspeed because, even in the hover, $\overline{V}$ will be equal to the induced flow speed.

188

It is evident that if this principle is satisfactory for measuring airspeed it can also be used to measure the vertical component of down wash under the helicopter rotor. Further, since in a "two axis" system the probe is always aligned with the local airflow vector, it provides a location for the static pressure vents which will furnish a repeatable static pressure source. The problem of relating the output of this static source to altitude (and altitude rate) is thus reduced to that of static source error compensation (SSEC) for the pressure field under the rotor.

2.1 <u>Verification of the Principle</u> - In 1968 an experimental single-axis system was built by Marconi-Elliott Avionics Systems Ltd. with the capability of measuring the horizontal component from 30 knots aft to 197 knots forward. This system is shown in figure 3. The system was test flown in England on a Westland Scout and by USAAEFA at Edwards AFB, where it was flown on a Bell UH1C in a variety of positions for measuring either forward or lateral IAS. All of the Flight Tests in both aircraft showed commonality in terms of repeatability as shown in Figure 4. Above approximately 30 knots IAS the probe was clear of the downwash and behaved like a normal airspeed indicator.

Below approximately 30 knots the instrument was repeatable for any given probe mounting position but each position produced a different characteristic. Generally a small discontinuity occured at one forward speed which could be minimized by choice of probe location. Subsequent tests have shown that the repeatable data can be corrected to give calibrated airspeed in a large range of probe locations, and so minimization of the discontinuity is not critical. The tests carried out on the UH1C also showed that the equipment could be used to provide valuable data about the behaviour of the airflow under the rotor. The induced flow speed and direction could be evaluated in a variety of flight conditions, including vertical climb and descent, autorotation, acceleration, and straight and turning level flight.

USAASTA Project 71-30 Final Report Number 1 contains a full description of the UH1C test program, methods and results which will not be repeated here except to comment that they demonstrate the ability of a single-axis system to measure helicopter airspeed accurately in one axis by the resolution of rotor downwash.

3. <u>PRODUCT DEFINITION</u>

On the basis of the excellent results obtained in this tests a new system was designed to extend the principle to a "two-axis" sensor (Figure 5). The prototype omni-directional system was purchased by USAAEFA in 1972 and has been used almost continuously since that time as a flight test reference. Prior to the employment of this system as a reference it was evaluated by USAAEFA in many flight conditions and the results are published in USAAEFA Project 71-30 Final Report Number 6. During this evaluation an altitude channel was added to the system to verify the theory that the sensor would provide accurate, repeatable altitude and altitude rate data.

I would like to state, with USAAEFA permission, the summary of findings in these tests as follows:-

3.1 FLIGHT TEST RESULTS SUMMARY

(a) The dual axis probe placed in the rotor downwash provides a good source for airspeed and flow direction information as well as static pressure and pressure changes.

(b) The dual axis system provides reliable measurements of longitudinal and lateral airspeed components.

(c) Linearization circuits greatly improve the system and render the discontinuity imperceptible to the pilot

(d) The altimeter produces altitude information superior to that obtained from the aircraft standard system at low speed.

(e) The vertical speed information from the system is better than that obtained from the standard system, the test boom system or the radar altimeter when flying over uneven terrain.

4. FUTURE PROGRAM

It has been shown from these tests and others in progress by U.S. Army U.S. Navy, British Ministry of Defense. and Messerschmidt-Bolkow-Blohm that the principle of air data measurement using a swivelling pitot-static probe can satisfy the total air data requirements of helicopters.

At present an air data computer is being flown which provides outputs of all of the parameters given in Table I from a single unit.

Tests are almost complete of a system which will also provide pilots with indications of engine efficiency, maximum torque and payload margin. This latter system will be incorporated into the air data computer with minimal hardware change.

Developments are in hand on advanced display techniques and all that remains technologically is to customize the system for your application.

5. HELICOPTER INTEGRATED AIR DATA SYSTEM

The definitive product consist of the following equipment:-

(a) Multi-axis Swivelling Pitot-Static Probe
(b) Digital Air Data Computer
(c) Displays of Altitude, Altitude Rate, Calibrated Airspeed, Sideslip Angle, Combined Torque and Maximum Torque, Payload Margin, Air Temperature. Engine Efficiency (display format optional).

190

5. <u>HELICOPTER INTEGRATED AIR DATA SYSTEM (CONT)</u>

The system can provide additional electrical analog or digital outputs of Altitude (Gilham coded for IFF), Angle of Attack, True Airspeed, air density, density ratio, density altitude, induced flow airspeed and direction.

The system excluding displays consumes about 80VA of 400Hz 115 volt single phase power and weighs about 22 lb. The MTBF is 3000 hours. The computer is housed in a 5 inch by 7 inch by 14 inch (½ ART short) case.
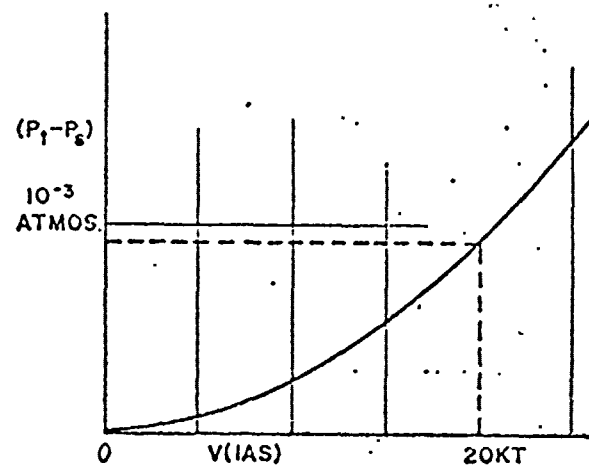
FIGURE 1 . IAS VERSUS $(P_t - P_s)$

$$V = \bar{V}.\cos\alpha - \upsilon.\sin i$$
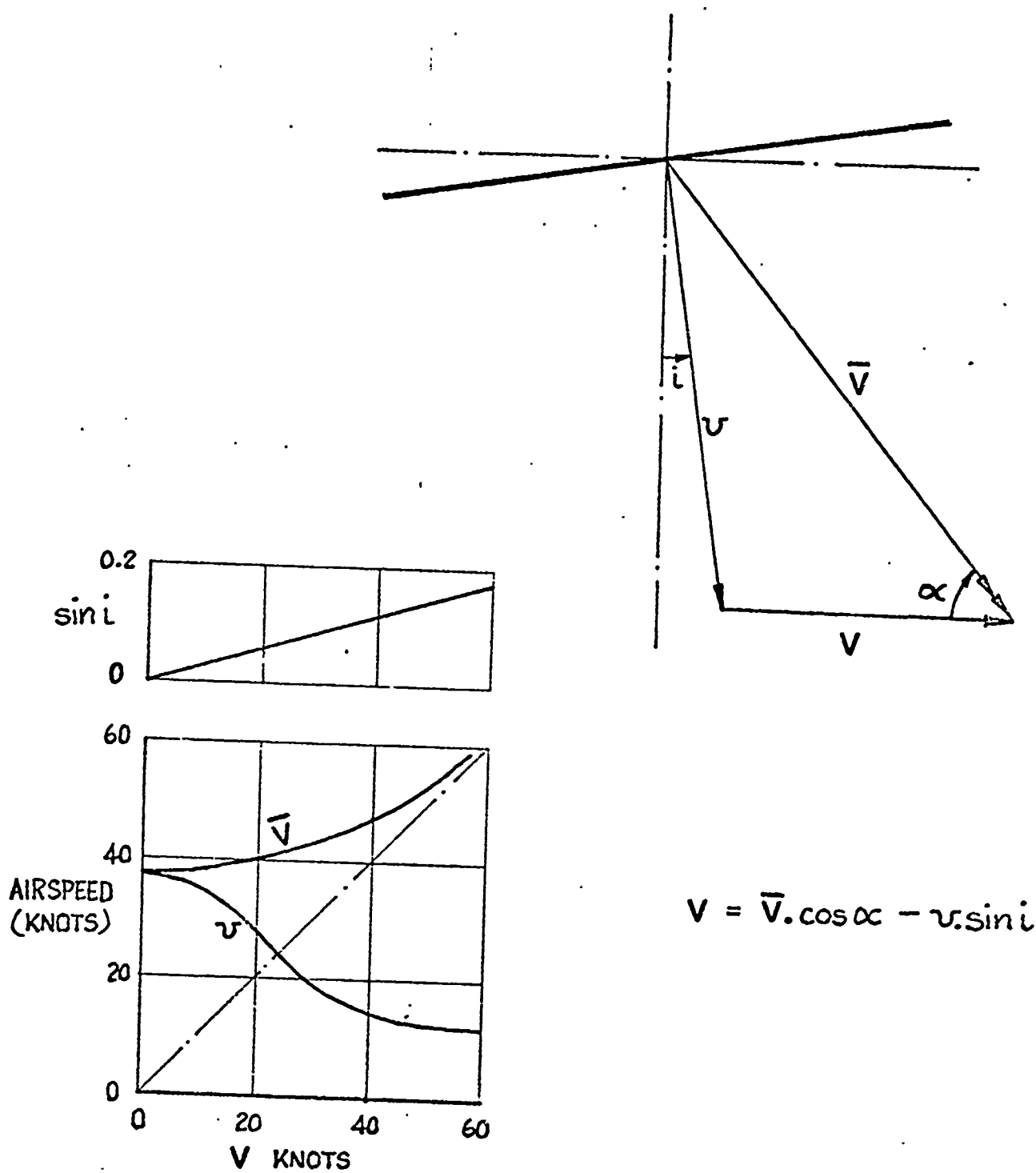
FIGURE 2. **INDUCED FLOW FIELD**

COMPUTER

SINGLE AXIS
PROBE

AIRSPEED
INDICATOR

E-A INDUSTRIAL
CORPORATION
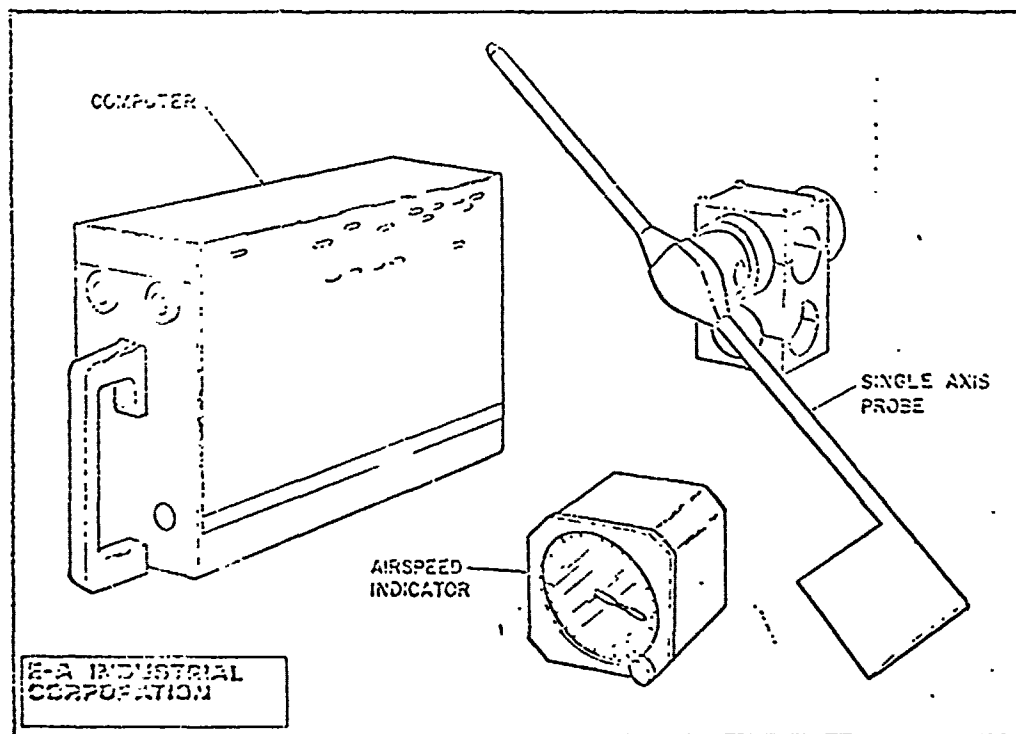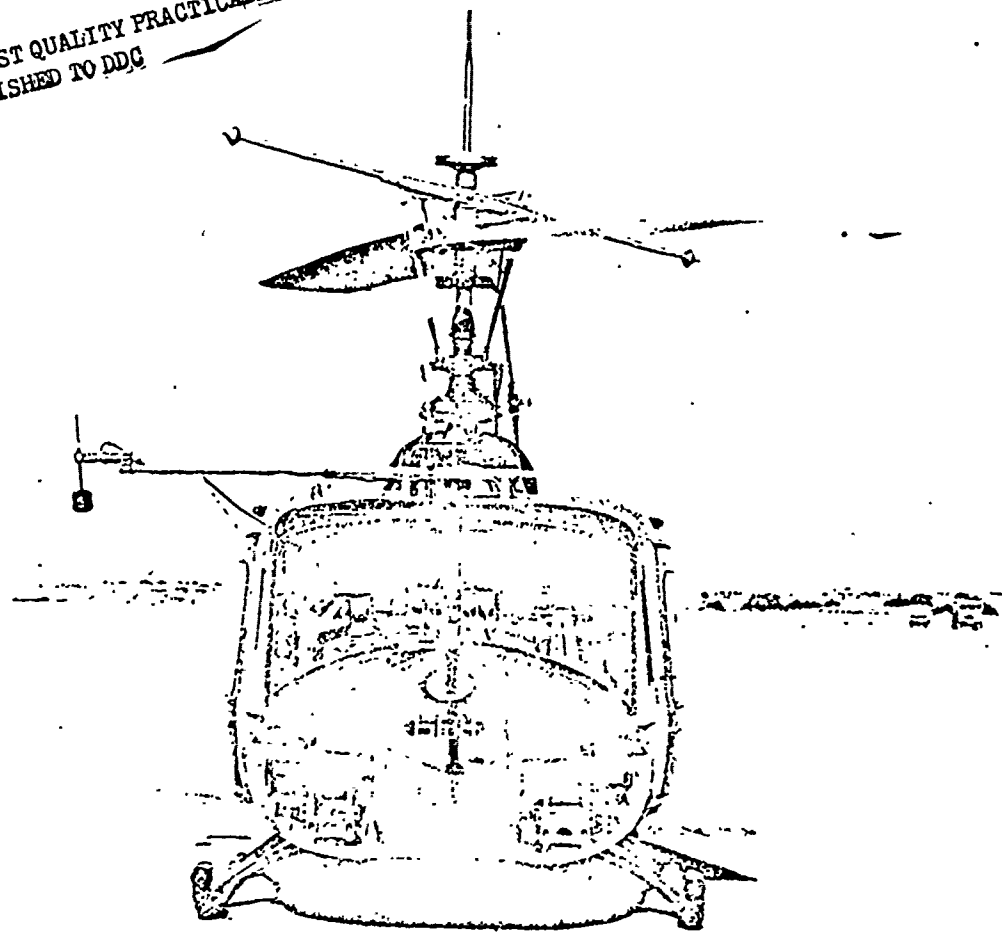
FIGURE 3. PROTOTYPE FORWARD AIRSPEED SYSTEM

FIGURE 4 .   PROTOTYPE TEST RESULTS — UH 1C

195
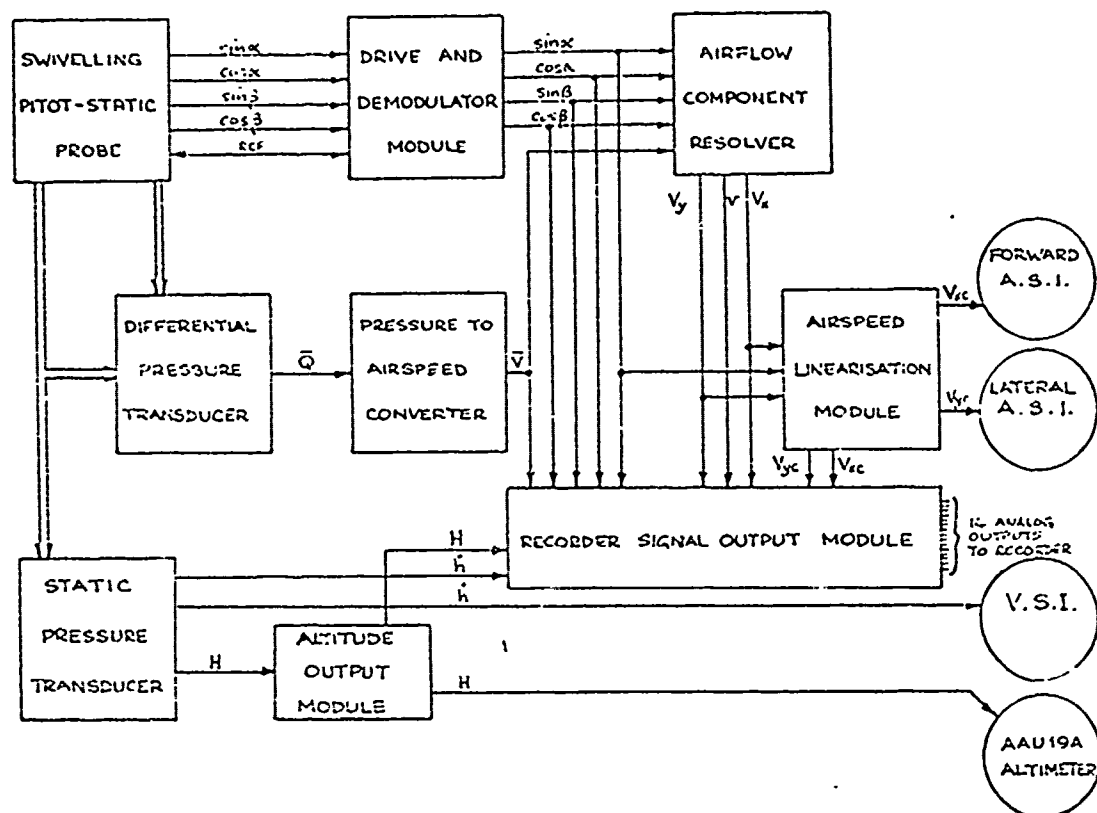
Displayed Data

(a) Forward Corrected Airspeed — Vxc

(b) Sideways Corrected Airspeed — Vyc

(c) Vertical Speed — $\dot{h}$

(d) Altitude — H

Electrical Outputs

(e) Local Airflow Speed — $\bar{V}$

(f) Sine Airflow Pitch Angle — $\sin \alpha$

(g) Cosine Airflow Pitch Angle — $\cos \alpha$

(h) Sine Airflow Yaw Angle — $\sin \beta$

(i) Cosine Airflow Yaw Angle — $\cos \beta$

(j) Forward Corrected Airspeed (Coarse) — $Vxcc = \bar{V} \cos \alpha \cos \beta + PEC$

(k) Forward Corrected Airspeed (Fine) — Vxcf

(l) Sideways Corrected Airspeed — $Vyc = \bar{V} \sin \beta + PEC$

(m) Forward Indicated Airspeed — $Vx = \bar{V} \cos \alpha \cos \beta$

(n) Sideways Indicated Airspeed — $Vy = \bar{V} \sin \beta$

(o) Vertical Component of Local Airflow — $v = \bar{V} \sin \beta \cos \alpha$

(p) Vertical Speed — $\dot{h} = dh/dt$

(q) Altitude (Coarse) — Hc

(r) Altitude (Fine) — Hf

FIGURE 5. EXPERIMENTAL AIR DATA SYSTEM 1972
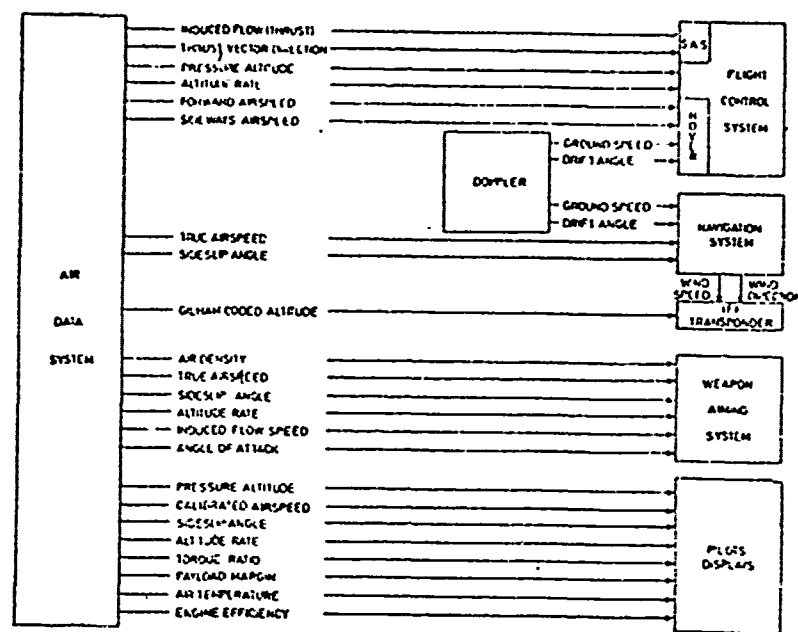
Output Function	Range	Accuracy (Plus & Minus)
Forward Calibrated Airspeed	40 Knots Aft to 250 Knots Fore	2 Knots or 1%
Lateral Calibrated Airspeed	40 Knots Left to 40 Knots Right	2 Knots
Total Calibrated Airspeed	0 Knots to 250 Knots	2 Knots or 1%
Total True Airspeed	0 Knots to 250 Knots	3 Knots or 1.5%
Sideslip Angle	350° Continuous	0.5 Degrees
Angle of Attack	360° Continuous	0.5 Degrees
Pressure Altitude	-2000 Ft. to 20000 Ft.	20 Ft. or 0.2%
Altitude Rate	6000 Ft./Min. Climb or Descent	50 Ft./Min.
Air Density	0.0026 slugs/Ft^3 to 0.0012 slugs/Ft^3	1%
Density Ratio	1.060 to 0.500	1%
Density Altitude	-2000 Ft. to 20000 Ft.	50 Ft.
Static Air Temperature	+50°C to -75°C	1 Degree
Torque Ratio	0 to 150%	1%
Engine Efficiency	85% to 110%	1%
Payload Margin	-200 lb to 10000 lb.	150 lb.

TABLE 1. HELICOPTER AIR DATA SYSTEM 1975
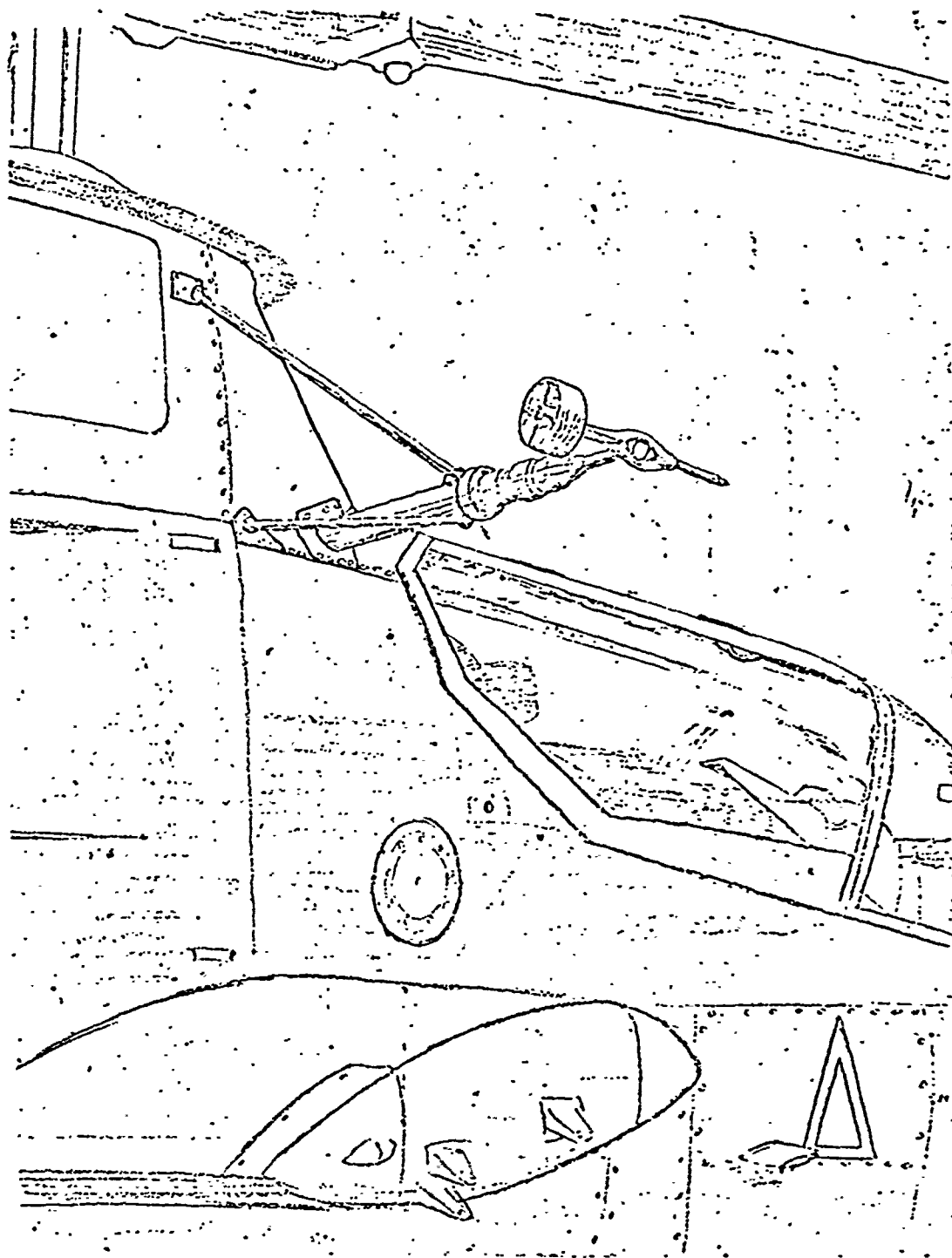
E-A INDUSTRIAL CORPORATION

MEASUREMENT OF HELICOPTER AIR DATA

USING A

SWIVELLING PITOT-STATIC PRESSURE PROBE

THE CORRELATION OF ACTUAL INDUCED FLOW WITH
THEORY FOR BELL NUH-1M HELICOPTER ROTOR
OPERATING IN LEVEL FLIGHT

JOHN CARTER
E-A INDUSTRIAL CORPORATION
4500 North Shallowford Road
Chamblee, Georgia   30341

ABSTRACT

This paper presents a simple theoretical analysis of the mean local flow
velocities at a point under a helicopter rotor for a range of horizontal and
vertical helicopter speeds.

This theoretical analysis is then compared with practical data obtained using
a swivelling pitot-static pressure probe mounted on a Bell NUH-1M helicopter
for the level flight case.

This comparison shows that for level flight good correlation between theory
and practice occurs over the complete forward speed range. The exception to
the good theoretical correlation is in the region of the induced flow field
wake boundary when the flow velocities are lower than expected.

The theory and experiment has only considered mean flow conditions and takes
no account of the flow modulation effects caused by each blade. A technique
is suggested by which the modulation effects can be evaluated under a helicopter
rotor.

1. Introduction

During the period 1968-1975 the Instrument Systems Division of Marconi-Elliott Avionic Systems Limited has been using a swivelling pitot-static probe to measure helicopter air data. During this period there has been from time to time a number of unexplained anomalies in the flight test data.

This paper is intended to present the classical theory underlying the induced flow velocities below a rotor in a form that can be easily related to actual practical results.

From this it is hoped to examine anomalous data in relation to theoretical expectations in order to assist in prediction of problem areas. If, in the light of practical results, the classical theory can be modified into a general empirical form it should be possible to predict all future air data system performance without recourse to flight evaluation.

2. Basis of Theoretical Analysis

The airflow at a point under a helicopter rotor is a function of two basic theoretical determinants. At low horizontal rotor speeds the point will be within the rotor induced flow pattern (Figure 1). The theoretical air velocity in this region can be determined for known values of horizontal and vertical helicopter speeds using the blade element theory (Mangler, RAE Report AERO 2247, 1948). At higher helicopter speeds the point under the rotor will be in the free airstream and, therefore, the local velocity will be obtained by direct solution of a triangle of velocities (Figure 2).
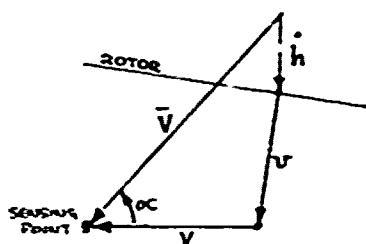
$\dot{h}$ = ALTITUDE RATE
υ = INDUCED VELOCITY
V = FORWARD AIRSPEED
$\bar{V}$ = LOCAL AIRSPEED
α = LOCAL FLOW ANGLE

FIGURE 1   INDUCED FLOW REGION
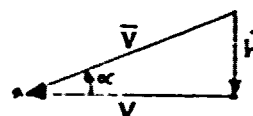   TRIANGLE OF VELOCITIES

FIGURE 2.   HIGH SPEED TRIANGLE
            OF VELOCITIES

3. Low Speed Flight Region

The blade element theory gives us a relationship between the rotor induced airflow velocity and the axial and radial rotor velocities. This relationship is plotted in Figure 3 in non-dimensional form. The value of v_h is given by the equation:-

$$v_h = \left(\frac{T}{2\pi\rho R^2}\right)^{\frac{1}{2}}$$

where T = the thrust of the rotor = weight of the helicopter
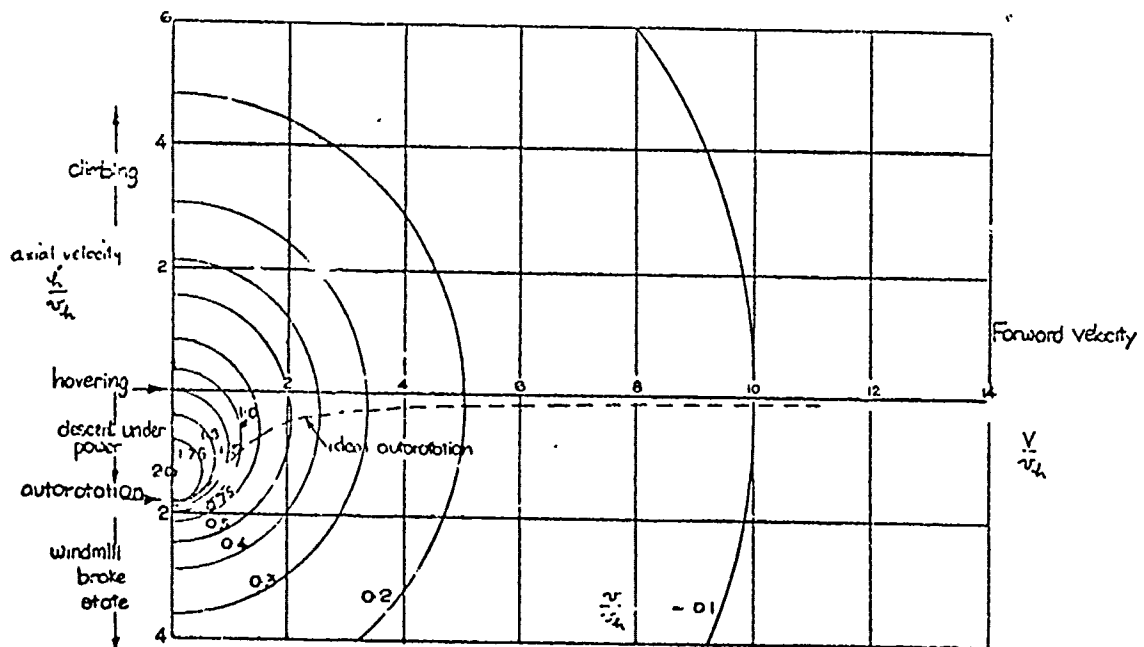
ρ = air density

R = rotor radius

FIGURE 3   Induced velocity in forward flight

By interpolation the values of induced velocity can be read from Figure 3 and the triangles of velocity can be solved to obtain local airflow velocity.

Figure 1 shows the velocity triangle in which it can be seen that

The local flow speed $(\overline{V}) \doteqdot [(h^{\cdot} + v)^2 + (V)^2]^{\frac{1}{2}}$

The airflow angle at the horizontal $(\alpha) = \tan^{-1}\left(\frac{h^{\cdot} + v}{V}\right)$

The values of $\bar{V}$ and α are plotted in Figure 4 for the range of horizontal and vertical speeds of interest. The graph is plotted in non-dimensional form.
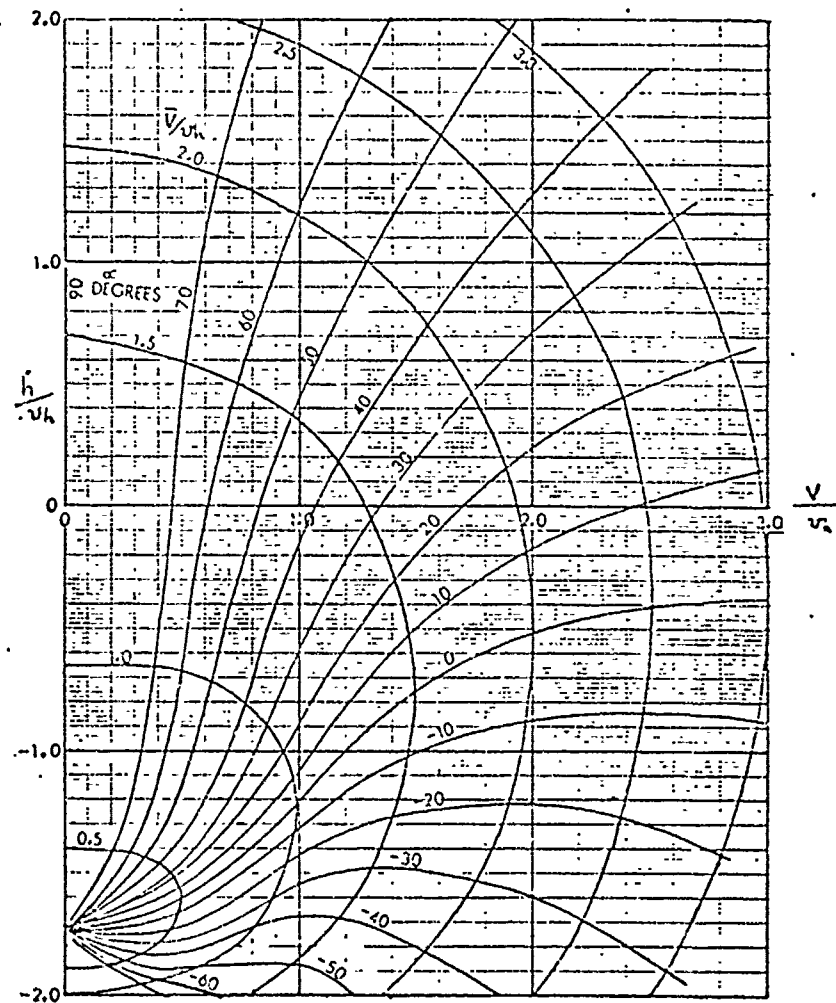

FIGURE 4. NON-DIMENSIONAL EVALUATION OF $\bar{V}$ AND α
FOR THEORETICAL INDUCED FLOW, IN
FORWARD, CLIMBING AND DESCENDING FLIGHT.

4. High Speed Flight Region

The high speed region velocities being a simple triangular solution (Figure 2) gives the following values:-

The local flow speed $(\overline{V}) = [\ (h^{\cdot})^2 + (V)^2\ ]^{\frac{1}{2}}$

The airflow angle at the horizontal $(\alpha) = \tan^{-1} \dfrac{h^{\cdot}}{V}$

The values of $\overline{V}$ and α are plotted in Figure 5 for the range of horizontal and vertical speeds of interest in non-dimensional form.
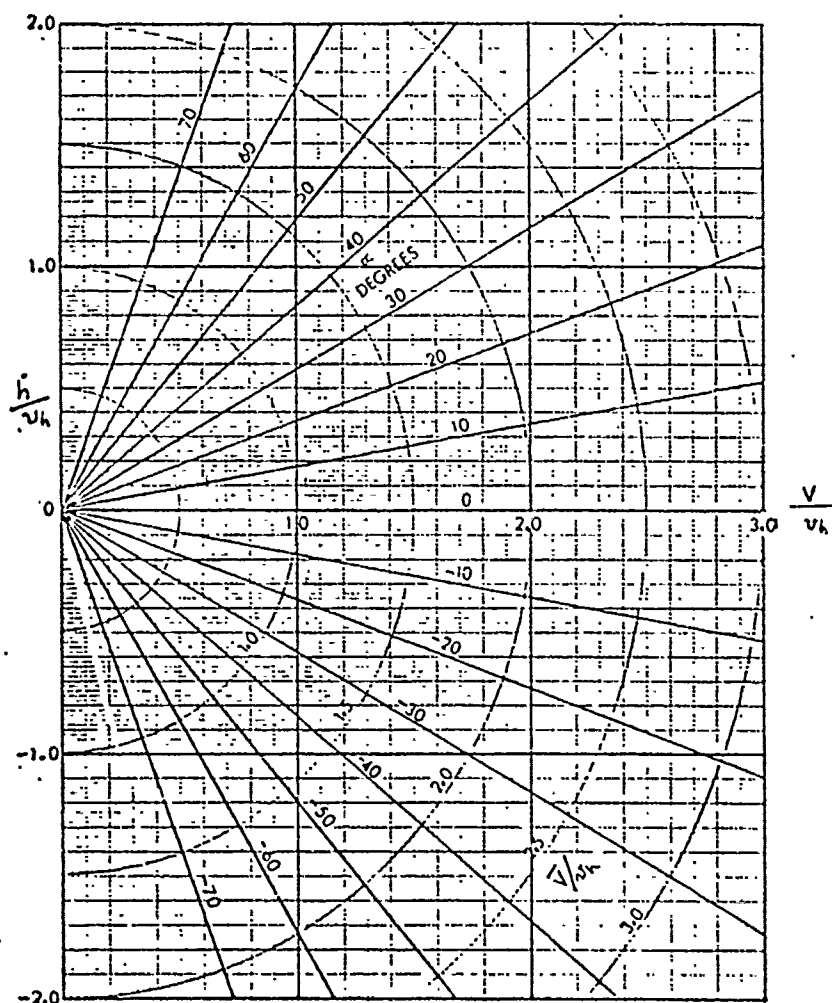

FIGURE 5. NON-DIMENSIONAL EVALUATION OF $\overline{V}$ AND α.
FOR FREE STREAM AIRFLOWS, IN
FORWARD, CLIMBING AND DESCENDING FLIGHT.

5. Practical Modification of the Theory

If we postulate a probe mounting position such that the probe transistions from the induced flow pattern to free stream at airflow angles less than 30°, the linear theory would give a velocity diagram as shown in Figure 6,
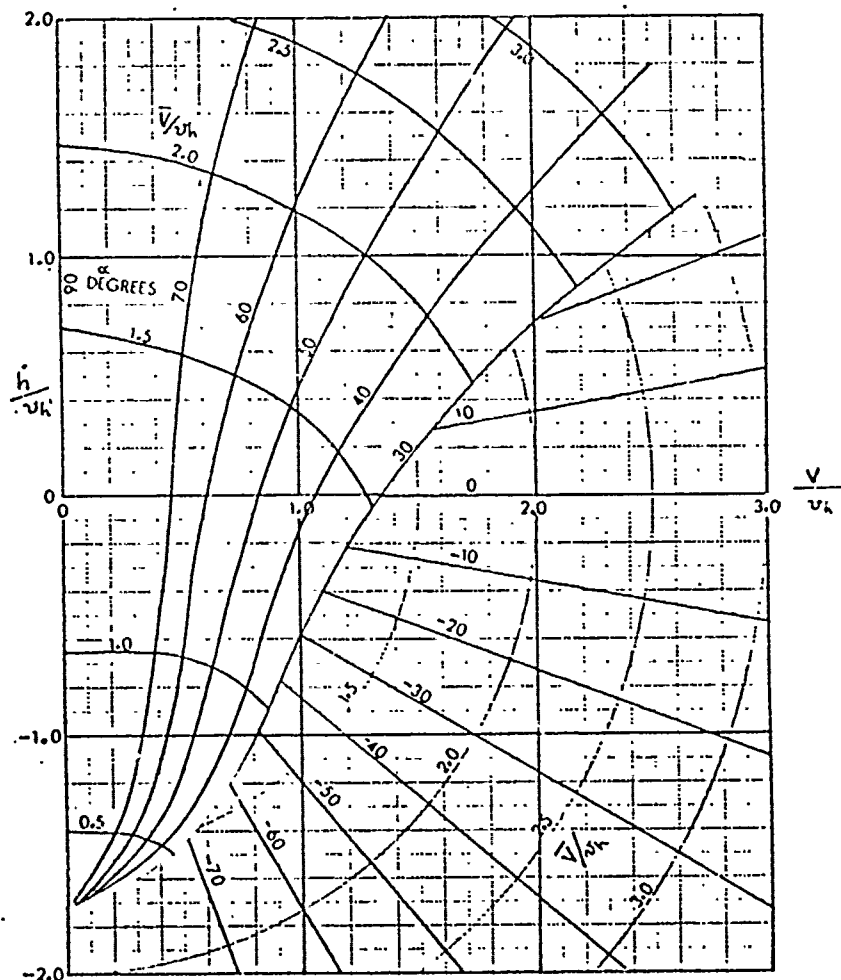

FIGURE 6. NON-DIMENSIONAL EVALUATION OF $\bar{V}$ AND $\propto$
FOR HYPOTHETICAL POINT , IN
FORWARD, CLIMBING AND DESCENDING FLIGHT.

There are two additional features in the practical case which modify this linear theory concept. These are:-

(a) The fact that there is a swirl component of induced flow such that actual airflow angle (α) varies from theoretical airflow angle (α) by a value up to 1°.

(b) The fact that under almost all conditions of flight there is upwash, rather than downwash at the tips of the rotor. Results suggest in the region of 80% to 120% of the rotor radius the induced flow is reversed. Hence the boundary between the low speed and high speed region will produce a non-linear behaviour above and below the discontinuity.

6. Comparison of Practical Results and Theory

Sufficient test data have been obtained at U.S. Army Aviation Engineering Flight Activity during level flight on a Bell UH-1C helicopter to be sure of the actual airflow conditions at one point under the rotor. Unfortunately there have been insufficient data in climbing or descending flight to carry out a full comparison of the theory at this time.

The results of the experimental measurements of $\overline{V}$ and α over a range of forward speeds are shown in Figure 7 in non-dimensional terms using the theoretical value of v_h as the speed normalizing term. The theoretical value of v_h is calculable for the UH-1C as being 21.5 knots.
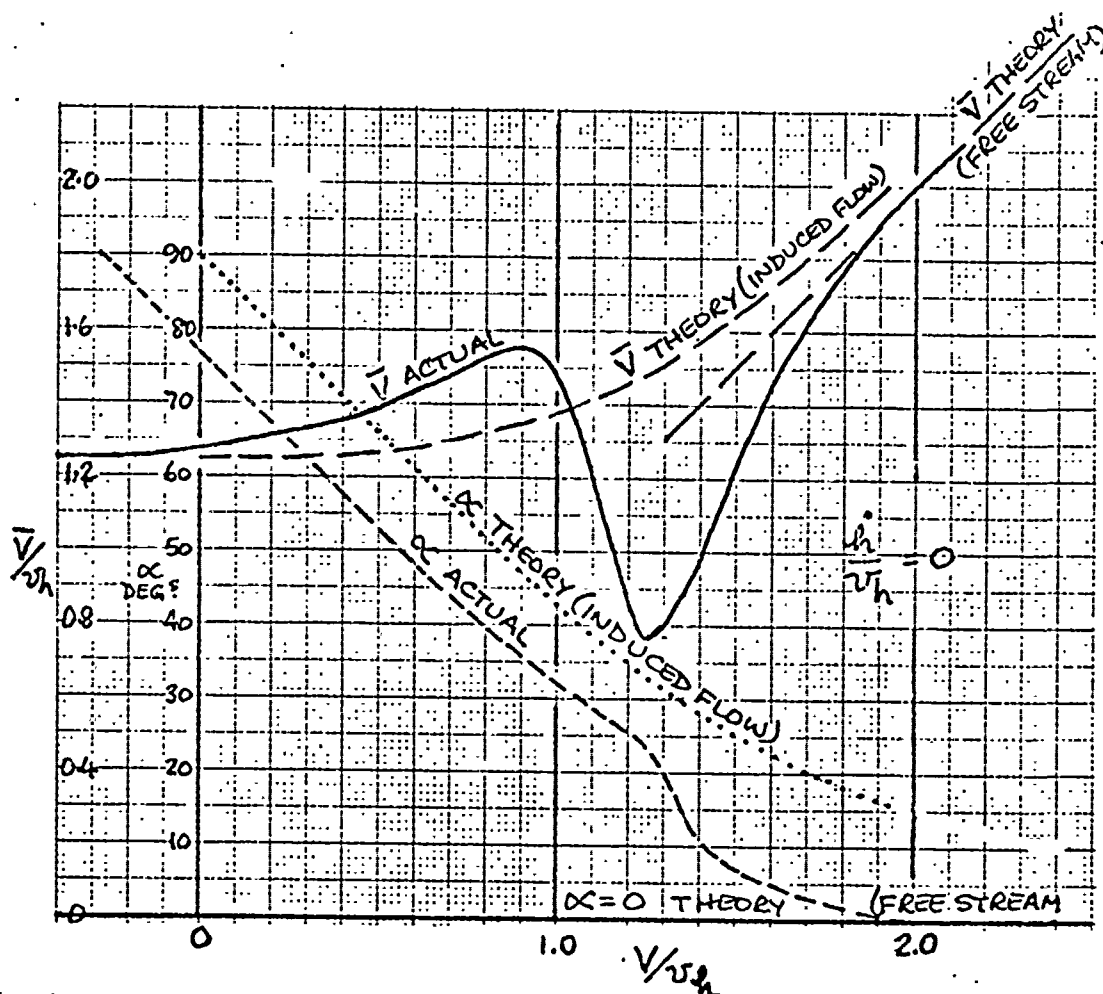

FIGURE 7. COMPARISON OF UH-1C DATA WITH THEORY — LEVEL FLIGHT.

From Figures 7 and 4 it can be seen that the values of α and $\bar{V}/v_h$ are in close agreement with the theory if the origin is displaced to $V/v_h = -0.25$ (i.e. the airspeed at which $\alpha = 90°$). This relationship holds up to the airspeed at which $\alpha = 25°$, that is $V/v_h = 1.5$. In the high speed region the values of $\bar{V}/v_h$ and α are in agreement with the theory above $V/v_h = 2.0$. In the region $1.5 < V/v_h < 2.0$ the theoretical notion of a sudden discontinuity based on α fails, but it seems logical to anticipate that this region is applicable over a region bounded approximately by lines of constant α as shown in Figure 8.
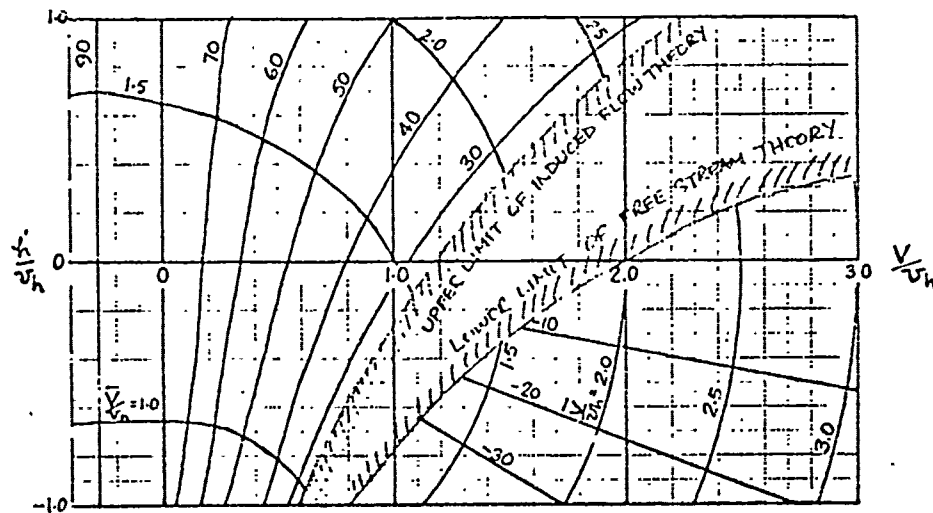

FIGURE 8   LIMITS OF THEORY FOR UH 1C INSTALLATION

The question then arises - "What does happen in the uncharted region?" From the test results obtained we do know the values of $\bar{V}/v_h$ and α across this region for $h'/v_h = 0$ and can extrapolate a probable contour as shown in Figure 9.
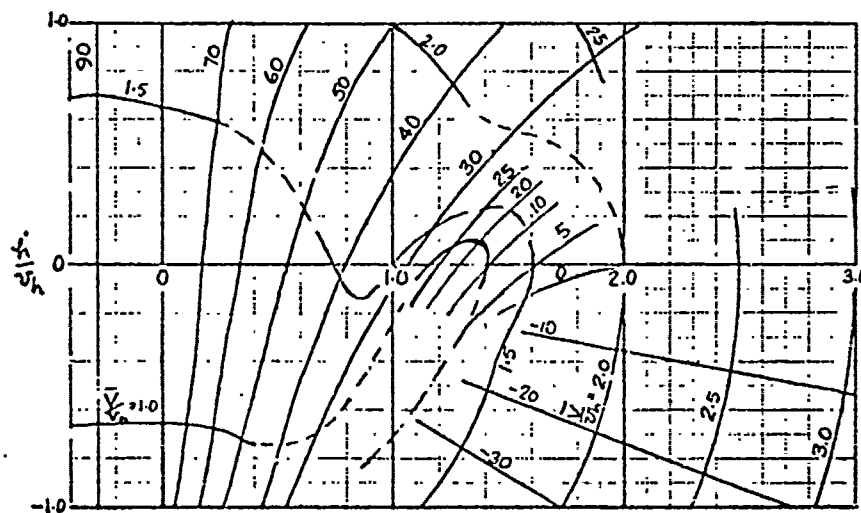

FIGURE 9   ESTIMATED LOCAL AIR VELOCITIES FOR UH 1C INSTALLATION.

206

THE CORRELATION OF ACTUAL INDUCED FLOW

WITH THEORY FOR BELL NUH-1M HELICOPTER ROTOR OPERATING

IN LEVEL FLIGHT

REVIEW OF LORAS CHARACTERISTICS
GENERAL REQUIREMENTS FOR AN OMNI DIRECTIONAL LOW RANGE AIRSPEED SYSTEM
LORAS DISPLAYS

DAVID L. GREEN
Pacer Systems, Inc
Arlington, Virginia

Presented at a Technical Conference on
"The Effects of Helicopter Downwash on Free Projectiles"
Held at US Army Aviation Systems Command, St. Louis, Missouri
12-14 August 1974

ABSTRACT

This abstract covers the next three papers.

PACER Systems, Inc. has developed and proven an omnidirectional airspeed
system (LORAS) capable of measuring airspeed between 0 and 200+ knots TAS,
360° about the sensor's vertical axis. The introduction will review the de-
velopment progress that has produced a system which is operationally ready
and in production, having been developed from concepts first explored in
the 1950's. The configuration being offered by PACER first operated in early
1972. Flight testing started in the fall of 1972. The results of this flight
test along with the results of wind tunnel and environmental testing led to
a Product Improvement Program which in turn resulted in an improved system
of lighter weight, increased accuracy and with reliability characteristics
suitable for operational use in current helicopters.

A short film clip will be presented. The clip includes several short
flight sequences of the first LORAS-helicopter evaluation flights, with the
sensor mounted on a nose boom. The film also contains an animated explana-
tion of how LORAS works.

Slides and view graphs will be used to review some of PACER's experience
with rotor mast mounts, boom mounts, and other under-rotor locations. The
impact of rotor flow will be reviewed with the conclusion that the main
rotor mast location is by far the superior location for an omnidirectional
airspeed sensor. A review of precedent and current design philosophy is
next offered to support the conclusion that the main rotor mast is both a
feasible and practical sensor location on current and future helicopters.
It simply remains for the Army to state this location requirement to have
it become a reality.

PACER Systems has studied operational requirements for an omnidirectional airspeed system. The results of this effort will be briefly reviewed. The objectives of this review are to first expose the multiplicity of the requirements for such a system and to conclude by identifying the several candidate applications which require an operational omnidirectional airspeed system today, tactical/NOE flight operations, Navigation (ASN-128) and the response to upcoming improvement in helicopter fire control.

The last segment will deal with specific integration techniques for Navigation, Fire Control and Cockpit Displays. View graphs will be used to present some ideas and a firm presentation will review PACER's development experience in cockpit displays.

REVIEW OF LORAS CHARACTERISTICS
AND
DEVELOPMENT HISTORY

D.L. Green
Director, Advanced Plans and Programs
PACER Systems, Inc.
Arlington, Virginia 22202

INTRODUCTION

LORAS is an omni-directional low range airspeed system capable of measuring airspeed down to and through zero knots. It can measure calibrated or true airspeed in any direction up to and beyond 200 knots.

Development of the concept began in the late 1950's and the first fully successful model of the current mechanization was first demonstrated in 1964 by Cornell Aeronautical Laboratories.

The original system was used as flight test equipment on the X-22A and the XV-6A V/STOL aircraft, with great success. As a result of this success and the emergence of new requirements for an omni-directional airspeed system, PACER Systems acquired the rights to develop, market and manufacture a productionized version of the system. This acquisition occurred in 1972 and was followed by a two phase development program.

The first phase of development involved demonstrations of the LORAS concept to prove LORAS could work on any type of aircraft. The second phase involved the further development of the equipment to achieve high reliability in the real world environment, maximize system performance and minimize weight and volume. In addition, PACER Systems continually interfaced with prospective military users during their development of new equipment, weapons and tactical scenarios. This interface has allowed PACER Systems to design a production system which is cost effective and which has the maximum achievable commonality among potential users. That is to say, the system is compatible with the needs of fire control, navigation, pilot displays, performance computers and flight control augmentation systems.

The first system to be flown by PACER Systems was designated LORAS II, weighed about 8 pounds and utilized a meter for lateral airspeed and a tape instrument for indication of forward and rearward airspeed. The first helicopter evaluation of this system involved a model FH-1100 Fairchild Industries helicopter. A nose boom was utilized on the FH-1100 to demonstrate the operation of LORAS in rotor inflow. The results, which are depicted in the film to follow, suggested that the frequency response of the system was too high. The three cycle per second capability of the LORAS II allowed it to measure too much of the turbulence associated with the main rotor and the natural turbulence contained in the free stream. We also found that the visual gain of the tape display was higher than necessary when utilized with the under-damped LORAS system. This high visual sensitivity of the tape display is easily observed in the film.

ORIGINAL PACER-LORAS II OMNIDIRECTIONAL LOW RANGE AIRSPEED SYSTEM

The impact of ground effect on a boom type sensor location is seen in the movie at the conclusion of an autorotative approach to a low hover. As power is applied in ground effect, the rotor downwash is turned by the ground plane and a rearward airspeed component is indicated by the LORAS system. Another rotor flow phenomenon is apparent during a climbing transition into forward climbing flight. In this case, the sensor appears to measure the tip vortex of a rotor blade as the sensor emerges from the rotor flow. In later models of the LORAS system, the damping was increased slightly, and display visual gains were decreased. Pilots rated the results as very satisfactory.
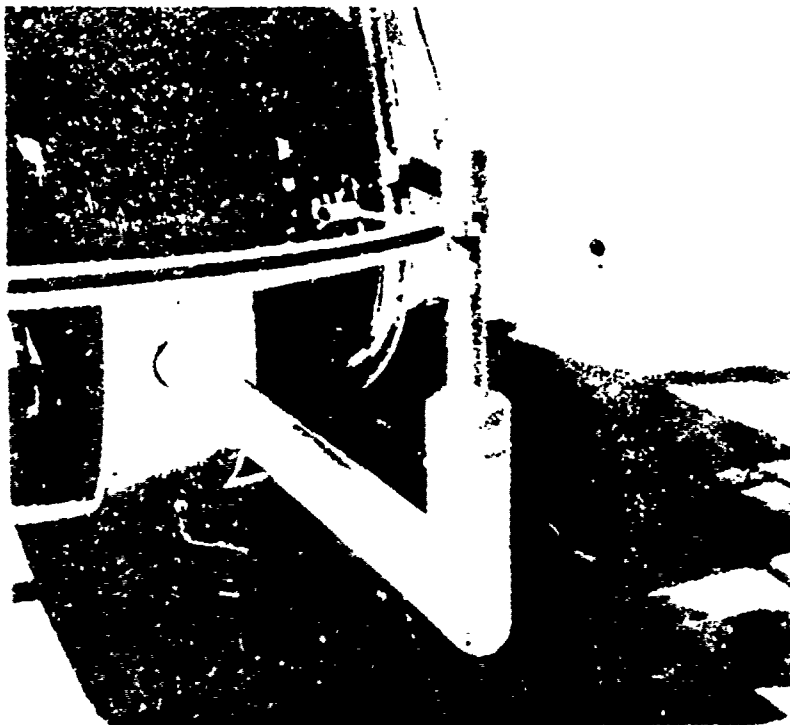
FIRST FLIGHT OF
LORAS SYSTEM ON
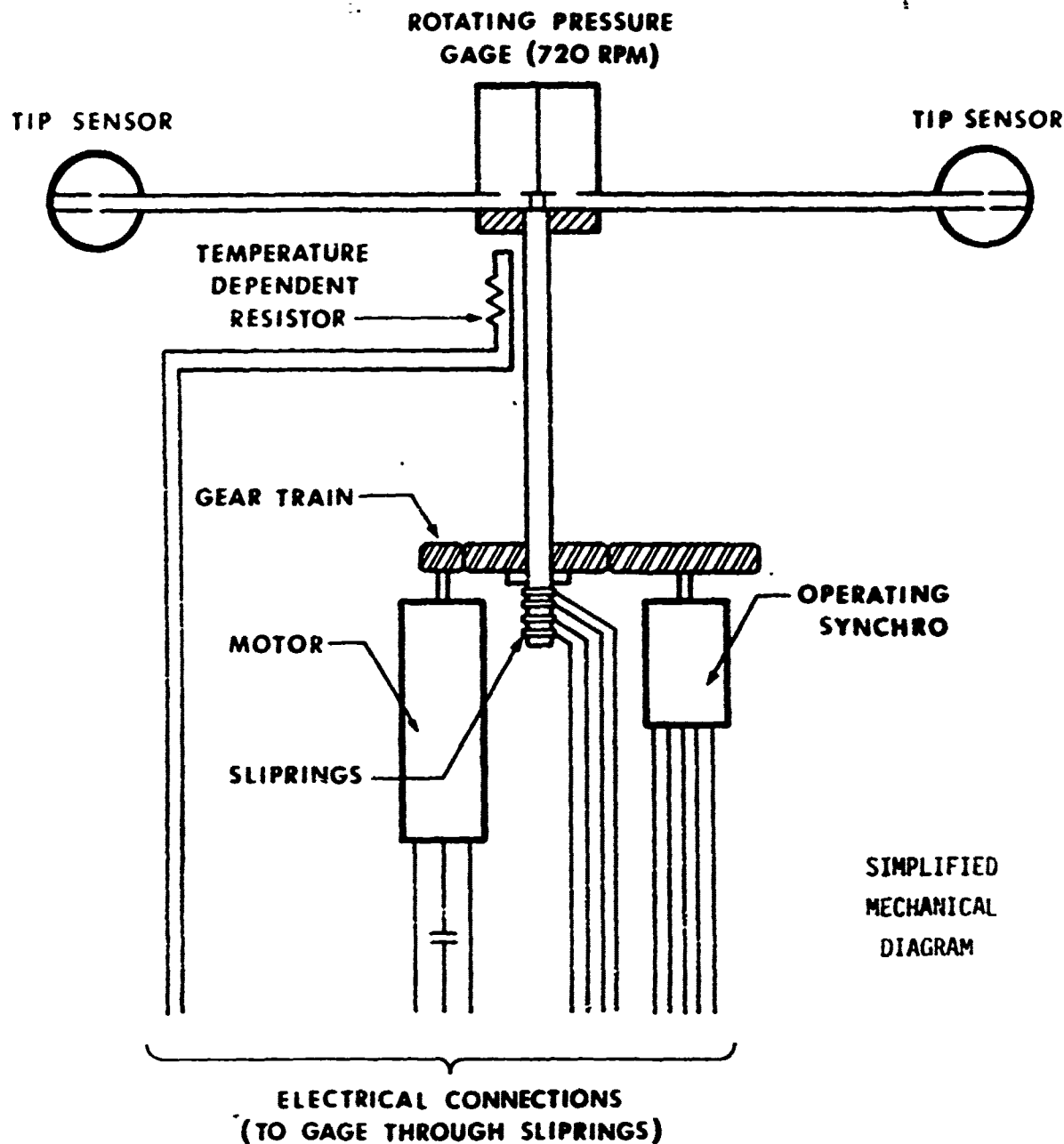A HELICOPTER
(FH-1100/OCT 1972)

AIRSPEED SENSOR (MOVIE EXCERPT)

The following explanation of sensor operation is adapted from the movie and is included here for continuity:

Primary outputs - The system provides either true or calibrated airspeed with three primary outputs: flight path airspeed, the component of airspeed along the aircraft heading and the component of airspeed at 90° angles to the aircraft heading. In addition, a density altitude signal is available when the true airspeed design is selected.

Sensor Operation - The Sensor, which measures 12 inches across and weighs about two pounds, is made of stainless steel (arms) and corrosion resistant aluminum (body). It is capable of measuring airspeeds with less than a one knot error in the slow speed regime and can withstand supersonic airloads.

At the heart of the Sensor concept is a rotating arm system. This system consists of two hollow rotating arms with Venturi-like sensors mounted at their respective ends. The arms are connected to a hub which is driven at a rate of 720 RPM by a constant speed motor in the base of the unit.

ROTATING PRESSURE
GAGE (720 RPM)

TIP SENSOR

TIP SENSOR

TEMPERATURE
DEPENDENT
RESISTOR

GEAR TRAIN

OPERATING
SYNCHRO

MOTOR

SLIPRINGS

SIMPLIFIED
MECHANICAL
DIAGRAM

ELECTRICAL CONNECTIONS
(TO GAGE THROUGH SLIPRINGS)

When the sensor is displaced through the air, the arms transmit cyclic
pressure inputs to a solid state differential pressure transducer in the hub.
The output of the transducer increases linearly with increases in the magnitude of the differential pressure. The rotation angle of the arm system is
tracked by a separate electronic subsystem.

The differential pressure signal and the arm rotation signal are fed
to the Air Data Converter, where they are used to determine the magnitude
of the airspeed and the component speeds which correspond to forward, rearward and sideward flight.

The sensor is insensitive to moderate angles of attack and has been repeatedly demonstrated satisfactory under severe climate conditions including
freezing rain.

213

Sensor Theory - Sensor behavior is best understood by considering the four basic wind conditions that characterize flight path operation.

No Wind Condition In a no-wind condition, the flow through both Venturis is equal and the transducer does not deflect.

TIP SPEED (t_E)

NO WIND
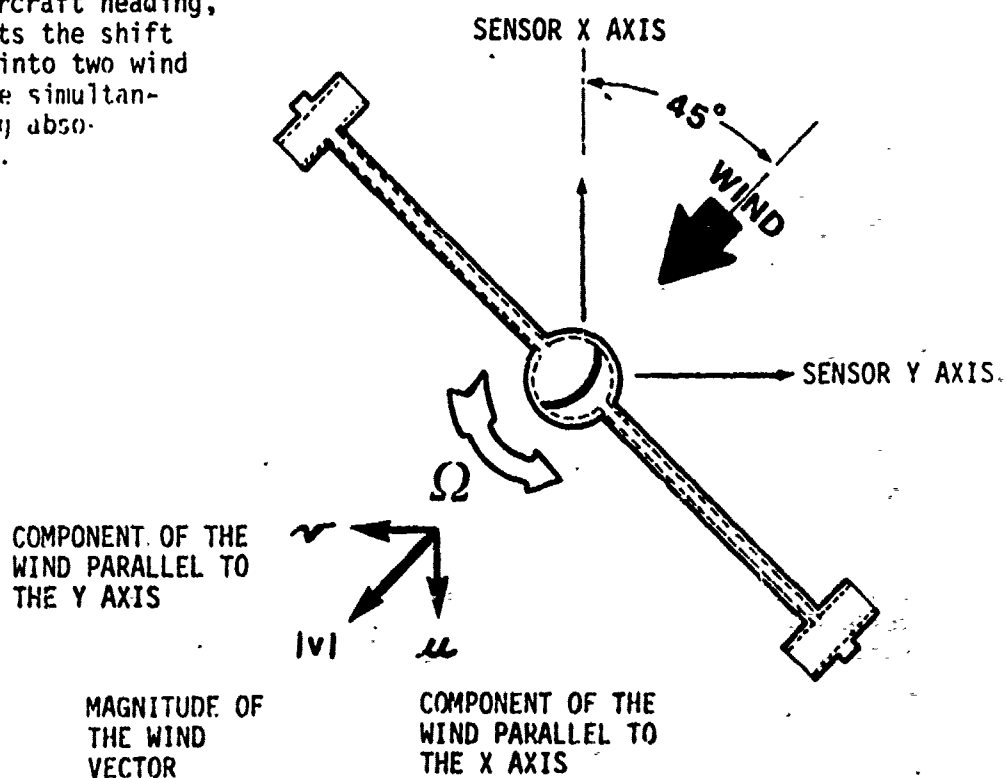
TIP SPEED (t_s)

Ω
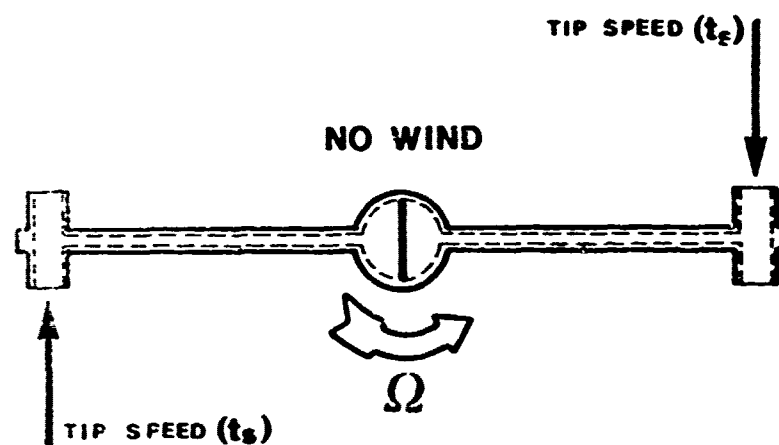
Wind Introduced When a wind is introduced, it adds to the tip speed of the advancing arm and, correspondingly, subtracts from the tip speed of the retreating arm. Low pressure is induced in the advancing arm due to the increased windspeed through the advancing Venturi. Higher pressure is induced in the retreating arm due to the lower airspeed through the retreating Venturi. The transducer deflects toward the low-pressure side, and the magnitude of the deflection represents the magnitude of the wind.

HIGHER PRESSURE IS
INDUCED IN THE
RETREATING ARM,
DUE TO THE LOWER
AIRSPEED THROUGH
THE RETREATING
VENTURI

WIND
(w)

w

r

t_s

r

t_s w

Ω

LOW PRESSURE IS INDUCED
IN THE ADVANCING ARM
DUE TO THE INCREASED
SPEED THROUGH THE
ADVANCING VENTURI

214
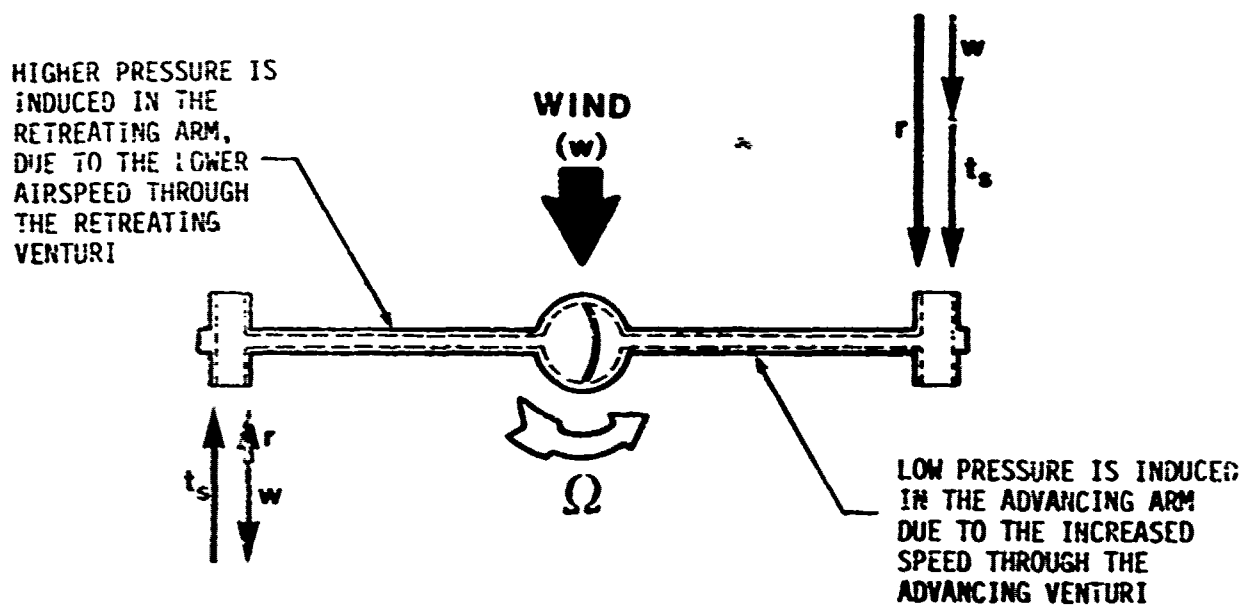
Wind Flow at Right Angles

When the wind flow is at right angles to the shrouds, the flow through both Venturis is equal and the transducer does not deflect.

WIND

Ω

SENSOR X AXIS
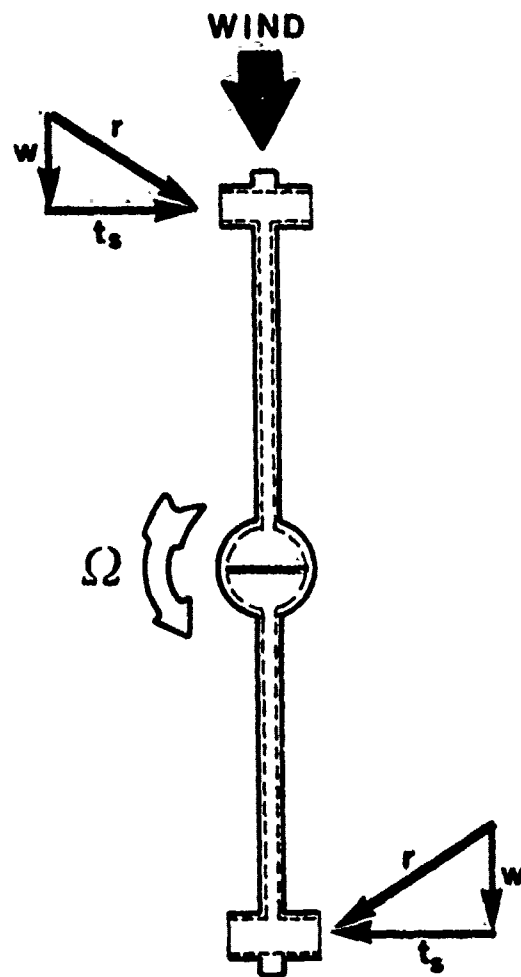
Wind Shifts Away From Heading

When the wind shifts away from the aircraft heading, the system detects the shift and resolves it into two wind components, while simultaneously outputting absolute windspeed v.

SENSOR X AXIS

45°

WIND

SENSOR Y AXIS

Ω

COMPONENT OF THE WIND PARALLEL TO THE Y AXIS

MAGNITUDE OF THE WIND VECTOR

$|v|$ u

COMPONENT OF THE WIND PARALLEL TO THE X AXIS

215

Air Data Converter - The Air Data Converter receives signals from the omni-directional airspeed sensor and outputs flight path information as either true or calibrated airspeed.

This solid state unit weighs less than three pounds, has a volume of under .12 cf, and is designed to meet the requirements of military specifications.

During operation, sensor output is coupled to the Air Data Converter via a single cable. The sensor input is first processed within a density compensation circuit which provides correction for air density. Inputs to the density compensation circuit are via self-contained static pressure and temperature sensors.

Absolute airspeed is derived directly from the density compensated signal and is presented unresolved as a signal equal to the vector sum of the longitudinal and lateral components.

Signals representative of the longitudinal and lateral velocities are obtained by multiplying the compensated velocity signal with the sine and cosine of the angular position of the rotating arms. The sine and cosine are obtained from a synchro/resolver combination. These signals are demodulated and filtered to remove the modulation frequency due to rotation.

The density compensation circuits can also be used to output a signal proportional to density altitude. This signal is suitable for pilot display or use in other systems.

The Air Data Converter is ruggedly constructed and can be hard- or soft-mounted in any helicopter or airplane. Special features include an electronic azimuth alignment control, a built-in gain adjustment, and a Built-In Test (BIT) circuit that provides the user with a GO/NO GO preflight checkout capability.

EXPERIENCE SINCE 1972

In the three years since the film was made PACER has delivered units for two types of utilization; first for use in evaluating LORAS performance and second for use as primary air data sensor. LORAS systems are now being used as primary air data sensors on V/STOL aircraft, airplanes and helicopters. The programs have included the T & E evaluation of the VAK-191 V/STOL fighter, and the X-22 research aircraft where the sensor is now being used to obtain vertical speed for the variable stability flight control system.

The sensor was mounted as instrumentation on the nose of AH-1G and AH-1J aircraft during evasive maneuver trials CDEC, Fort Ord, California. The reports of these trials established that LORAS was essential to the safety of flight during the maneuvers associated with TOW missile attack and post attack maneuvers.

The Army Aviation Engineering flight test activity at Edwards first tested a LORAS unit in the Spring of 1973. This test activity is currently using a LORAS system on an AH-1G as part of a MICOM project at Edwards Air Force Base. On this project the pilot references LORAS forward, rearward
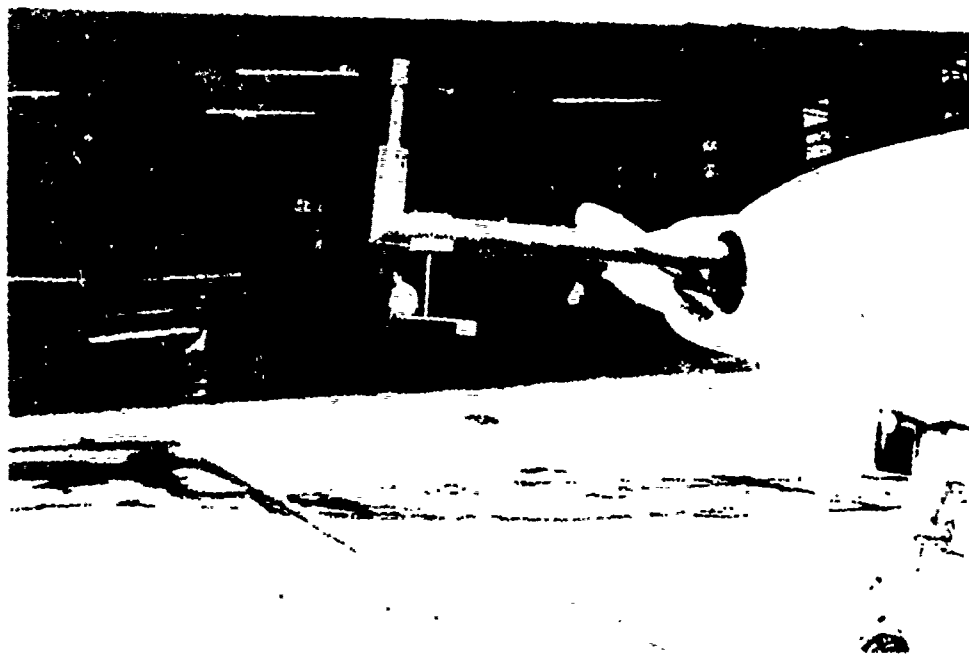
LORAS II SENSOR MOUNTED ON STANDPIPE
MANUFACTURED BY PACER SYSTEMS, INC.

and lateral airspeed to fly the aircraft during a flight program to survey rotor downwash characteristics. A second Army unit has been in service for over a year at Fort Rucker on a UH-1H helicopter involved in human factors experiments associated with NOE flight. Additional evaluations were conducted on an H-46 at the Naval Test Pilot School, a Bell model 212 at Bell Helicopter, a UH-1N at the Naval Air Test Center, and an OH-58 at the Aerospace Engineering Test Establishment at Cold Lake, Alberta, Canada. Most recently LORAS has been proven on an S-61 Sikorsky helicopter. This last effort involved demonstration for commercial applications and was also used to demonstrate preliminary suitability of LORAS for the Navy SH-3 series helicopter.

One LORAS Unit has been subjected to operations in a salt water environment via its installation on a Japanese sea plane. This installation also subjected the LORAS unit to high speed forward flight. In addition, PACER Systems has also conducted its own high speed trials, using a Beech Barron to fly at true airspeeds in excess of 200 knots.

LORAS data has been used for automatic speed control during "hands off" ILS approaches and it has been used to develop official performance Stability and Control data for V/STOL aircraft and helicopters.

LORAS II SENSOR MOUNTED ON NOSE BOOM OF FIXED WING AIRPLANE FOR
HIGH SPEED TRIALS

PRODUCTION LORAS SENSOR
MOUNTED ON A MODEL S-61
HELICOPTER FOR FAA
PRODUCTION APPROVAL
DEMONSTRATION
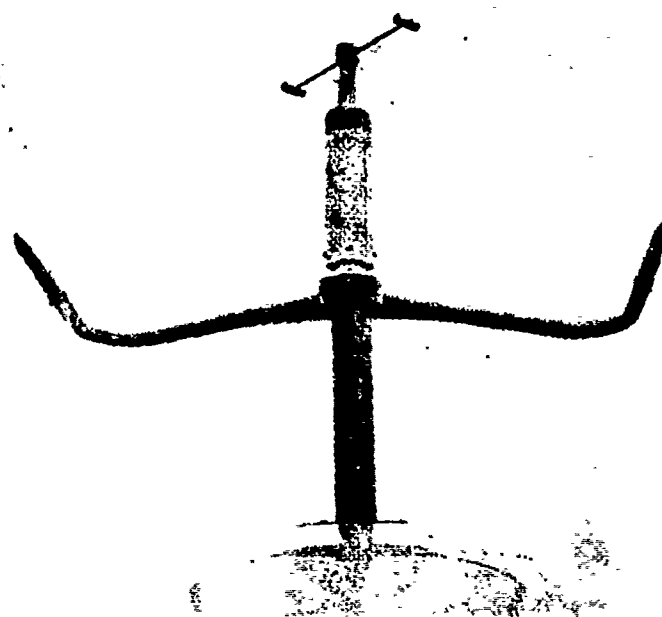
Slow speed calibration of LORAS normally takes a single flight of about one hour. A second flight is flown to spot check the correctness of any gain change which may have been made to match the LORAS output with the airspeed standard being used.

Over 450 hours of wind tunnel work have been conducted by PACER in this development. In addition, thousands of hours of environmental testing and life cycle testing have been completed on PACER's laboratory truck and on a fixed test stand mounted above PACER's Boston facility.

ENVIRONMENTAL EFFECTS

The sensor has been operated for long periods in freezing rain, thunder-storm "cloud burst" levels of rain, sand, dust, and snow. No system degradation due to environment has been observed. The excellent results obtained during operations in snow and freezing rain have suggested that conventional pitot-static anti-ice and de-ice heat is not required, nevertheless, provisions have been included, should that requirement be established by a user. It should be emphasized that PACER expects the current unheated LORAS system has a capacity to function in freezing rain which equals or exceeds the capacity of any current helicopter to operate in freezing rain.

PRODUCT IMPROVEMENT PROGRAM

PACER has conducted a product improvement program concomitant with the development of current operational requirements. This program has produced a sensor weighing 2.25 pounds and an airdata converter weighing 2.88 pounds. The system has been made smaller and more streamlined by the substitution of solid state components, such as the pressure transducer in the hub of the
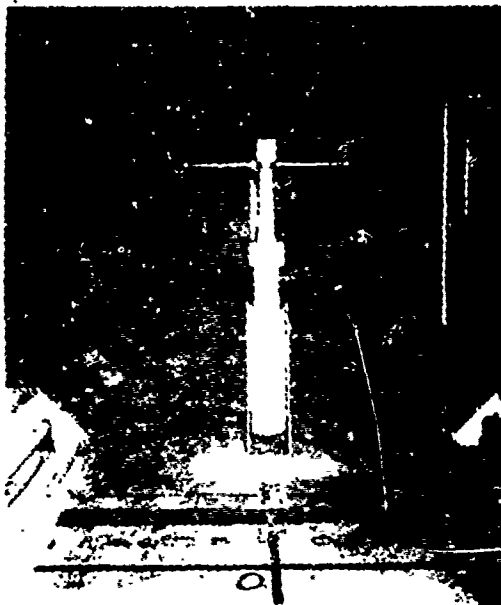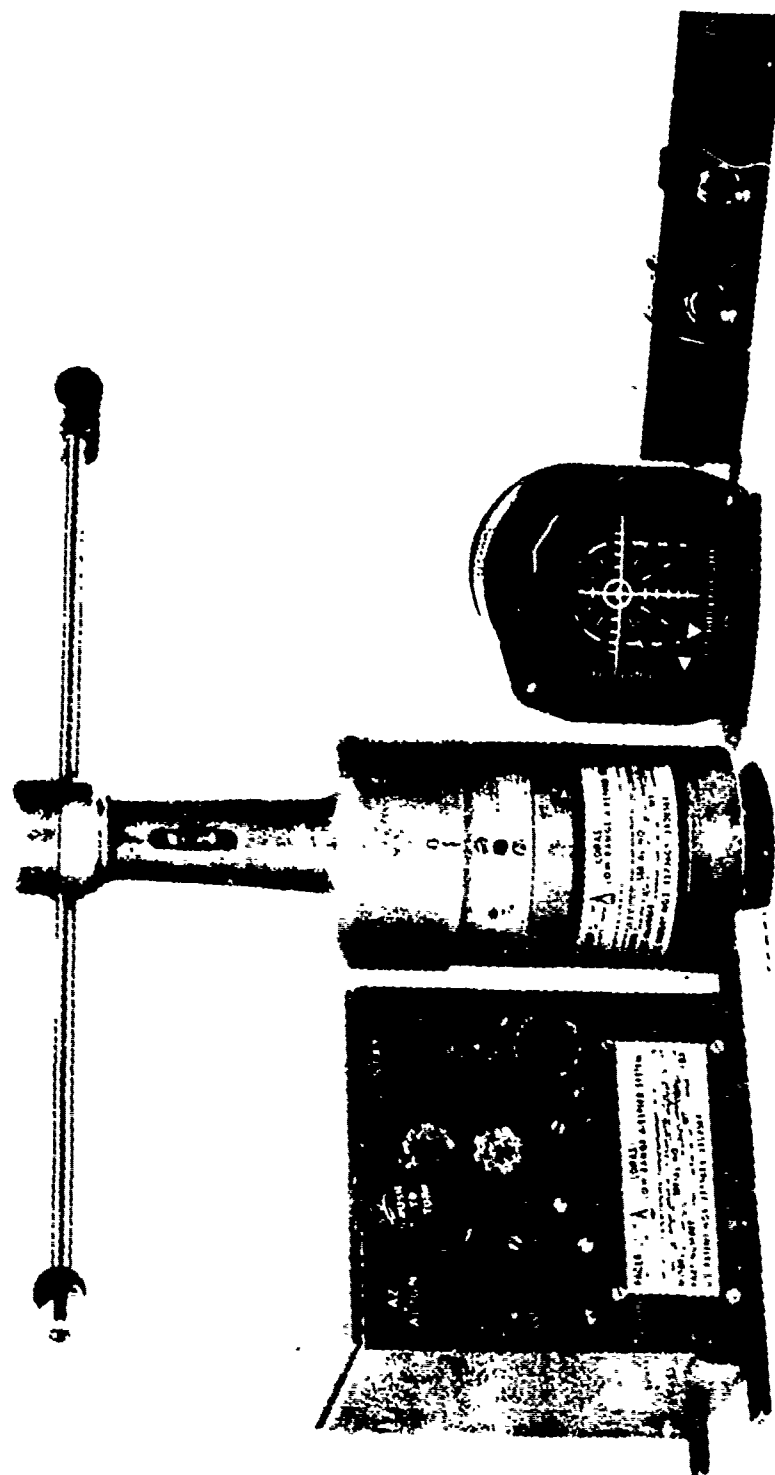

LORAS SENSOR MOUNTED IN
NBS SUBSONIC WIND TUNNEL
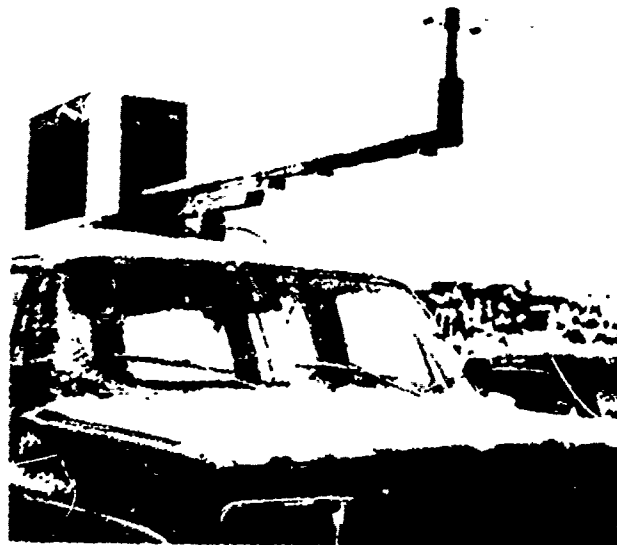
LORAS SENSOR TEST INSTALLATION,
SHOWN FOLLOWING HIGHWAY TESTING
IN FREEZING RAIN

220

PRODUCTION LORAS SYSTEM. The basic system includes the airdata converter and the sensor unit. The omni-directional airspeed indicator and control panel are optional.

sensor. Superior reliability in the helicopter environment has been a con-
tinuing design goal. This goal has been achieved by overdesigning the power
train, underloading the motor, cooling the motor with a fan, and using grooved
slip rings made of gold (to compensate for vibration and to protect against
corrosion). In addition, operational type features have been added. For
example, an azimuth alignment knob on the front of the case allows maintenance
personnel to electrically align the X axis of the sensor with X axis of the
aircraft via a bore-sighting alignment type adjustment. A Built-In Test
feature provides for a "go-no go" preflight check and allows maintenance
personnel to check the calibration of the system in the field with simple
DC voltmeters.

RECENT DATA

The most recent data available on the LORAS was obtained at the Army
Aviation Engineer Test Activity, Edwards Air Force Base, in June of 1975.
This system did not include many of the product improvements included in
the current production equipment, but nevertheless, it provided excellent
results in slow speed flight. Even though the data were observed in an 8
knot wind, most of the points fell within about 2 knots of the ideal cali-
bration line in the four directions tested. In February of 1975, PACER
tested the preproduction prototype LORAS at the National Bureau of Standards.
The results were gratifying in that the errors were by and large less than
1 knot and the repeatability was within about 0.25 knots.

The current system is essentially insensitive to moderate angles of
attack, although it is designed to ignore the vertical components during
high angle of attack operations, where rotor induced flow approaches or
exceeds 45 degrees. The system is responsive, and has no measurable dead-
band during transitions through zero airspeed or zero sideslip angles.

SENSOR LOCATION

The best aerodynamic location for
the LORAS sensor is on top of the main
rotor mast, above the rotor hub. This
location minimizes the obstructions to
the sensor's view of the free stream.

The LORAS sensor will function
above or below the main rotor disk, but
certain fuselage and rotor flow charac-
teristics tend to make the "under rotor"
position the least desirable. First, if
the sensor is mounted below the rotor,
the free stream flow can be deflected
and the speed can be changed by fuselage
interference. For example, a sensor
mounted below the nose will work in
portions of the forward and sideward
flight profile only. Descending flight
provides the best results, while rear-
ward climbing flight may yield no out-
put at all.
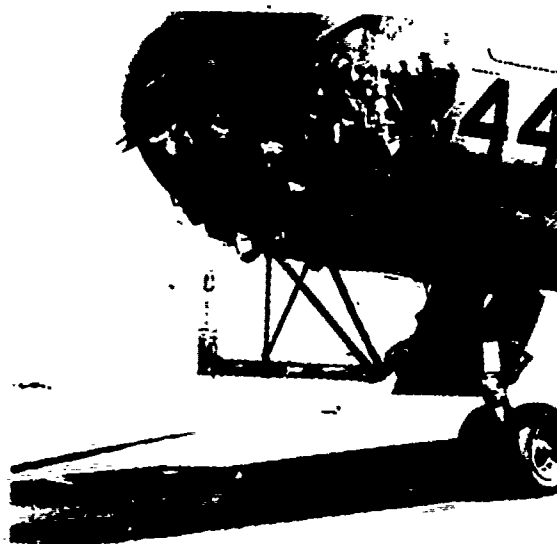
LORAS SENSOR MOUNTED BELOW NOSE

OF A MODEL UH-46A HELICOPTER

222

TYPICAL STANDPIPE INSTALLATION

When a sensor is mounted in the flow of the rotor, the sensor must deal with variations in the flow at the sensor which occur due to variations in the flight path, density altitude, power, gross weight and ground proximity. There are methods which allow the variables to be measured and used to develop corrections but this approach requires a considerable calibration effort. This calibration effort must be conducted for each model aircraft and the calibration will vary for each sensor location on a given aircraft. The calibration may also change significantly with changes in the external stores configuration of a given helicopter.

Rotor flow is turned or deflected by the ground plane when a helicopter hovers at a wheel height of one rotor diameter or less. This can impact the flow seen by a sensor mounted under the rotor but clear of the airframe. For example, when a heavily loaded AH-1J helicopter was hovered at about a 2 foot skid height, a nose boom mounted LORAS reported an 18 knot tail wind (on a no wind day). At a skid height of about 50 feet, the LORAS read a correct "zero zero" airspeed.

Under some conditions rotor twist and rotor slip stream contraction, will induce additional errors in measured airspeed. These effects are dependant upon sensor location, yet the sensor locations which permit rotor flow effects to be minimized, tend to constrain the useful flight envelop due to the interference of the free stream with basic airframe.

All-in-all, the most consistent and continuous flow is found near the rotor hub. A vertical component of rotor flow is generally expected in the hub area, but the LORAS sensor is designed to ignore this high angle type flow.

A "standpipe" type installation is required to accomodate the location of the LORAS sensor on top of the main mast. This standpipe is non-rotating and is attached to the bottom of the main transmission. A bearing is used to center the standpipe at the top of the main rotor mast. The standpipe does not need to have a large outside diameter, and when properly designed, it need not weigh over four pounds. The other additional fixtures might add another three or four pounds but the total added weight of an operational standpipe should not exceed seven pounds.

Many helicopters have standpipe type installations for such things as rotor blade formation lights, blade fold, pitot-static airspeed, rotor blade de-ice, rotor mast bending instrumentation, and numerous special purpose instrumentation installations. There is no reason why a standpipe is not feasible on all current and future operational helicopters. The user must simply state the requirement, and the contractor will be responsive (or non-responsive). The sooner the user establishes the standpipe requirement, the less the likelihood of conflicts with respect to other features which similarly need access to the main rotor mast.
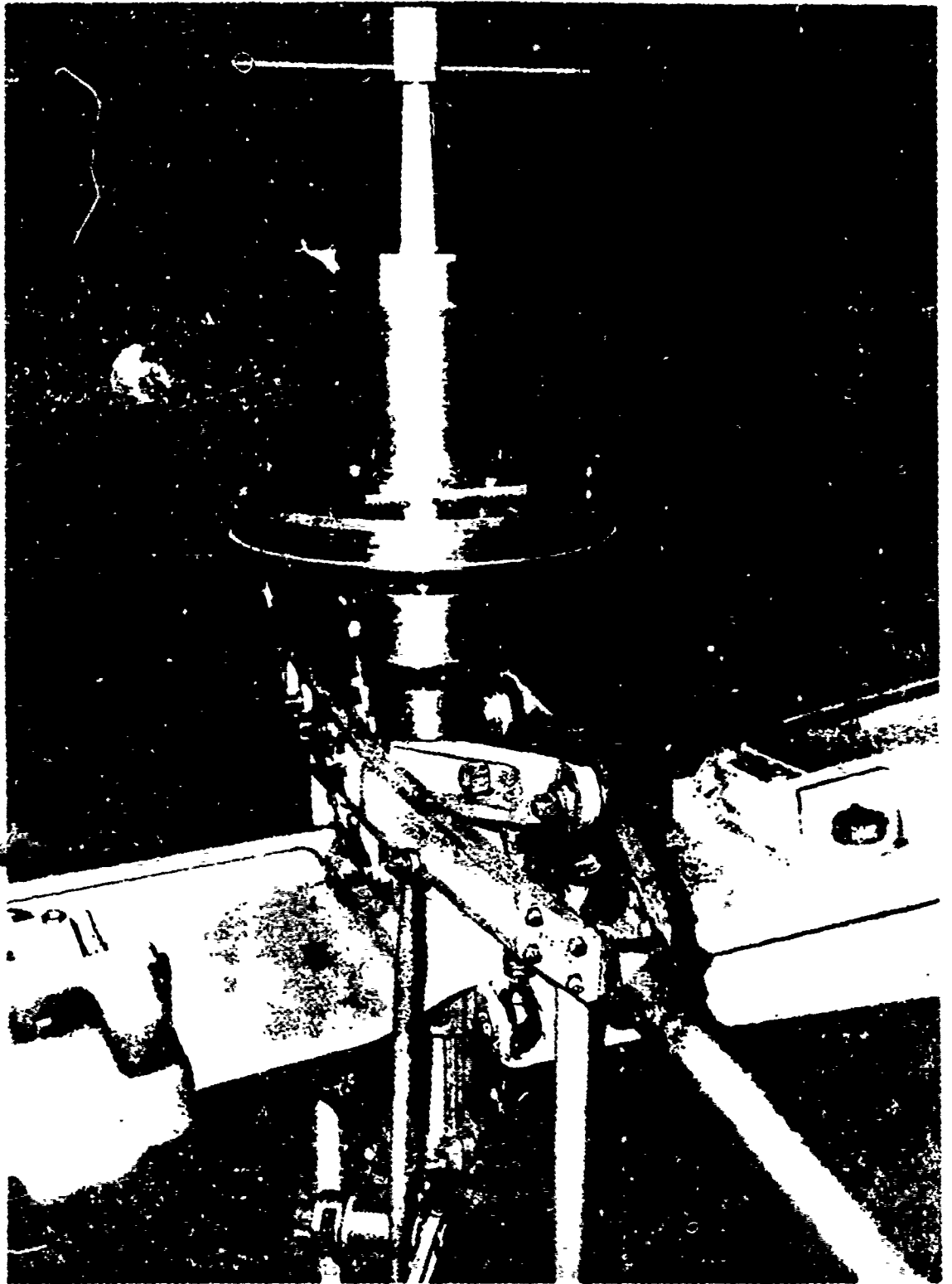
FIRST STANDPIPE SENSOR INSTALLATION. The first LORAS II unit was mounted on a non-rotating platform atop a non-rotating standpipe. The standpipe, installed on a UH-1C at the U.S. Army Aviation Engineering Test Activity, was originally designed for other purposes.

General Requirements
For An
OMNIDIRECTIONAL LOW RANGE AIRSPEED SYSTEM (OMNI-LORAS)
On The
AH-1 Model Helicopter.

D.L. Green
Director, Advanced Plans and Programs
PACER Systems, Inc.
Arlington, Virginia 22202

GENERAL

There are a number of common reasons for the installation of an OMNI-LORAS on most military helicopters, but certain helicopter missions have unique requirements which justify priority consideration. For example, Navy ASW helicopters need an OMNI-LORAS to prevent accidents due to spacial disorientation under night IFR conditions. USMC/USA cargo/transport helicopters urgently need an improved capability to compute slow speed lift performance. Similarly, scout and attack helicopter have a separate set of requirements due to the evolution of NOE operations. In particular, helicopters equipped with the TOW missile, 2.75 rockets, or gun systems appear to have a broad spectrum of similar and urgent requirements for an OMNI-LORAS. These requirements can be verified by an analysis of available technical information in combination with a review of current tactical doctrine.

Aside from the system requirements, an analysis will show that the conglomerate justification for OMNI-LORAS on the AH-1 helicopter is very similar to the justification which the fixed wing community has advanced for angle of attack indicators, mach indicators and 'g' meters. Only by reference to angle of attack can fighter pilots exploit maximum turning performance in combat, or slow to the minimum safe landing speed with full confidence that the aircraft will not suddenly pitch up into a fatal stall spin. Only with mach meters and 'g' meters can combat maneuvers be conducted while staying inside the design structural envelope (particularly during combat training). OMNI-LORAS provides these same functions. It allows the pilots to aggresively maximize performance of the weapon system while confidently avoiding loss of control and avoiding operations outside design limits of the aircarft.

SUMMARY OF FIRE CONTROL REQUIREMENTS

Man Machine - There are a number of man machine performance criteria which impact the successful delivery of ordinance from a helicopter. For example, the more stable the platform, the smaller the dynamic disturbance will be to the fire control problem. In this regard, the helicopter has not exhibited superior rigidity with respect to pitch, roll or yaw attitude, in slow speed flight, and performance is typically dependent upon the:

. Direction, magnitude and gust content of the relative wind
. Open-loop stability of the basic (or augmented) aircraft, and
. Skill of the pilot in efforts to reduce or eliminate residual sinusoid or random aircraft motion.

The pilot therefore needs a cockpit presentation of omnidirectional airspeed to allow him to learn to fly the aircraft into the relative wind conditions which will minimize the need for compensation by the fire control system.

Airdata - There are a number of airdata requirements. The high speed problem involves the need for true airspeed, angle-of-attack and angle of sideslip. In slow speed flight there is a need to compensate for rotor inflow, and the relative wind over, the aircraft. In addition, some designers want to know the airmass and wind (relative to the earth's surface as opposed to the aircraft).

OMNI-LORAS can provide true airspeed and sideslip angle. Rotor inflow can be predicted as a function of specific aircraft parameters (including the longitudinal and lateral airspeed component outputs of an OMNI-LORAS). The wind over the ground can be determined by using an OMNI-LORAS and a DOPPLER NAV System or by having the pilot visually establish a zero groundspeed hover and noting OMNI-LORAS outputs (earth wind).

Flight Profile - There are a number of requirements for an OMNI-LORAS which are important during the approach to, and the withdrawal from, the attack site. These requirements involve:

. Slow speed "Lift" or "Maneuver Margin" performance
. Controlability of the aircraft in the NOE profile (down/cross wind controlability).
. Navigation to and from the attack site (OMNI-LORAS providing basic or redundant navigation input).
. Pilot cueing during recovery from inadvertent rearward/sideward flight when visual flight references are lost near the ground (night blindness or an inadvertent encounter with a low overcast).

THE DESIGN ENVELOPE

The structural integrity and controlability of the AH-1 is defined for the operational pilot by the flight envelope found in the pilot's flight manual. The low speed end of this envelope is defined by the clearance to turn 360° in a wind of some limited magnitude (30 knots to 40 knots depending upon helicopter model). This envelope has the effect of limiting the maximum rearward speed to zero (0) knots whenever the aircraft is operating at the maximum sideward airspeed (and vice versa). This envelope characteristic is important since the odds are that at least-half of all combat engagements by attack helicopters will be conducted under wind conditions where some down wind component exists.

What happens if the pilot attempts to operate outside the flight envelope? First of all, he may be unable to fly outside the envelope due to loss of directional control as yaw control limits are reached. This keeps the aircraft inside the envelope but represents an unacceptable situation from a weapons deployment standpoint. In addition, the temporary loss of heading control

under conditions of poor external visibility may precipitate a yaw-roll-pitch couple that is not noted by the pilot and subsequently produces an unusual attitude with a spacially disoriented pilot at the controls. Thus, loss of heading control is not acceptable warning that envelope limits are being exceeded.

If the pilot is able to fly outside of the flight envelope while maintaining adequate controlability, the result may well be an over-stressed aircraft. The out-of-limits operation may involve airframe structure, tail rotor blade fatigue, unusually high gearbox stresses or any other airframe component. This abuse may show up as a flight failure but most probably the overstress will be reflected as unexplained accelerated wear. Remember the loads used to compute components' wear were established while flying with reference to the handbook flight envelope.

It is impossible for operational AH-1 pilots to use pitch or roll angle as an indicator of airspeed in order to avoid "out of limits" operations. Normal variations in CG loadings (longitudinal and lateral displacement), variations in external store configurations, and variation in gross weight, all alter the pitch and roll attitudes which define component speeds. In addition, the variation of pitch attitude with variations in forward or rearward airspeed is characteristically non-linear and misleading for any given configuration. The same is true for the relationship between sideward flight and bank angle. In the same vein, control positions are normally not a reliable indication of speed, either.

The lack of speed cues is even more serious during accelerations and decelerations. The rate of change of airspeed which can be commanded is so high that envelope limits can be exceeded almost as soon as the longitudinal or lateral control input is completed. There is no bank angle or pitch angle cue to warn the pilot that a limit speed is being approached or exceeded. Everything is happening too fast. Even fewer warning cues are observed during wings level skidding stops, induced by rapid full displacement of the directional control. The skidding stop is a common maneuver and is probably the easiest way to exceed the structural limits of single rotor helicopters.

PRECISION CONTROL AND ATTACK SITE SELECTION

Precision control of heading and bank angle is required to achieve a satisfactory launch of the TOW missile and 2.75 rockets. The bank angle must be within certain small limits, and oscillations in heading must be held inside small limits.

These piloting requirements are important for a number of reasons yet an indepth discussion of launch constraints is beyond the scope of this presentation. Let is suffice to say that there is a launch envelope which the pilot must fly into (even for the TOW). An OMNI-LORAS will allow the pilot to avoid bad attack sites before exposing the aircraft. The OMNI-LORAS will permit the pilot to expeditiously and deliberately fly into the launch envelope with a minimum of abortive, non-firing launch attempts or iterations.

With a properly marked OMNI-LORAS display, pilots will be able to deliberately and positively fly into flight conditions which will insure that pre-launch exposure time is minimized. Once they learn this technique they will

be able to evaluate attack sites before they expose themselves to the enemy.

SIDEWARD FLIGHT AND TACTICAL MANEUVERS

High sideward flight airspeeds are encountered during post-fire maneuvers involving the TOW Missile System. When the weapon fires, the crew of the target vehicle may be alerted by the flames and smoke associated with the missile. When the target is alerted to the missile, there immediately exists a requirement to conduct one of two high sideward flight maneuvers:

    (1) Maneuver to maintain line of sight
    (2) Maneuver to avoid defensive fire (jigging)

The time of flight of the missile, when fired at long ranges, is sufficient in some cases for the target to maneuver so as to obtain concealment behind a tree clump type obstruction or behind defilade. High speed lateral maneuvering may allow the helicopter gunner to maintain line of sight even during such evasive target maneuvers. Line of sight is required to obtain a hit. It is not desirable to close range on the target in an effort to maintain line of sight contact, because the target and escorts will have defensive weapons. The pilot can not turn his aircraft and fly on a heading 90° to the weapons tract to maintain line of sight without concern. Such maneuvers increase visual, electronic and IR Signatures, enhancing detection and the probability of successful counter fire. Hand-held IR missiles, radar guided mobile AA guns, and other similar weapons are expected in the combat environment. Thus, the smallest frontal profile is the best profile.

Pilots will be required to fly these high speed sideward flight maneuvers in the presence of existing wind conditions. The existing wind may be a tailwind, a crosswind or a headwind. Wind direction is important in all cases, but the downwind situation is probably the most important of all. The downwind situation effectively decreases the allowable crosswind component (as specified by structural design limits or as defined by loss of heading controlability). In actual combat, structural limits may not be an overriding consideration, but these limits should certainly be observed during training exercises where unnecessary damage can be avoided by prudent piloting techniques. In any case, the pilot may select a second location with a better wind situation before exposing his aircraft in an attack. A second course might be to adjust the initial attack point so that a small increment of forward ground speed can be commanded, thereby reducing the tailwind component and expanding the allowable sideward airspeed component. These alternatives are not even thinkable without training in an aircraft equipped with OMNI-LORAS.

NAP OF THE EARTH MANEUVERS (NOE)

NOE maneuvers are required in the operational environment where the AH-1 helicopter is expected to be employed. NOE flight requires slow ground speeds and it even requires stops in downwind and crosswind conditions.

THRUST MARGIN FOR SLOW SPEED AGILE MANEUVERS

The margin of power available, above that required for level flight, decreases as airspeed decreases (in the slow speed regime). This margin of excess power available defines to a significant degree, the slow speed agility

of the AH-1. At high Density Altitudes (D.A.) and high Gross Weights (G.W.) the thrust margin may even become negative. It is possible to fly NOE profiles and similar maneuvers while purposefully staying above some minimum airspeed, an airspeed which will insure the availability of the minimum desired maneuver margin (excess thrust margin).

Slow speed operations in a left crosswind typically require less power required to hover than in "head-on" or right crosswind conditions. As much as a 07% decrease in power required can be achieved via piloting techniques utilizing an OMNI-LORAS sensor-display in a 25 knot wind. This could mean a 25% increase in dead weight lift capability over the "head-on" capability.

SPEED STABILITY AUGMENTATION

An OMNI-LORAS system can be used to provide speed cue inputs to a slightly modified version of the current SCAS. Longitudinal and lateral airspeed signals could be used to provide positive static stability (where it is now not present). This would allow the pilot to trim the aircraft so that it would hold most combinations of speed components in the low speed regime. This stability enhancement would reduce pilot workload, especially at night when the pilot must concentrate on tactical maneuvers and terrain avoidance.

HELICOPTER FIRE CONTROL

There are a number of design options available using a single LORAS sensor. In every case, flight path true airspeed $|v|$ is used throughout the entire flight envelope. In every case we recommend that the longitudinal component of LORAS airspeed $|u|$ and the lateral component of LORAS airspeed $|v|$ be used within the low airspeed regime (under 60 knots in any direction). In some cases $|v|$ (the lateral airspeed component) is recommended for use at all speeds. The general idea of all options is to complement LORAS air data with vane or non-vane aerodynamic sensors of angle-of-attack. The absolute velocity of LORAS $|V|$ is used with angle of attack to compute the vertical speed component in forward flight. Other means are used to compute the vertical speed component of the aircraft in slow speed flight.

SHORT RANGE TACTICAL NAVIGATION

Pilots can enhance DR navigation accurancy by observing the lateral and longitudinal airspeed components and by using the LORAS True Airspeed Mode of operation.

Current air mass navigation systems are failures because they do not measure inherent sideslip information. (Sideslips are induced by tail rotor thrust and by "out of trim" flight.) OMNI-LORAS outputs can be ground stabilized and fed into a navigation computer. This provides the pilot with short term, synthetic ground speed, and short range navigation.

GROUND OPERATIONS

Engine Over Temperature (out of limits) operations may occur during start attempts in high downwind conditions. Pilot start techniques, based on wind direction and speed, can be used to avoid overtemp, or the aircraft may be turned into the wind prior to a start attempt.

Rotor Engagement/Disengagement in high winds exposes the aircraft to mast bumping. The pilot can develop control placement techniques to minimize the problem if OMNI-LORAS data is displayed in the cockpit. The pilot can also observe the OMNI-LORAS output during operations near thunderstorms and engage the rotor during the lower wind conditions, which are often present just after a large gust passes.

Dynamic Roll Over often involves takeoffs in crosswind conditions. The sideforce caused by the crosswind in turn causes the downwind skid to "dig in" as the aircraft starts to lift off.

SUMMARY

An OMNI-LORAS is required on all AH-1 helicopters in order that pilots may fly inside the low range airspeed limits prescribed by the pilot's handbook.

Incorporating LORAS as a basic Air Data sensing and display system:

. Increases the probability of Accomplishing Mission Objective.
. Enhances OPERATIONAL Flight Safety and Survivability.
. Reduces Total Maintenance Activity and Increases Operational Availability.

LORAS DISPLAYS

D.L. Green
Director, Advanced Pla·· and Programs
PACER Systen Inc.
Arlington, Vi·:· 22202

INTRODUCTION

PACER Systems, Inc. has conducted numerous studies of display require-
ments. In addition, PACER has offered a series of displays for flight
evaluation. Additional display formats have been provided by cooperative
evaluators and research activities while pursuing their own interest.

PACER elected to work in the display design area because of the ·ob-
vious fact that display is a critical component of the omnidirectional air-
speed system. It's a simple fact that the pilot must see the data to use
it. In most cases, it is impossible for pilots (and engineers) to agree on
airdata usability or suitability for a given mission unless the display is
satisfactory.

One can expect a lot of different ideas to emerge as omnidirectional
low range airspeed systems are incorporated in research and operational air-
craft. Nevertheless, there should be no question that the current level of
experience has been adequate to define a safe and practical first generation
production display.

MOVING TAPE

A moving tape display has been evaluated extensively on a number of air-
craft. This type of display was found to provide a very strong visual gain
to the pilot. Speed changes are much more apparent to the pilot when the
scale numbers (printed on the tape) move past a pointer as opposed to the
pointer moving by a fixed scale on a fixed face plate. When such a display
is used in conjunction with a very sensitive (or very responsive) airspeed
sensor, the result can be a nervous display and a somewhat annoyed pilot.
One is tempted to overdamp the sensor (or display) to eliminate the undesired
sensitivity. This temptation should be resisted, since responsiveness can
be used as a design tradeoff. The designer can compress the airspeed scale
and retain the desired visual cue strength (with a more economical use of
display area) when adequate sensor responsiveness is available. This con-
cept of compressing the display scale was used in PACER's adaptation of the
conventional Doppler hover display.

DIGITAL DISPLAY

A digital LED type display was available during one flight evaluation.
No conclusions or recommendations are available as a result of this one flight
effort. A study of the concept suggests that certain digital formats would
be acceptable for certain applications, yet the digital format has the same
limitation as the single axis meter type display. Neither of these display
schemes can easily incorporate a simple presentation of the slow speed flight
envelope.

SIMPLE LIGHT SYSTEMS

Simple light displays can play a very important role in the "heads up" display mode. In the area of performance, the minimum airspeed for tactical flight can be "set in" to an analog light display. Such a display could indicate fast (safe), on minimum speed, and below minimum speed. The display could take the form of the one used for years by the Navy for displaying angle-of-attack during landing approach. The idea is to mount the display up in the pilot's view where it is continually visible, even during tactical maneuvers. This visibility requirement may dictate two units, one on both sides of the cockpit.

The same type of display can be used to indicate the magnitude of the sideward flight component. A center light would light when the lateral speed is under say ±5 knots. Additional lights would indicate higher sideward speeds.

SIMPLE LIGHT DISPLAY
FOR INDICATING "MIN"
SAFE AIRSPEED

GREEN
.Fast
.Safe

YELLOW
.On Speed
.Caution

RED
.Slow
.Danger

Yellow   Green   Yellow
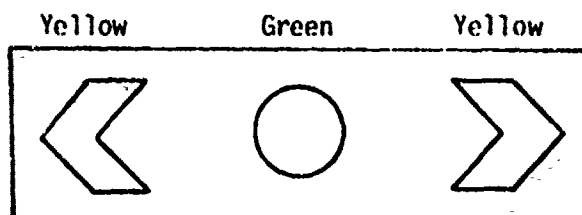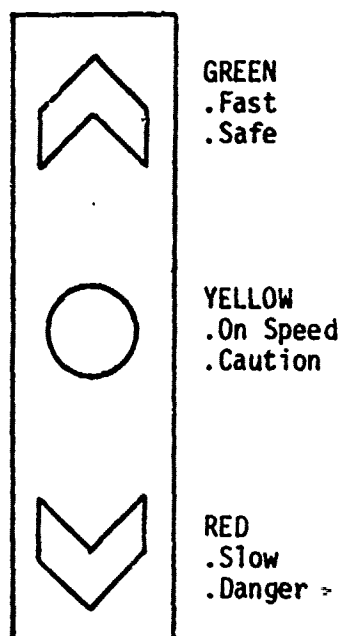
DISPLAY FOR ZEROING SIDEWARD
AIRSPEED OR AVOIDING LIMITS

SINGLE AXIS METERS

Two sizes of single axis meters have been evaluated. The original system used a meter for reporting the lateral airspeed component. This meter was marked for right and left lateral flight out to 30 knots. One early discovery was that the meter scale needed to be resized to provide for flight out to 50 knots. Pilots were sometimes flying outside of the design envelope of their aircraft. They needed to know how far out they were going.

A set of meters was later developed for installation vertically (for forward-rearward airspeed) and horizontally (for right and left airspeed). The idea was to locate these displays along side and below a HUD or gunsight. These displays worked nicely for their intended purpose but they do not allow "hover type" flight envelope information to be displayed.

FLIGHT DIRECTOR BARS

Most current production attitude indicators (ADI) incorporate flight director bars or have provisions for the installation of flight director bars. On one occasion LORAS component airspeed information was fed to the flight director bars of our ADI for evaluation. The results were very positive. The scaling was selected so that the horizontal bar reached full down deflection, as a forward airspeed of 50 knots was attained. The vertical bar deflected to the right and left indicating speeds up to 50 knots, left and right respectively.

This arrangement put attitude and airspeed information all on one device. This proved to be an excellent arrangement for "heads down" instrument type flight operations. It is an excellent arrangement because of the tie between attitude control and speed control in the low speed flight regime.

The ADI - LORAS integrated display also saves space on the instrument panel for heads down formats. The multi-use ADI approach would allow LORAS airspeed and Doppler ground speed to be available (presented) heads down at the same time (assuming a Doppler Hover Display were also installed).
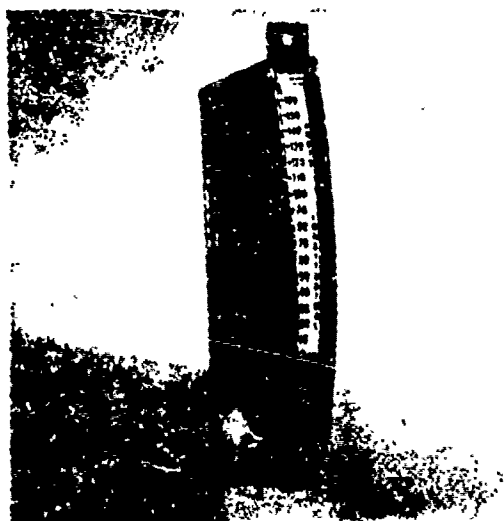
LONGITUDINAL AIRSPEED METER   LATERAL AIRSPEED METER

ADAPTING THE DOPPLER HOVER DISPLAY

The Navy, Air Force, and Coast Guard have used a crossbar-type indicator to present doppler radar derived ground speed cues to helicopter pilots. This is an inexpensive type indicator, available in large quantities in the government supply system.

This indicator format provides the pilot with omnidirectional information in that the intersection of the two bars tells the pilot which direction the relative wind is coming from. That is, a line between the intersection of the two bars and the "zero-zero" airspeed point (center of the small circle on the face of the display), portrays the bearing of the relative wind line. This omnidirectional quality makes it possible to mark the face of the display with omnidirectional limitations important to structural flight envelopes and controlability envelopes.

The bars of this type indicator provide very strong visual cues which can provide useful piloting information even in a peripheral scan.

The center of the display can be offset so that more of the display face is allocated to forward flight and less is allocated to rearward flight. Offsetting the center is proposed by PACER as the best way to provide continuous information in the slow speed regime.

There are two approaches which can be used when connecting the LORAS outputs to the bars of the indicator. All current applications of the display use only one of these alternatives. That is, when forward speed is generated, the horizontal bar moves down scale, and when right sideward speed is generated, the vertical bar moves to the left. This is the display technique that doppler installations have used for over 15 years.
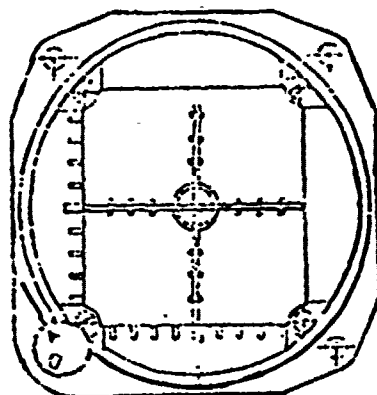

STANDARD
OMNI-SPEED
INDICATOR FOR
LORAS AND DOPPLER
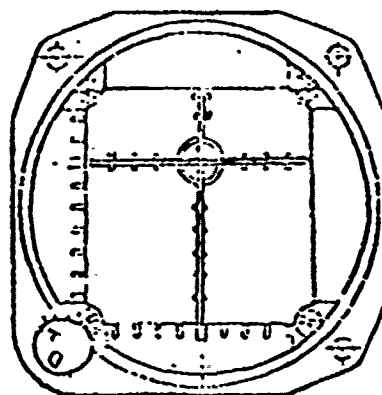
MODIFIED
OMNI-SPEED
INDICATOR FOR
LORAS AND DOPPLER

235

There is a second approach, which
may be more desirable for USMC and U.S.
Army applications. This alternate
approach would have the bar move up
for forward speed and right for
right sideward flight. There is :
no problem in providing different
display formats to separate custc
mers.
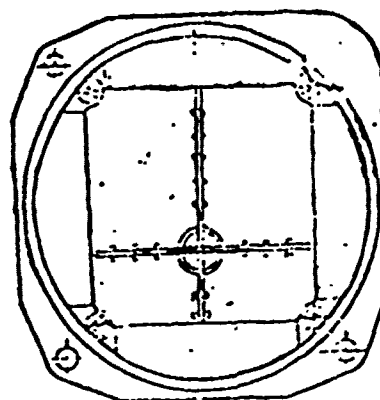
There are also a number of approches
which can be taken to mark the face of
the display. A simple dashed line has
been used here to suggest how the dis-
play would be marked for the AH-1 G/Q
model cobra helicopter. The marking
depicts a sideward airspeed limit of
30 knots in forward flight, plus the
clearance to turn 36° in a 30 knot
wind.
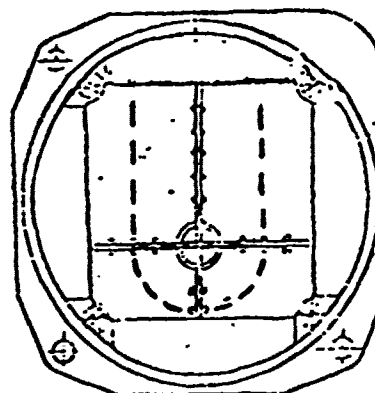
OMNIDIRECTIONAL DISPLAY

The display, which PACER offers as an optional accessory, is tailored
after conventional Doppler groundspeed displays and weighs about 1.6 pounds.

The horizontal and vertical bars indicate aircraft speed in knots along
the fore-aft and lateral axes respectively. When the bars cross in the center
of the circle, true airspeed is zero. As the aircraft moves into forward
flight, the horizontal bar moves downward. As the aircraft moves into right
sideward flight, the vertical bar moves left. The convention used to corre-
late bar motion with airspeed direction has been readily accepted during
flight evaluation and agrees with the convention used in Doppler groundspeed
displays.

When the pilot desires to zero airspeed along a given axis, he flies
(displaces the cyclic control) toward the appropriate bar. To zero the side-
slip by yawing the aircraft, he steps on the "ball"---center circle of the
display. This technique is consistent with the prudential rule of "stepping
on the ball" of the turn and bank indicator to achieve balanced flight.

Angle reference cues are provided by the dash marks extending outward
from the center of the display. The ends of the marks form circles of con-
stant flight path airspeed. These dash marks also provide the display face
with visual texture, making bar movement easier to monitor.

236
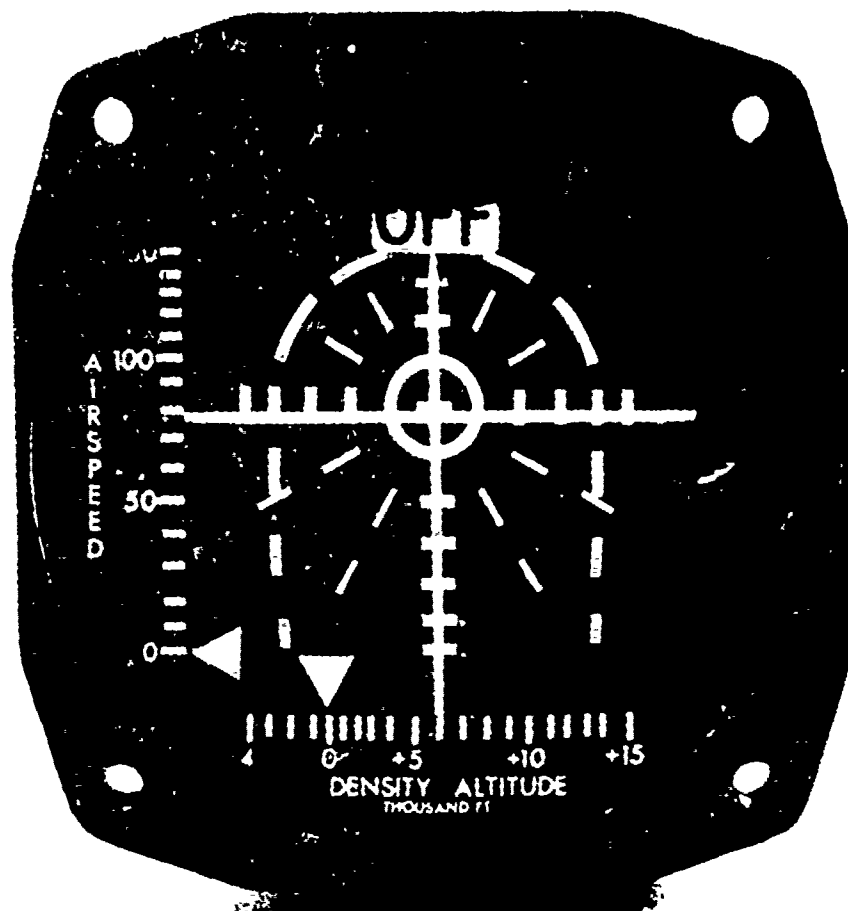
The intersection of the bars also indicates the azimuth angle of the relative wind. This angle is measured clockwise from the top of the vertical bar to an imaginary line connecting the center cross mark to the point at which the bars intersect.

The horseshoe-shaped dashed line on the face of the display represents the aircraft's safety-of-flight envelope limits. The location of the bar intersection with respect to this dashed line tells the pilot at a glance if he is in or out of this envelope. The relative motion of the bar intersection with respect to this dashed line lets the pilot instantaneously evaluate the "trend" in the changing margin of safety.

A pointer on the left edge of the display indicates the magnitude of flight path airspeed. For example, if the pilot executes a 360-degree turn in a 30-knot wind, the pointer maintains its 30-knot indication.

Density altitude is presented across the lower edge of the display within the range of -4000 to +15000 feet. Scaling and range can be adjusted to fit customer needs.

The omnidirectional LORAS display concept has been evaluated on a tandem and a single rotor helicopter. The results were positive. A few minor marking changes might be desirable but, otherwise, pilots have found the display satisfactory.

MANEUVER MARGIN DISPLAY

Hover performance charts are provided in helicopter flight manuals for pilot reference. The impact of wind is depicted on these charts as causing a reduction in power required. As the magnitude of the wind increases above zero knots, the power required to hover decreases. PACER has determined that these wind-power characteristics can be cross-plotted onto the face of an x-y type display. When airspeed and engine torque signals are used to drive the x-y bars, the product is an inexpensive Maneuver Margin Display. There are many small improvements which enhance the basic concept but we will constrain this disclosure to the rudimentary design principles and applications.
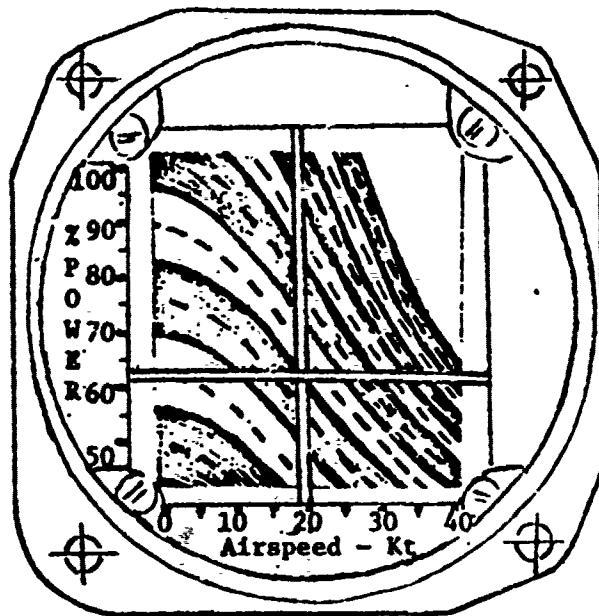

MANEUVER MARGIN DISPLAY

MULTI-MODE DISPLAYS

A multi-mode display could be used to present either doppler groundspeed or LORAS airspeed, as selected by the pilot.

A slow speed maneuver margin display and a standard OMNI-LORAS display may both be required in the cockpit. In some cases it will be possible to use one display for both formats, if the display has sufficient flexibility. A properly designed CRT display could provide the desired capability and allow more engineering flexibility in the design of the basic airspeed display format as well. This is considered a long range design objective.

HEADS UP vs. HEADS DOWN

A "Heads Up" type display is required for "eyes out" tactical maneuvering. PACER has suggested that the omni-directional airspeed display be located above the sun shield, over the instrument panel. It should be located next to the Pilot Steering Indicator for TOW equipped aircraft and next to the Fire Control HUD for guns and rocket equipped helicopters.

238

LORAS
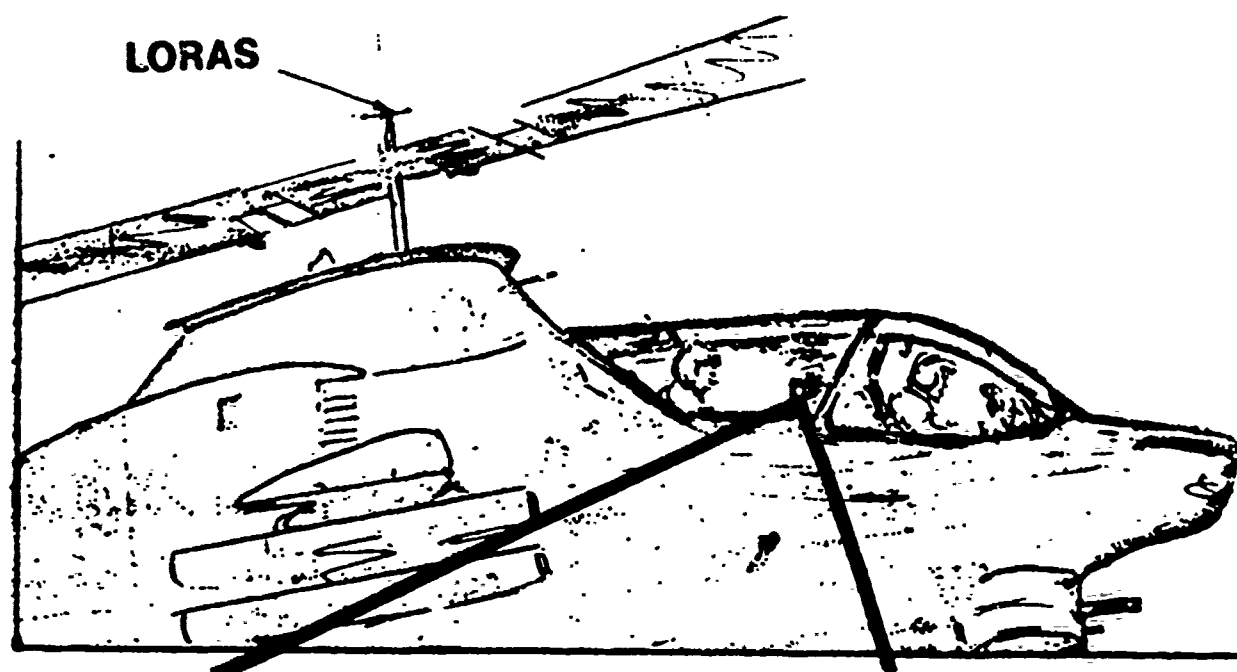
OMNIDIRECTIONAL
AIRSPEED INDICATOR(OAI)

PILOT STEERING
INDICATOR (PSI)
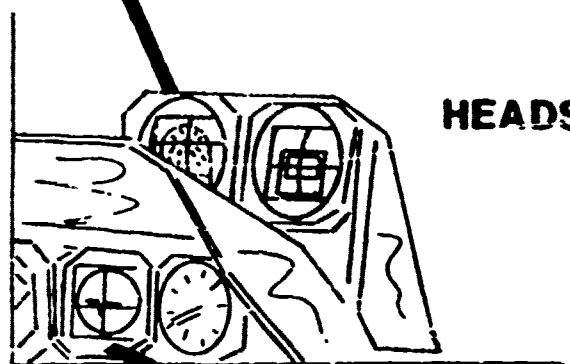
HEADS UP

ALTERNATIVE A

ALTERNATIVE B

ATTITUDE
DIRECTOR
INDICATOR (ADI)

HEADS DOWN

● PLANED INSTRUMENT
FLIGHT

● NIGHT/INSTRUMENT
PILOT DISORIENTATION

LEARNING TO FLY

With LORAS information available, pilots quickly learn to execute control displacement patterns which produce the desired speed change. The control manipulation is a "learned" input and it is executed in a very conventional manner. The manipulation and cross-reference to airspeed is conducted much as a 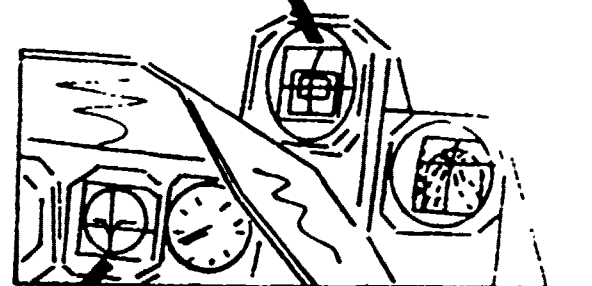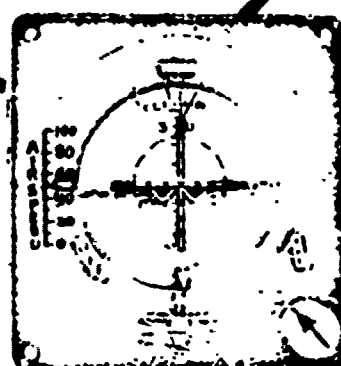speed change is accomplished at higher airspeeds where it is possible to reference the pitot static airspeed indicator. The pilot notes his present speed and executes the control input he anticipates will achieve the desired results. As the maneuver nears completion he will cross check LORAS to adjust the conclusion of the speed change. Pilots can not properly judge the control displacement magnitude or the time frame for the displacement until they have a speed cue feedback. Once pilots learn "control"/ "speed change" relationships, they need to spend less time in directly monitoring the omnidirectional airspeed indicator (OAI).

Low range airspeed information allows pilots to learn the sound, feel and capability of their aircraft throughout the low speed regime. This process is in fact the learned correlation of aircraft characteristics to airspeed. It changes some from day to day and from aircraft to aircraft, but the start of each flight will be a recalibration of man and machine. This knowledge in turn allows pilots to augment the displayed airspeed information with perceived information gained peripherally via aural, visual and other perceptual cues. It is this integrated mode of operation that provides the maximum benefits from an omnidirectional low range airspeed system.

ULTRASONIC WIND VECTOR SENSOR

F. J. Ferrin
Honeywell Inc.
Government and Aeronautical Products Division
St. Louis Park, Minnesota

and

M. Yurescko
Frankford Arsenal
Aircraft Weapons Branch
Philadelphia, Pennsylvania

ABSTRACT

A sensor that accurately measures the relative wind on helicopters for reliable rocket fire control solutions has been developed. This sensor, which operates on a principle involving ultrasonic signal transmissions through a moving air mass, contains no moving parts. It uses an ultrasonic transmitter and receiver configuration to determine wind vector information from wave transit times, thus giving immediate response to rapid changes in wind magnitude and direction. Tests on board an Army Cobra helicopter indicate that the Ultrasonic Wind Vector Sensor (UWVS) performs satisfactorily both at low speeds having large off-axis components as well as at high speeds, providing an improvement in rocket delivery.

INTRODUCTION

Fire control solutions for reliable rocket delivery from helicopters require that the effect of the relative wind be determined accurately. The ability to sense the relative wind on a rotary wing aircraft is difficult because of the large variations in the wind magnitude and direction. A sensor is needed which will be sensitive and stable at low speed having large off-axis components as well as giving satisfactory performance at high speeds. The Ultrasonic Wind Vector Sensor (UWVS) shown in Figure 1 was developed to provide an accurate measure of the relative wind while utilizing no moving parts, giving linear sensitivity over the entire speed range, and responding to rapid changes in wind magnitude and direction. As the name suggests, the UWVS operates on a principle involving ultrasonic signal transmissions through the moving air mass. This paper describes the UWVS concept which uses an ultrasonic transmitter and receiver configuration to determine wind vector information from wave transit times. Performance characteristics demonstrated during wind tunnel testing are discussed. The paper concludes with a summary of the flight test results to date on an Army Cobra helicopter employing the UWVS in a rocket delivery system.

FUNCTIONAL CONCEPT

Defining the wind velocity components requires a geometric arrangement of three ultrasonic transmission paths deployed in the airflow. From this, three equations can be derived to express the velocity components as functions of the measured transmission times along the paths. Figure 2 illustrates the relationship of the wind velocity components to the standard aircraft angles of attack and sideslip. Also shown are the three transmission paths and the associated transit times t_1, t_2, and t_3. The temperature sensor is needed

in order to compute the wave velocity in air as a function of temperature. The transmitters are simultaneously pulsed and at a later time, typically 200 to 300 microseconds, the wave arrives at the receivers. Figure 3 shows the vector relationships from which the equations are derived. The resulting equation for one transmitter/receiver pair is shown in Figure 3. As can be seen, it contains three unknowns, the W_x, W_y, W_z wind vectors, and the

measured transit time for the particular path. By writing the equations for the other two transmitter/receiver pairs as a function of their respective transit times, three equations with the three unknown vectors result. After rearranging the equations, the expressions shown in Figure 4 result. These are not of a closed form because the vectors are a function of W and therefore must be solved by iterative or feedback methods.

With zero relative wind velocity, the three transit times will be identical and equal to the ultrasonic wave transit time at the particular temperature. At 25°C, the times would be as follows:

$$t = \frac{R\sqrt{2}}{346.192}$$

R in meters

With a relative wind along the X axis only, the times are also equal, but now increase in value for forward aircraft motion. For relative wind speeds up to 100 meters per second, the times increase by about 30 percent. For relative wind in an arbitrary direction, the three times will be different in value. In general, the times can be considered as quantities which vary by a percentage around the still air value. Because of this, the equations were rewritten to provide simplified computation which is dependent on difference times. Using numerical approximation methods, the equations in Figure 5 result. The computation involves time differences around the still air transit time at 25°C and temperature differences around 25°C. These equations have been shown to provide results which contribute negligible mathematical errors.

242
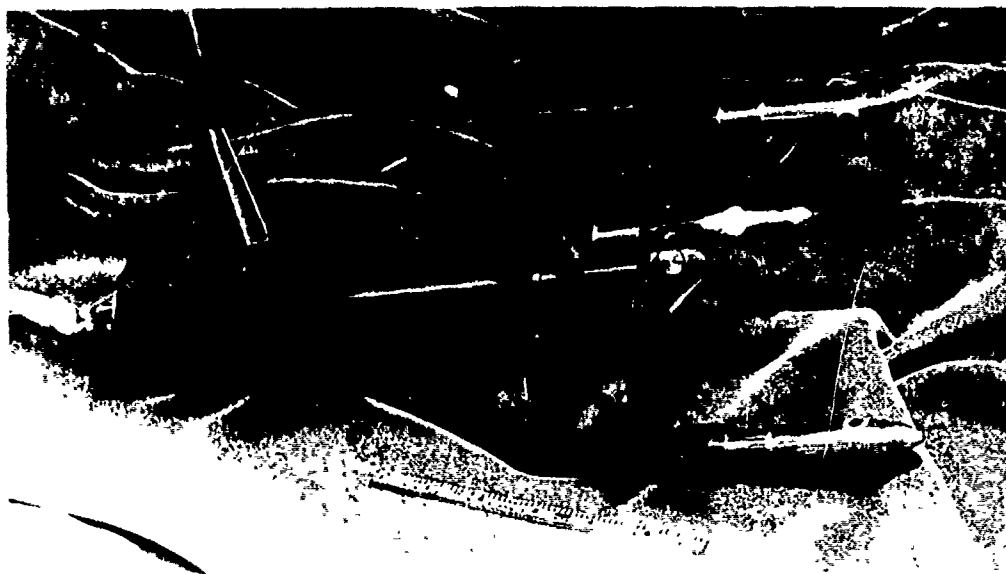
Figure 1. Ultrasonic Wind Vector Sensor (UWVS)

α = AIRCRAFT ANGLE OF ATTACK
β = AIRCRAFT ANGLE OF SIDESLIP
W = WIND VECTOR

3 TRANSMITTERS

TEMPERATURE SENSOR

RECEIVER 2

RECEIVE.: 3

RECEIVER 1

+X (FORWARD)
+Y (RIGHT)
+Z (DOWN)

AIRCRAFT AXES
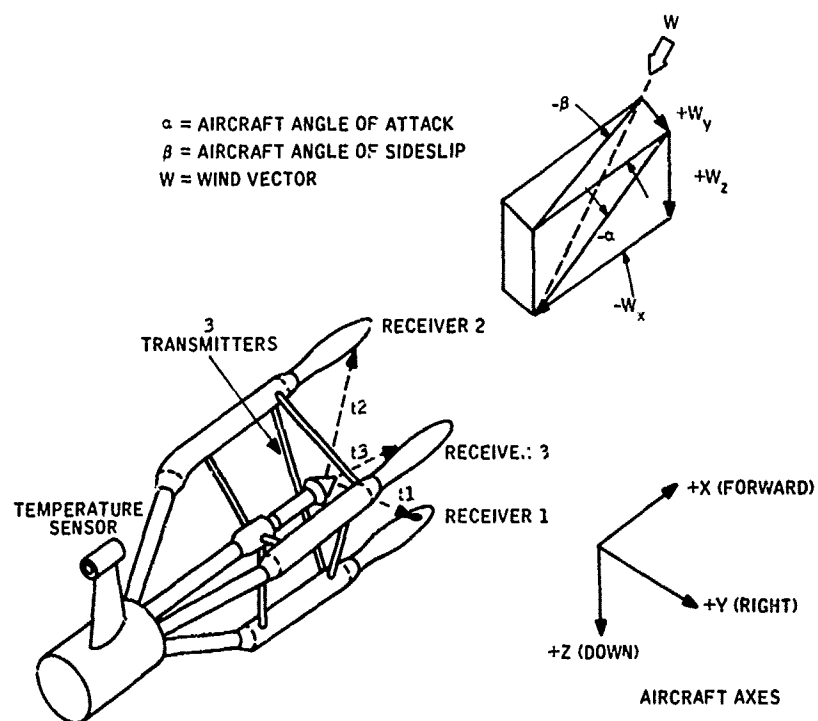
Figure 2. Wind Vector Definition

UWVS GEOMETRY

W = WIND VECTOR
L = TRANSMITTER TO RECEIVER VECTOR
M = RESULTANT WAVE TRANSIT VECTOR
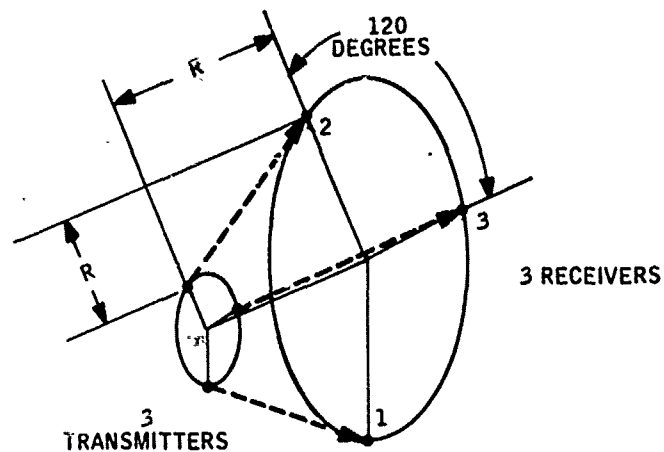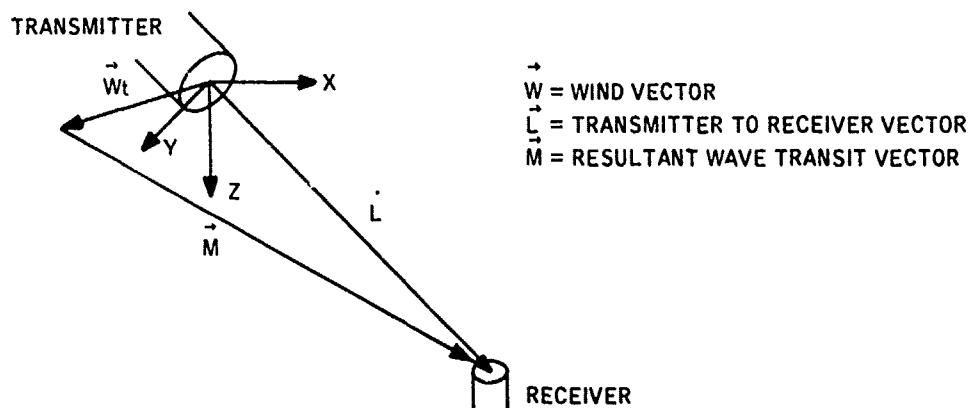
VECTOR DEFINITION

$$\vec{M} = \vec{L} - \vec{W}t$$

$$\vec{W} = w_x\hat{i} + w_y\hat{j} + w_z\hat{k}$$

$$\vec{L} = \ell_x\hat{i} + \ell_y\hat{j} + \ell_z\hat{k}$$

$$|\vec{M}| = Ct$$

C = SPEED OF ULTRASONIC WAVE

$$(\ell_x - w_xt)^2 + (\ell_y - w_yt)^2 + (\ell_z - w_zt)^2 = C^2t^2$$

Figure 3. UWVS Geometry and Vector Definition

244

$$W_x = \frac{-R}{3}\left(\frac{1}{t_1} + \frac{1}{t_2} + \frac{1}{t_3}\right) + \frac{\left(C^2 - W^2\right)}{6R}\left(t_1 + t_2 + t_3\right)$$

$$W_y = \frac{R\sqrt{3}}{3}\left(\frac{1}{t_2} - \frac{1}{t_3}\right) - \frac{\left(C^2 - W^2\right)\sqrt{3}}{6R}\left(t_2 - t_3\right)$$

$$W_z = \frac{-R}{3}\left(\frac{2}{t_1} - \frac{1}{t_2} - \frac{1}{t_3}\right) + \frac{\left(C^2 - W^2\right)}{6R}\left(2t_1 - t_2 - t_3\right)$$

$$W^2 = W_x^2 + W_y^2 + W_z^2$$

$$C^2 = C_0^2\left(\frac{T + 273}{298}\right)$$

$$C_0 = 346.192 \text{ METERS PER SECOND}$$

Figure 4. UWVS Equations

$$W_x = S_1 W^2 + \left[S_2 + S_3 W^2 + S_4 (T-25)\right]\left[t_1 + t_2 + t_3 - 3t_0\right] + \left[S_5 (T-25) + S_6 (T-25)^2\right]$$

$$W_y = Q_1\left[Q_2 + Q_3 W_x + Q_4 (T-25)\right]\left[t_2 - t_3\right]$$

$$W_z = Q_5\left[Q_2 + Q_3 W_x + Q_4 (T-25)\right]\left[2t_1 - t_2 - t_3\right]$$

$$W^2 = W_x^2 + W_y^2 + W_z^2$$

- $S_1 \rightarrow S_6$ AND $Q_1 \rightarrow Q_5$ ARE CONSTANTS
- $t_1, t_2,$ AND t_3 = TRANSIT TIMES
- t_0 = REFERENCE TIME AT W = 0 AND T = 25°C
- (T-25) = TEMPERATURE - 25°C

Figure 5. Simplified Equations

245

MECHANIZATION

The UWVS was mechanized as shown by the functional diagram illustrated in Figure 6. This is part of a 2.75-inch rocket delivery system. The transmitters utilized are piezo-electric transducers resonant at 75 kilohertz, while the receivers are wide bandwidth ceramic microphones with response out to 400 kilohertz. These are isloation mounted in a lightweight tubular aluminum structure as shown in Figure 1. The temperature sensor is a platinum element, thermally isolated from the structure. The sensor unit also contains a temperature sensor amplifier and three receiver preamplifiers. The transmitter drive, timing logic, pulse detection circuitry, and the electronics used to solve the equations are contained for the time being in a separate electronics unit.

The equations, previously discussed, are not very difficult to solve. Either a digital processor can be utilized for the solutions or analog methods can be employed. Because of their simplicity, the equations in the present mechanization are solved using a unique analog multiply/divide technique. The accuracy of the circuitry is sufficient to contribute negligible error to the wind vector determination.

PERFORMANCE ANALYSIS

Performance analysis indicates that there are six primary areas that can influence the UWVS accuracy. A summary of each of these effects is presented below.

Transducer Locations

This is associated with the location of a particular receiver with respect to its transmitter. Calibration is accomplished in a straightforward manner by merely positioning the receiver booms, with zero wind, until the transit time is equal to the theoretical value for that temperature and the specified value of transmitter/receiver distance. Doing this to within ±0.1 microsecond has shown to be satisfactory and is readily accomplished.

Aerodynamic Effects

Inserting any finite volume into an airstream modifies the flow to some extent. In the case of the UWVS, tests have shown that the equations require only a fixed scaling change to minimize the effect for the sensor geometry used. It should be noted that, depending on the sensor mounting location, the flow around the aircraft structure will change the sensor measurements. This obviously is not a sensor related error because any sensor used can only be expected to measure the actual flow over it. It is appropriate, however, to compensate for mounting location flow irregularities in the wind vector computation. The UWVS mechanization includes terms in the equation processing which can provide compensation so that the computed wind vectors are an accurate measure of the aircraft motion through the air mass.

Signal Noise

The limiting noise source in the UWVS occurs as the flow across the sensor becomes turbulent at high speeds. With the present structure, the noise from local air turbulence becomes significant at wind velocities over 200 knots, which is above practical maximum helicopter speeds. The effect of this noise is to cause jitter in the computed wind vector values.

Installation Alignment

Alignment of the UWVS to the aircraft reference frame is quite simple to achieve in that it can be accomplished during aircraft leveling and alignment. Because of the geometry, a level can be used for two axes and a boresight tool for the other axis.
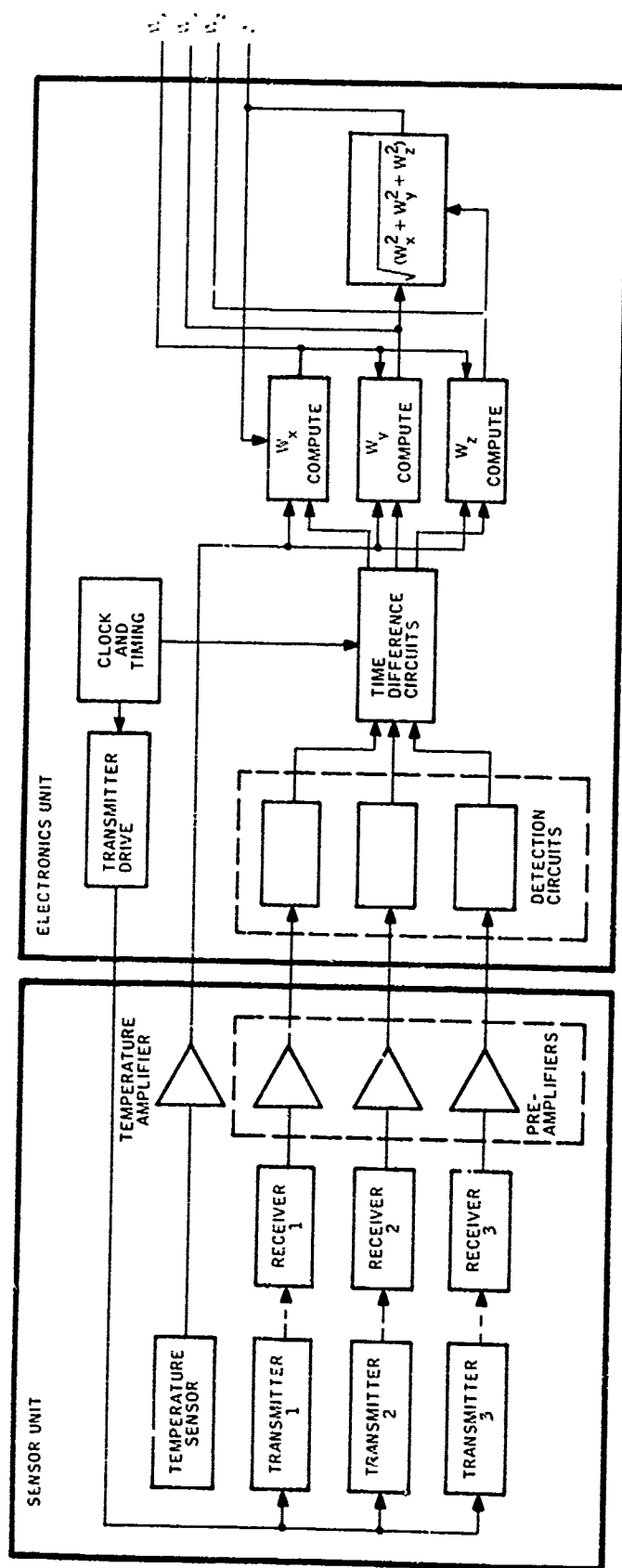
Figure 6. UWVS Functional Block Diagram

Environmental Conditions

Temperature, altitude, and vibration tests have been conducted on the UWVS. Temperature tests from -40°F to +140°F have shown no significant effect on performance. Altitude tests show ultrasonic signal attenuation as expected, with 6 decibels per 18,000 feet being measured. The signal attenuation, however, did not affect operation. Vibration tests show that any resonances are well above those input frequencies experienced on rotary wing aircraft. Flight tests to date on an Army Cobra helicopter also indicate that no structural or functional problems exist.

Electronic Circuitry

Another contribution to UWVS performance is associated with the pulse detection and time difference circuitry. The stability of these functions has been measured and found satisfactory. After the receiver boom position calibration has been performed, the time difference values as determined electronically do not change significantly enough to influence overall performance.

PERFORMANCE TESTS

The UWVS has been evaluated in two wind tunnel facilities. Early developmental testing was accomplished in a Honeywell wind tunnel with a small test section. During this phase of the program, various structural shapes, transmitter types, receiver types, and transducer orientations were evaluated which led to the present configuration. Development continued with sensor performance testing under varying wind magnitudes and directions. More recently, testing was accomplished in a larger facility having a 7 x 10 foot test section (LTV low speed wind tunnel, Dallas, Texas). The test setup used is shown in Figure 7. Measurements were made with tunnel wind velocities up to 200 knots. Flight conditions having angle of attack and sideslip were simulated by rotating the UWVS 90 degrees in its mount from that shown and positioning at angles up to 90 degrees in the tunnel. This extreme orientation allowed evaluation under simulated helicopter downwash at hover. The test results obtained in the wind tunnel are summarized in Table 1.

Table 1.   Wind Tunnel Test Result Summary

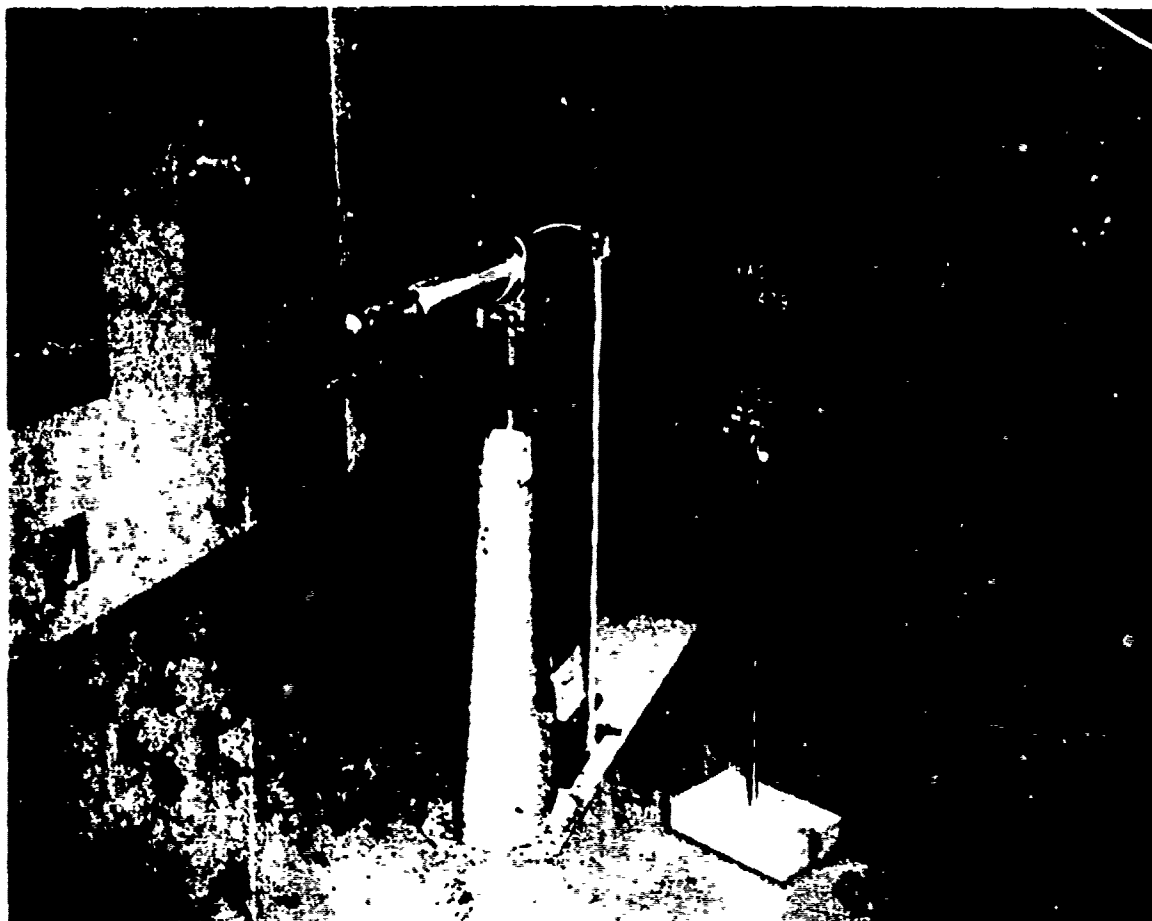| Condition	Wind Velocity	Performance
$\alpha = 0$, $\beta = 0$	0-180 knots	W_x linear within 2 knots
$\alpha = 0$, $\beta = -30°$ to $+30°$	0-100 knots	W_y linear within 1 knot
$\beta = 0$, $\alpha = -20°$ to $+20°$	0-100 knots	W_z linear within 1 knot
$\beta = 0$, $\alpha = 0°$ to $-45°$	60 knots	W_x linear within 1 knot
$\beta = 0$, $\alpha = 0°$ to $-45°$	60 knots	W_z linear within 2 knots
$\beta = 0$, $\alpha = -90°$ (hover)	60 knots	W_x accurate within 1.4 knots
$\beta = 0$, $\alpha = -90°$ (hover)	60 knots	W_z accurate within 0.9 knot

Figure 7. UWVS Wind Tunnel Test Setup

Analysis of sensor requirements for accurate rocket delivery indicate that the most critical parameter is measurement of slant range to the target. In addition, the next greatest influence on delivery accuracy is the relative wind components on the rocket after launching. The UWVS performance demonstrated during wind tunnel testing was evaluated in regard to UWVS usage in a rocket delivery fire control system. It was determined that, typically, a 1 knot error in measuring the W_y and W_z components and a 5 knot error in measuring the W_x component would contribute an acceptably low amount to rocket miss distance. This was established by examining the error budget, which included all contributors to delivery accuracy.

It should be noted that computation of the ballistic path when firing from hover has not been finalized. The actual influence of the downwash component W_z on the rocket and the appropriate fire control equations for this flight condition require further analysis. The UWVS provides a measure of the W_z wind vector at and near hover which is stable, although with slightly reduced linearity.

FLIGHT TESTING

The UWVS is part of a rocket delivery system which contains not only the wind sensor, but the pilot's sight, computation electronics, and the other necessary aircraft sensors as well. The system is presently undergoing evaluation on the Army Cobra helicopter shown in Figure 8. As shown in Figure 8, the UWVS is mounted on a short boom on the aircraft nose. The flight test is in its early stages so that the UWVS evaluation is not complete. However, test results to date indicate that the UWVS performs very well in the helicopter environment. The UWVS measured wind information has provided an improvement in 2.75-inch rocket ballistic computation over a number of different flight conditions. Rocket delivery accuracy to date with the system has proven very satisfactory. As predicted by earlier wind tunnel testing, the wind vectors as measured by the UWVS have remained stable and have provided an accurate input to the ballistic computation. Further testing is underway to gather more complete information on the UWVS performance. More detailed data analysis will be available through the use of an on-board recorder to monitor measured data. A summary of tests to date follows below.

Airspeed

Several timed runs were made over fixed ranges at a fixed aircraft altitude and attitude to obtain a measure of the W_x wind vector. It was determined that, at the UWVS location, the relative wind was about 10 percent lower in velocity than the true aircraft wind speed through the air mass for airspeeds tested (0 to 150 knots).

Angle of Attack

It was observed that the airflow at the UWVS location is several degrees more downward than expected theoretically when the aircraft is in level flight at constant altitude with a particular pitch attitude. As an immediate compensation, the UWVS mount was rotated upward the required angle so that the measured vertical wind vector was correct. Another form of compensation, being considered as an alternate, is to incorporate modifications to the computation.

Sideslip

The measured values of the lateral wind vector during flight testing were correct as expected because of the aircraft symmetry in this axis.

Figure 8. Army Cobra Helicopter for UWVS Flight Test

Hover

The UWVS forward wind vector W_x made a smooth transition from zero to the particular velocity when the aircraft was flown from a hover condition and slowly maneuvered to a forward velocity away from hover. The UWVS downward wind vector W_z also changed as expected from the value at hover (about 50 knots) to the particular value resulting at the aircraft attitude with a forward velocity. It was found that the downwash component moves behind the aircraft nose as forward velocities exceed 20 to 30 knots. It is hoped that additional data can be taken with a recorder to provide more detailed data analysis.

CONCLUSIONS

The UWVS provides a needed function for accurate 2.75-inch rocket delivery. The device is particularly suited to the Army helicopter environment in its ruggedness while offering almost instantaneous linear response over the entire flight envelope. The wind tunnel testing performed during the developmental effort demonstrated that the UWVS is capable of providing the necessary performance. The UWVS operation as observed during flight testing to date on an Army Cobra helicopter has been very satisfactory. Additional flight testing is underway to provide a more detailed performance analysis.

APPLICATION OF REMOTE WIND SENSORS

DAVID H. DICKSON
ATMOSPHERIC SCIENCES LABORATORY
WHITE SANDS MISSILE RANGE, NEW MEXICO

ABSTRACT

Modern weapon systems and Army operations cannot attain maximum
potential effectiveness in correcting for the influence of the
atmosphere where the correction are based on periodic point measurements
of the atmospheric parameters. Since the army operates principally
in the planetary boundary layer where parameters such as wind, temperature,
moisture, precipitation, visibility, etc., vary rapidly, remote wind
sensing is needed to supply real-time data to the fire control computer
so proper correction can be made. This paper speaks to the application
of remote wind sensors currently being developed by ASL which are capable
of fulfilling the Army's need.

INTRODUCTION

The following paper is a condensation of the information presented
during the conference on The Effects of Helicopter Downwash on Free
Projectiles.

Remote sensing is based on measurements of the interaction of waves with
the medium of study. It has been found possible to use acoustic, radio,
and optical waves, each having unique advantages for certain uses.
Although many types of remote sensing are being investigated, the great-
est effort is being devoted to optical sensing. Any systems we devise
must have the objectives of real-time measurement and automatic operation,
and must be tailored to specific Army needs.

ADVANTAGES OF REMOTE WIND SENSORS

The major potential advantages of remote sensing techniques are:

1. Measurements are taken remotely, i.e., without requiring that
in situ instrumentation be carried to the region of atmosphere to be
measured.

2. Remote sensing permits the measurement of the relevant parameters
of the atmosphere in one, two, or three spatial dimensions, all as a
function of time.

3. Excellent space and time resolution is obtainable.

4. The remote sensing measurements typically provide a line, area,
or volume integration which helps to insure that the observations are
more representative of the medium than those of a single-point sensor,
which may be adversely affected by local or transient perturbation.

5. Remote sensing instrumentation is usually automatic and often
can provide fully processed data 24 hours a day with a minimum of
manpower.

Modern weapons systems and Army operations cannot attain maximum poten-
tial effectiveness in correcting for the influences of the atmosphere
where the corrections are based on periodic point measurements of the
atmospheric parameters. The Army operates principally in the planetary
boundary layer where parameters such as wind, temperature, moisture,
precipitation, visibility, etc., vary rapidly both temporally and
spatially.

254

CONCEPT

A relatively new concept in atmospheric measurements for the support of
Army weapons systems and field operations is needed. This concept must
be based upon instantaneous (real-time) measurement of atmospheric param-
eters at the point or region of the atmosphere where the supported opera-
tion is taking place. The measurement system must be capable of rapidly
reaching any desired point in the atmosphere or of rapidly scanning a
particular region or volume.

PROGRAM OBJECTIVES

The objective of the program in the Atmospheric Sensing Technical Area of
the Atmospheric Sciences Laboratory (ASL) is to conduct basic and applied
research leading to the development of remote atmospheric measurement
systems required by the Army for support of specific tactical operations
or weapon systems.

Developments in microwave radar, laser radar, passive radiometry, and
acoustic sounding have demonstrated the feasibility of remote real-time
measurement of almost all the atmospheric parameters, and it is now
feasible to consider new real-time atmospheric sensing systems for the
field Army.

DEVELOPMENT PROGRAM

In FY-76 ASL began a developmental effort for design, fabrication,
installation, and testing of a remote wind sensor for helicopters.

A helicopter-carried remote wind sensor will be capable of functioning
in a Class IB, i.e., MSL to 15,000 ft over a temperature range of -40c
to 55c and over the shock and vibration ranges shown in Table 1,
page 27, MIL-E-5400P. Provisions for personnel safety will be made so
that inadvertent exposure to hazardous sources (if any) are minimized.
Remote Sensor Measurement Capabilities for this effort are divided into
two distinct measureable volumes: (1) that volume which surrounds the
helicopter firing platform, specifically the effects of downwash, and
(2) crosswinds from the firing platform to the intended target. Cross-
winds to target are considered long-range winds and state-of-the-art
studies are being planned for this.

Downwash wind field measurements are currently within the state-of-the-
art. By considering laser doppler velocimeter techniques, with certain
modifications, real-time downwash wind fields should be attainable.

The design measurement capabilities are currently planned to measure
three dimensional winds so that the downwash direction is within ± 2 degrees,
downwash speed is within ± 2 ft/sec, and the range (normal to downwash)
is 0-100 ft attainable through 2-ft increments with full or partial
integration at points or the total path.

255

The data output will be real-time analog voltage proportional to the components measured. The three dimensional position (x y z) of the centered volume of space measured and the three vector velocities (x y z) at that point will be obtainable.

EFFECTS OF AIR FLOW ON JETTISON OF MULTIRAIL
LAUNCHERS FROM HELICOPTERS

ERNEST S. STOOPS and RALPH D. EHRICH
ROCKWELL INTERNATIONAL
MISSILE SYSTEMS DIVISION
COLUMBUS, OHIO

ABSTRACT

The relative effects of free stream airflow, local air flow,
and jettison force on the behavior of a helicopter carried,
three-rail missile launcher with various missile loads were
investigate . The study was conducted to determine the sensitivity
of the predicted motions of the jettisoned store configurations
to increasingly sophisticated aerodynamic flow representations.
The results presented can be used as a guide in the early develop-
ment of new missile-launcher configurations to obtain approximate
launcher dynamic motions during jettison, either before the aero-
dynamic date exist, or for minimum cost of the analysis. The
effects of zero jettison force on launcher motion are included,
both to exaggerate the relative aerodynamic force effects and to
show the desirability/need for the ejector. AH-1G helicopter
data were used in the analyses and that helicopter was used in
a subsequent flight verification program. A short film of the
flight jettison tests is presented.

Missile Systems Division
Rockwell International

SUMMARY

An analytical investigation was conducted to determine the sensitivity of
the predicted motions of multi-rail missile launchers with various missile
loads to the aerodynamic flow around the helicopter. The analyses were
conducted for both 2-rail launchers, jettisoned from the inboard store
stations and 3-rail launchers jettisoned from the outboard store stations
of the AH-1G helicopter. Although the majority of the data are for
jettison at 120 knots, variations in airspeed were included. The results
showed that the worst case aerodynamic effects caused less than two inches
lateral motion of the launcher-missile combination, when compared to the
"zero-air" case. In-flight jettison tests of a fully loaded outboard
launcher confirmed safe separation of that configuration.

GENERAL

One of the problems associated with the carriage of external stores on
aircraft is the ability to safely jettison those stores during emergency
conditions. When multiple weapons are carried under one pylon, the
effort required to establish flight clearance is significantly increased.
The major input to determining safe jettison of a store are the geometry
involved, mass, and inertia of the store, the ejector force and the
aerodynamic effects on store motion. For helicopters, if the store
density is high, the aerodynamic effects tend to be relatively small
because of the low q's involved. (For example, q at 120 kts is only
approximately 5% of that at Mach = 0.9.)

If one could show that for some practical store configurations, the
effects of the aerodynamic forces are small, predictable and the direction
($\pm$) of the effect can be known, then one could investigate a relatively
few cases to determine store jettison clearances. Even if it were con-
sidered necessary to include aerodynamic effects for "final" analyses, much
effort might be saved early in the design process.

Rockwell Missile Systems Division (MSD) has conducted comparative studies
of the effects of zero air and "free stream" air on the translational
and rotational motions of selected missile-launcher combinations during
jettison from the AH-1G helicopters.

The 3-rail missile-launcher configuration analyzed is shown in Figure 1.
It represents the hardware used during the Laser HELLFIRE Operational/
Technical Test (LHOTT) program, funded by the U.S. Army Missile Command
under contract number DAAH01-74-C-0585. Figure 2 shows the loaded 2-
rail (inboard) and 3-rail (outboard) configurations installed on the AH-1G
wing pylons.

Figure 3 shows the values and directions of the ejector forces during
jettison. In addition, the problem of clearing the launcher skid is
readily apparent.

The list of store configurations analyzed is provided in Table 1.

258

OUTBOARD EJECTOR
FOOT LOCATION

SWAY BRACE
LOCATION

INBOARD
EJECTOR FOOT
LOCATION
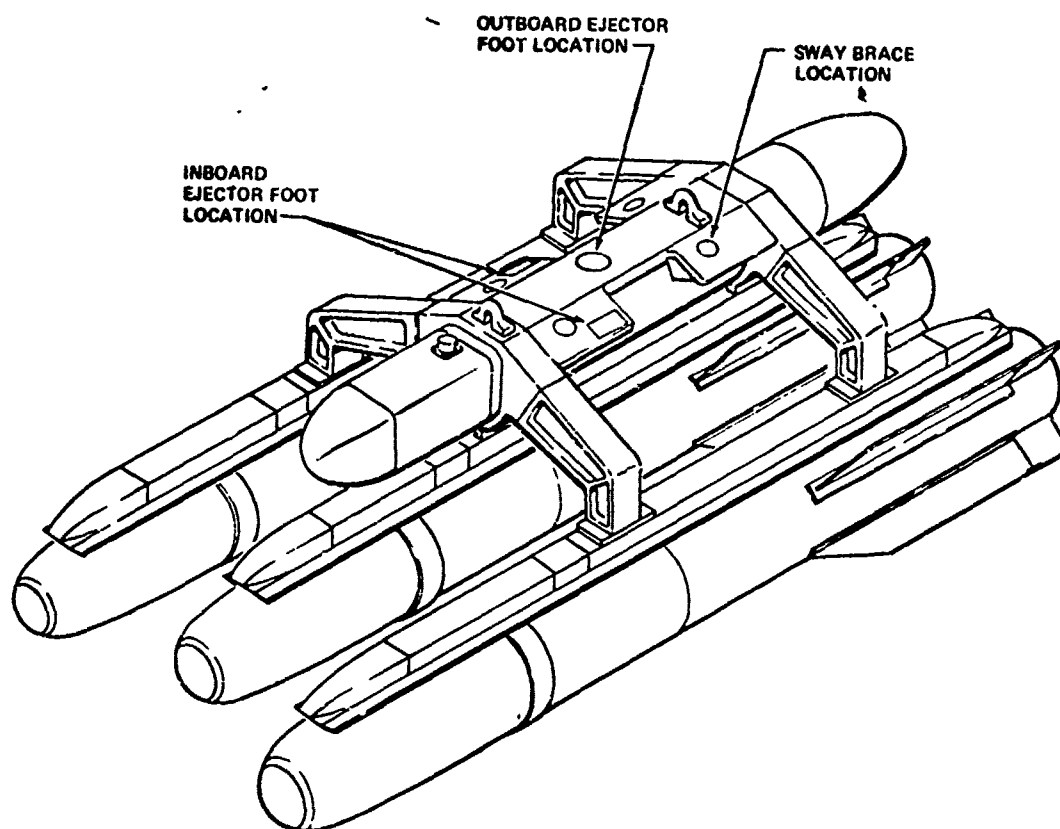
Figure 1. 3-Rail Missile-Launcher Configuration

Parts Commonality

Outboard/Inboard
Store Station Compatibility

Standard Lugs

Ground
Clearance

Front Loading
One or Two Men

Figure 2. Launcher Installation on AH-1G

259

Figure 3. Ejectory Force Geometry

Table 1. Missile-Launcher Configurations Analyzed

CONFIGURATION NO.	2-RAIL LAUNCHER MISSILES		3-RAIL LAUNCHER MISSILES		
1			I/B	₵	O/B
2	NA		—	₵	O/B
3			—	—	O/B
4			I/B	—	—
5	I/B	₵			
6	—	₵		NA	
7	I/B	—			

The ejector force-time history representations for both the inboard and outboard ejectors are provided in Figure 4. The force actually experienced by the missile is limited by the stroke of the ejector which is 4.5 inches.

Figure 4. Ejector Force Time History

Table 2 provides the major mass properties of the loaded 2-rail and 3-rail launchers, although the simulation also included cross products of inertia.

Table 2. Launcher Mass and Inertia Properties
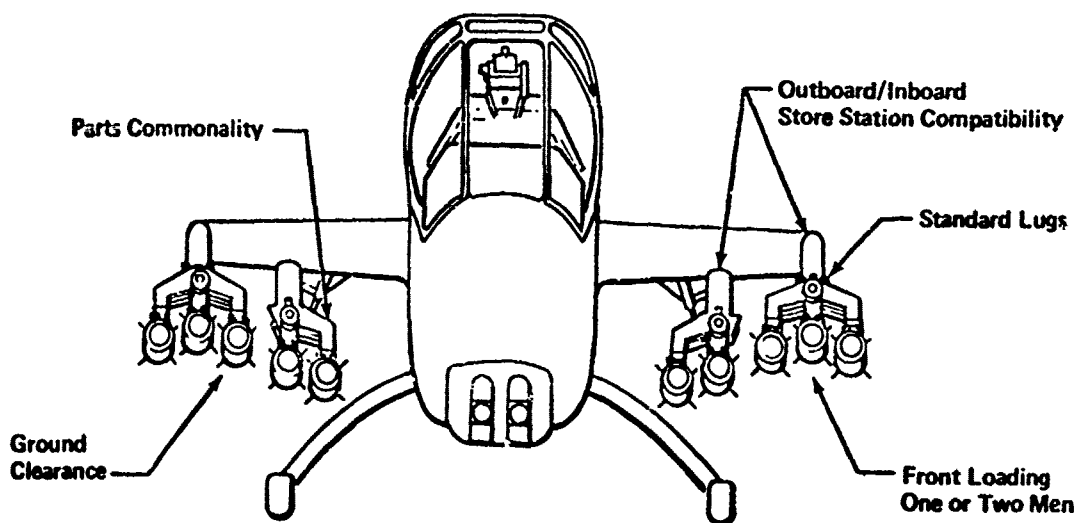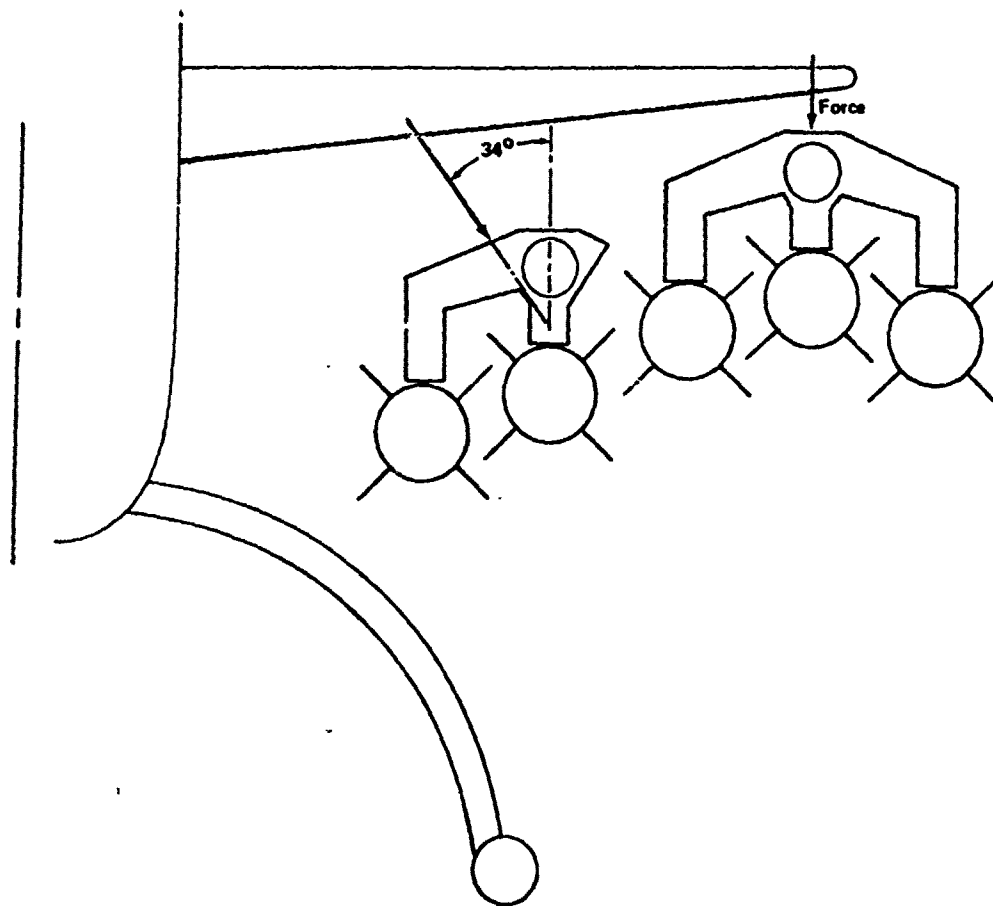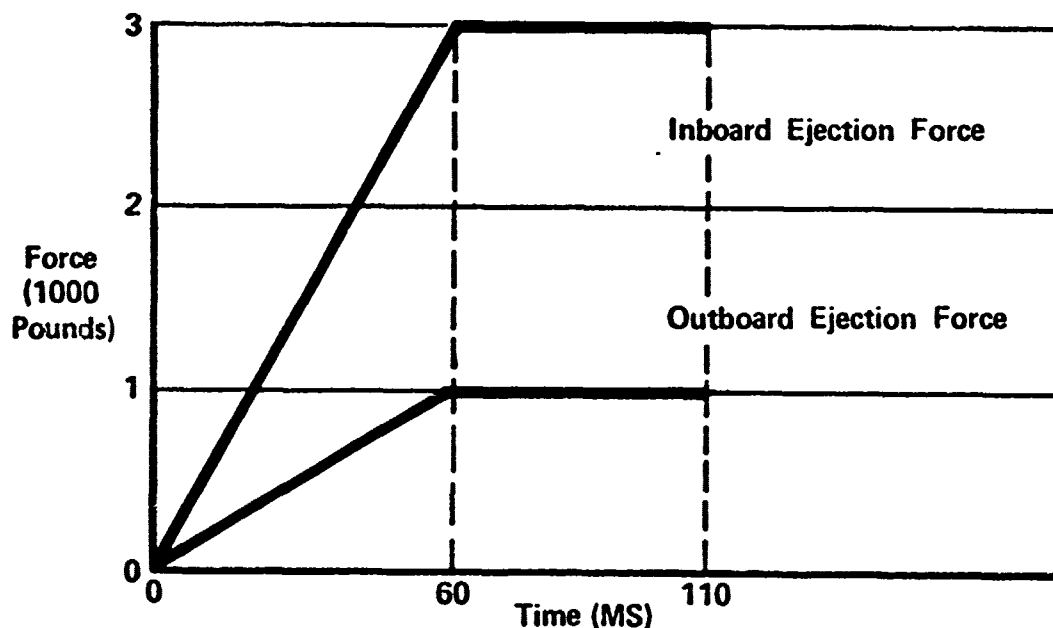
	Three Rail Launcher (Outboard)	Two Rail Launcher (Inboard)
Mass (Slug)	9.062	6.772
I_{xx} (Slug-Ft^2)	3.364	1.772
I_{yy} (Slug-Ft^2)	20.84	14.50
I_{zz} (Slug-Ft^2)	23.71	15.236

Aerodynamic Coefficients

Force and moment coefficients were derived for each of the missile-launcher configurations. These data were generated from a combination of sources, including wind tunnel test data and analyses of single and clustered weapons. Both interpolation and extrapolation techniques were used. The final data were produced in the form of plots of the individual coefficients as functions of angle of attack and yaw angle. The variations of the configuration center of pressure as functions of pitch and yaw angle were accounted for.

Helicopter Flight Parameters

During the LHOTT program, the U.S. Army Missile Command provided data showing the nominal AH-1G pitch, roll and yaw angles as a function of airspeed for helicopter "level flight". These data are shown in Figure 5. In addition, it has been stated that for airspeeds above 40 knots, the helicopter downwash effect does not significantly influence the air flow below the helicopter wing.
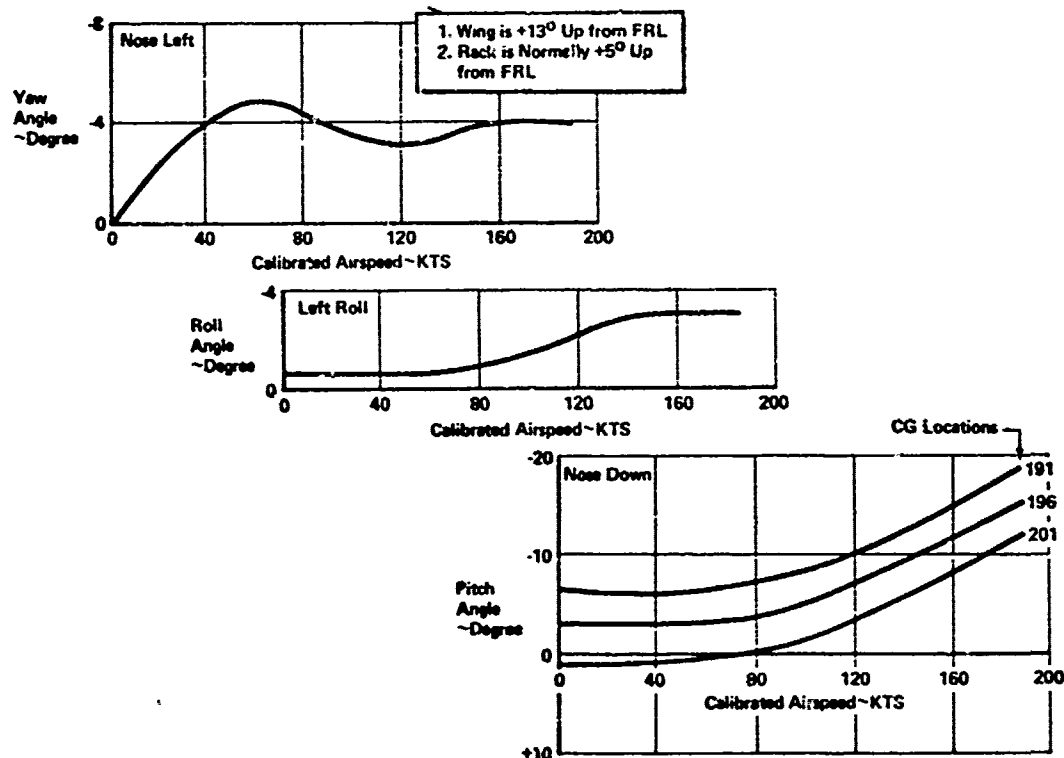
Figure 5. AH-1G Attitudes Vs. Calibrated Airspeed

Free Stream Aerodynamics

A simplified approach to the aerodynamic flow around the missile-launcher combinations considered that the angle of attack was controlled by the helicopter pitch attitude and the angle of incidence between the launcher and helicopter fuselage reference line. The windward side yaw angle seen by the missile-launcher combination was considered equal to the yaw angle of the helicopter, while the leeward side yaw angle was arbitrarily chosen to be half the windward side angle, as shown in Figure 6.

263
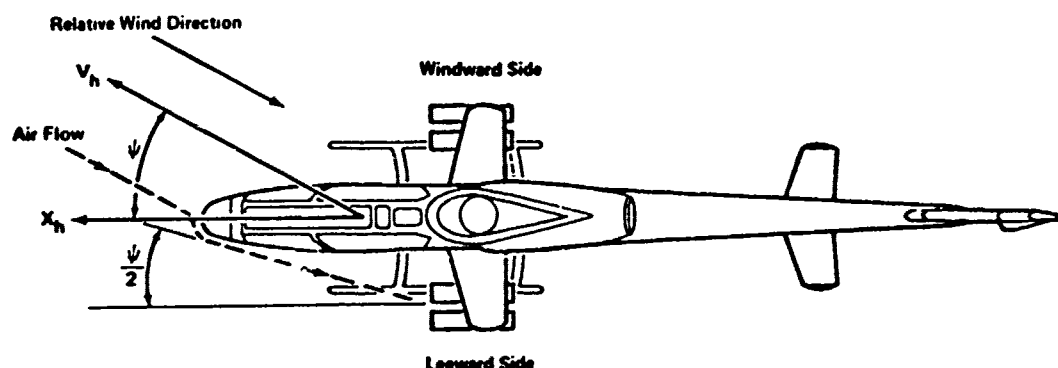
Figure 6. Air Flow Directions for Leeward and Windward Launchers

Launcher Configuration

The launcher configurations analyzed were shown in Table 1. As would be expected, ejection of 3-rail missile-launcher configurations which are not symmetrical about the launcher plane of symmetry induce rolling motions. For outboard cg's on the right hand wing, the roll is counterclockwise, and for inboard cg's, the roll is clockwise. For the inboard 2-rail missile-launcher configurations, the roll induced by the jettison force (at an angle of 34°) is always clockwise on the right hand wing and counterclockwise on the left hand wing. The roll rate is increased or decreased by the specific missiles carried, as they affect the total system cg, changing the lever arm between the line of the ejector force and the cg.

Analyses

The analyses were conducted using a full six degree-of-freedom digital program in IBM CSMP. The program provided for integration every .005 seconds. Aerodynamic data were inserted in a "Table look-up" approach. The program calculated the relative positions of the missile fins and selected launcher points as measured from the skids for every intermediate solution, thereby providing the minimum clearances directly.

In the first series of analyses, the gometry, inertia and ejector force terms were included. For the second series, free-stream aerodynamic terms were added. The third series showed the effects of airspeed for the free stream aerodynamic representation for missile-launcher configurations 3 and 6.

Results

Figures 7 and 8 show typical motions of the missile launcher configurations as the system is ejected from the helicopter. Notice that significant rotation occurs for all but the three missile launcher fully loaded. Figures 9 through 12 show the minimum clearance between the launcher and the skid. In each case, the solution with no aerodynamic forces and that with "free stream air" are shown. For the outboard launcher on the windware side, the air tends to reduce the clearance except for one case. This

264

Three-Missile Load

Two-Missile Load

5 In.

Helicopter
Skid

Helicopter
Skid
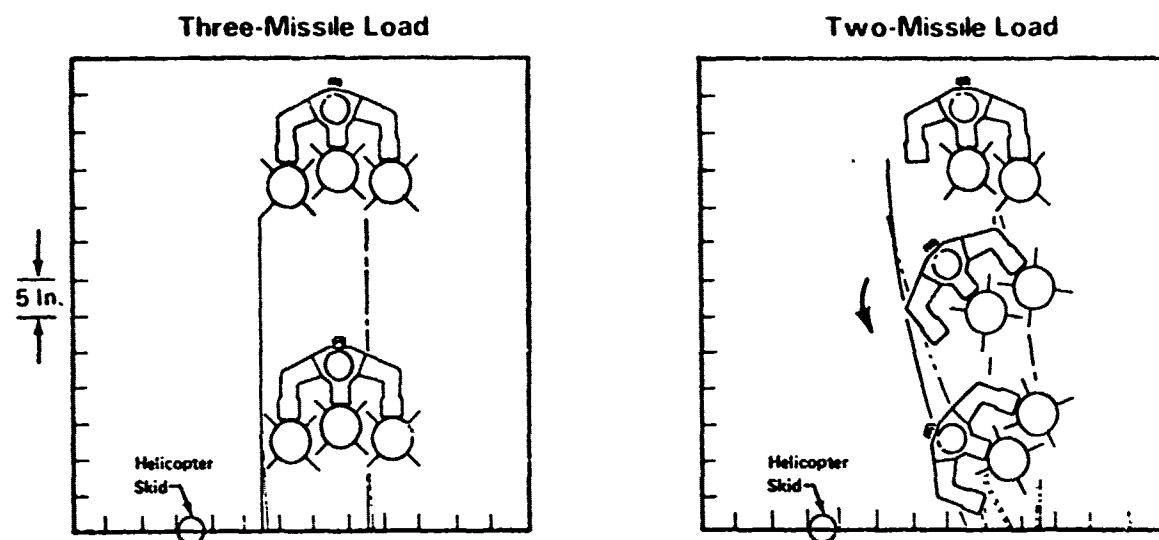
Figure 7. Outboard Launcher Jettison - Typical Trajectories

Single-Missile Load

Two-Missile Load

5 In.

Helicopter
Skid

Helicopter
Skid
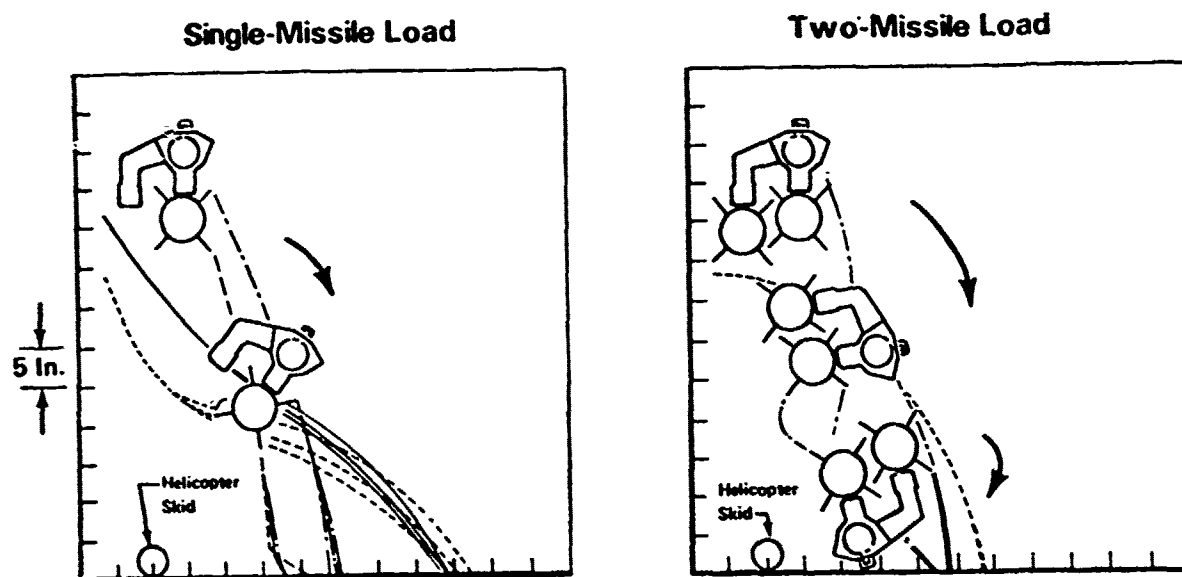
Figure 8. Inboard Launcher Jettison - Typical Trajectories

265
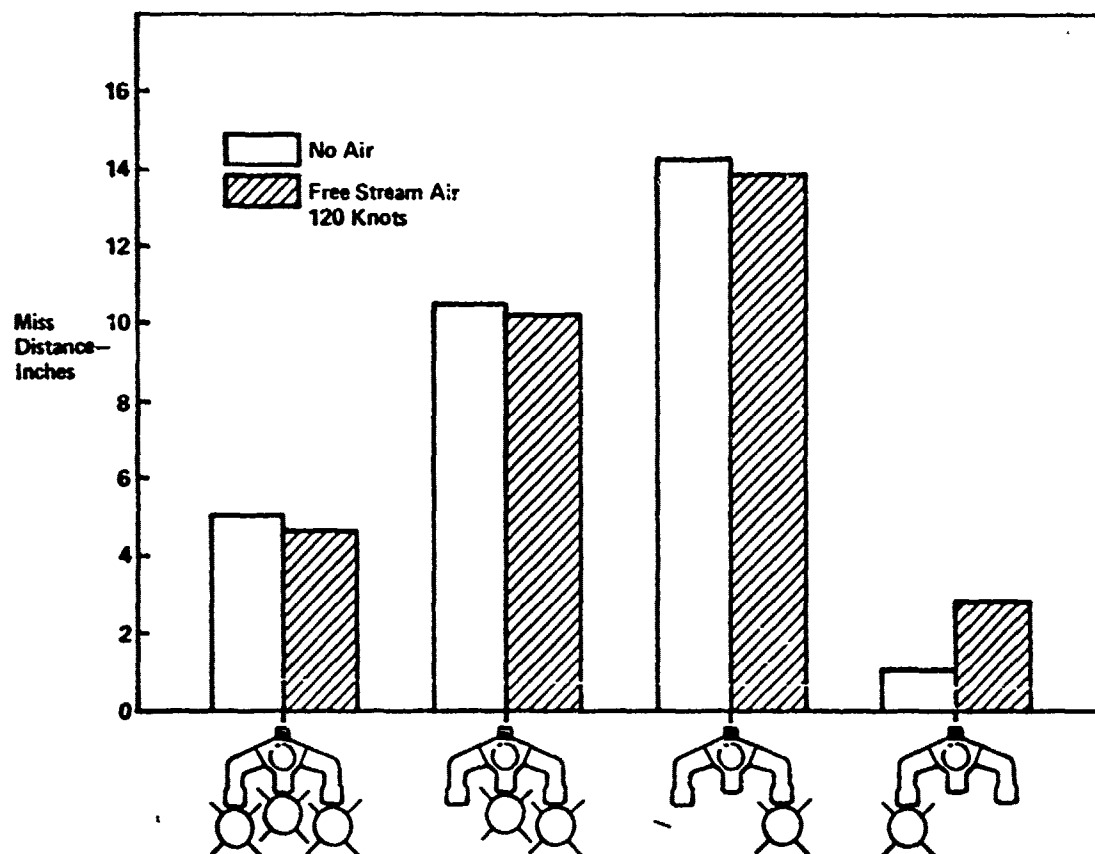
Figure 9. Outboard Launcher - Windward Side
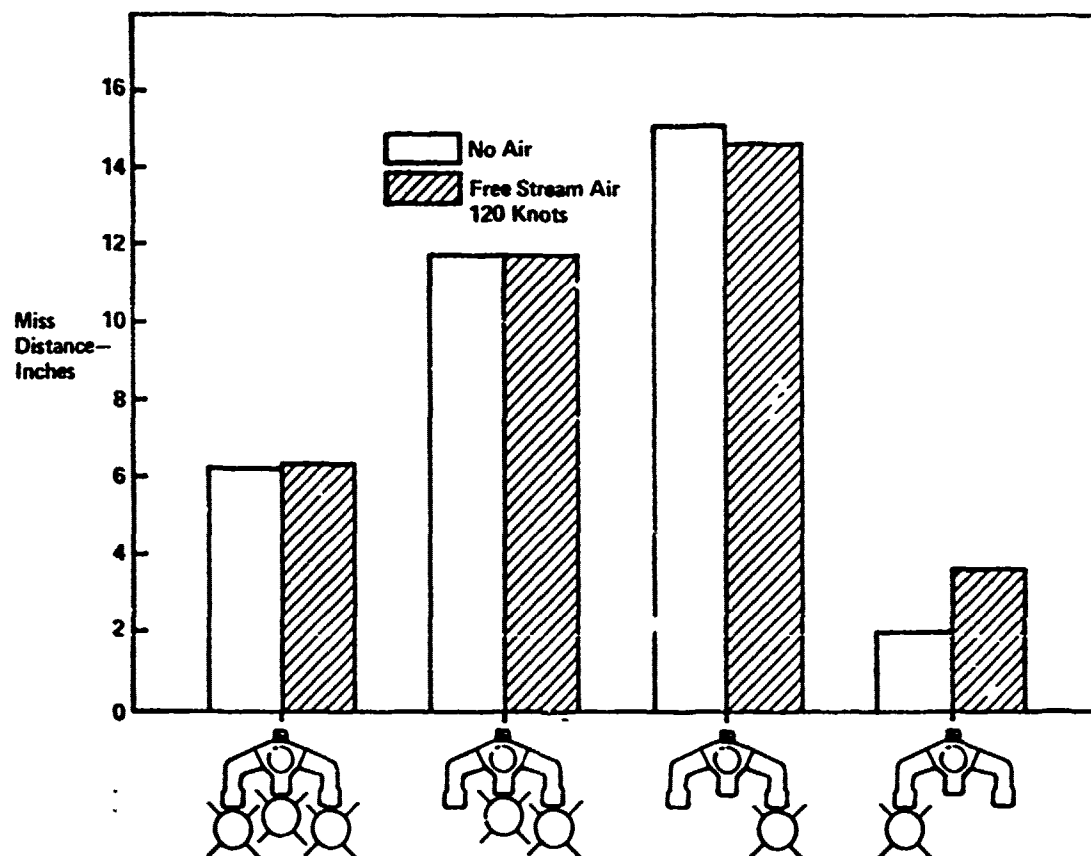
Figure 10. Outboard Launcher - Leeward Side
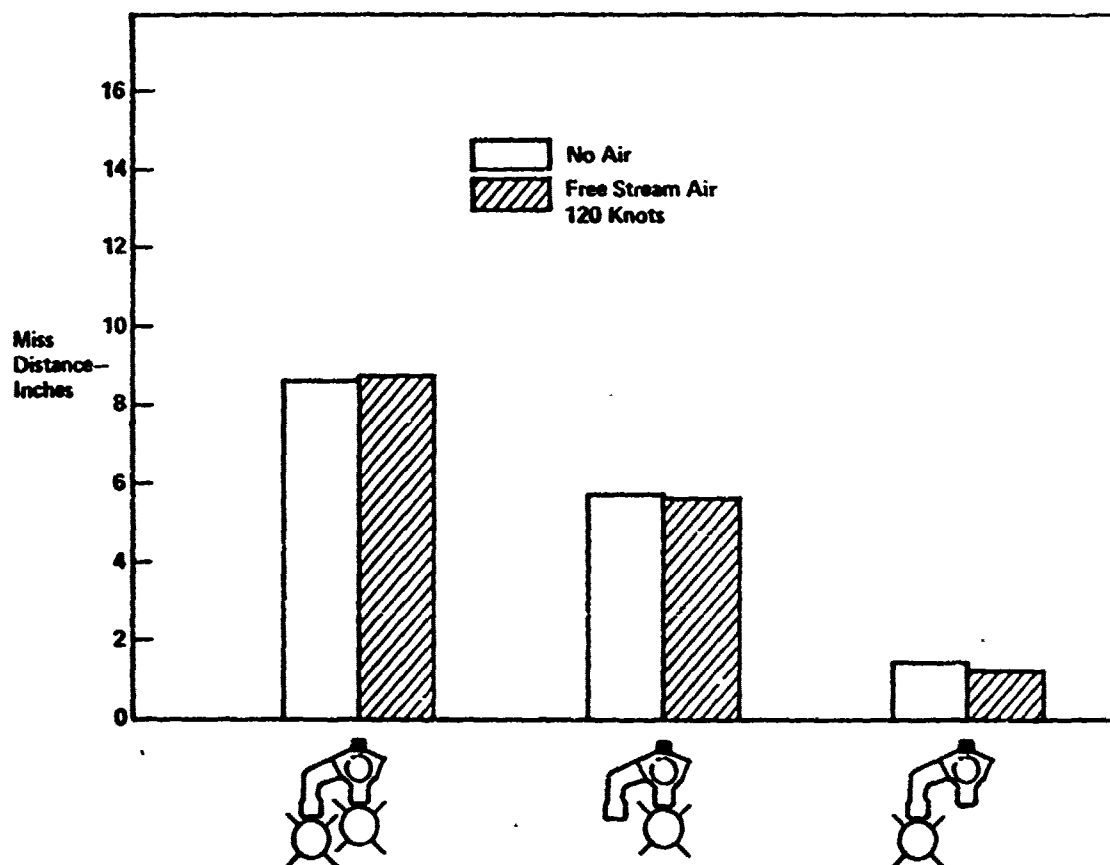
Figure 11.   Inboard Launcher - Windward Side
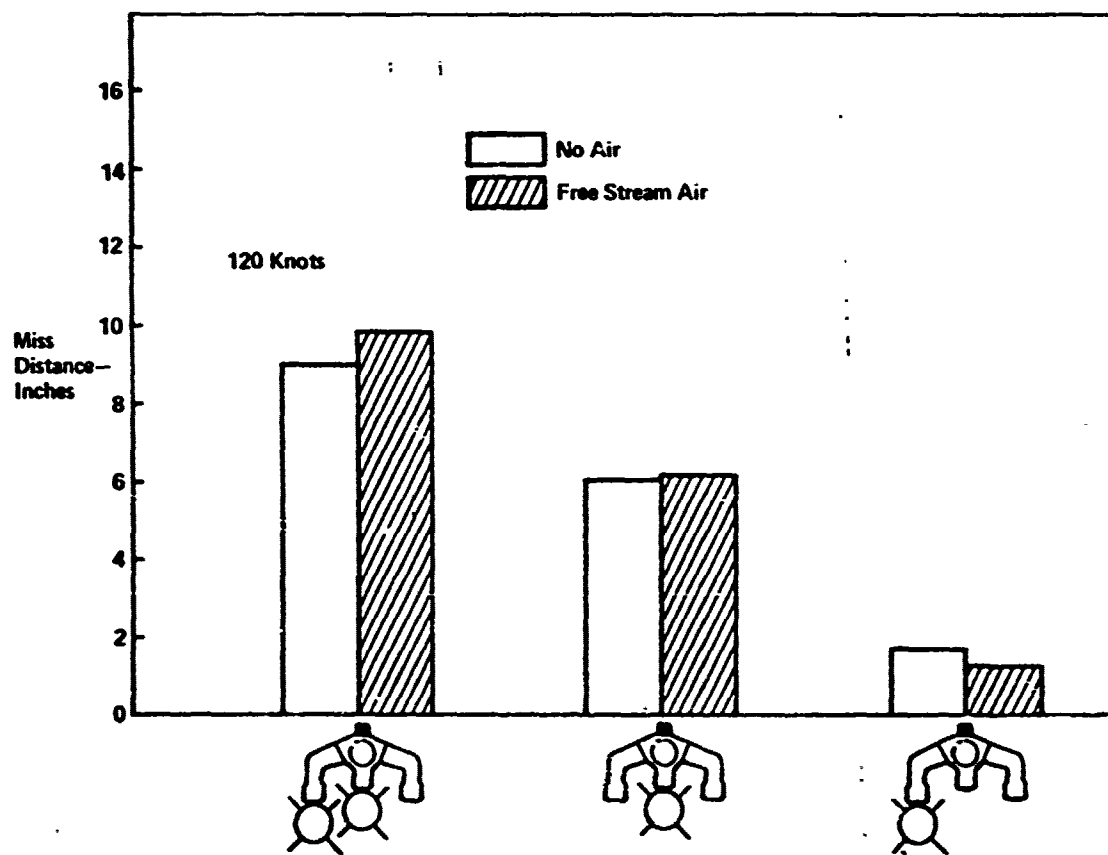
Figure 12. Inboard Launcher - Leeward Side

case involves a single inboard missile. For the leeward side, the air tends to increase clearance except for the case of a single outboard missile. Figures 13 and 14 show the incremental miss distances for the configurations analyzed. Figure 15 shows the effects of variable air-speed on miss distance for configuration number 2.
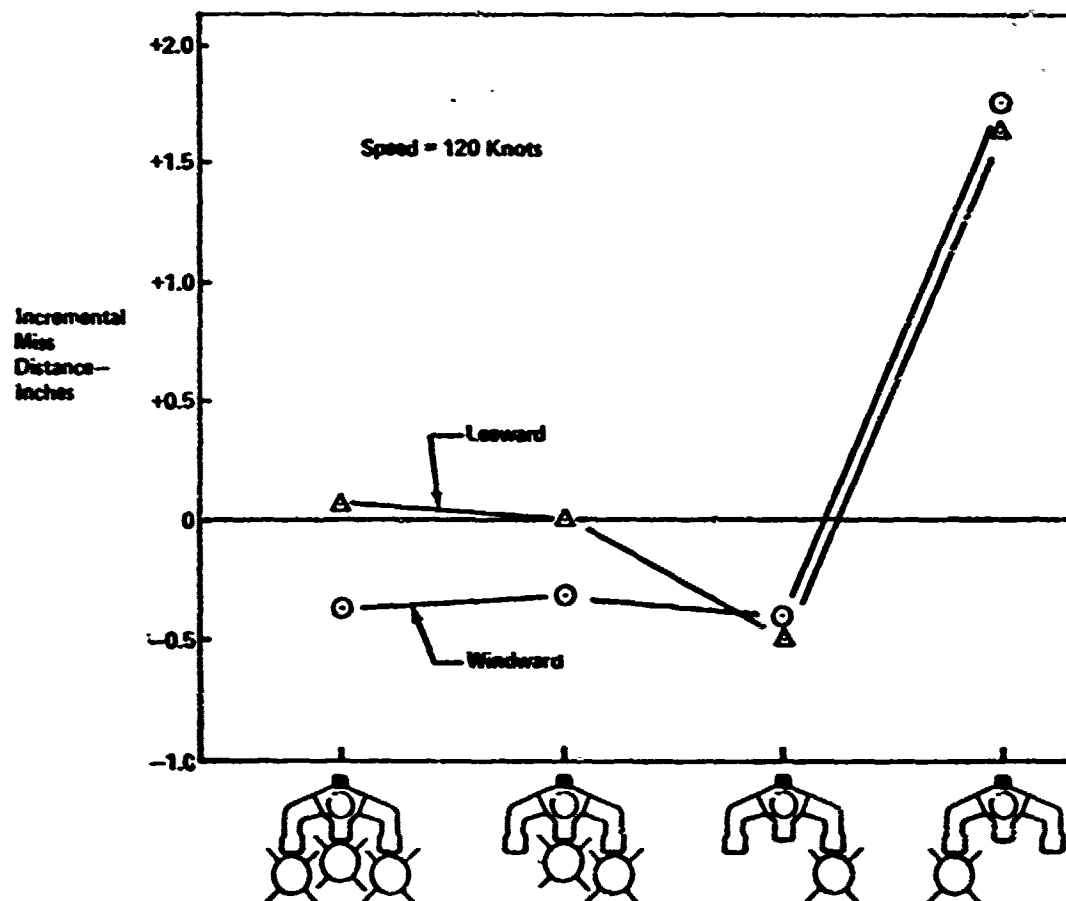
Figure 13. Air Effect - Outboard Launcher
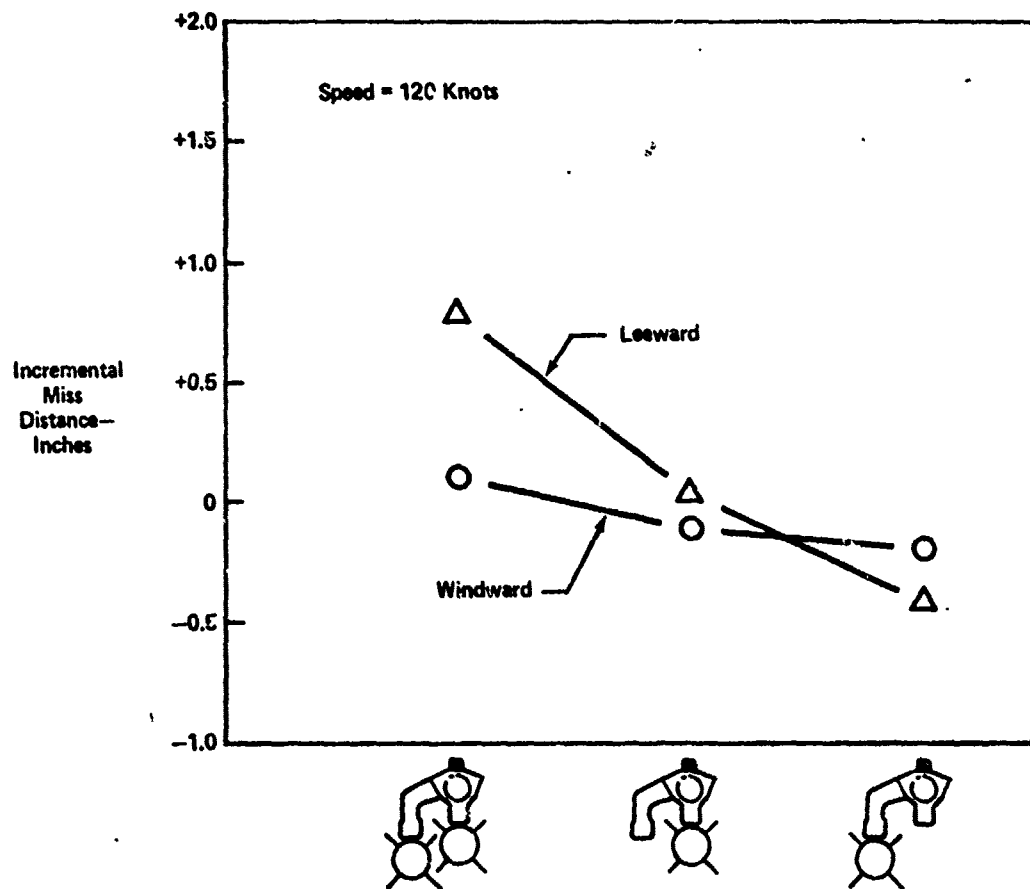
Figure 14. Air Effect - Inboard Launcher
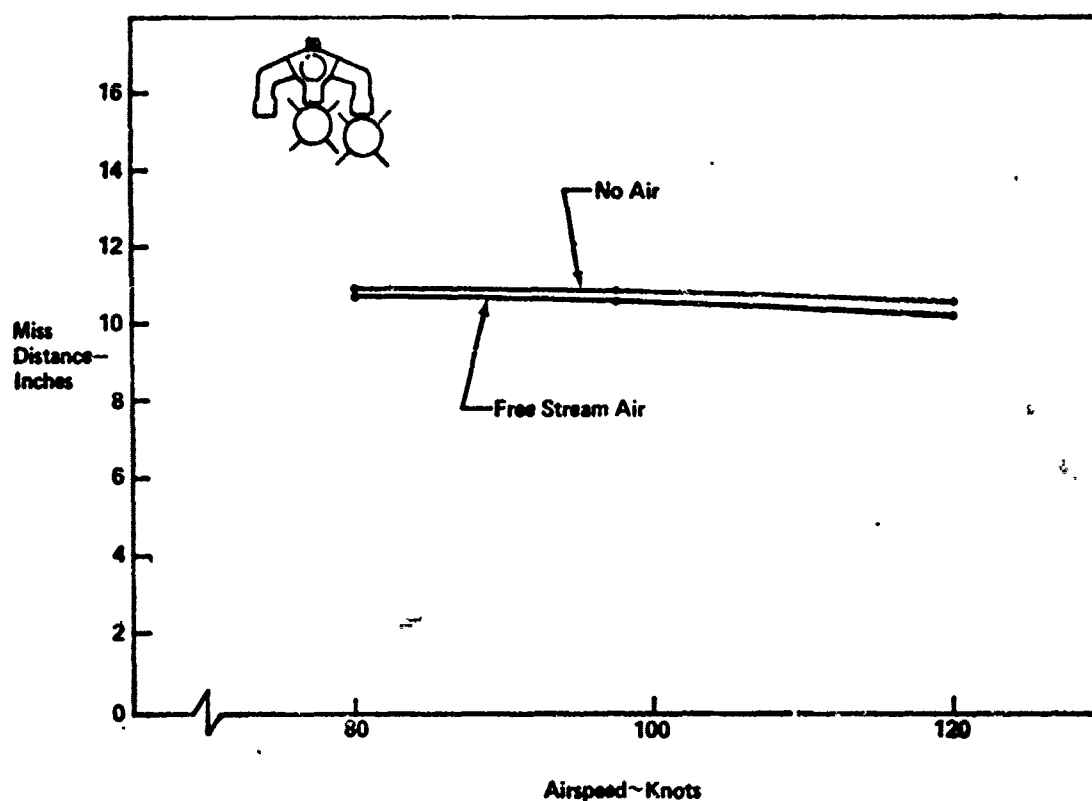
Figure 15. Outboard Launcher - Windward Side

CONCLUSIONS

The motions of the jettisoned missile-launcher configurations are strongly dependent on the location of the system cg with regard to the line of the ejector force.

In summary, it appears that aerodynamic effects can be ignored for early "proof of design" jettison analyses of dense stores. Further, the use of a "free stream" aerodynamic representation provides conservative results.

For final analyses of a particular store configuration, it may be useful or even necessary to include the best aerodynamic data available, depending on the particular store configuration, the predicted clearances and the consequences of store impact on the helicopter skids.

VA 210-220 SERIES, LOW SPEED INDICATOR, 1 TO 150K AND
AIR SPEED/DIRECTIONAL SENSOR, 2 AXIS, VT 1003

R. Colton and R. Joy

Paper Not Available for Presentation

273

CHRONOLOGICAL BIBLIOGRAPHY ON ROTOR DOWNWASH: 1922 - 1975

Air Warfare Division
Army Materiel Systems Analysis Activity
Aberdeen Proving Ground, Maryland 21005

10 July 1975

274

CHRONOLOGICAL BIBLIOGRAPHY ON ROTOR DOWNWASH

1922

1. "Notes on the Vortex Theory of Airscrews" (U), ARC Report and Memorandum No. 869, H. Glauert, Aeronautical Research Council, London, England, December 1922 (Unclassified)

1925

2. "An Investigation of the Air-Flow Pattern in the Wake of an Aerofoil of Finite Span" (U), A. Fage and L. F. G. Simmon, Philosophical Transactions of the Royal Society of London, Vol. 225, No. A632, pp. 303-330, 1925 (Unclassified)

1926

3. "An Extension of the Vortex Theory of Airscrews with Applications to Airscrews of Small Pitch, Including Experimental Results" (U), ARC Report and Memorandum No. 1014, C. N. H. Lock, H. Bateman and H. C. H. Townsend, Aeronautical Research Council, London, England, 1926 (Unclassified)

4. "Further Development of Autogiro Theory" (U), ARC Report and Memorandum No. 1014, C. N. H. Lock, Aeronautical Research Council, London, England, 1926 (Unclassified)

5. "The Analysis of Experimental Results in the Windmill Brake and Vortex Ring States of an Airscrew" (U), ARC Report and Memorandum No. 1026, H. Glauert, Aeronautical Research Council, London, England, 1926 (Unclassified)

6. "On the Contraction of the Slipstream of an Airscrew" (U), ARC Report and Memorandum No. 1067, H. Glauert, Aeronautical Research Council, London, England, 1926 (Unclassified)

7. "A General Theory of the Autogiro" (U), ARC Report and Memorandum No. 1111, H. Glauert, Aeronautical Research Council, London, England, 1926 (Unclassified)

1929

8. "On the Vortex Theory of Screw Propellers" (U), S. Goldstein, Proceedings of the Royal Society (A), Vol. 123, pp. 440, 1929 (Unclassified)

1931

9. "The Application of Goldstein's Theory to the Practical Design of Airscrews" (U), Aeronautical Research Council R&M No. 1377, C. N. H. Lock, 1931 (Unclassified)

1934

10. "Applied Hydro and Aeromechanics" (U), O. G. Tietjens, McGraw-Hill Book Company, Inc., New York, 1934 (Unclassified)

1935

11. "Rolling Up of the Surface of Discontinuity Behind an Aerofoil of Finite Span" (U), ARC Report and Memorandum No. 1692, F. L. Westwater, Aeronautical Research Council, London, England, August 1935 (Unclassified)

12. "Full-Scale Wind-Tunnel Tests of a PCA-2 Autogiro Rotor" (U), NACA Report No. 515, J. B. Wheatley and M. J. Hood, National Advisory Committee for Aeronautics, 1935 (Unclassified)

13. "Airplane Propellers" (U), H. Glauert, Vol. IV, Div. L. Aerodynamic Theory, edited by W. F. Durand, Springer, Berlin, 1935 (Unclassified)

1937

14. "The Ground Effect on Lifting Propellers" (U), NACA Technical Note No. 836, A. Betz, National Advisory Committee for Aeronautics, 1937 (Unclassified)

1939

15. "Applied Aerodynamics" (U), L. Bairstow, Second Edition, Longmans, London, 1939 (Unclassified)

1941

16. "A Simplified Theoretical Model of Determining the Characteristics of a Lifting Rotor in Forward Flight" (U), NACA Report No. 716, F. J. Bailey, Jr., National Advisory Committee for Aeronautics, 1941 (Unclassified)

17. "Analysis of Ground Effect on the Lifting Airscrew" (U), NACA Technical Note No. 835, M. Knight and R. A. Hefner, National Advisory Committee for Aeronautics, 1941 (Unclassified)

1943

18. "The Elements of Aerofoil and Airscrew Theory" (U), H. Glauert, MacMillan Company, New York, 1943 (Unclassified)

1944

19. "Round Jets in a General Stream" (U), ARC Report and Memorandum No. 1974, H. B. Squire and J. Trouncer, Aeronautical Research Council, London, England, January 1944 (Unclassified)

20. "Periodic Aerodynamic Forces on Rotors in Forward Flight" (U), C. Seibel, Journal of Aeronautical Sciences, Vol. 11, No. 4, pp 339-342, October 1944 (Unclassified)

21. "Induced Velocity in Level Flight (YR-4A)" (U), SER Report No. 74, Sikorsky Aircraft Company, Stratford, Connecticut, 22 December 1944 (Unclassified)

1945

22. "Evaluation of the Induced-Velocity Field of an Idealized Helicopter Rotor" (U), NACA Report No. WR L-126, (formerly NACA Report No. ARR L5E10), R. P. Coleman, A. M. Feingold and C.W. Stempin, National Advisory Committee for Aeronautics, 1945 (Unclassified)

23. "Hydrodynamics" (U), H. Lamb, Sixth Edition, Dover Publications, New York, 1945 (Unclassified)

1946

24. "A Machine Method for Calculating Helicopter Rotor Performance Including Stall and Drag-Divergence Effects" (U), UACRL Report No. R-0725-3, N. Kemp. Research Laboratories, United Aircraft Corporation, East Hartford, Connecticut, 2 January 1946 (Unclassified)

25. "Helicopter Main Rotor Blades" (U), CAL Report No. BB-427-S-1, G. B. Martin, Cornell Aeronautical Laboratory, Buffalo, New York, 2 May 1946 (Unclassified)

26. "A Preliminary Design Study of Main Rotor Blades for a Variable Stiffness Flight Test Program" (U), CAL Report No. BB-427-S-2, H. Hirsch, J. Kline and R. Mertens, Cornell Aeronautical Laboratory, Buffalo, New York, 16 September 1946 (Unclassified)

27. "The Performance of Model Propellers, Part I, Static Conditions" (U), LSARA Report No. 40, P. R. Payne and N. K. Walker, 1946 (Unclassified)

1947

28. "Structural Analysis of Fiberglass Main Rotor Blade for the R-5 Helicopter" (U), CAL Report No. BB-472-S-3, J. Kline, Cornell Aeronautical Laboratory, Buffalo, New York, 18 February 1947 (Unclassified)

29. "An Investigation in Flight of the Induced Velocity Distribution Under a Helicopter Rotor when Hovering" (U), RAE Report No. Aero-2212, P. Brotherhood, Royal Aircraft Establishment, Farnborough, England, June 1947 (Unclassified)

30. "Note on the Characteristic Curve for an Airscrew or Helicopter" (U), ARC Report and Memorandum No. 2673, C. N. H. Lock, Aeronautical Research Council, London, England, June 1947 (Unclassified)

31. "YR-6A Helicopter Vibration Absorber and Vibration Isolator-Flight Test Survey" (U), CAL Report No. SB-429-F-1, H. Weichsel, Jr., Cornell Aeronautical Laboratory, Buffalo, New York, August 1947 (Unclassified)

32. "Rotor Systems and Control Problems in the Helicopter" (U), R. Hafner, World Aeronautical Engineering Conference, London, England, 5 September 1947 (Unclassified)

33. "Fabrication Procedure for Fiberglass Main Rotor Blades for the R-5 Helicopter" (U), CAL Report No. BB-427-S-4, H. Hirsch and J. Mertens, Cornell Aeronautical Laboratory, Buffalo, New York, 17 September 1947 (Unclassified)

34. "R-5 Helicopter Variable Stiffness Blade Program Instrumentation and Shakedown Flight Proposal" (U), CAL Report No. BB-427-S-5, H. Weichsel, Jr., Cornell Aeronautical Laboratory, Buffalo, New York, 18 September 1947 (Unclassified)

35. "Ground Effect on the Lifting Rotor"(U), RAE Technical Note No. Aero-1903, J. Zbrozeck, Royal Aircraft Establishment, Farnborough, England, 1947 (Unclassified)

36. "An Experimental Investigation of the Flow through a Helicopter Rotor in Forward Flight" (U), ARC Report and Memorandum Report No. 2734, P. Brotherhood and W. Stewart, Aeronautical Research Council, London, England, 1947 (Unclassified)

1948

37. "Structural Test of a Main Rotor Blade for the R-5 Helicopter, Blade Stiffness" (U), CAL Report No. BB-427-S-6, J. E. Carpenter and J. R. Mertens, Cornell Aeronautical Laboratory, Buffalo, New York, 23 January 1948 (Unclassified)

38. "Calculations of the Induced Velocity Field of a Rotor" (U), RAE Report No. Aero-2247, K. W. Mangler, Royal Aircraft Establishment, Farnborough, England, February 1948 (Unclassified)

39. "Fourier Coefficients for Downwash at a Helicopter Rotor" (U), RAE Technical Note No. Aero-1958, K. W. Mangler, Royal Aircraft Establishment, Farnborough, England, May 1948 (Unclassified)

40. "Downwash Measurements Behind a 12-Foot Diameter Helicopter Rotor in the 24-Foot Wind Tunnel" (U), ARC Report and Memorandum No. 2810, R. A. Fail and R. C. W. Eyre, Aeronautical Research Council, London, England, 1948 (Unclassified)

41. "Effect of Wind Velocity on Performance of Helicopter Rotors as Investigated with the Langley Helicopter Apparatus" (U), NACA Technical Note No. 1698, P. J. Carpenter, National Advisory Committee for Aeronautics, 1948 (Unclassified)

42. "Flight Testing of Helicopters" (U), W. Stewart, Journal of the Royal Aeronautical Society, Volume 52, No. 449, 1948 (Unclassified)

43. "Rotor Systems and Control Problems in the Helicopter" (U), R. Hafner, edited by J. L. Pritchard and J. Bradbrooke, Journal of the Royal Aeronautical Society, pp. 579-632, London, England, 1948 (Unclassified)

44. "Theoretical Aerodynamics" (U), W. R. Sears, Part I, Edwards Brothers, Inc., Ann Arbor, Michigan, 1948 (Unclassified)

45. "Theory of Propellers" (U), T. Theodorsen, McGraw Hill, New York, 1948 (Unclassified)

1949

46. "Helicopter Flight Test Technique, Variable Blade Stiffness Program" (U), H. Weichsel, Jr., Presented at the 5th Annual Forum of the American Helicopter Society, 12-13 May 1949 (Unclassified)

47. "A Theory of Airflow through Rotors and Its Application to some Helicopter Problems" (U), J. M. Drees, Journal of the Helicopter Association of Great Britain, Vol. 3, No. 2, pp. 79-104, July, August and September 1949 (Unclassified)

48. "An Experimental Investigation of the Flow through a Helicopter Rotor in Forward Flight" (U), ARC Report and Memorandum No. 2734, P. Brotherhood and W. Stewart, Aeronautical Research Council, London, England, September 1949 (Unclassified)

49. "Airflow through Helicopter Rotors in Vertical Flight" (U), No. V 1535, J. M. Drees, L. R. Lucassen and W. P. Hendal, Versl. Nat. Luchtv. Lab., Amsterdam, 1949 (Unclassified)

50. "Flow through Helicopter Rotor in Vertical Descent" (U), Report and Memorandum Report No. 273J, P. Brotherhood, Aeronautical Research Council, London, England, 1949 (Unclassified)

51. "Loss of Static Thrust Due to a Fixed Surface under a Helicopter Rotor" (U), RAE Technical Note No. Aero-2008, R. A. Fail and R. C. Eyre, Royal Aircraft Establishment, Farnborough, England, 1949 (Unclassified)

1950

52. "The Rolling Up of the Trailing Vortex Sheet and Its Effect on the Downwash Behind Wings" (U), J. R. Spreiter and A. H. Sacks. Aerodynamics Session, Eighteenth Annual Meeting, I.A.S., New York, January 23-26, 1950 (Unclassified)

53. "The Field of Flow through a Helicopter Rotor Obtained from Wind Tunnel Smoke Tests" (U), Report No. A1205, J. M. Drees and W. P. Hendal, Versl. Nat. Luchtvlab., Amsterdam, February 1950 (Unclassified)

54. "A Balsa-Dust Technique for Air-Flow Visualization and Its Application to Flow through Model Helicopter Rotors in Static Thrust" (U), NACA Technical Note No. 2220, M. K. Taylor, National Advisory Committee for Aeronautics, November 1950 (Unclassified)

55. "Hovering and Low-Speed Performance and Control Characteristics of an Aero-Dynamic-Servocontrolled Helicopter Rotor System as Determined on the Langley Helicopter Tower" (U), NACA Technical Note No. 2086, P. J. Carpenter and R. S. Paulnock, National Advisory Committee for Aeronautics, 1950 (Unclassified)

56. "The Field of Flow through a Helicopter Rotor Obtained from Wind Tunnel
Smoke Tests" (U), No. V 1205, J. M. Drees and W. P. Hendal, Versl. Nat.
Luchtv. Lab., Amsterdam, 1950 (Unclassified)

1951

57. "The Rolling-Up of the Trailing Vortex Sheet and Its Effects on the Down-
wash Behind Wings" (U), J. R. Spreiter and A. H. Sacks, Journal of
Aeronautical Science, Vol. 18, No. 1, January 1951 (Unclassified)

58. "Vibration Measurements of a Sikorsky H-5 Fuselage with CAL Fiberglass
Blades" (U), CAL Report No. BB-427-S-11, E. A. Kidd, Cornell Aeronautical
Laboratory, Buffalo, New York, 9 February 1951 (Unclassified)

59. "H-5 Variable Stiffness Blade Program, Instrumentation and Shakedown
Flight Phase" (U), CAL Summary Report No. BB-427-S-9, H. Hirsch, E. Guske,
and H. Weichsel, Jr. (edited by E. A. Kidd), Cornell Aeronautical
Laboratory, Buffalo, New York, 15 April 1951 (Unclassified)

60. "Airflow Patterns in the Neighborhood of Helicopter Rotors" (U), J. M.
Drees and W. P. Hendal, Aircraft Engineering, Vol. 23, No. 266, pp 107-111,
April 1951 (Unclassified)

61. "Desirable Longitudinal Flying Qualities for Helicopters and Means to
Achieve Them" (U), F. B. Gustafson, Aeronautical Engineering Review,
Vol. 10, No. 6, pp. 27-33, June 1951 (Unclassified)

62. "Helicopter Behaviour in the Vortex Ring Conditions" (U), Current Papers
No. 99, W. Stewart, Aeronautical Research Council, London, England,
November 1951 (Unclassified)

63. "H-5 Variable Stiffness Blade Program - an Experimental Investigation.
Part I - Harmonic Reduction of Measured Blade Beam Bending Moment Data"
(U), CAL Report No. BB-427-S, (AF Technical Report No. 6329 Part 1),
H. Hirsch and J. Kline, Cornell Aeronautical Laboratory, Buffalo, New
York, December 1951 (Unclassified)

64. "Dynamic Effects in Rotor Blade Bending" (U), CAL Report BB-427-S-10,
A. H. Flax and L. Goland, Cornell Aeronautical Laboratory, Buffalo, New
York, December 1951 (Unclassified)

65. "Dynamic Effects in Rotor Blade Bending" (U), A. H. Flax and L. Goland,
Journal of Aeronautical Sciences, Vol. 18, No. 12, December 1951
(Unclassified)

66. "The Normal Component of the Induced Velocity Near a Vortex Ring and Its
Application to Lifting Rotor Problems" (U), J. H. DeLeeuw, Master's Thesis,
Daniel Guggenheim School of Aeronautics, Georgia Institute of Technology,
Atlanta, Georgia, December 1951 (Unclassified)

67. "Full-Scale-Tunnel Investigation of the Static-Thrust Performance of a Coaxial Helicopter Rotor" (U), NACA Technical Note No. 2318, R. D. Harrington, National Advisory Committee for Aeronautics, 1951 (Unclassified)

68. "Empirical Relation between Induced Velocity, Thrust, and Rate of Descent of a Helicopter Rotor as Determined by Wind-Tunnel Tests on Four Model Rotors" (U), NACA Technical Note No. 2474, W. Castles, Jr., and R. B. Gray; National Advisory Committee for Aeronautics, 1951 (Unclassified)

1952

69. "H-5 Variable Stiffness Blade Program - an Experimental Investigation. Part II - Blade Beam Bending Moment Envelopes" (U), CAL Report No. BB-427-S (AF Technical Report No. 6329, Part 2), H. Hirsch and J. Kline, Cornell Aeronautical Laboratory, Buffalo, New York, January 1952 (Unclassified)

70. "H-5 Variable Stiffness Blade Program - an Experimental Investigation Part III - Evaluation of Rotor Blade Resonant Bending Efforts" (U), CAL Report No. BB-427-S, (AF Technical Report No. 6329, Part 3), H. Hirsch and J. Kline, Cornell Aeronautical Laboratory, Buffalo, New York, January 1952 (Unclassified)

71. "The Contribution of Higher Mode Resonance to Helicopter Rotor Blade Bending" (U), H. Hirsch, Presented at Institute for Aeronautical Sciences Meeting, January 1952 (Unclassified)

72. "H-5 Variable Stiffness Blade Program - an Experimental Investigation. Part IV - Harmonic Reduction of Measured Blade Motion and Control Force Data" (U), CAL Report No. BB-127-S, (AF Technical Report No. 6329, Part 4), J. Kline, Cornell Aeronautical Laboratory, Buffalo, New York, April 1952

73. "The Low Speed Performance of a Helicopter" (U), Current Papers No. 122, A.L. Oliver, Aeronautical Research Council, London, England, May 1952 (Unclassified)

74. "H-5 Variable Stiffness Blade Program - an Experimental Investigation. Part V - Evaluation of Blade Beam Bending Data Measured by Three Helicopter Manufacturers" (U), CAL Report No. BB-427-S, (AF Technical Report No. 6329, Part 5), J. Kline, Cornell Aeronautical Laboratory, Buffalo, New York, June 1952 (Unclassified)

75. "An Experimental and Theoretical Study of the Low Frequency Flapping - Pitching Flutter of a Hovering Rotor Blade" (U), CAL Report No. SB-680-S-2, F. A. DuWaldt and C. Gates, Cornell Aeronautical Laboratory, Buffalo, New York, September 1952 (Unclassified)

76. "H-5 Variable Stiffness Blade Program - an Experimental Investigation. Part VI - A Tentative Empirical Criterion for the Design of Rotor Blades for Higher Mode Resonances" (U), CAL Report No. BB-427-S, (AF Technical Report No. 6329, Part 6), H. Daughaday and J. Kline, Cornell Aeronautical Laboratory, Buffalo, New York, November 1952 (Unclassified)

77. "Aerodynamics of the Helicopter" (U), A. Gessow and G. C. Myers, Jr., MacMillan Co., 1952 (Unclassified)

1953

78. "Flow about a Hovering Rotor" (U), Report R-12514-1, H. Kessler, Research Department, United Aircraft Corporation, East Hartford, Connecticut, January 1953 (Unclassified)

79. "An Approach to the Determination of Higher Harmonic Rotor Blade Stresses" (U), CAL Report No. 52, H. Daughaday and J. Kline, Proceedings Ninth Annual Forum, American Helicopter Society, Cornell Aeronautical Laboratory, Inc., Buffalo, New York, May 1953 (Unclassified)

80. "The Physics of Blown Sand and Desert Dunes" (U), R. A. Bagnold, FRS, Methuen and Company Ltd., London, July 1953 (Unclassified)

81. "Effect of a Rapid Blade-Pitch Increase on the Thrust and Induced - Velocity Response of a Full-Scale Helicopter Rotor" (U), NACA Technical Note No. 3044, P. J. Carpenter and B. Fridovich, National Advisory Committee for Aeronautics, 1953 (Unclassified)

82. "Elements of Propeller and Helicopter Aerodynamics" (U), D. O. Dommasch, Pitman Publishing Corporation, 1953 (Unclassified)

83. "The Induced Velocity Field of a Rotor" (U), ARC Report and Memorandum No. 2642, K. W. Mangler and H. B. Squire, Aeronautical Research Council, London, England, 1953 (Unclassified)

1954

84. "A Flutter Theory for a Flexible Helicopter Rotor Blade in Vertical Flight" (U), CAL Report No. SB-862-S-1, T. T. Chang, Cornell Aeronautical Laboratory, Buffalo, New York, July 1954 (Unclassified)

85. "An Investigation of the Effect of Virtual Delta-Three Angle and Blade Flexibility on Rotor Blade Flutter" (U), CAL Report No. SB-862-S-2, H. Daughaday and J. Kline, Cornell Aeronautical Laboratory, Buffalo, New York, August 1954 (Unclassified)

86. "Semi-Monthly Progress Reports on XHR2S-1 Helicopter, SER Report No. 3012, Sikorsky Helicopter Corporation, Stratford, Connecticut, 30 September 1954 (Unclassified)

87. "Aspects of Internal Flow System Design for Helicopter Propulsive Units" (U), NACA Report No. RM L54F29, J. R. Henry, National Advisory Committee for Aeronautics, 1954 (Unclassified)

88. "Preliminary Results from Flow-Field Measurements around Single and Tandem Rotors in the Langley Full-Scale Tunnel" (U), H. H. Heyson. Langley Aeronautical Laboratory, Langley Field, Virginia, 1954 (Unclassified)

89. "Helicopter Research" (U), F. O'Hara, Journal of the Helicopter Association of Great Britain, Vol. 7, No. 4, 1954 (Unclassified)

90. "The Normal Component of the Induced Velocity in the Vicinity of a Lifting Rotor and some Examples of Its Application" (U), NACA Report No. 1184, (Supersedes NACA Technical Note No. 2912, 1953), W. Castles, Jr. and J. H. DeLeeuw, National Advisory Committee, 1954 (Unclassified)

91. "Charts for Estimating Tail-Rotor Contribution to Helicopter Directional Stability and Control in Low-Speed Flight" (U), NACA Technical Note No. 3156, K. B. Amer and A. Gessow, National Advisory Committee for Aeronautics, Langley Aeronautical Laboratory, Langley Field, Virginia, 1954 (Unclassified)

92. "Wind Tunnel Studies of the Performance of Multi-Rotor Configurations" (U), NACA Technical Note No. 3236, R. C. Dingeldin, National Advisory Committee for Aeronautics. 1954 (Unclassified)

93. "Review of Information on Induced Flow of a Lifting Rotor" (U), NACA Technical Note No. 3238, A. Gessow, National Advisory Committee for Aeronautics, Langley Aeronautical Laboratory, Langley Field, Virginia, 1954 (Unclassified)

1955

94. "Wind Tunnel Corrections for a Helicopter Rotor in Forward Flight" (U), UACEL Report No. M-00554-4, W. J. Wells, United Aircraft Corporation, East Hartford, Connecticut, 12 September 1955 (Unclassified)

95. "The Effect of Blade Root Properties on the Natural Mode Shapes, Bending Moments and Shears of a Model Helicopter Rotor Blade" (U), CAL Report No. SB-862-S-3, H. Daughaday and F. DuWaidt, Cornell Aeronautical Laboratory, Buffalo, New York, September 1955 (Unclassified)

96. "A Two-Dimensional Approximation to the Unsteady Aerodynamics of Rotary Wings" (U), CAL Report No. 75, R. G. Loewy, (IAS Preprint No. 605), Cornell Aeronautical Laboratory, Buffalo, New York, October 1955 (Unclassified)

97. "Aeroelasticity" (U), A. Bisplinghoff and Halfman, Addison-Wesley Publishing Company, Inc., 1955 (Unclassified)

98. "Determination of Inflow Distributions from Experimental Aerodynamic Loading and Blade-Motion Data on a Model Helicopter Rotor in Hovering and Forward Flight" (U), NACA Technical Note No. 3492, G. Falabella, Jr., and J. R. Meyer, Jr., National Advisory Committee for Aeronautics, 1955 (Unclassified)

99. "The Effect of the Ground on a Helicopter Rotor in Forward Flight" (U), ARC Report and Memorandum No. 3021, I. C. Cheeseman and W. E. Bennett, Aeronautical Research Council, London, England, 1955 (Unclassified)

100. "The Mechanics of Flow on Annular Wings" (U), W. Seibold, Interavis Vol. 10, No. 1, 1955 (Unclassified)

1956

101. "The Effect of Blade Root Properties on the Natural Mode Shapes, Bending Moments and Shears of a Model Helicopter Rotor Blade" (U), H. Daughaday and F. DuWaldt, Journal of the American Helicopter Society, Vol. 1, No. 2, April 1956 (Unclassified)

102. "Static-Thrust Measurements of the Aerodynamic Loading on a Helicopter Rotor Blade." (U), NACA Technical Note No. 3688, J. P. Rabbott, Jr., National Advisory Committee for Aeronautics, July 1956 (Unclassified)

103. "Investigation of Helicopter Rotor Flutter and Load Amplification Problems" (U), CAL Report No. SB-862-S-4, H. Daughaday, F. DuWaldt, and C. Gates, Cornell Aeronautical Laboratory, Buffalo, New York, August 1956 (Unclassified)

104. "An Aerodynamic Analysis of a Single-Bladed Rotor in Hovering and Low-Speed Forward Flight as Determined from Smoke Studies of the Vorticity Distribution in the Wake" (U), PU/AED Report No. 356, R. B. Gray, Aeronautical Engineering Department, Princeton University, Princeton, New Jersey, September 1956 (Unclassified)

105. "Experimental Investigation of the Aerodynamic Loading on a Helicopter Rotor Blade in Forward Flight" (U), NACA Report No. RM-L56I07, J. P. Rabbott, Jr., and G. B. Churchill, National Advisory Committee for Aeronautics, 25 October 1956 (Unclassified)

106. "The Wall Jet" (U), M. B. Glauert, Journal of Fluid Mechanics, Vol. 1, Pt. 6, December 1956 (Unclassified)

107. "Amount of Dust Recirculated by a Hovering Helicopter" (U), Kaman Aircraft Corporation Report No. R-169, E. Watzen, Bloomfield, Connecticut, December 1956 (Unclassified)

108. "Investigation of Vertical Drag and Periodic Airloads Acting on Flat Panels in a Rotor Slipstream" (U), NACA Technical Note No. 3900, R. A. Makofski and G. F. Menkick, National Advisory Committee for Aeronautics, 1956 (Unclassified)

109. "Distribution of Normal Component of Induced Velocity in Lateral Plane of a Lifting Rotor" (U), NACA Technical Note No. 3841, W. Castles, Jr., and H. L. Durham, Jr., National Advisory Committee for Aeronautics, 1956 (Unclassified)

110. "Investigation of Helicopter Blade Flutter and Load Amplification Problems" (U), IAS Preprint No. 705, F. Duwaldt, C. Gates, and H. Daughaday, Institute for Aeronautical Sciences, Cleveland, Ohio, 31 January 1957 (Unclassified)

111. "A Two Dimensional Approximation to the Unsteady Aerodynamics of Rotary Wings" (U), R. G. Loewy, Journal of the Aeronautical Sciences, Vol. 24, No. 2, February 1957 (Unclassified)

112. "The Effect of Wing Geometry and Lower Surface Boundary Layer on the Rolled-up Tip Vortex" (U), Terence L. Grow, M.S. Thesis, The Pennsylvania State University, University Park, Pennsylvania, June 1957 (Unclassified)

113. "Investigation of Helicopter Blade Flutter and Load Amplification Problems" (U), H. Daughaday, F. DuWaldt and C. Gates, Journal of the American Helicopter Society, Vol. 2, No. 3, July 1957 (Unclassified)

114. "Theory of the Annular Nozzle in Proximity to the Ground" (U), Model Basin Aero Report No. 923, N. R. Chaplin, David W. Taylor, July 1957 (Unclassified)

115. "Approximate Solution for Streamlines about a Lifting Rotor Having Uniform Loading and Operating in Hovering or Low-Speed Vertical-Ascent Flight Conditions" (U), NACA Technical Note No. 3921, W. Castles, Jr., National Advisory Committee for Aeronautics, 1957 (Unclassified)

116. "Induced Velocities Near a Lifting Rotor with Non-Uniform Disc Loading" (U), NACA Report 1319, (Supersedes NACA Technical Note No. 3690 and 3691) H. H. Heyson and S. Katzoff, National Advisory Committee for Aeronautics, 1957 (Unclassified)

1958

117. "Induced Velocity Near a Rotor and Its Application to Helicopter Problems" (U), H. H. Heyson, Proceedings of the 14th Annual National Forum, American Helicopter Society, Inc., pp. 63-71, 16 - 19 April, 1958 (Unclassified)

118. "Review of Present Knowledge and Outline of a Research Program Pertaining to Rotor-Airframe Aerodynamic Problems" (U), Report No. 1272-90-2, R. Pruyn and D. Gebhard, Kellett Aircraft Corporation, March 1958

119. "Flow Field Measurements for a Hovering Rotor Near the Ground" (U), E. A. Fradenburgh, Presented at American Helicopter Society 5th Annual Forum, Sikorsky Aircraft Company, Stratford, Connecticut, September 1958 (Unclassified)

120. "Conversion of Blade Bending Moment Measurements to Blade Deflections" (U), SER Report No. 50053, R. Caseria and W. Marlatt, Helicopter Section, Sikorsky Aircraft Co., Stratford, Connecticut, 24 October 1958 (Unclassified)

121. "Flow Induced by a Rotor in Power-On Vertical Descent" (U), NACA Technical Note No. 4430, W. Castles, Jr., National Advisory Committee for Aeronautics, 1958 (Unclassified)

122. "Hovering Rotor Flow Patterns" (U), Research Memorandum No. 8, Research Section, Sikorsky Aircraft Company, Stratford, Connecticut, 1958 (Unclassified)

1959

123. "HU2K-1 Analysis of Main and Directional Control Rotors" (U), Report No. S-113, E. Schuett, B. Bellow and A. Berman, Kaman Aircraft Corporation, Bloomfield, Connecticut, 26 February 1959 (Unclassified)

124. "Induced Flow Near a Helicopter Rotor" (U), H. H. Heyson, Aircraft Engineering, Vol. XXXI, No. 360, pp. 4C-44, February 1959 (Unclassified)

125. "Comparison of Measured Flapwise Structural Bending Moments on a Teetering Rotor Blade with Results Calculated from the Measured Pressure Distribution" (U), NASA Memo 2-28-59L, A. P. Mayo, National Aeronautics and Space Administration, March 1959 (Unclassified)

126. "The Computed Instantaneous Velocities Induced at the Blade Axes by the Skewed Helical Vortices in the Wake of a Lifting Rotor in Forward Flight" (U), W. Castles, Jr., and H. L. Durham, Jr., Georgia Institute of Technology, Atlanta, Georgia, March 1959 (Unclassified) (AD 210 613)

127. "Experimental Downwash Velocity, Static Pressure, and Temperature Distributions in Ground Effect for a 75-Foot Jet Driven Rotor" (U), Journal of the American Helicopter Society, Vol. 4, No. 2, M. Bolonovich, April 1959 (Unclassified)

128. "The Loading of Helicopter Rotor Blades in Forward Flight" (U), RAE Report Naval 2-N-76935 No. 8, M. A. Willmer, Royal Aircraft Establishment, Farnborough, England, April 1959, (Unclassified) (AD 227 736)

129. "Investigation of Helicopter Rotor Blade Flutter and Flapwise Bending Response in Hovering" (U), WADC Technical Report No. 59-403, F. A. Duwaldt, C. A. Gates and R. A. Piziali, Wright Air Development Center, Wright Patterson Air Force Base, Dayton, Ohio, August 1959 (Unclassified)

130. "An Investigation to Determine Conditions Under Which Downwash from VTOL Aircraft will Start Surface Erosion from Various Types of Terrain" (U), NASA Technical Note No. D-56, R. E. Kuhn, National Aeronautics and Space Administration, September 1959 (Unclassified)

131. "Experimental Investigation of the Pressure Fluctuations on a Flat Plate and a Cylinder in the Slipstream of a Hovering Rotor" (U), NASA Technical Note No. D-112, J. McKee, National Aeronautics and Space Administration, September 1959 (Unclassified)

132. "An Evaluation of VTOL Aircraft Concepts" (U), P. L. Michel, Presentation to the Scientifi Institute for Aeronautics, Hamburg, Germany, 1959 (Unclassified)

133. "An Evaluation of Linearized Vortex Theory as Applied to Single and Multiple Rotors Hovering in and out of Ground Effect" (U), NASA Technical Note No. D-43, H. H. Heyson, National Aeronautics and Space Administration, 1959 (Unclassified)

134. "Charts of the Induced Velocities near a Lifting Rotor" (U), NASA Memorandum 4-15-59L, J. W. Jewel, Jr., National Aeronautics and Space Administration, 1959 (Unclassified)

135. "Helicopter Dynamics and Aerodynamics" (U), P. R. Payne, Sir Isaac Pitman and Sons, Ltd., London, 1959 (Unclassified)

136. "Normal Component of Induced Velocity for Entire Field of a Uniformly Loaded Lifting Rotor with Highly Swept Wake as Determined by Electromagnetic Analog" (U), NACA Technical Report No. R-41, (Supersedes NACA Technical Note No. 4238), W. Castles, Jr., H. L. Durham, Jr., and J. Kevorkian, National Advisory Committee for Aeronautics, Georgia Institute of Technology, Atlanta, Georgia, 1959 (Unclassified)

1960

137. "A Note on the Mean Value of Induced Velocity for a Helicopter Rotor" (U), NASA Technical Note No. D-240, H. H. Heyson, National Aeronautics and Space Administration, May 1960 (Unclassified)

138. "Investigation of the Flutter of a Model Helicopter Rotor Blade in Forward Flight" (U), WADD Technical Report No. 60-328, F. A. DuWaldt, C. A. Gates and R. A. Piziali, Wright Air Development Center, Wright Patterson Air Force Base, Dayton, Ohio, July 1960 (Unclassified)

139. "Comparison of Theoretical and Experimental Flutter Results for a Full-Scale Helicopter Rotor" (U), WADD Technical Report No. 60-692, F. A. DuWaldt and R. A. Piziali, Wright Air Development Center, Wright Patterson Air Force Base, Dayton, Ohio, July 1960 (Unclassified)

140. "Measurements of the Time-Averaged and Instantaneous Induced Velocities in the Wake of a Helicopter Rotor Hovering at High Tip Speeds" (U), NASA Technical Note No. D-393, H. H. Heyson, National Aeronautics and Space Administration, July 1960 (Unclassified)

141. "Equations for the Induced Velocities near a Lifting Rotor with Non-Uniform Azimuthwise Vorticity Distribution" (U), NASA Technical Note No. 3-394, H. H. Heyson, National Aeronautics and Space Administration, August 1960 (Unclassified)

142. "Experimental and Theoretical Study of Local Induced Velocities over a Rotor Disc for Analytical Evaluation of the Primary Loads Acting on Helicopter Rotor Blades" (U), Engineering Division Report No. DE2012, S. Tararine and M. Deleste, European Research Office, U. S. Department of the Army, Giravions Dorand Co., 15 October 1960 (Unclassified)

143. "A Review of Theoretical and Experimental Investigations of the Rotor Aerodynamic Problem" (U), Report R-217, R. G. Loewy, D. J. Smyers and R. Gabel, Vertol Division of Boeing Aircraft Corporation, Renton, Washington, October 1960 (Unclassified)

144. "VTOL Downwash Impingement Study - Surface Erosion Tests" (U), TREC Technical Report No. 60-67, A. Morse and H. Newhouse, Transportation Research Command, U.S. Army Aviation Materiel Laboratories, Fort Eustis, Virginia, October 1960 (Unclassified)

1961

145. "Tables and Charts of the Normal Component of Induced Velocity in the Lateral Plane of a Rotor with Harmonic Azimuthwise Vorticity Distribution" (U), NASA Technical Note No. 809, H. H. Heyson, National Aeronautics and Space Administration, April 1961 (Unclassified)

146. "Information and Preliminary Data on H-34 Helicopter Rotor Blade Dynamic Airloads and Motions Measured in Flight" (U), National Aeronautics and Space Administration, May 1961 (Unclassified)

147. "Information and Preliminary Data on Helicopter Rotor Blade Dynamic Airloads and Moments as Measured in Flight" (U), F. L. Thompson, NASA Letter to J. G. McHugh, U. S. Army TRECOM, National Aeronautics and Space Administration, May 1961 (Unclassified)

148. "Method for Calculating Induced Velocities at the Blades of a Slightly Inclined Propeller with Constant Circulation" (U), NASA Technical Note No. D-818, H. H. Heyson, National Aeronautics and Space Administration, May 1961 (Unclassified)

149. "An Investigation of VTOL Operational Problems Due to Downwash Effects" (U), Report No. 179T80-2, L. Goland, N. Miller and R. Pruyn, Kellett Aircraft, June 1961 (Unclassified)

150. "Comparison of Theoretical and Experimental Model Helicopter Rotor Performance in Forward Flight" (U), TCREC Technical Report 61-103, U. S. Army Transportation Research Command, Ft. Eustis, Virginia, July 1961 (Unclassified)

151. "The Influence of Two-Dimensional Stream Shear on Airfoil Maximum Lift" (U), CAL Report No. A1-1190-A-7, (TRECOM Technical Report 61-93), R. J. Vidal, J. T. Curtis and J. G. Hilton, Cornell Aeronautical Laboratory, Buffalo, New York, August 1961 (Unclassified)

152. "The Effects of Axisymmetric Shear on Airfoil Characteristics" (U), CAL Report No. A1-1190-A-8, (TRECOM Technical Report 61-138), R. J. Vidal and J. T. Curtis, Cornell Aeronautical Laboratory, Buffalo, New York, December 1961 (Unclassified)

153. "Studies of Rotorcraft Aerodynamic Problems Aimed at Reducing Parasite Drag, Rotor-Airframe Interference Effects and Improving Airframe Static Stability" (U), WADD Technical Report No. 61-124, R. R. Pruyn and N. J Miller, Wright Air Development Center, Wright Patterson Air Force Base, Dayton, Ohio, 1961 (Unclassified)

154. "Aerodynamic Processes in the Down Wash Impingement Problem" (U),
IAS Paper No. 62-36, R. J. Vidal, Institute for Aeronautical Sciences,
Cleveland, Ohio, January 1962 (Unclassified)

155. "Rotor Blade Harmonic Air Loading" (U), IAS Paper No. 62-82, R. H.
Miller, Presented at the Institute for Aeronautical Sciences' 30th
Annual Meeting, New York, New York, January 1962 (Unclassified)

156. "Experimental and Theoretical Investigation of the Flutter Characteristics
of a Model Helicopter Rotor Blade in Forward Flight" (U), CAL Report No.
BB-1504-S-1, (ASD Technical Report No. 67-712), F. A. Duwaldt and C. A.
Gates, Cornell Aeronautical Laboratory, Buffalo, New York, February
1962 (Unclassified)

157. "On the Computation of Airload Acting on Rotor Blades in Forward Flight"
(U), R. H. Miller, Journal of the American Helicopter Society, Vol. 7,
Part 2, April 1962 (Unclassified)

158. "Computation of Rotary Wing Harmonic Airloads and Comparison with
Experimental Results" (U), R. A. Piziali and F. DuWaldt, Paper presented
at the American Helicopter Society Eighteenth Annual National Forum,
Washington, D. C., 2-4 May 1962 (Unclassified)

159. "Measurement of Dynamic Airloads of a Full Scale Semi-Rigid Rotor" (U),
Bell Report No. 525-099-001, (TRECOM Technical Report No. 62-42), F.
Burpo, Bell Helicopter Corporation, Fort Worth, Texas, June 1962
(Unclassified)

160. " A Method for Computing Rotary Wing Airload Distributions in Forward
Flight" (U), CAL Report No. BB-1495-S-1, (TRECOM Technical Report
TCREC No. 62-44), R. A. Piziali, F. A. DuWaldt, Cornell Aeronautical
Laboratory, Buffalo, New York, July 1962 (Unclassified)

161. "Evaluation of SS-11 Missile Firings from HU-1 Helicopter" (U), Army
Ordnance Corps Technical Memorandum No. RH-TM-62-1, Redstone Arsenal,
Huntsville, Alabama, July 1962 (Unclassified)

162. "A Digital Analysis for Helicopter Performance and Rotor Blade Bending
Moments" (U), B. Blankenship and K. Harvey, Journal of the American
Helicopter Society, October 1962 (Unclassified)

163. "An Investigation of the Induced Velocity in the Vicinity of a
Propeller and Its Influence on Wing Lift" (U), L. Goland, Doctoral
Dissertation, University of Pennsylvania, Philadelphia, Pennsylvania,
December 1962 (Unclassified)

164. "The Normal Induced Velocity in the Vicinity of a Thrust Rotor" (U),
DCR Report No. 12, L. Goland, University of Pennsylvania Dissertation,
1962, Dynasciences Corporation, December 1962 (Unclassified)

165. "Studies of Rotocraft Aerodynamic Problems Aimed at Reducing Parasite Drag, Rotor-Airframe Interference Effects and Improving Airframe Static Estability" (U), Air Force WADD Technical Report No. 61-124, M. George, N. Miller and R. Pruyn, Wright Air Development Division, Wright Patterson Air Force Base, Dayton, Ohio, 1962 (Unclassified)

1963

166. "Introduction to Ground Effect Recirculation Theory" (U), FEDC Report No. 142-2, Frost Engineering Development Corporation, Englewood, Colorado, January 1963 (Unclassified)

167. "Preliminary Performance Measurements with a Frost Fan Model Exhausting to Ambient" (U), FEDC Report No. 142-4, Frost Engineering Development Corporation, Englewood, Colorado, February 1963, (Unclassified)

168. "A Note on the Optimum Thickness and Angle of an Annular Jet with Zero Translational Velocity" (U), FEDC Report No. 142-5, Frost Engineering Development Corporation, Englewood, Colorado, February 1963. (Unclassified)

169. "A Note on Viscous Mixing of Annular Jets" (U), FEDC Report No. 142-6, Frost Engineering Development Corporation, Englewood, Colorado, February 1963 (Unclassified)

170. "Performance Measurements with a Frost Fan Model" (U), FEDC Report No. 142-7, Frost Engineering Development Corporation, Englewood, Colorado, February 1963 (Unclassified)

171. "Aerodynamic Theory of the Hinged-Blade Frost Fan for Annular Jet Ground Effect Machines" (U), FEDC Report No. 142-8, Frost Engineering Development Corporation, Englewood, Colorado, March 1963 (Unclassified)

172. "Representation of Wakes and Propellers in Ground Effect by Ring Vortex Systems" (U), CAL Report No. BB-1665-S-1, A. Sowyrda and F. DuWaldt, Cornell Aeronautical Laboratory, Buffalo, New York, April 1963 (Unclassified)

173. "Theoretical and Experimental Studies of Impinging Uniform Jets" (U) CAL Report No. BB-1657-S-1, (TRECOM Technical Report TCREC 63-11), W. G. Brady and G. R. Ludwig, Cornell Aeronautical Laboratory, Buffalo, New York, April 1963 (Unclassified)

174. "Computer Induced Velocity, Induced Drag, and Angle of Attack Distributions for a Two-Bladed Rotor" (U), R. A. Piziali and F. A. DuWaldt, Presented at the American Helicopter Society Nineteenth Annual National Forum, Washington, D. C., 2 May 1963 (Unclassified)

175. "2.75-Inch FFAR Rocket/UH-1B, Aerial Firing" (U), Analytical Laboratory Report No. 63-AL-81, Development and Proof Services, Aberdeen Proving Ground, Maryland, 10 May 1963 (Unclassified)

176. "A Method for Determining the Fully Coupled Aeroelastic Response of Helicopter Rotor Blades" (U), E. Wood and K. Hilzinger, American Helicopter Society Forum, May 1963 (Unclassified)

177. "A Note on the Comparative Hover Performance of Annular Jet and Plenum Chamber Ground Effect Machines" (U), FEDC Report No. 142-9, Frost Engineering Development Corporation, Englewood, Colorado, May 1963 (Unclassified)

178. "An Introduction to the Theory of the Cross-Flow Fan" (U), FEDC Report No. 142-10, Frost Engineering Development Corporation, Englewood, Colorado, June 1963 (Unclassified)

179. "Experimental and Theoretical Study of Local Induced Velocities over a Rotor Disc" (U), V. S. Tararine, CAL/TRECOM Dynamic Load Problems Symposium, June 1963 (Unclassified)

180. "Rotor Airloads" (U), R. A. Piziali, H. Daughaday and F. A. DuWaldt, CAL/TRECOM Dynamic Load Problems Symposium, June 1963 (Unclassified)

181. "A Discussion of Rotor Blade Harmonic Airloading" (U), R. H. Miller, CAL/TRECOM Dynamic Load Problems Symposium, June 1963 (Unclassified)

182. "HU-1/SS-11/AN/ASW-12 Weapons Systems Flight Evaluation" (U), AFSWC Technical Documentary Report No. 62-35, D. A. Davis and G. L. Calvin, Air Force Special Weapons Center, Kirtland Air Force Base, New Mexico, June 1963 (Unclassified)

183. "Correlation of UH-2A Rotor Stall Analyses with Flight Tests" (U), Analytical Information Report No. 63-3, A. F. Smith and A. Lemnis, Kaman Aircraft Corporation, Bloomfield, Connecticut, 26 August 1963 (Unclassified)

184. "Determination of Optimized Propellers for Ground Effect Machines" (U), TRECOM Technical Report No. 63-16, N. J. Miller and M. George, U. S. Army Transportation Research Command, Fort Eustis, Virginia, August 1963 (Unclassified)

185. "A Method of Assessing the Performance of a Ground Effect Machine Configuration" (U), FEDC Report No. 142-14, Frost Engineering Development Corporation, Englewood, Colorado, August 1963 (Unclassified)

186. "Performance and Efficiency of the Frost Fan" (U), FEDC Report No. 142-13, Frost Engineering Development Corporation, Englewood, Colorado, August 1963 (Unclassified)

187. "Results of Research Laboratories Investigation of Rotor Inflow Methods and Recommendations for Future Work, (U), UAR Report No. B130, P. J. Areidiacono, United Aircraft Research Laboratories, East Hartford, Connecticut, August 1963 (Unclassified)

188. "The Influence of Leakage on the Performance of an Annular Jet GEM" (U), FEDC Report No. 197-3, Frost Engineering Development Corporation, Englewood, Colorado, September 1963 (Unclassified)

189. "The Theory of Heave Stability of an Annular Jet GEM" (U), FEDC Report No. 142-15, Frost Engineering Development Corporation, Englewood, Colorado, September 1963 (Unclassified)

190. "Observation of Some Recirculating Flow Phenomena" (U), FEDC Report No. 142-16, Frost Engineering Development Corporation, Englewood, Colorado, September 1963 (Unclassified)

191. "Generalized Rotor Performance Method" (U), SER Report No. 50355, S. W. Herdes, Sikorsky Aircraft Company, Stratford, Connecticut, September 1963 (Unclassified)

192. "VTOL Operational Problems Due to Downwash Effects" (U), L. Goland and M. George, Presented at Symposium on Environmental Effects on Aircraft and Propulsion Systems, (Dynasciences Report DCR-125) U. S. Navy NARDAC, September 1963 (Unclassified)

193. "VTOL Aircraft Downwash Impingement Design Criteria" (U), DC Report No. 725, A. A. Perlmutter and M. George, U. S. Army Contract DA 44-177-AMC-65 (T), Dynasciences Corporation, Blue Bell, Pennsylvania, 15 October 1963 (Unclassified)

194. "Unsteady Airloads on Helicopter Rotor Blades" (U), R. H. Miller, The Royal Aeronautical Society Fourth Cierva Memorial Lecture, October 1963 (Unclassified)

1964

195. "Effects of Airframe Geometry on Downwash Problems of Tandem Ducted - Propeller VTOL Aircraft" (U), KAC Report No. 179T80-6, R. R. Pruyn, Kellett Aircraft Corporation, Willow Grove, Pennsylvania, January 1964 (Unclassified)

196. "The Development of a Vortex Meter" (U), Donald M. May, M.S. Thesis, The Pennsylvania State University, University Park, Pennsylvania, June 1964 (Unclassified)

197. "Theoretical and Experimental Studies of Impingement Uniform and Nonuniform Jets" (U), TRECOM Technical Report No. 64-42, G. R. Ludwig and W. G. Brady, Transportation Research Command, U.S. Army Aviation Materiel Laboratories, Fort Eustis, Virginia, August 1964 (Unclassified)

198. "Downwash Impingement Design Criteria for VTOL Aircraft" (U), TRECOM Technical Report No. 64-48, M. M. George, A. A. Perlmutter, and L. Butler, Transporation Research Command, U.S. Army Aviation Materiel Laboratories, Fort Eustis, Virginia, August 1964 (Unclassified)

199. "Airflow near the UH-1B" (U), Thor Letter Report, R. J. Pipino, Ballistic Analysis Laboratory, The Johns Hopkins University, Baltimore, Maryland, 21 October 1964 (Unclassified)

200. "Airflow in the Vicinity of the UH-1B" (U), Thor Letter Report, R. J. Pipino, Ballistic Analysis Laboratory, The Johns Hopkins University, Baltimore, Maryland, 26 October 1964 (Unclassified)

201. "Velocity of the Airstream near the Trajectories of Rounds Fired from the UH-1B" (U), Thor Letter Report, R. J. Pipino, Ballistic Analysis Laboratory, The Johns Hopkins University, Baltimore, Maryland, 30 October 1964 (Confidential)

202. "Preliminary Analysis of Rotor-Induced Airflow near the UH-1B" (U), Thor Technical Note No. 53, R. J. Pipino, P. McInnis and T. Reeves, Ballistic Analysis Laboratory, The Johns Hopkins University, Baltimore, Maryland, October 1964 (Unclassified)

203. "Charts for Estimating Rotary Wing Performance in Hover and at High Forward Speeds" (U), NASA Contractor Report No. 114, W. H. Tanner, National Aeronautics and Space Administration, November 1964 (Unclassified)

1965

204. "Representation of Propeller Wakes by Systems of Finite Core Vortices" (U), CAL Report No. BB-1665-S-2, W. G. Brady and P. Crimi, Cornell Aeronautical Laboratory, Inc., Buffalo, New York, February 1965 (Unclassified)

205. "Theoretical Prediction of the Flow in the Wake of a Helicopter Rotor, Part 1 - Development of Theory and Results of Computations" CAL Report No. BB-1994-S-1, P. Crimi, Cornell Aeronautical Laboratory, Inc., Buffalo, New York, September 1965 (Unclassified)

206. "Theoretical Prediction of the Flow in the Wake of a Helicopter Rotor, Part 2 - Formulation and Application of the Rotor-Wake-Flow Computer Program" (U), CAL Report No. BB-1994-S-2, P. Crimi, Cornell Aeronautical Laboratory, Inc., Buffalo, New York, September 1965 (Unclassified)

207. "VTOL Periodic Aerodynamic Loadings, the Problems - What is Being Done and What Needs to be Done" (U), R. P. White Jr., Proceedings of the Symposium on Noise and Loading Actions on Helicopter V/STOL Aircraft and Ground Effect Machines, University of Southhampton, England, September 1965 (Unclassified)

208. "Final Report of Engineering Test of XM151 Warhead for 2.75-Inch FFAR Rocket" (U), DPS Report No. 1804, D. M. Potter, Development and Proof Services, Aberdeen Proving Ground, Maryland, October 1965 (Confidential)

209. "Downwash Tests of the Dual Tandem Ducted Propeller VTOL Research Aircraft Configurations to Evaluate Engine Inlets, Protection Devices and Study Aerodynamic Interference" (U), KAC Report No. 179T80-12, N. C. Curtis, Jr., Kellett Aircraft Corporation, Willow Grove, Pennsylvania, November 1965 (Unclassified)

210. "Analysis and Correlation of Helicopter Rotor Response in a Variable Inflow Environment" (U), USAAVLABS Technical Report No. 65-51, R. G. Carlson and K. D. Hilzinger, U. S. Army Aviation Materiel Laboratories, Fort Eustis, Virginia, 1965 (Unclassified)

211. "A Method for Predicting the Aerodynamic Loads and Dynamic Response of Rotor Blades" (U), USAAVLABS Technical Report No. 65-74, R. A. Piziali, U.S. Army Aviation Materiel Laboratories, Fort Eustis, Virginia, January 1966 (Unclassified)

212. "Theoretical Prediction of the Flow in the Wake of a Helicopter Rotor, Addendum - Effects due to a Fuselage in a Constant Nonuniform Flow" (U), CAL Report No. BB-1994-S-3, P. Crimi and A. K. Trenka, Cornell Aeronautical Laboratories, Buffalo, New York, April 1966 (Unclassified)

213. "Experimental Study of the Unsteady Aerodynamic of a Tandem Rotor Operating in the Vortex Ring State" (U), K. Washizu, A. Azuma, J. Koo, and T. Oka, Proceedings of the Twenty-Second Annual National Forum, American Helicopter Society, Washington, D.C., May 1966 (Unclassified)

214. "Model Studies of Helicopter Rotor Flow Patterns in a Water Tunnel" (U), A. F. Lechman, Proceedings of the 24th Annual Forum of the American Helicopter Society, May 1966 (Unclassified)

215. "A Theory for Static Propeller Performance" (U), J. C. Erickson and D. E. Ordway, CAL/AAVLABS Symposium Proceedings, Vol. I, June 1966 (Unclassified)

216. "Experiments on a Model Helicopter Rotor Operating in the Vortex Ring State" (U), Journal of Aircraft, Vol. 3, No. 3, K. Washizu, A. Azuma, J. Koo, and T. Oka, May-June 1966 (Unclassified)

217. "The Movement, Structure and Breakdown of Trailing Vortices from a Rotor Blade" (U), I. A. Simons, CAL/USAAVLABS Symposium Proceedings, Vol. 1, June 1966 (Unclassified)

218. "Experimental Boundary Layer Study on Hovering Rotors" (U), W. H. Tanner and P. F. Yaggy, Journal of the American Helicopter Society, Vol. 2, No. 3, July 1966 (Unclassified)

219. "1965 Measurements of Rotor Downwash by D&PS" (U), Thor Letter Report, R. J. Pipino, Ballistic Analysis Laboratory, The Johns Hopkins University, Baltimore, Maryland, 29 August 1966 (Confidential)

220. "Tip Vortex Core Thickening for Application to Helicopter Rotor Noise Reduction" (U), USAAVLABS Technical Report No. 66-1, Barnes W. McCormick, Jr., H. Sternfeld and R. H. Spencer, U.S Army Aviation Materiel Laboratories, Fort Eustis, Virginia, September 1966 (Unclassified)

1967

221. "Chronological Bibliography of Reports on Rotor Downwash" (U), Thor Technical Note No. 102, R. J. Pipino, Ballistic Analysis Laboratory, The Johns Hopkins University, Baltimore, Maryland, March 1967 (Unclassified)

222. "The Helicopter Rotor at High Mach Numbers" (U), W. H. Tanner, J. P. Van Wyckhouse, P. Cancro and J. McCloud, III, Presented at the Twenty-Third Annual National Forum of the American Helicopter Society, 10-12 May 1967 (Unclassified)

223. "Rotary Wing Boundary Layer and Related Researches" (U), W. H. Tanner, Presented at Advisory Group for Aerospace Research and Development (AGARD), NATO, Specialist's Meeting on "Fluid Dynamics of Rotor and Fan Supported Aircraft at Subsonic Speeds", Gottingen, Germany, 11-13 September 1967 (Unclassified)

224. "CH-54A and CH-53A Engine Air Particle Separator (EAPS) Development" (U), Report No. 67-ENV-7, C. D. Stephenson, H. H. Shohet, and E. F. Speiden, Proceedings of the Seventh Annual National Conference on Environmental Effects on Aircraft and Propulsion Systems, Report No. 67-ENV-7, Princeton, New Jersey, September 1967 (Unclassified).

225. "Development of the Lycoming Internal Particle Separator" (U), Report No. 67-ENV-5, H. D. Connors, Proceedings of the Seventh Annual National Conference on Environmental Effects on Aircraft and Propulsion Systems, Princeton, New Jersey, September 1967 (Unclassified)

226. "Field Evaluation of an Air Cleaner for the T63 Engine Powered OH-6A Aircraft" (U), Report No. 67-ENV-6, G. V. Bianchini, Proceedings of the Seventh Annual National Conference on Environmental Effects on Aircraft and Propulsion Systems, Princeton, New Jersey, September 1967 (Unclassified)

227. "Study of Rotor Configurations for Minimum Power and Rotor-Wake Pressure Distributions" (U), CAL Report No. BB-2293-S-2, C. Tung, and W. G. Brady, Cornell Aeronautical Laboratory, Inc., Buffalo, New York, September 1967 (Unclassified)

228. "Effects of Downwash Upon Man" (U), USAARU Report No. 68-3, W. P. Schane, LTC, MC, U.S. Army Aeromedical Research Unit, Fort Rucker, Alabama, November 1967 (Unclassified)

229. "Investigation of Compound Helicopter Aerodynamic Interference Effects" (U), USAAVLABS Technical Report No. 67-44, L. J. Bain and Anton J. Landgrebe, United Aircraft Corporation Research Laboratories, East Hartford, Connecticut, U.S. Army Aviation Materiel Laboratories, Fort Eustis, Virginia, November 1967 (Unclassified)

230. "Effects of a Porous Wingtip on an Aircraft Trailing Vortex" (U), H.C. Smith, M.S. Thesis, The Pennsylvania State University, University Park, Pennsylvania, December 1967 (Unclassified)

231. "Aerodynamics of the Helicopter" (U), A. Gessow and G. C. Meyers, Frederick Ungar Publishing Company, New York, 1967 (Unclassified)

1968

232. "Evaluation of the Dust Cloud Generated by Helicopter Rotor Blade Downwash" (U), USAAVLABS Technical Report No. 67-81, S. J. Rodgers, U.S. Army Aviation Materiel Laboratories, Fort Eustis, Virginia, March 1968 (Unclassified)

233. "A Reassessment of Rotor Hovering Performance Prediction Methods" (U),
D. S. Jenney, J. R. Olson and A. J. Landgrebe, Journal of the American
Helicopter Society, Vol. 13, Part 2, April 1968 (Unclassified)

234. "Structure of Trailing Vortices" (U), Journal of Aircraft, Vol. 5, No. 3,
B. W. McCormick, J. L. Tangler, and H. E. Sherrieb, May 1968 (Unclassified)

235. "Investigation of the Downwash Environment Generated by V/STOL Aircraft
Operating in Ground Effect" (U), USAAVLABS Technical Report No. 68-52,
Dynasciences Corporation Report No. DCR-275, M. George, E. Kisielowski, and
D. S. Douglass, Dynasciences Corporation, Blue Bell, Pennsylvania, for
U.S. Army Aviation Materiel Laboratories, Fort Eustis, Virginia, July 1968
(Unclassified)

236. "Induced Flow Variation of the Helicopter Rotor Operating in the Vortex
Ring State" (U), Journal of Aircraft, Vol. 5, No. 4, A. Azuma and A. Obata,
July-August 1968 (Unclassified)

237. "An Analysis of the Stall Flutter Instability of Helicopter Rotor
Blades" (U), F. O. Carta, Journal of the American Helicopter Society,
Vol. 12, Part 4, October 1968 (Unclassified)

238. "Two-Dimensional Tests of Advanced Instrumentation for Rotors" (U),
BHC Report No. 606-099-001, F. B. Burpo and W. H. Tanner, Prepared
under Contract NAS 2-4466, Bell Helicopter Company, Fort Worth, Texas,
December 1968 (Unclassified)

1969

239. "A Reassessment of Rotor Hovering Performance Prediction Techniques". (U),
D. S. Jenney, J. R. Olson, and Anton J. Landgrebe, American Helicopter
Society 25rd Annual National Forum, May 1969 (Unclassified)

240. "Inviscid Flow Field Induced by a Vortex in Ground Effect" (U), NASA Report
No. CR-1027, M. D. Greenberg and A. L. Kaskel, National Aeronautics and
Space Administration, Washington, D.C., May 1969 (Unclassified)

241. "Vortex Field, Tip Vortex, and Shock Formation on a Model Propeller"
(U), W. H. Tanner and R. M. Wohfeld, Paper presented at the CAL/AVLABS
1969 Symposium on "Aerodynamics of Rotary Wing and VTCL Aircraft",
18 - 20 June 1969 (Unclassified)

242. "An Analytical Method for Predicting Rotor Wake Geometry" (U), Anton J.
Landgrebe, Journal of the American Helicopter Society, Volume 14, No. 4,
October 1969 (Unclassified)

243. "Vortex Field, Tip-Vortex, and Shock Formation on a Model Propeller" (U),
W. H. Tanner and R. M. Wohlfeld, Proceedings of CAL/AVLABS Symposium on
Aerodynamics of Rotary Wing and VTOL Aircraft, 1969 (Unclassified)

1970

244. "The Free Wake Analysis; A Method for the Prediction of Helicopter Rotor Hovering Performance" (U), Journal of the American Helicopter Society, Vol. 15, No. 1, David R. Clark and Albert C. Leiper, Senior Research Engineers, Sikorsky Aircraft, Division of United Aircraft Corporation, Stratford, Connecticut, January 1970 (Unclassified)

245. "Study of Modification of Rotor Tip Vortex by Aerodynamic Means" (U), RASA Report No. 70-02 for ONR, S. A. Rinehart, Rochester Applied Science Associates, Inc., Rochester, New York, January 1970 (Unclassified) (AD 704 804)

246. "Effect of Wing Tip Configuration on the Strength and Position of a Rolled-up Vortex" (U), NASA Report No. CR-66916, R. Padakannaya, A Thesis in Aerospace Engineering, National Aeronautics and Space Administration, Washington, D.C., March 1970 (Unclassified)

247. "New Experimental Techniques in Rotorcraft Aerodynamics and their Application" (U), W. H. Tanner and R. M. Wohlfeld. Journal of the American Helicopter Society, Vol 15, No. 2, April 1970 (Unclassified)

248. "An Exploratory Wind-Tunnel Investigation of the Wake Effect of a Panel Tip-Mounted Fan-Jet Engine on the Left-Induced Vortex" (U), NASA Report No. TN D-5729, J. C. Patterson, Jr., and S. G. Flechner, National Aeronautics and Space Administration, Washington, D.C., May 1970 (Unclassified)

249. "Thor Presentation to AMSAA 28 October 1970" (U), Thor Letter Report, R. J. Pipino, Thor Division, Falcon Research and Development Company, Cockeysville, Maryland, 28 October 1970 (Unclassified)

250. "Flow Field Beneath the Rotor of a Helicopter and Considerations of Its Effect upon Missile Motion" (U), Memorandum for the Record, C. Raymond Dietz, AMXRD-AMM, Army Materiel Systems Analysis Agency, Aberdeen Proving Ground, Maryland, 17 November 1970 (Unclassified)

251. "Chronological Bibliography on Rotor Downwash: 1922-1970" (U), Thor Technical Note No. P42, R. J. Pipino and C. D. McGarry. Thor Division, Falcon Research and Development Company, Cockeysville, Maryland, December 1970 (Unclassified)

1971

252. "An Experimental Study of Tip Vortex Modification by Mass Flow Injection" (U), RASA Report No. 71-01 for ONR, S. A. Rinehart, J. C. Balcerak and R. P. White, Jr., Rochester Applied Science Associates, Inc., Rochester, New York, January 1971 (Unclassified) (AD 726 736)

253. "NASA Aircraft Trailing Vortex Research" (U), W. A. McGowan, Presented at the Federal Aviation Administration Symposium on Turbulence, Washington, D.C., 22-24 March 1971 (Unclassified)

254. "Aircraft Configuration Effects on Wake Turbulence" (U), J. Olsen, Paper presented at FAA Symposium on Turbulence, Washington, D.C., 22, 23, 24 March 1971 (Unclassified)

255. "Tip Vortices - Velocity Distributions" (U), N. A. Chigier and V. R. Corsiglia, Paper presented at the 27th Annual National Forum of the American Helicopter Society, Preprint No. 522, Washington, D.C., 19-21 May 1971 (Unclassified)

256. "An Analytical and Experimental Investigation of Helicopter Rotor Hover Performance and Wake Geometry Characteristics" (U), USAAMRDL Technical Report No. 71-24, Anton J. Landgrebe, United Aircraft Corporation Research Laboratories, East Hartford, Connecticut, for Eustis Directorate, U.S. Army Air Mobility Research and Development Laboratory, Fort Eustis, Virginia, June 1971 (Unclassified)

257. "Wake and Boundary Layer Effects in Helicopter Rotor Aerodynamics" (U), AIAA Paper No. 71-581, D. R. Clark and Anton J. Landgrebe, AIAA Fourth Fluid and Plasma Dynamics Conference, June 1971 (Unclassified)

258. "An Investigation of the Trailing Vortex System Generated by a Jet-Flapped Wing Operating at High Wing Lift Coefficients"(U), Journal of the American Helicopter Society, Vol. 16, No. 4, William J. Schumacher, Major, U.S. Army, United States Military Academy, West Point, New York, October 1971 (Unclassified)

259. "Design Considerations for Tilt-Rotor VTOL Aircraft to Minimize the Effects of the Recirculating Downwash Environment" (U), Journal of the American Helicopter Society, Vol. 16, No. 4, Richard R. Pruyn and Robert B. Taylor, The Boeing Company, Vertol Division, Boeing Center, Philadelphia, Pennsylvania, October 1971 (Unclassified)

260. "An Investigation of the Quantitative Applicability of Model Helicopter Wake Patterns Obtained from a Water Tunnel" (U), USAAMRDL Technical Report No. 71-69, Anton J. Landgrebe and E. D. Bellinger, United Aircraft Corporation Research Laboratories, East Hartford, Connecticut, for Eustis Directorate, U.S. Army Air Mobility Research and Development Laboratory, Fort Eustis, Virginia, December 1971 (Unclassified)

261. "Development and Application of a Method for Predicting Rotor Free Wake Positions and Resulting Rotor Blade Airloads" (U), NASA Report No. CR-1911, S. G. Sadler, National Aeronautics and Space Administration, Washington, D.C., 1971 (Unclassified)

1972

262. "An Investigation of the Mixing of Linear and Swirling Flows" (U), RASA Report No. 72-04 for ONR, R. P. White, Jr., and J. C. Balcerak, Rochester Applied Science Associates, Inc., Rochester, New York, February 1972 (Unclassified)

263. "Analytical Prediction of Vortex-Ring Boundaries for Helicopters in Steep Descents" (U), Journal of the American Helicopter Society, Vol. 17, No. 3, Julian Wolkovitch, Manager, Guidance and Control Department, Mechanic Research, Inc., Los Angeles, California, July 1972 (Unclassified)

264. "Investigation of the Dissipation of the Tip Vortex of a Rotor Blade by Mass Injection" (U), USAAMRDL Technical Report No. 72-43, R. P. White, Jr., and J. C. Balcerak, U.S. Army Air Mobility Research and Development Laboratory, Fort Eustis, Virginia, August 1972 (Unclassified)

265. "Main Rotor Free Wake Geometry Effects on Blade Airloads and Response for Helicopters in Steady Maneuvers, Volume I - Theoretical Formulation and Analysis of Results" (U), NASA Report No. CR-2110, S. G. Sadler, National Aeronautics and Space Administration, Washington, D.C., September 1972 (Unclassified)

266. "Rotor Wakes - Key to Performance Prediction" (U), AGARD-CP-111, AGARD Conference Proceedings No. 111 on Aerodynamics of Rotary Wings, Fluid Dynamics Panel Specialists Meeting, Anton J. Landgrebe and M. C. Cheney, September 1972 (Unclassified)

267. "Rotor Wakes - Key to Performance Prediction" (U), Paper presented at the Symposium on Status of Testing and Modeling Techniques for V/STOL Aircraft, Mideast Region of the American Helicopter Society, Anton J. Landgrebe and M. C. Cheney, October 1972 (Unclassified)

268. "The Wake Geometry of a Hovering Helicopter Rotor and Its Influence on Rotor Performance" (U), Journal of the American Helicopter Society, Vol. 17, No. 4, Anton J. Landgrebe, October 1972 (Unclassified)

1973

269. "Investigation of the Effects of Mass Injection to Restructure a Trailing Tip Vortex at Transonic Speeds" (U), RASA Report No. 73-03 for ONR, J. C. Balcerak and A. D. Zalay, Rochester Applied Science Associates, Inc., Rochester, New York, February 1973 (Unclassified)

270. "Experimental Investigation of Model Variable-Geometry and Ogee Tip Rotors" (U), AHS Paper No. 703, 29th Annual National Forum of the American Helicopter Society, Anton J. Landgrebe and E. D. Bellinger, May 1973 (Unclassified)

271. "Elimination of the Trailed Tip Vortex from a Helicopter Rotor Blade" (U), Rochester Applied Science Associates, Inc., NASA/Langley Research Center, Hampton, Virginia, Contract NAS1-11409, March 1971 - May 1973 (Unclassified)

272. "An Investigation of the Vibratory and Acoustic Benefits Obtainable by the Elimination of the Blade Tip Vortex" (U), Journal of the American Helicopter Society, Vol. 18, No. 4, Richard P. White, Jr., Executive Vice President and Director of Engineering, Rochester Applied Science Associates, Inc., Rochester, New York, October 1973 (Unclassified)

273. "Downwash Effects on Rocket Trajectory" (U), Report No. 2418, Electronics and Space Division, Emerson Electric Company, St. Louis, Missouri, 12 December 1973 (Unclassified)

274. "Vortex Modification by Mass Injection and by Tip Geometry Variation" (U), USAAMRDL Technical Report No. 73-45, J. C. Balcerak and R. F. Feller, U.S. Army Air Mobility Research and Development Laboratory, Fort Eustis, Virginia, 1973 (Unclassified)

1974

275. "Experimental Investigation of Model Variable-Geometry and Ogee Tip Rotors"
(U), NASA Report No. CR-2275, Anton J. Landgrebe and F. D. Bellinger, United
Aircraft Corporation Research Laboratories, East Hartford, Connecticut,
for Langley Research Center, NASA, February 1974 (Unclassified)

276. "Measure of Model Helicopter Rotor Flow Velocities with a Laser Doppler
Velocimeter" (U), Journal of the American Helicopter Society, Vol. 19,
No. 3, Anton J. Landgrebe and B. V. Johnson, July 1974 (Unclassified)

1975

277. "A Simplified Approach to Generalized Helicopter Configuration Modeling
and the Prediction of Fuselage Surface Pressures" (U), Proceedings of the
National Symposium on Helicopter Aerodynamic Efficiency, American Helicopter
Society, T. W. Sheehy, March 1975 (Unclassified)

278. "Prediction of Rotor Wake Induced Flow Along the Rocket Trajectories
of an Army AH-1G Helicopter" (U), Technical Report No. 4797,
Anton J. Landgrebe and T. Alan Egolf, United Aircraft Corporation
Research Laboratories, East Harford, Connecticut, for Picitinny
Arsenal, Dover, New Jersey, March 1975 (Unclassified)

No Date

279. "Ames Full Scale Wind Tunnel Tests" (U), TRECOM Contract DA-44-177-AMC-S3(t), Transportation Research Command, Fort Eustis, Virginia, (Unclassified)

280. "Introduction to Helicopter Aerodynamics" (U), W. Z. Stepniewski, revised edition, Rotorcraft Publication Comm., Morton, Pennsylvania, (Unclassified)

281. "Slipstream Flow Around Several Tilt-Wing VTOL Aircraft Models Operating Near Ground" (U), NASA Report No. TND-1382, W. A. Newson and L. P. Tosti, National Aeronautics and Space Administration, Washington, D.C., (Unclassified)

282. "Unpublished Data on the Effects of Foreign Object Ingestion on the Mission Endurance of the Vertol Model 107 (CH-46A) Helicopter"(U), Anon., Vertol Division of the Boeing Company, Morton, Pennsylvania (Unclassified)